NIR Absorption with adoptive Aromaticity: the paradigmatic cases of dicarba porphyrinoids and monocarba Vinylogous porphyrinoids

Thesis

Submitted for the Degree of

Doctor of Philosophy (Science)

At

Jadavpur University

by

Sumit Sahoo

School of Chemical Sciences

Indian Association for the Cultivation of Science

Jadavpur, Kolkata 700 032

India

March-2022

INDIAN ASSOCIATION FOR THE CULTIVATION OF SCIENCE
2A & 2B Raja S. C. Mullick Road, Jadavpur, Kolkata 700 032, INDIA

Dr. Harapriya Rath
Associate Professor

CERTIFICATE FROM THE SUPERVISOR

This is to certify that the thesis entitled "**NIR Absorption with adoptive Aromaticity: the paradigmatic cases of dicarba porphyrinoids and monocarba Vinylogous porphyrinoids**" submitted by Mr. Sumit Sahoo Index No. 105/18/ *Chem./ 25*, who got his name registered on 28. 02. 2018 for the award of Ph. D. (Science) degree of Jadavpur University, is absolutely based upon his own work under the supervision of Dr. Harapriya Rath and that neither this thesis nor any part of it has been submitted for either any degree/diploma or any other academic award anywhere before.

Dr. Harapriya Rath
Associate Professor
School of Chemical Sciences
Indian Association for the Cultivation of Science
Jadavpur, Kolkata-700 032

Harapriya Rath 09.03.22
Signature & Date with official seal

Dr. Harapriya Rath
Thesis Supervisor
School of Chemical Sciences

Phone: +91-33-2473-4971 Fax: +91-33-2473-2805 Mail: ichr@iacs.res.in

Dedicated to

My Dida & Parents

Preface

I hereby declare that the matter manifested in this thesis, "**NIR Absorption with adoptive Aromaticity: the paradigmatic cases of dicarba porphyrinoids and monocarba Vinylogous porphyrinoids"**, is the result of research carried out by me in the School of Chemical Science, Indian Association for the Cultivation of Science, Kolkata, India under the supervision of **Dr. Harapriya Rath**.

In keeping with general practice of reporting scientific observations, due acknowledgements have been made wherever the work described is based on the findings of other investigators. Attention has been given to incorporate all the current references related to this contemporary area of research.

Sumit Sahoo 09.03.22

Signature & Date

(Sumit Sahoo)
School of Chemical Science
Indian Association for the Cultivation of Science
Jadavpur, Kolkata – 700032
India

Acknowledgement

*It fills my heart with unspeakable joy, that after five years of hard work I am able to reach a position when I can write a full thesis entitled "**NIR Absorption with Adoptive Aromaticity: the paradigmatic cases of dicarba Porphyrinoids and monocarba Vinylogous Porphyrinoids**" from School of Chemical Sciences, Indian Association for the Cultivation of Science, Kolkata -32, for my doctoral degree. It is one of the finest moments in my academic life when I get the opportunity to express my indebtedness to all of my near and dear ones and to all who have contributed to the successful completion of this research work and who have given me the support and guidance. My heartfelt thanks to all the people mentioned here and others whose names I might have omitted unwillingly.*

To start with, I would like to acknowledge my supervisor Dr Harapriya Rath, for her enthusiastic support throughout my stay in his laboratory and without whom none of this would have been possible. Her mentorship, guidance, scientific acumen have not only enriched my scientific insight, it made me capable for analyzing and observing the details of any process. I thank her especially for her encouragement and ideas. I also wish to thank her for giving me the opportunity to work on this project, for trusting my judgement, and allowing me to grow and develop as a better researcher and scientific professional. She has been an inspiration, a philosopher and of course the guide in this scientific journey and beyond.

I am indebted to my collaborator Dr. D. Usharani, Prof. Peter Comba, Dr. S. J. Prathapa who helped me complete my work

I take the opportunity to express my thanks to Prof. R. Goswami, Prof. P. Ghosh, Prof. S. Sinha, Dr. T. K. Paine and their groups, School of Chemical Sciences, for their kind help and valuable suggestions.

During my undergraduate and post graduate studies, I have come in contact with some remarkable teachers Syed Sirajul Islam, Prof. Braja Gopal Bag, Prof. Ajay

Kumar Misra, Prof. Sudipta Dalai, Dr. Sumita Roy, Dr. Subal Chandra Manna, Dr. Maidul Hossain of my University (Vidyasagar University) and Dr. Nirmal Kumar Hazra (NKH), Sukhendu Das Adhikary (SDA), Biswajit Patra (BP), Gopalchandra Das from my college life who had enlightened me with the basic essence of this subject without them I would not be able to achieve this platform. It is an honor for me to express my sincere gratitude to them.

. I would like to especially mention Dr. Nirmal Kumar Hazra Sir. He is the key person behind the set-off of my journey.

I thank my fellow chemistry lab mates in Dr. Harapriya Rath's group: Abhijit da, Nyancy Di, Buddhadeb, Manik and Anirban and would also add names of some project fellows, Soumita, Shiney, Paramashivam, Poulami, Prabir for the stimulating discussions and all the fun we have had in the last five years. They rendered me enormous support in every possible way they could.

I consider myself extremely fortunate to have Lakshman da, Debasis da, Prabir, Anirban, Sanjit, Sambu da, Sourav da, as my friends. Thanks for being there for me in all sorts of fun and difficulties.

It is a pleasure to thank my friends at this institute Sanu, Jayanta da, Debu da, Abhishek,Ujjal, Suman da,, Sridhar da, Rahul da, Manish Da, Novendu da, Pratap da.

My other friends and relatives, whom I never treated with time and patience, should be thanked for their resilience to continue to be by my side supporting silently.

I would like to acknowledge the official and technical personnel in IACS for their cooperation. They have allowed me working in flexibility, agreed to help me in the best possible way.

I take the opportunity of acknowledging my institute Indian Association for the Cultivation of Science for providing me this platform and our director for providing me all the laboratory and institutional facilities. I sincerely thank CSIR (NEW Delhi) for providing me Junior and Senior Research Fellowships.

I have never seen God in my life yet. I owe everything I am today to my family, maa, baba, dada, boudi, vhai, niece (Supriti), and my lovely grandmother who are truly the reflection of almighty for me in Earth. Their unwavering faith and confidence in my abilities and in me are what has shaped me to be the person I am today. I find this opportunity to thanks them from my full heart who has always felt my every pain and cherished my every success and provided me everything they can for my bright and happy living without considering their own needs.

I apologise in advance, if I missed out anyone. Everyone and everything around me have been a teacher and inspiration to me in some way or other.

Finally, all praise to God Almighty, for His mercy that has given me the strength and ability to step strong and smooth in the way of my doctoral research. I can feel You are always holding my weak hand and helping me to proceed in the right path. Lastly, I wish to pray to You to get the opportunity to serve better for mankind.

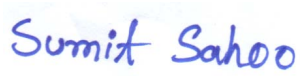

(Sumit Sahoo)
School of Chemical Sciences
Indian Association for the Cultivation of Science

ABSTRACT

Index No. *105/ 18/ Chem./ 25*

NIR Absorption with adoptive Aromaticity: the paradigmatic cases of dicarba porphyrinoids and monocarba Vinylogous porphyrinoids

Submitted by: Sumit Sahoo

Aromaticity is considered as of the most important concepts in modern organic chemistry that determines structure, stability, and reactivity of the molecules. Aromatic compounds having absorptions and emissions in the red or near-infrared (NIR) region are capable materials for a broad range of applications such as photodynamic therapy dyes, semiconductors in light-emitting diodes, photo-sensitizers in solar cells and microscopic imaging agents. Carbaporphyrins are porphyrin analogous in which one or more of the pyrrolic nitrogens have been replaced by carbon atoms. One of the most interesting properties of such carbaporphyrinoids is model of aromaticity and stabilisation of metal in higher oxidation state.

In my thesis, I have focused on design and synthesized of NIR active aromatic carbaporphyriods. I my third chapter, I have synthesized of dithia/diselena aromatic core modified *trans*-doubly *N*-Confused porphyrins with strong NIR absorption. Acid catalyzed condensation of N-TIPS pyrrole and 2,5-bis(*p*-tolylhydroxymethyl)selenophene/2,5-bis(p-tolylhydroxymethyl)thiophene (1:1 molar ratio) using$BF_3.OEt_2$ and subsequent chloranil oxidation has led to the isolation of *meso*-aryl substituted core modified *trans*-doubly *N*-Confused porphyrins **1** and **2.** The Aromaticity of these macrocycle are strongly supported by in-depth solution state spectroscopic measurements and DFT level theoretical calculations

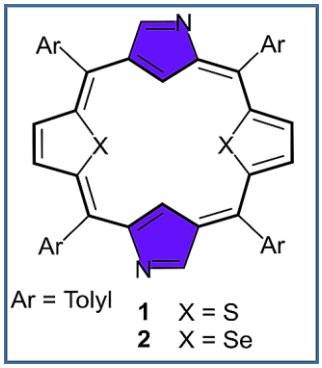

Figure **1**

My fourth chapter is an attempt in arriving at Hückel aromatic/antiaromatic dithia [26]/[24] core modified expanded azuliporphyrinoids (1.3.3.1.0). Acid catalyzed condensation of azulene-1, 3-bis-acrylaldehyde and bithiophenetetrapyrrane in methylene chloride using trifluoroacetic acid (TFA) as catalyst followed by oxidation with DDQ led to the exclusive isolation of Carbasapphyrins **3** and **4**.

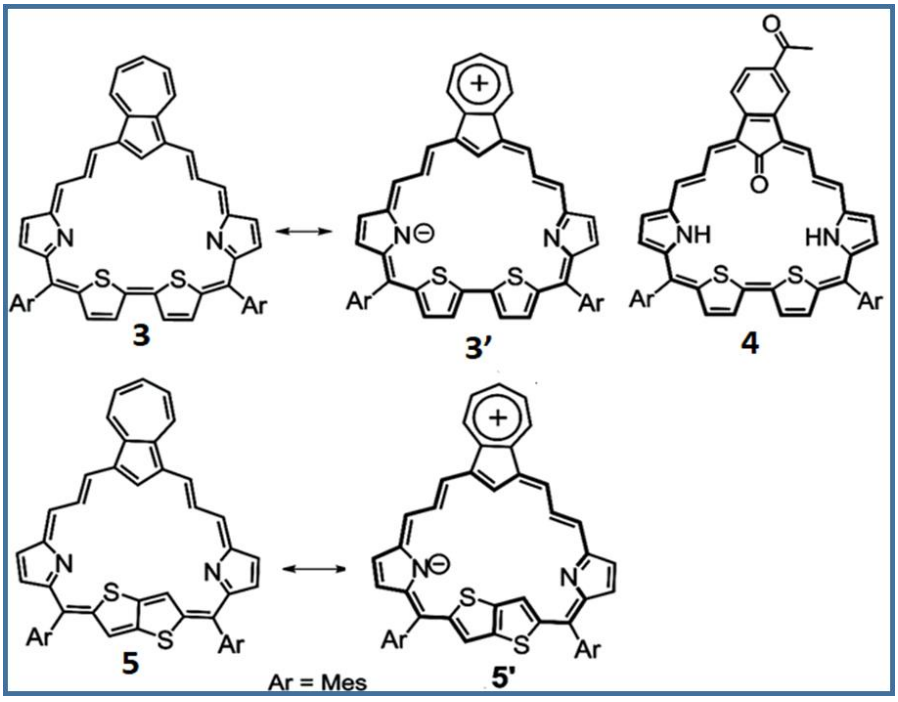

Figure **2**

The charge separated resonance delocalized tropylium cation is surmising the aromatic nature of the this carbaporphyrinoid **3'**. Contrarily, swiping the bithiophene

moiety with fused thieno [2,3, b] thiophene has anticipated anti aromatic nature of the corresponding azuliporphyrinoid (1.3.3.1.0) **5**. The spectroscopic preclusion of aromaticity/antiaromaticity have been well supported by supported by solution state spectroscopic measurements, DFT level theoretical calculations and solid state X-ray crystal structure.

Introducing aromatic spacer linker inside the expanded macrocycles have been challenging to researcher as such porphyrinoids exhibits dual conjugated path and allowing multi-metal coordination site. My fifth chapter is an attempt in arriving at aromatic bridge expanded carbaporphyrinoids following literature known acid catalyzed condensation protocol from its easy precursors. The aromaticity of these macrocycles **6** and **7** are supported by UV-Vis-NIR and NMR spectroscopy.

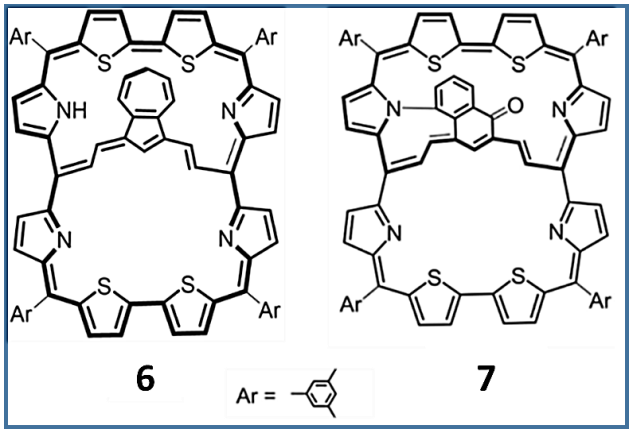

Figure **3**

Harapriya Rath. 09.03.2022
Signature of Supervisor

Sumit Sahoo
Signature of Student

(Dr. Harapriya Rath)

(Sumit Sahoo)

Dr. Harapriya Rath
Associate Professor
School of Chemical Sciences
Indian Association for the
Cultivation of Science
Jadavpur, Kolkata-700 032

ABBREVIATIONS

Me	Methyl
DBU	1,8-Diazabicyclo(5.4.0)undec-7-ene
NaOH	Sodium hydroxide
DMF	*N,N*-dimethylformamide
DCM	Dichloromethane
THF	Tetrahydrofuran
DDQ	2,3-Dichloro-5,6-dicyano-1,4-benzoquinone
HCl	Hydrochloric acid
HNO_3	Nitric acid
H_2SO_4	Sulphuric acid
Chloranil	Tetrachloro-1,4-benzoquinone
TFA	Trifluoroacetic acid
PTLC	Preparative Thin-layer Chromatography
ESI	Electron Spray Ionization
MALDI	Matrix-Assisted Laser Desorption/Ionization
TOF	Time of Flight
MS	Mass Spectrometry
UV-vis	Ultra Violet- visible
A (in UV-vis spectrum)	Absorbance
NIR	Near-Infrared
NMR	Nuclear Magnetic Resonance
ppm	parts-per million
1,2-DCE	1,2-dichloroethane
CV	Cyclic Voltammetry
DPV	Differential Pulse Voltammetry
FMO	Frontier Molecular Orbital
HOMO	Highest Occupied Molecular Orbital
LUMO	Lowest Unoccupied Molecular Orbital
BLA	Bond Length Alternation
HOMA	Harmonic Oscillator Model of Aromaticity
DFT	Density Functional Theory
GIAO	Gauge Including Atomic Orbitals

NICS	Nucleus Independent Chemical Shift
ACID	Anisotropy of the Current Induced Density
NCP	N-Confused Porphyrin
N_2CP	Doubly N-Confused Porphyrin
TPP	Tetra-Phenyl Porphyrin
DDQ	2,3-Dichloro-5,6-dicyano-1,4-benzoquinone
NCTPP	N-Confused Tetra Phenyl Porphyrin

CONTENTS

Chapter 4: NIR Absorbing monocarba Vinylogous porphyrinoids with adoptive Aromaticity

Chapter 5: Siamese Vinylogous Carbaporphyrinoids

General Introduction

Chapter 1

1.1. Introduction

The design and synthesis of NIR absorbing chromophores are challenging to researchers due to their application of all-direction of sciences.[1a-g] NIR absorbing chromophores are more applicable in biology as near-infrared (NIR) light holds more superior penetrability than the visible range in biological tissues because of less light scattering and absorption ratio in longer wavelengths.[1h]

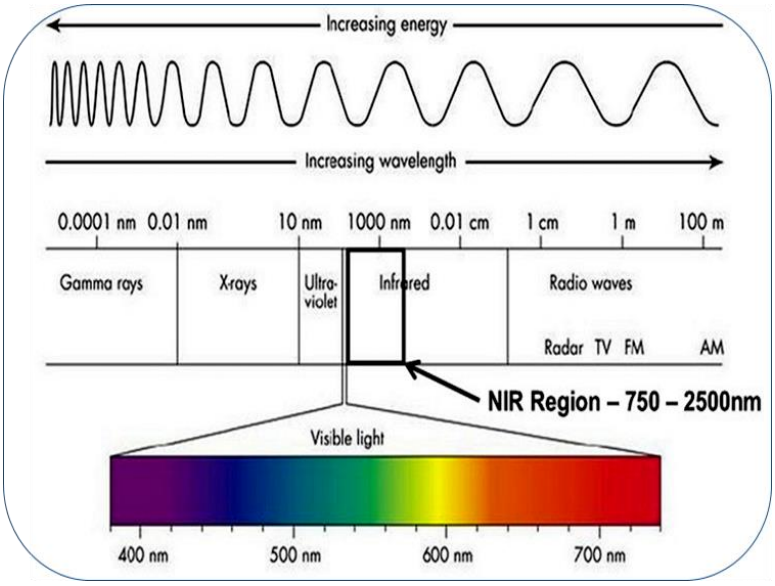

Figure 1.1 Electromagnetic Spectrum

NIR materials we can classify into two ways one is Organic based molecule, and another is inorganic-based. Quantum dots (QDs) are composed of inorganic fluorescent material. Near-infrared (NIR) emission QDs have outstanding application advantages in laser, energy, photodetection.[2] Soga et al. developed novel nanoparticles composed of Y_2O_3 and YPO_4 with well-controlled particle size able to be excited by near-infrared (NIR) light.[3] Such inorganic based NIR active materials are highly toxic for biological study.

Chapter 1

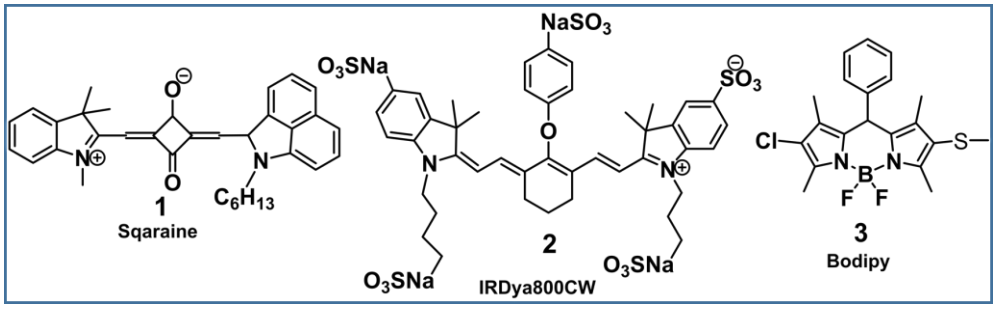

Figure 1.2 Organic molecules exhibiting NIR absorption

Organic aromatic compounds having absorptions and emissions in the red or near-infrared (NIR) region are capable materials for a broad range of applications such as photodynamic therapy dyes,[4] semiconductors in NIR light-emitting diodes,[5] and photo-sensitizers in NIR-utilizing solar cells[6] microscopic imaging agents[7] etc. Cyanines,[8] phthalocyanines /porphyrins,[9] squaraines[10] or BODIPYs[11] are the most common organic chromophores which exhibits strong NIR absorption/emission properties. The acyclic chromophore which are shown in (Figure 1.2) are not aromatic. Commercially available NIR dyes, such as cyanine and polyene dyes possess intrinsic disadvantage(s) for practical use owing to poor photostability and low solubility.[12a-b] To circumvent such issues, organic chemists have tremendously benefited from the synthesis and isolation of soluble and stable aromatic organic NIR chromophore. As aromatic compounds give stability to the molecules[12c] and play important roles in biochemistry and industry.

1.2. Criteria for Organic NIR chromophores

The optical and electronic properties of organic molecules are determined by the energy gap between HOMO and LUMO. The redshift in absorption and emission spectra results from narrowing the HOMO-LUMO gap. Therefore, the HOMO- LUMO gap is the key parameter to design a molecule of the low energy gap and often involves chemical modification at the molecular level. Organic compounds that absorb or emit in the NIR region are all considered to have a conjugated π system.

For a chromophore to absorb at wavelengths above 750 nm, the π electron must be effectively delocalized along the conjugated path. Research on NIR materials and technology is motivated by curiosity in the fundamental study and practical applications in several important sectors such as energy, communication, bioimaging, sensing, and advanced optoelectronics.[13]

Several design factors which are the reason for NIR absorbing organic molecules are

- Extended π-conjugated chromophores
- Donor–acceptor charge transfer.
- The polar effect is caused by the heavy atoms.

1.2.1. Extended π-conjugated chromophores

It is generally found that the bandgap decreases with increasing conjugation length. Cyclic conjugated systems are generally rigid compare to acyclic system. If we increase the conjugation path in cyclic conjugated system, then molecule will show bathochromic shift. Porphyrins are 18π conjugated aromatic compound. The torsional angle between the adjacent rings of porphyrin partially interrupts the conjugation and leads to an effective increase of the band gap.[14]

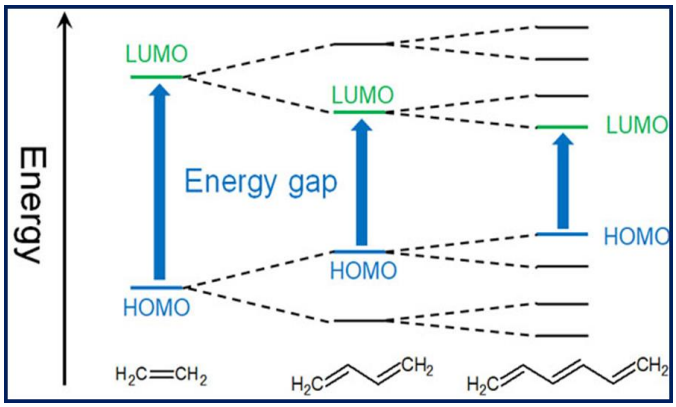

Figure 1.3 Variation of the HOMO–LUMO gap with increasing conjugation length

1.2.2. Donor–acceptor charge transfer

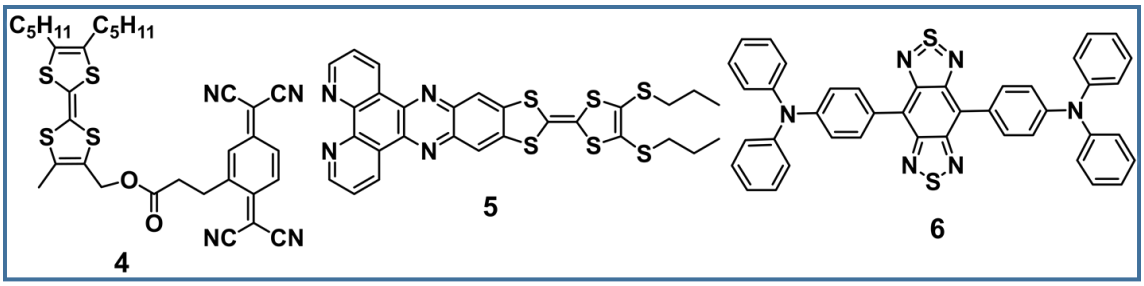

Figure 1.4 Doner-acceptor Charge transfer molecules

Intramolecular charge-transfer (CT) chromophores can be defined as chromophores in which movement of π -electron density from the donor to the acceptor accompanies to the first excitation. A strong electron donor (D) and a strong electron acceptor (A) in small molecules and polymers become a common strategy for lowering the energy gap. On one hand, the D–A type of chromophores exhibit two resonance forms (D-A $\rightarrow$ $^{+}$D=A^{-}), which give rise to an increased double bond character between the D and A units, thus reducing the bond length alternation, resulting in a decrease of the HOMO- LUMO gap.[15] On the other hand, hybridization of the energy levels of the donor and acceptor can raise the energetic level of the HOMO higher than that of the donor and lower the energetic level of the LUMO below that of the acceptor, leading to an unusually small HOMO–LUMO separation.[16]The use of an electron donor (high-lying HOMO) and an electron acceptor (low-lying LUMO) in molecular design is a widely accepted and used approach. The donor and acceptor units can be linked either by a nonconjugated σ spacer or a conjugated π spacer. For the σ spacer linked compound since the mixing of HOMO and LUMO orbital is precluded, the HOMO and LUMO level can be tuned independently.[17]

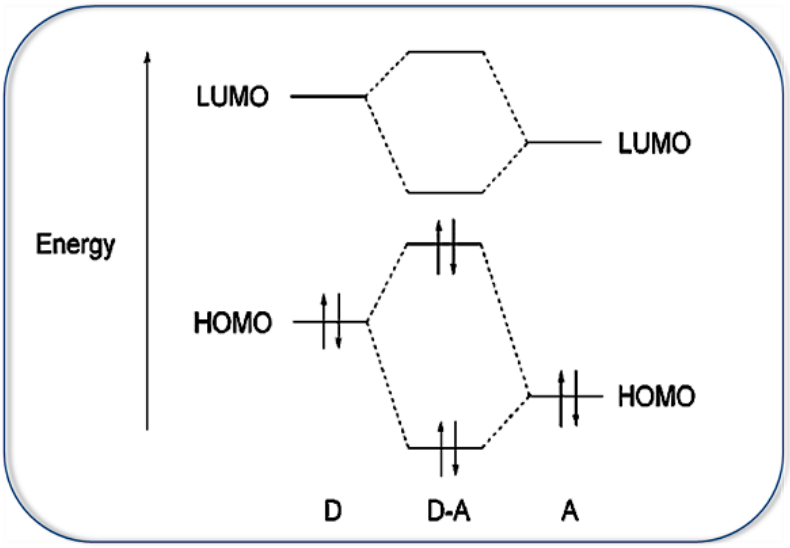

Figure 1.5. Interaction of energy levels of a donor (D) and acceptor (A) leading to a narrower HLG.

1.2.3. The polar effect caused by the heavy atoms

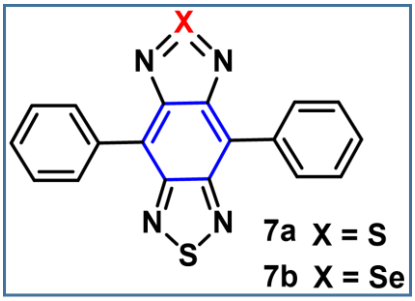

Figure 1.6. Diphenylbenzobisthiadiazole

The polar effect caused by the heavy atoms on the energy gap should also be considered when designing NIR chromophores. The well-known cases of lowering the energy gap typically involve the replacement of sulfur and oxygen atoms with heavier ones such as selenium and tellurium in a conjugated system.[18] A redshift of 67 nm in absorption maximum was observed in a simple

diphenylbenzobisthiadiazole compound when the sulfur is replaced with selenium.[19]

1.3. Aromaticity in general

In 1931, German chemist and physicist Sir Erich Hückel proposed a theory to determine the aromaticity of a molecule. According to rules the criteria for Aromaticity of molecule are (a) The molecule is cyclic (a ring of atoms) (b) The molecule is planar (all atoms in the molecule lie in the same plane) (c) The molecule is fully conjugated (p orbitals at every atom in the ring) (d) The molecule has 4n+2 π electrons (n=0 or any positive integer).[20]

1.3.1. Nucleus-Independent Chemical Shift (NICS)

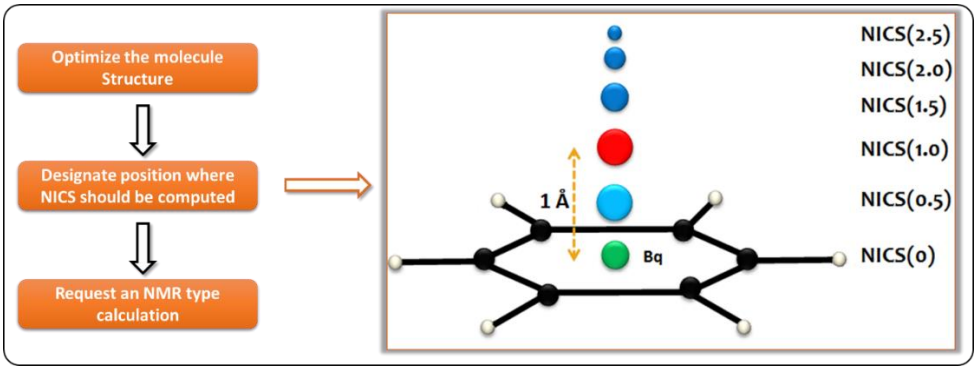

Figure 1.7. Schematic presentation of NICS

The nucleus-independent chemical shift (NICS) is a computational method that analyzes the negative or positive of the absolute magnetic shielding or deshilding at the center of a ring. If the NICS values at the center of the ring is negative (i.e. Magnetically shielded) indicate the presence of induced diatropic ring currents or "aromaticity", whereas positive values (i.e., deshielded) indicate the presence paratropic ring currents and "antiaromaticity".[21] *Bq* ghost atoms (Banquo, that is, ghost atoms, taken from Macbeth) are used to designate the positions for the NICS evaluations.

1.3.2. Anisotropy of the Current-Induced Density (ACID)

Anisotropy of the Current-Induced Density (ACID) is another computational method for the investigation and visualizing delocalization of a molecule. [22]. From the direction of ring current vectors, we can have judged easily either it is aromatic or antiaromatic. If the direction of the ring current vector is clockwise(diatropic) then it is aromatic and anticlockwise (paratropic) is antiaromatic.

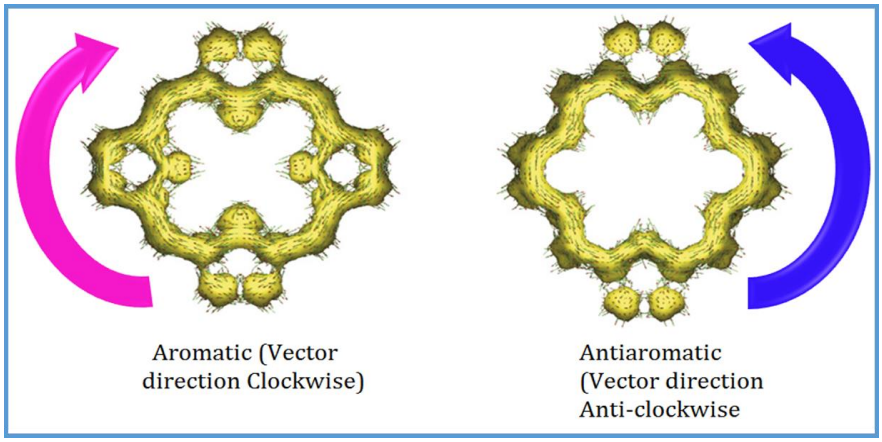

Figure 1.8: Isosurfaces of the anisotropy of the induced current density of aromatic and antiaromatic systems

1.3.3. Harmonic Osciletor Model of Aromaticity (HOMA)

Harmonic Oscillator Model of Aromaticity (HOMA) is another structural criterion based on experimental data from single-crystal X-ray diffraction studies or the optimized geometry structure. It is easily calculating from the given equation. From the value of HOMA, we can easily judge the Aromaticity of a molecule. Benzene is well known Aromatic stable compound, its HOMA value considers as one. The HOMA values of other Aromatic molecules are compared with respect to that of benzene.

$$\mathrm{HOMA} = 1 - \frac{1}{n}\sum_{i=1}^{n} \alpha_i \left(R_{\mathrm{opt},i} - R_i \right)^2$$

Where α is constant, n is the number of peripheral bonds with individual bond lengths R_{opt} and R_i is their mean value. [23]

1.3.4 Bond length alternation

Bond-length alternation (BLA) is defined as the average of the difference in the length between adjacent carbon-carbon single and double bonds. The smaller the bond length alternation is, the lower the HOMO- LUMO energy gap.[24] Most π Aromatic hydrocarbon geometries have bond lengths that fall in between that of a C–C single bond (1.54 Å from ethane) and a C-C double bond (1.34 Å from ethylene) as a result of the "partial" bonding in the electron delocalization. For instance, benzene is acknowledged to have bond lengths of around 1.40 Å, nearer to that of the double bond. True Kekulé geometries would alternate the single and double bonds, giving an average bond size between the two, as benzene exhibits. Hence, the average bond size might also be beneficial as a simple, first-order prediction of aromaticity. Planar, aromatic molecules defined in the traditional sense have average C–C bond lengths of 1.41 Å or less whereas planar, cyclic antiaromatic species have average bond lengths of between 1.41 - 1.50 Å.[25]

1.4. Porphyrin and modified Porphyrin

Porphyrin is 18 π conjugated aromatic compound in which four pyrrole units are connected with α–α linkage through four *meso* carbons. Various synthetic strategies have been used to build up novel artificial porphyrin homologs, such as *meso* and *β*-substitution, ring-contraction, ring-expansion, isomerization and core-modification, to regulate their structural and optoelectronic properties.[26] Modifications of porphyrinoid core, which involves the replacement of the nitrogen atoms by other hetero atoms have led to a new class of macrocycles known as core-modified porphyrins.[27]

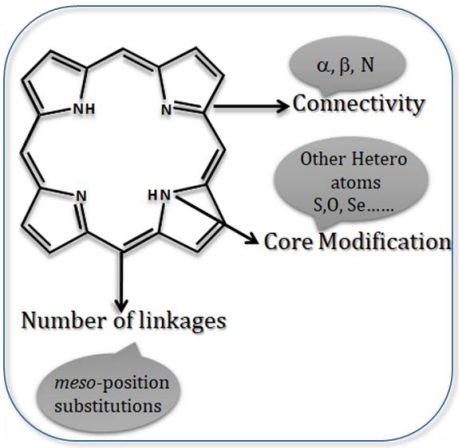

Figure 1.9 Schematic Diagram of Porphyrin

1.5. Criteria for porphyrinoids exhibiting Aromaticity with NIR absorption

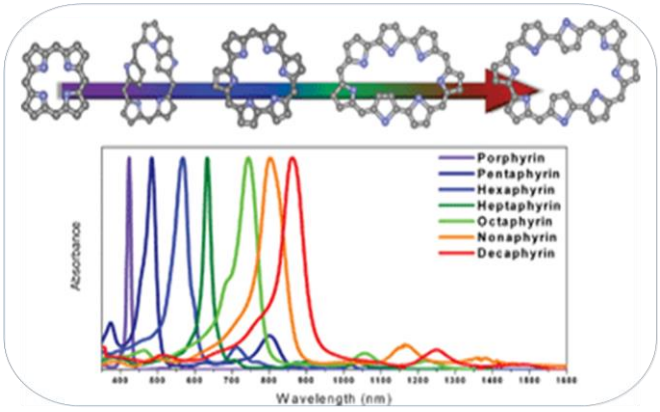

Figure 1.10. π-conjugated expanded porphyrins

Retro synthetically, we can design a porphyrin which exhibits aromaticity with NIR absorption. The porphyrin exhibit aromaticity with NIR absorption are

(a) Expanded Porphyrin

(b) Fused porphyrins (Fused in the periphery)

(c) Fused porphyrins (Fused in the core)

(d) Carbaporphyrinoids

(e) Vinylogous Porphyrins

1.5.1. Expanded Porphyrins

Expanded porphyrins are the class of conjugated macrocyclic compounds in which more than four pyrrole rings are connected via *meso*-methine bridges. They have been found to exhibit NIR absorption and emission due to extend of π conjugation. Another way to increase the number of π-electrons in the macrocycle is by increasing the *meso* carbon between the four pyrrole/heterocycle rings.[28] Due to the extent of π conjugation, such macrocycles have revealed significant photophysical properties and reactivity and display absorption bands from visible to near IR range. Expanded porphyrins have potential application such as, sensitizers for photodynamic therapy (PDT),[29] as contrast agents in magnetic resonance imaging (MRI),[30] as radiation therapy enhancer,[31]rapidly developing biomedical applications, and as nonlinear-optical materials.[32]

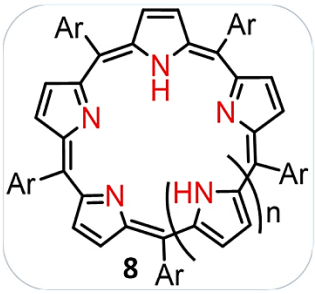

Figure 1.11. Schematic diagram of expanded Porphyrin

Due to the structural distortion, expanded porphyrin does not maintain its planarity. As a result, the delocalization of π-electrons along the molecular framework is hindered. So, they exhibit broad and ill-defined absorption spectra.

meso-aryl substituted hexaphyrin **9** exhibits two potentially valuable properties, one is excellent NIR absorption for less invasive photothermal therapy (PTT) and another is multiple fluorine atoms at a *meso*-aryl group for ^{19}F MRI.[33]

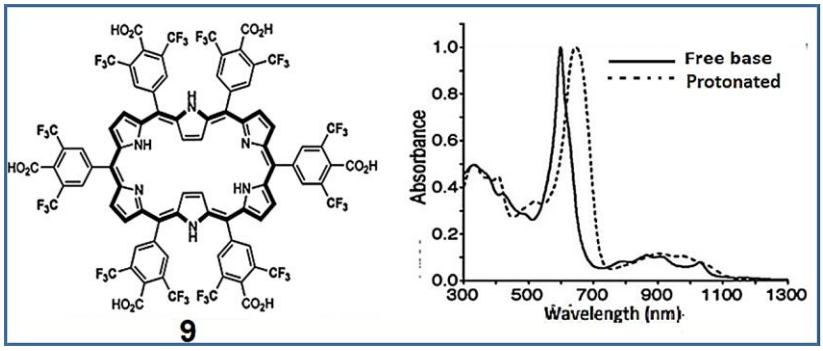

Figure 1.12. NIR absorption of hexaphyrin **9** in free base (solid) and protonated in dotted line

It is found that the structural preference, inverted versus planar, is very sensitive to the *meso* substituents temperature and solvent polarity. In this context [28]Hexaphyrin(1.1.1.1.1.1) **10** and [32]Heptaphyrin(1.1.1.1.1.1.1) **11** have been shown to exist as a dynamic equilibrium between Hückel antiaromatic and Möbius aromatic conformers in solution, in which distribution of conformers is dependent upon temperature and solvent polarity and metalation .[34]

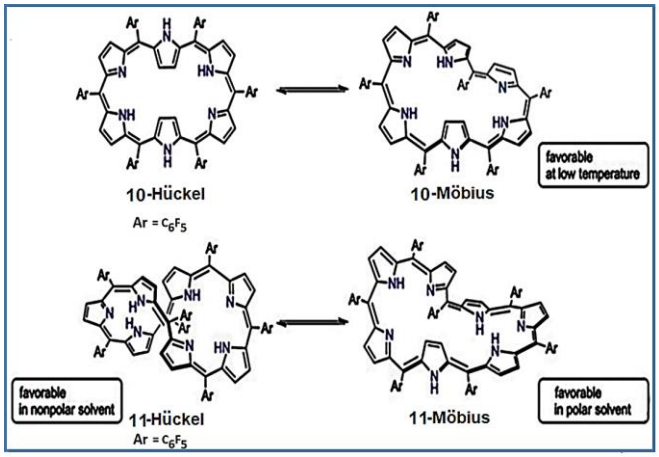

Figure 1.13. Equilibrium between Huckel antiaromatic and Mobius aromatic conformers

Oxidation and reduction induces the conformational changes of expanded porphyrin. Oxidations of 28 π Mobius aromatic molecule **12** gave rise to formations of non-twisted 26π Hückel aromatic species **13** with related topological changes. Interestingly, NNNC palladium(II) coordination in **12** is changed to NNCC palladium(II) coordination in **13** with a molecular topology change from a twisted Möbius conformation to a planar Hückel conformation.[35]

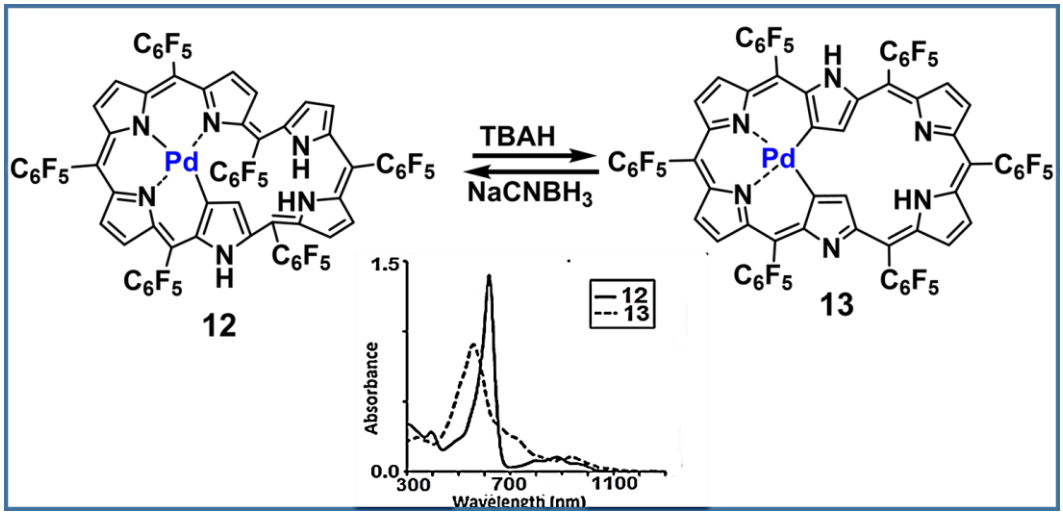

Figure 1.14. UV –vis-NIR spectra of **12** and **13**

1.5.1.1. External stimuli triggering aromaticity and NIR absorption in Various Expanded porphyrins:

From a structural point of view, extended porphyrins with *meso* aryl substituents exhibit structural diversity,[36] where depending on the number of twists it can be triggered its aromaticity and reactivity.[37].

1.5.1.2. Temperature-Dependent aromaticity and NIR absorption

Macrocycle **14** exhibits an unusual ^{1}H NMR spectrum, it shows a moderate diatropic ring current at room temperature itself, in spite of its [4n] π electrons. At room temperature, meso-hexaaryl-substituted [28]hexaphyrins(1.1.1.1.1.1) **14** in solution exist an equilibrium between planar antiaromatic and distorted Möbius aromatic conformers.Upon lowering the temperature, the equilibrium shifted to the distorted Möbius aromatic conformation.The temperature-dependent absorption and fluorescence spectra of **14** in the range 293–173 K are presented in(figure 1.15.) As the temperature is lowered, the B-like band in the absorption spectra of **14** is red-shifted, with the appearance of a small band at 650 nm and intensifying with well-resolved Q-bands. [38]

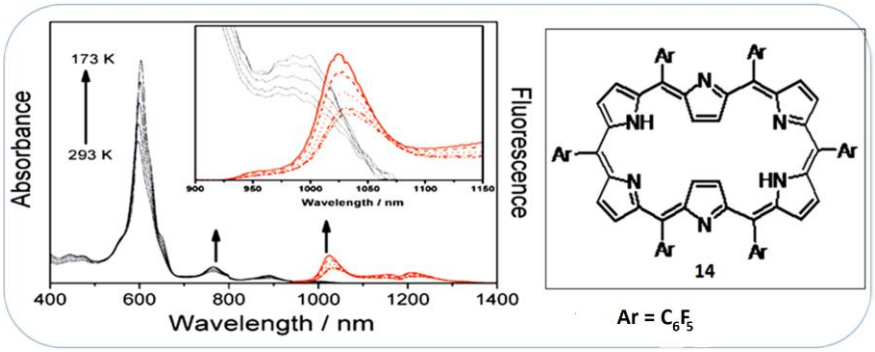

Figure 1.15. NIR absorption (black) and emission (red)of hexaphyrin **14**

1.5.1.3. Protonation induced Aromaticity with NIR absorption

Various protic acids like MSA, TFA, DCA, TCA, etc have been found to protonated porphyrin. In this context, upon titration with trifluoroacetic acid, the expanded porphyrin **15** & **16** (Figure 1.16) shows a dramatic change in its absorption spectra. Upon protonation, the molecules are changed to their geometry from figure-eight to planner structure results red-shifted absorption.[39a]

Chapter 1

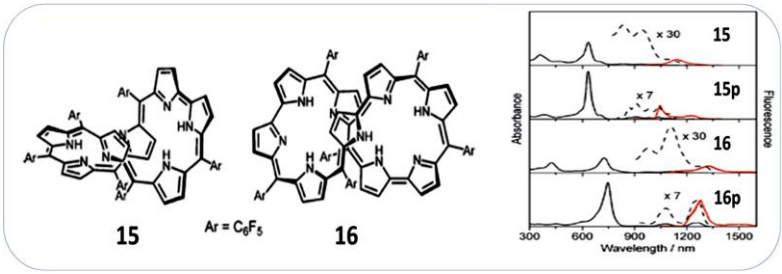

Figure 1.16. UV –vis-NIR of protonation induced conformational changes and NIR absorption of expanded porphyrin **15** &**16**

In continuation 5,20-Di(pyridin-2-yl)-[28]hexaphyrin(1.1.1.1.1.1) Hückel antiaromatic molecule **17** was reported by Osuka and co-worker. Upon protonation of **17** with methanesulfonic acid (MSA) the formation changes from Hückel antiaromatic molecule to twisted conformations with Möbius aromaticity with NIR absorption.[39b]

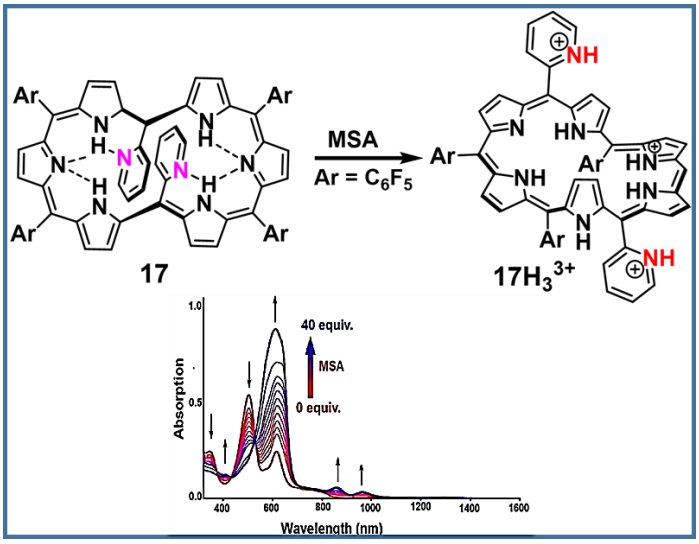

Figure 1.17. Protonation induced conformational changes and NIR absorption of hexaphhyrin **17**

1.5.1.4. Deprotonation induced aromaticity and NIR absorption.

Upon treatment with tetrabutylammonium fluoride (TBAF), [32] heptaphyrins **18a** and **18b** underwent conformational changes to form Möbius aromatic species. These changes were accompanied by red-shifted and sharp soret-like bands, two distinct Q-like bands in the NIR region and elongated S1-state lifetime. [40]

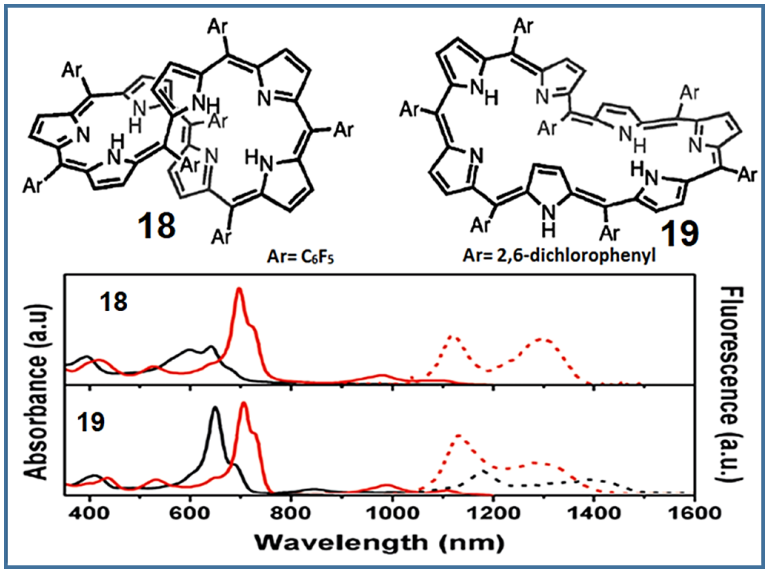

Figure 1.18. Absorption spectroscopy of [32]heptaphyrins upon deprotonation neutral (black line) and deprotonated (red line) species

1.5.1.5. Metalation induced NIR absorption

Transition metals have been found as an effective tool for the metallated complexes. The Metal complexes of expanded porphyrin have found potential application as photosensitizers in photodynamic therapy,[41a] contrast agents in magnetic resonance imaging,[41b] and enzyme models in bioinorganic chemistry.[41c] Mono-Au(III) complex **20**a and bis-Au- (III) complex **20**b were reported by Osuka and co-worker.[41d] The mono-Au(III) complex **20**a was more planner compare to bis-Au- (III) complex **20**b. The presence of diatropic ring corrent of these complexes were evident from 1H NMR spectra Both the complexes exhibited NIR absorption

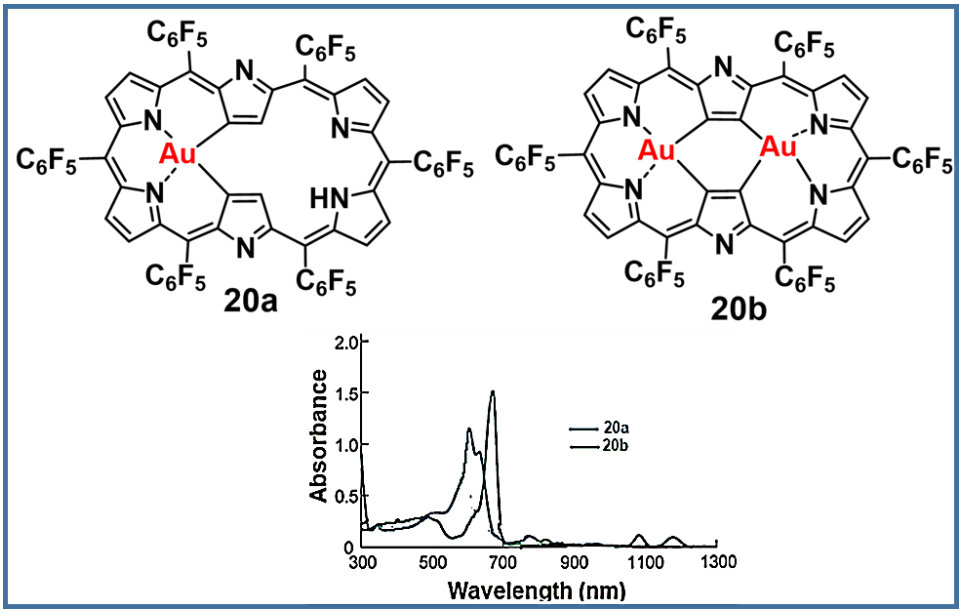

Figure 1.19. Metalation induced NIR absorption of macrocycles

1.5.1.6. Directly *meso–meso* linked linear porphyrin arrays exhibiting NIR absorption (Z_N)

The molecular design of directly *meso–meso* linked linear porphyrin arrays called $\mathbf{Z}_N$,(where N =1, 2, 3, 4, 6, 8, 12, 16, 32, 64 and 128) was evident to bring the porphyrin units closer for rapid energy transfer.

1.5.1.7. Fused linear porphyrin arrays (T_N)

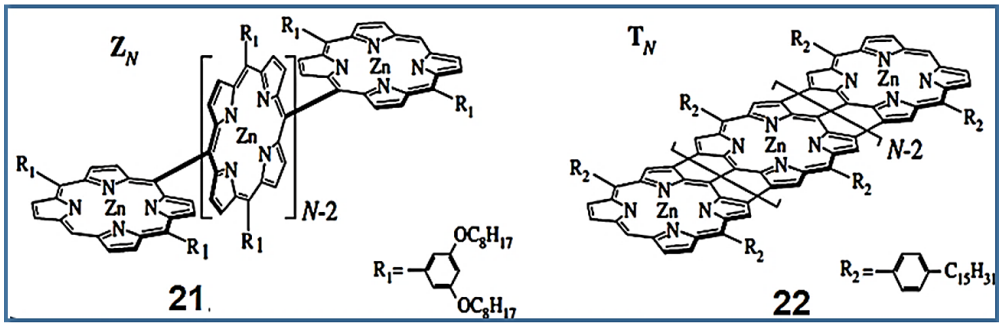

Figure 1.20. Molecular structures of directly *meso–meso* linked ($\mathbf{Z}_N$) and *meso–meso*, β–β, β–β triply linked ($\mathbf{T}_N$) linear porphyrin arrays.

As a straightforward strategy for maximizing π-overlap among the porphyrins, triply *meso–meso*, β–β, β–β linked linear porphyrin arrays called $\mathbf{T}_N$, (*N* =2, 3, 4, 5, 6, 8 and 12) were reported by Osuka and co-workers(Figure1.20). These fully conjugated porphyrin arrays have planar tape-shaped structures and display drastically red-shifted absorption spectra that reach into the far-IR region, reflecting extensive π conjugation.[44]

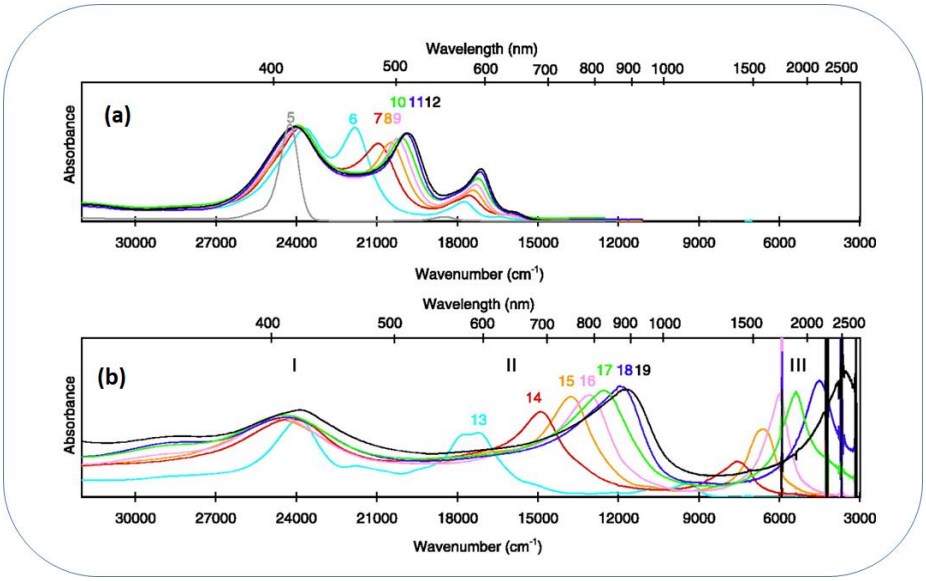

Figure 1.21. Steady-state absorption spectra of (*a*) Z_N and (*b*) T_N taken in $CHCl_3$ at room temperature

1.5.1.8. Porphyrin tapes exhibiting NIR absorption

meso-meso, β–β, β–β triply-linked porphyrin arrays so-called porphyrin tapes possess a unique position in terms of extending linear planar structures, fully conjugated π-electronic networks, and exceptionally red-shifted absorption bands [42] *meso-meso* linked porphyrin–hexaphyrin hybrid **23**, **24**, and **25** were reported by Osuka and co-worker. The flexibility of macrocycles **24** and **25** is reduced compare to macrocycle **23** due to β–β fusion of pyrrole β positions. The hybrid tapes **23, 24** and **25** exhibited NIR absorption due to effective π-electronic delocalization.[43]

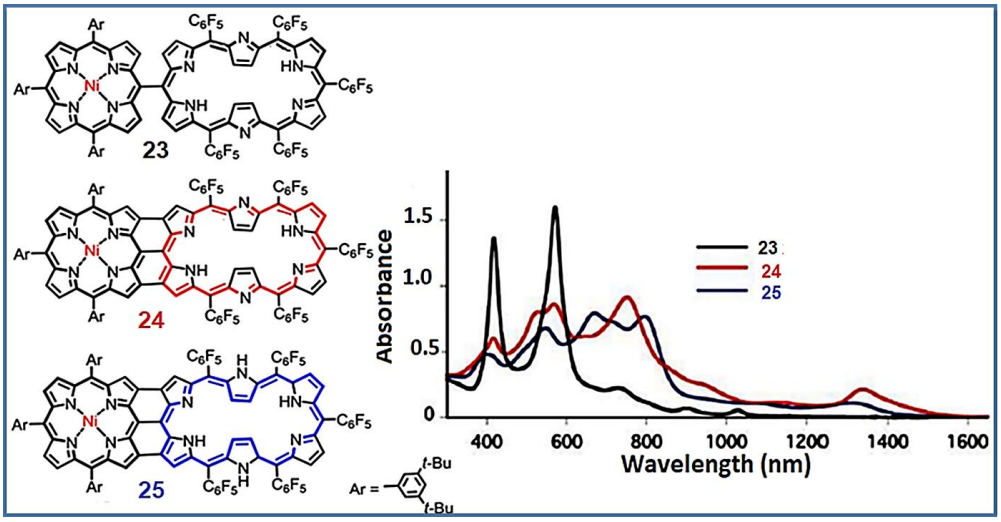

Figure 1.22. UV –vis-NIR spectra of of *meso-meso*, β–β, fused porphyrins.

. 1.5.2. Fused Heterocycle Incorporated macrocycle with NIR absorption and aromaticity

Porphyrinoids, which are embedded with fused heterocycles in their periphery can adopt planar or near planar conformation and show strong absorption in the NIR region. Due to the fused system in their periphery, the molecular flexibility is reduced and the macrocycle becomes rigid conformation. Furthermore, the unique local aromatic features of these constructing blocks have an effect the global aromatic properties of porphyrinoids. Fused porphyrin has an unusually narrow HOMO-LUMO energy gap and exhibits absorption in the near infrared (NIR) region [45]

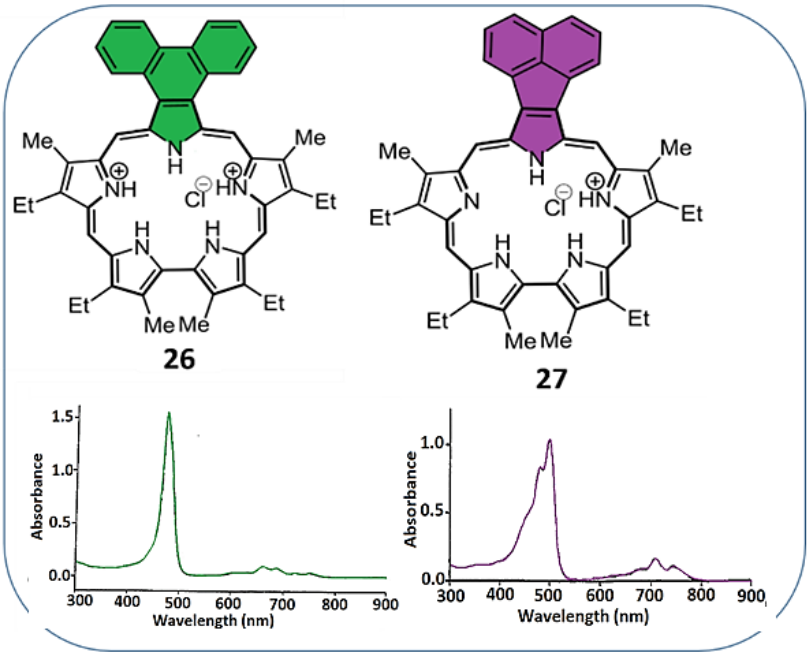

Figure 1.23. UV –vis-NIR spectra of Phenanthrene and acenaphthylene fused sapphyrins

Macrocycles **26** and **27** were reported by T. D. Lash and co-workers.[46] Introducing to inbuilt fused part (phenanthrene and acenaphthylene) inside macrocycle gave phenanthro and acenaphthosapphyrins. The extant of π conjugation increases due to the inbuilt fusion portion in the conjugation path leading to red-shifted UV- vis spectra in macrocycles **26** and **27.**

Macrocycle **28** benzodipyrrole sapphyrin was reported by C. H. Lee and co-workers. [47] The free base and diprotonated species of benzodipyrrole sapphyrin **28** exhibits NIR absorption. In continuation when two pyrrolic nitrogen atoms were replaced by two oxygen atoms, it formed more rigidified dioxabenzosapphyrin **29** [48]

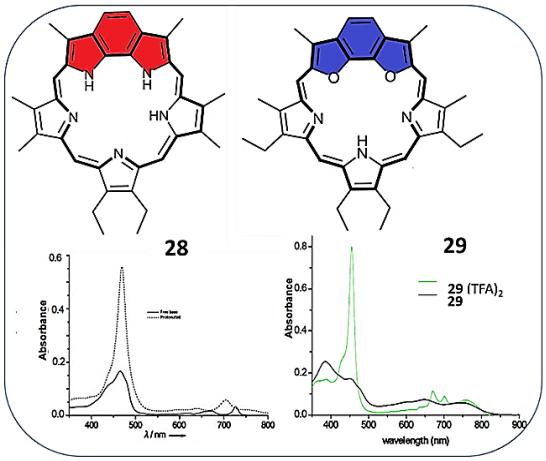

Figure 1.24. UV-Vis spectra of benzodifuran & benzodifuran Derived Sapphyrin.

The fused naphthorubyrin **30** and naphthosapphyrin **31** were reported by the same group. The π–extended naphthorubyrin was isolated as its monoprotonated form, whereas in naphthosapphyrin where one of the pyrrole ring was inverted. The reinversion of the inverted pyrrole was observed upon monoprotonation, while in presence of excess acid led to the formation of a diprotonated form with spectral features that is the ‘‘NH out’’ arrangement of the pyrrolic subunit. Both the macrocycles are aromatic and exhibit NIR absorption in the free base as well as protonated form.[49]

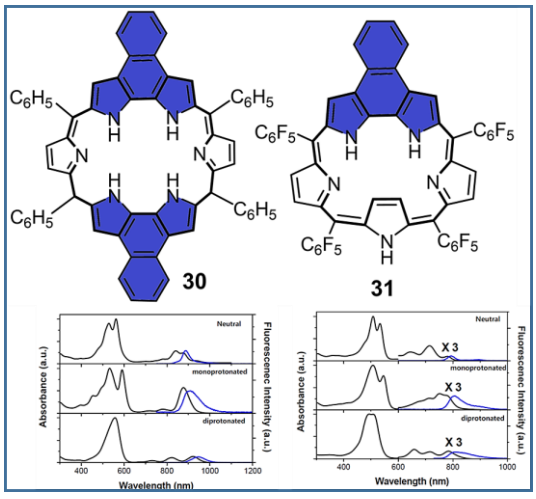

Figure 1.25. UV-vis-NIR spectra of naphthorubyrin **30** and naphthosapphyrin **31**

Naphthobipyrrole-Derived Cyclo[8]pyrroles **32** was reported by P. K. Panda and co-workers.[50] The macrocycle **32** exhibits strong NIR absorption at 1100 nm. owing to the induced structural rigidification and extended π conjugation In addition, a planar β,β' -phenylene-bridged hexaphyrin (1.0.1.0.1.0), 24 π–electron antiaromatic rosarian derivative was reported by J. L. Seslorad co-workers. Upon protonation with HCl proton-coupled electron transfer (PCET) takes place and formed 26π-electron aromatic triprotonated monocationic species via an intermediate-but stable-25π-electron non-aromatic triprotonated monoradical dication.[51]

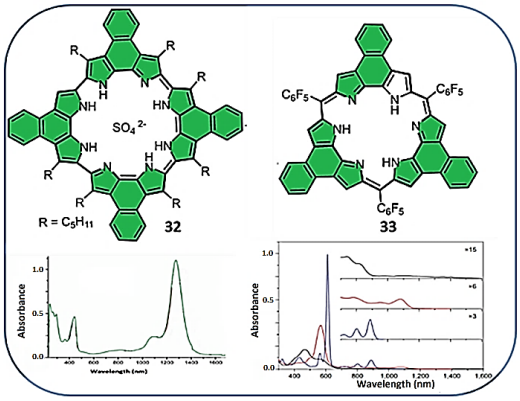

Figure 1.26. UV-vis-NIR spectra fused macrocycles **32** and **33** (black line), H_3**33**.Cl_2· (red line) and H_3**33**.Cl (blue line) in CH_2Cl_2

Shen and co-workers had reported a core-modified phenanthrene-fused pyrrole with bi-thiophene and bi-selenophene rubyrins **34** and **35**. [52] Ring fusion has led to 26π (when conjugation path is through two bi- thiophene and two pyrrole ring) and 52π (when conjugation path is through two bi-thiophene and two phenanthrene moity) electronic system. The spectroscopic and redox features of indicate that ring fusion results in the formation of a dye with the Hückel [4n+2] aromaticity of the [26] chromophore both macrocycle. The electronic absorption spectra of **34** exhibited with a Soret band at 596 nm and three Q bands at 714, 784 and 1076 nm. Rubyrin **34** has been utilised for selective detection of the Hg2+ ion in aqueous

solution Macrocycle **35** exhibited NIR absorption and used as an acidic pH-activatable targeted photosensitizer for selective NIR photodynamic therapy against cancer.

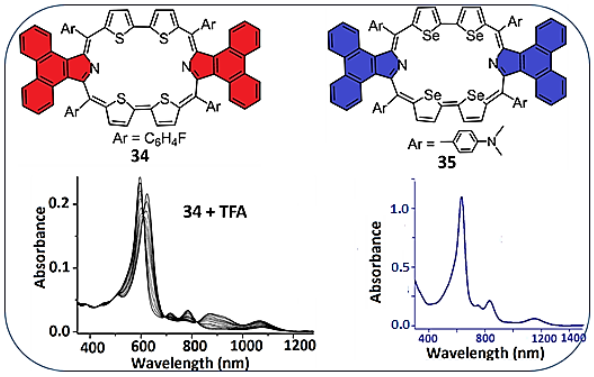

Figure 1.27 UV –vis-NIR spectra of phenanthreen fused Core modified expanded porphyrins

Dithienothiophene fused core modified expanded porphyrins **36** to **39** were reported by Chandrasekhar and co-workers. Both the macrocycles display aromatic characteristics in freebase and protonated forms and their electronic absorption exhibited NIR absorption. [56]

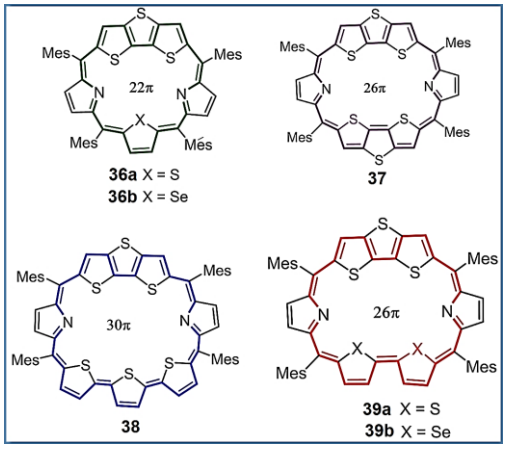

Figure 1.28. Dithienothiophene fused core modified aromaticexpanded porphyrins

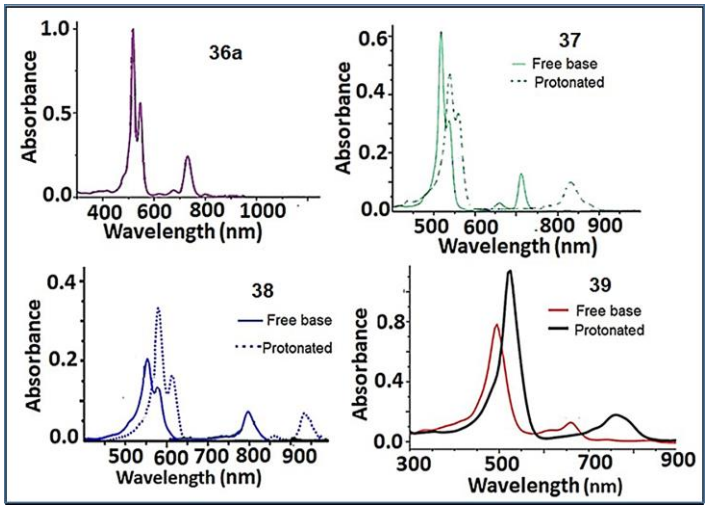

Figure 1.29. UV –vis-NIR spectra of dithienothiophene fused core modified expanded porphyrins

Our group recently reported a core-modified 22 π electron aromatic smallest fused with build-in thienothiphene phenanthrene-annulated pyrrole macrocycles **40**, and **41**. The fused macrocycle **40, 41a** and **41b** exhibited strong NIR absorption in the free base also in their protonated form.[53]

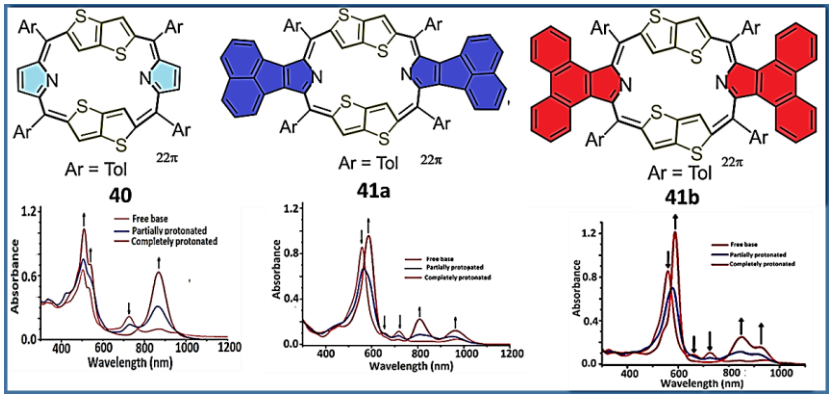

Figue.1.30. UV –vis-NIR spectrum of thieno thiophene fused macrocycles

Our group also reported thioenophene fused aromatic [30]π porphyrinoids **42a** and **42b**. (1.1.0.1.1.0) exhibiting sharp Soret band at 551 and 553 nm Q-like

bands in the range of 692–1088 nm.[54] In continuation upon increasing the number of *meso* carbon the macrocycle **43a** and **43b** become 32π electrons Hückle anti aromatic. Upon protonation, the conformation changes from Hückel anti aromatic to Möbius Aromatic and exhibiting NIR absorption.[55]

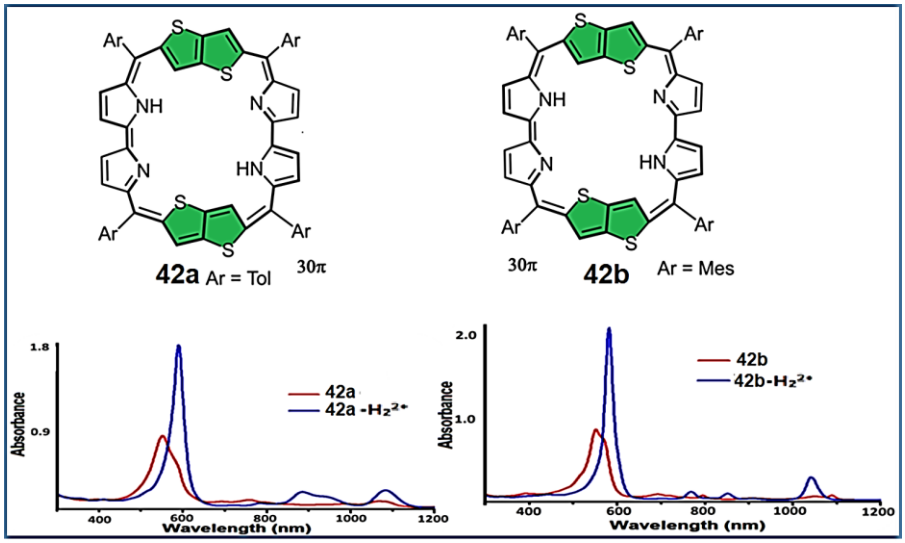

Figue.1.31. UV –vis-NIR spectrum of thieno thiophene fused macrocycles **39a** and **39b**

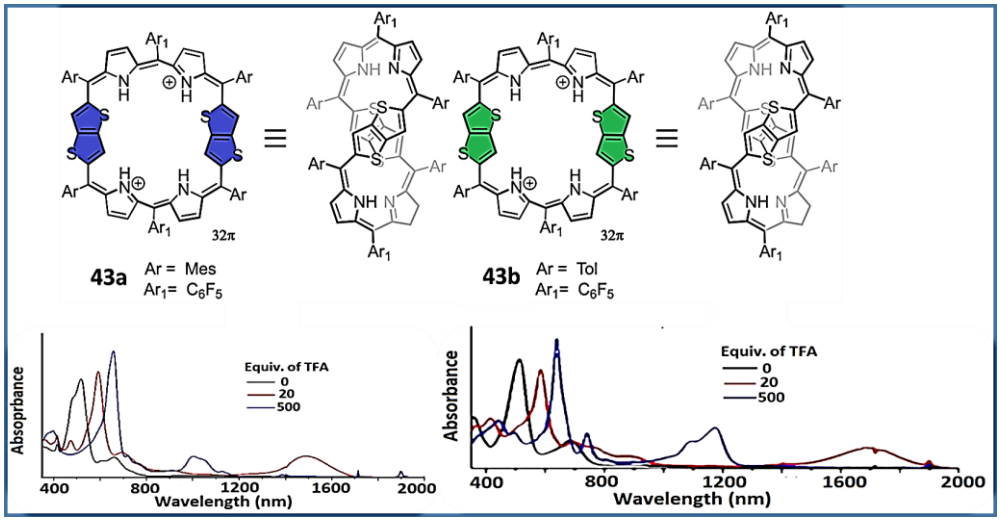

Figue.1.32. UV –vis-NIR spectrum of thieno thiophene fused macrocycles **43a** and **43b**

1.5.3. Fused Porphyrin (Fused in the core)

1.5.3.1. N-confused Porphyrin

First N-confused porphyrin was reported by Furuta and Grazynasky group independently. N-confused porphyrin is one type of carbaporphyrin where one the pyrrole unit is connected with α,β′- linkage. NCP has the same backbone structure as porphyrin (1,1,1,1) and Hückel aromatic 18 π electrons. Upon protonation, it becomes red-shifted and the Q band up to 900 nm. [57]

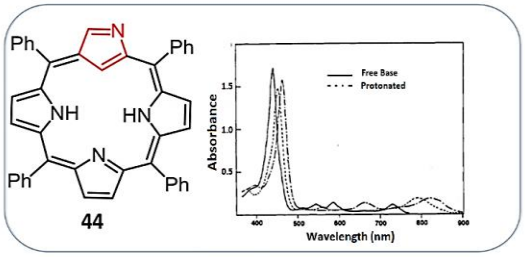

Figure 1.33. UV –vis-NIR spectra of N-confused porphyrin free base (solid) and (doted) protonated form.

Tetrakis(pentafluorophenyl)NCP can stabilize both Cu(II) and Cu(III) species. The two Cu complexes are interconvertible by oxidation and reduction. The electron-withdrawing C_6F_5 group at the *meso* position raises both the acidity of the outer NH and the oxidation potential of the π-ring system that exhibiting NIR absorption for **45b**.[58]

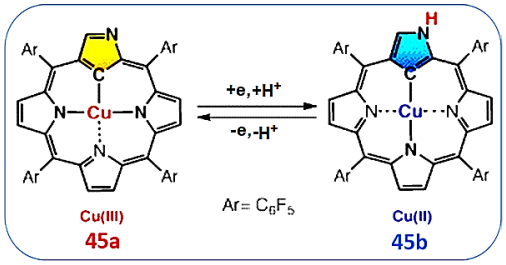

Figure 1.34. Cupper complex of N-confused porphyrin

1.5.3.2. N-Fused Porphyrin

Fusion is a relatively new concept to produce unique members of the porphyrin family. N-Fused porphyrin has an unusually narrow HOMO-LUMO energy gap and exhibits absorption in the near-infrared region up to 1100 nm.[59] The first N-fused porphyrin **47** was obtained from di-bromo-NCP via inversion of the confused pyrrole and subsequent nucleophilic substitution of the adjacent pyrrolic nitrogen. Upon fusion of the molecular flexibility reduced exhibiting red-shifted absorption in the free base as well as in protonated its form.[60]

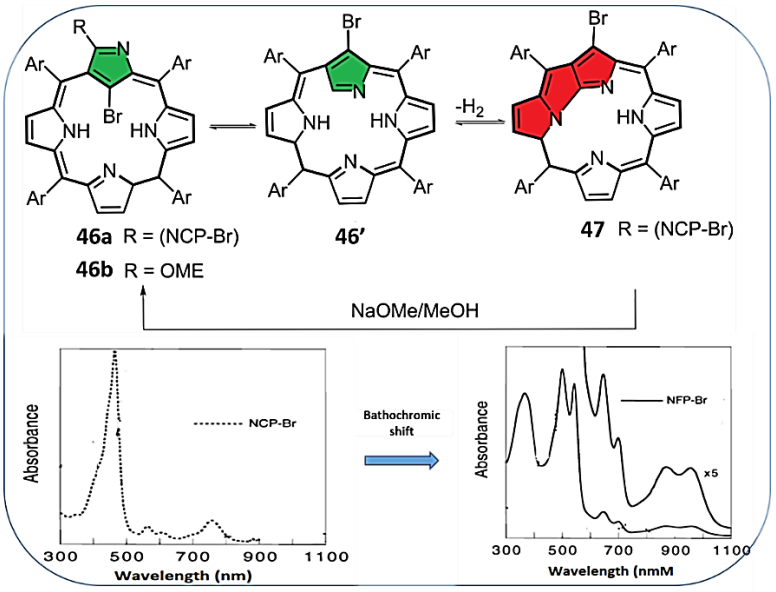

Figure 1.35. UV –vis-NIR spectra of N fused porphyrin and protonated form

Apart from the dibromo-NCP route, the NFP skeleton was synthesized by Furuta and co-workers directly by a treatment of NCP with Re_2CO_{10} that exhibited NIR absorption.[61]

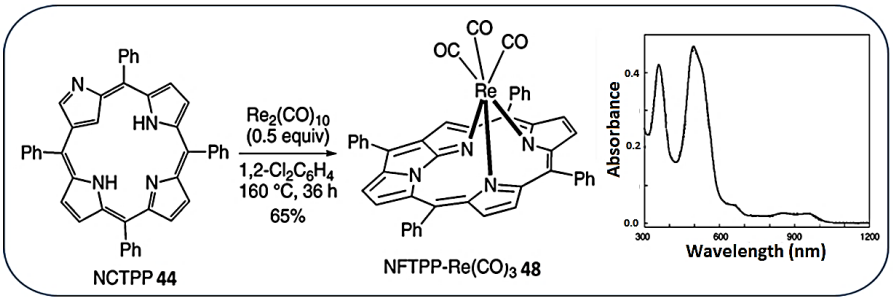

Figure 1.36. UV –vis-NIR spectra of N-fused porphyrin from N-confused porphyrin**.**

1.5.3.3. Doubly N-fused porphyrin.

In continuation doubly N-fused porphyrin **49** was reported by same group. The macrocycle has an unusually narrow HOMO-LUMO energy gap as a 18π aromatic compound and its electronic absorption is exhibited in the NIR region up to 1600 nm.[62]

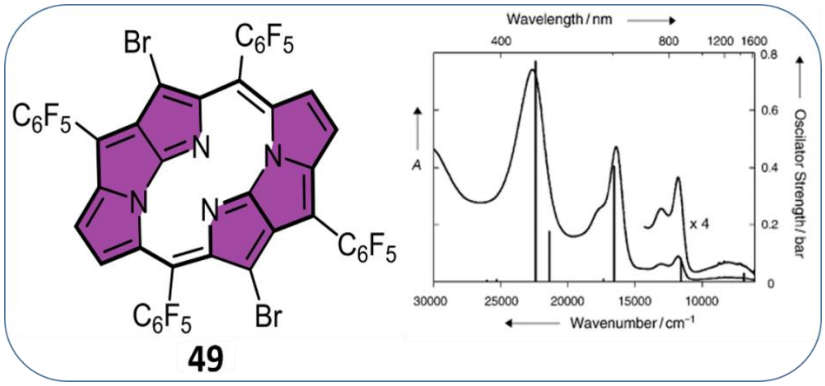

Figure 1.37. UV –vis-NIR spectra of doubly N-fused porphyrin

Also N-fused pentaphyrin (NFP5) **50a** which contains a fused tri-pentacyclic ring in the core, was reported by Furuta and co-worker exhibiting aromaticity with NIR absorption.[63]

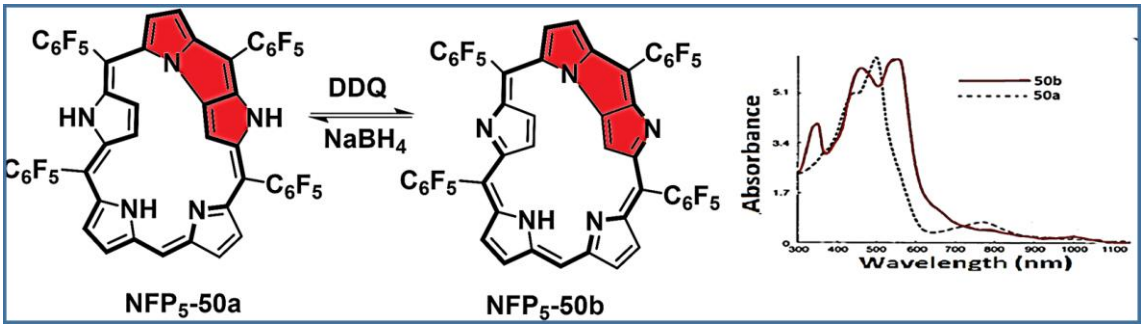

Figure 1.38. UV –vis-NIR spectra of N-fused pentaphyrin.

N-fused porphyrin serves as a versatile mononegative tridentate ligand, which can bind variety of metal centers tightly. A hybrid molecule of double-decker ferrocene-type NFTPp complex **52** was reported by Furuta and co-workers. The macrocycle exhibited NIR absorption. [64] In addition a hybrid molecule of ruthenocene and N-fused porphyrin, [Ru(NFp)Cp] **53** was reported by the same group. The molecular orbitals of [Ru(NFp)Cp] spread over the whole molecule, thereby constructing a fascinating 3D d–p system and exhibiting NIR absorption.[65]

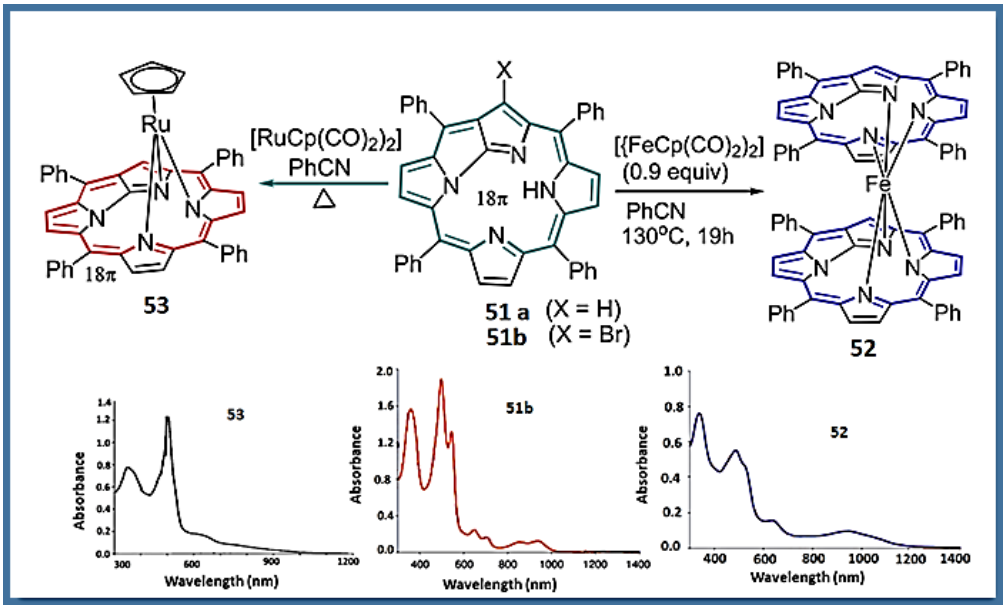

Figure 1.39. UV –vis-NIR spectra of N-fused metal complexes **52**.and **53**

1.5.4 Carbaporphyrinoids.

Carbaporphyrins are porphyrin analogs in which one or more of the pyrrolic nitrogens have been replaced by carbon atoms.[66] Azuleporphyrins are the carbaporphyrins where one of the pyrrole unit is replaced by azulene moiety. The first azuliporphyrin **54** was reported by T. D. Lash and co-workers. Spectroscopic properties reveal that these types of macrocycles show borderline porphyrin aromaticity with dipolar canonical forms **54'** making important contributions for its aromaticity. The aromaticity is further increased upon protonation.[67]

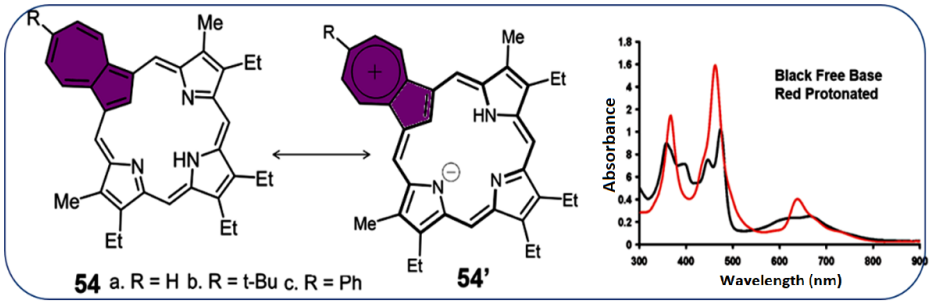

Figure 1.40. UV –vis-NIR spectra of azuliporphyrin **54**

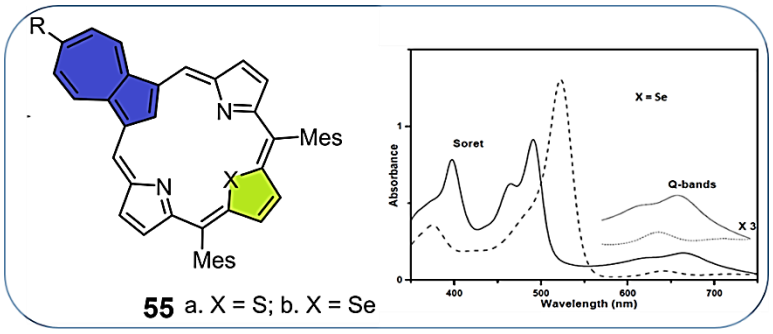

Figure 1.41. UV –vis-NIR spectra of core modified azuliporphyrins **55**

Core modified azuliporphyrins was reported by T. K Chandrasekhar **55.** The NMR spectra for **55**a-b indicated that the heteroanalogues have similar diatropic characteristics like azuliporphyrins **54**.[68]

Chapter 1

Core modified diazuliporphyrins **56a-b** were reported by L. Grazynski. and co-workers which are revealed as Near-IR redox switchable chromophore. The macrocycles are nonaromatic readily and reversibly oxidizable to its cation radical to aromatic carbaporphyrinoid dication, indicates fused tropylium rings are responsible for aromaticity. Significantly, the replacement of oxygen atom by sulfur in the case of dication yields a remarkable bathochromic shift and exhibiting the NIR band from 1148 to 1320 nm. [69]

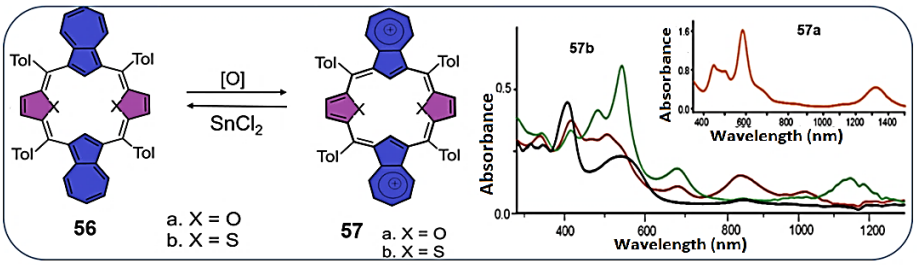

Figure 1.42. UV –vis-NIR spectra of ditropylium fused carbaporphyrin.

In continuation, our group recently reported core modified tropylium cation-fused aromatic [26]dicarbaporphyrinoids **58**$^{2+}$and **59**$^{2+}$. The ditropylium fused macrocycles exhibited NIR absorption up to 1400 nm.[70]

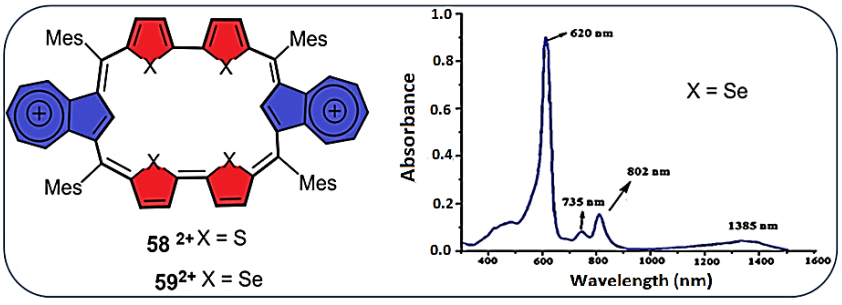

Figure 1.43. UV –vis-NIR spectrum of core modified tropylium fused expanded carbaporphyrin

Anderson et al. reported azulene-fused porphyrins **60**, **61** and **62** in the periphery of the macrocycles. The azulene fused strategy allowed the realization of

highly π-conjugated porphyrinic electronic systems. These azulene-fused porphyrins exhibited relatively broad absorption spectra in the NIR region (λ_{max} ¼ 855 nm for **60**, 1014 nm for **61**, and 1136 nm for **62**).[71]

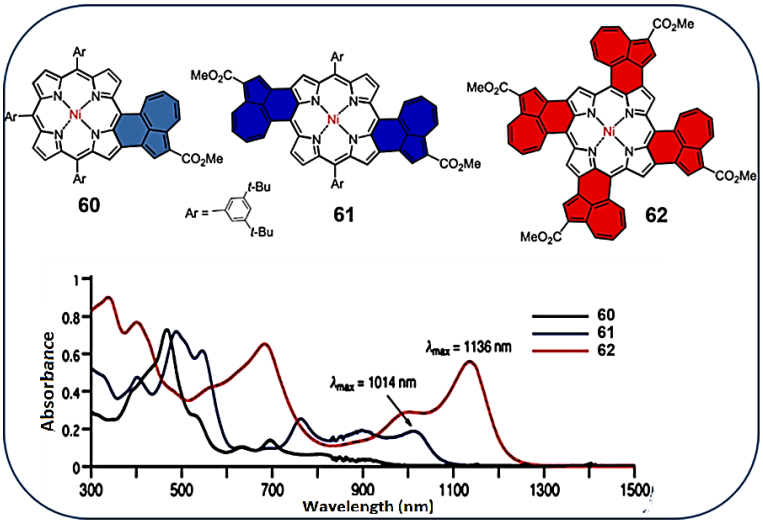

Figure 1.44. UV –vis-NIR spectroscopy of azulene fused porphyrins

The first expanded azuliporphyrinoid, **63** was reported by T. D. Lash and co-workers. The electronic absorption spectrum for this azuliporphyrin exhibited a series of bands between 420 and 511 nm and a broad absorption at 742 nm, although azulisapphyrin **63'H$_2$** $^{2+}$ exhibited a strong diamagnetic ring current. In addition, evidence for the formation of aromatic pyrrolidine adduct **64** was presented, but this species was also very unstable [72]

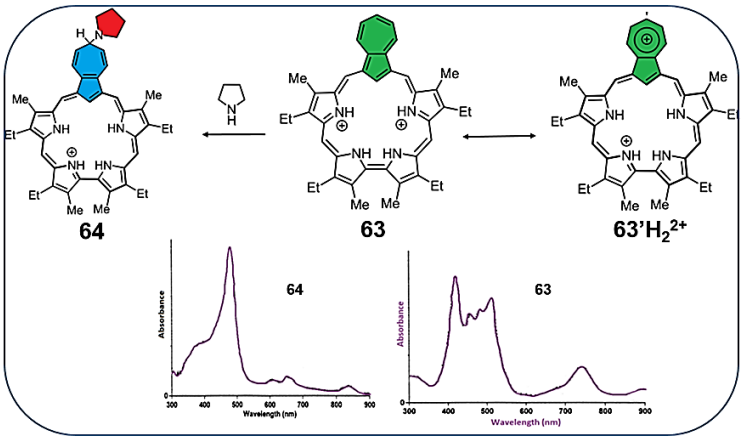

Figure 1.45. UV –vis-NIR spectra of expanded azuliporphyrinoids

1.5.5. Vinylogous Porphyrins

Tetrapyrrolic [18]porphyrins(1.1.1.1)are connected by four *meso* carbon (p =1 q= 1) (Figure 1.46.) More specifically, by inserting two carbon atoms into opposite sides of the porphyrin (p = q = 1) skeleton results in a bis-vinylogous structure, (p= 1, q = 3), which has been elongated at two of the *meso*-sites. Further expansion in this way gives rise to tetravinylogous porphyrin (p =1 q = 5) and the octavinylogous (p = q= 3) porphyrins. The diatropic behavior of the vinylogous porphyrins is greater compared to tetrapyrrolic [18] porphyrin(1.1.1.1). This is because they typically contain extended conjugation pathways in a rather rigid and planar framework. They have been found to exhibit remarkable photochemical and spectroscopic properties significantly red-shifted absorption spectra. [74] Vinylogous porphyrins are attractive as potential sensitizers for use in various light-based therapeutic applications (e.g., photodynamic therapy).[75]

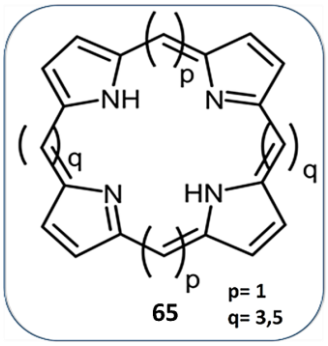

Figure 1.46. Schematic diagram of of vinylogous porphyrin

The synthesis of tetravinylogous [26] porphyrin **66a**, the alkyl- and phenylsubstituted [26] porphyrins **66b** and **66c** respectively and a [26] azaporphyrin **67** were reported by Franck and co-worker. [76] The 1H NMR spectrum of **66a** as arene, shows significant diatropic ring current effects with the maximum difference between the δ values of the inner and outer protons being Δδ = 24.1 ppm. The diatropicity of these derivatives decreases from **66a** via **66b** to the aza

derivative **67**. The UV/VIS absorption spectra of the bisprotonated forms of the new [26] porphyrins, measured in $CHCl_3$/TFA are very similar with the Soret band absorption at 512 nm (**66a**), 520 nm (**66b**), 525 nm (**66c**) and 503 nm (**67**), while the corresponding Q-band absorptions were at 694, 711, 710 and 735 nm respectively.

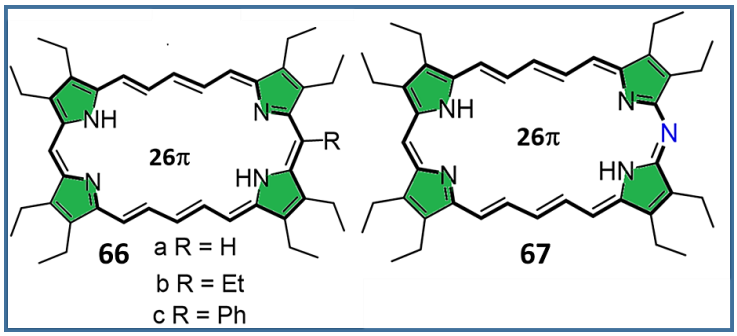

Figure 1.47. Tetravinylogous porphyrins

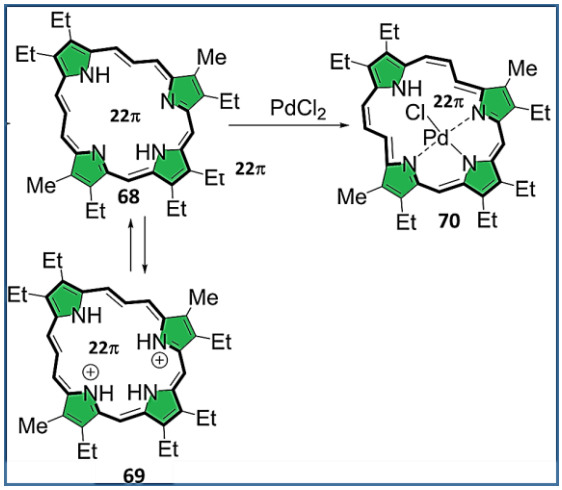

Figure 1.48. Vinylogous [22]porphyrin **68** and its Pd- complex

A new type of vinylogous [22]porphyrin-(3.1.1.3)**68** synthesized by Lash and co-worker.[77,] its dication **69** and palladium(II) complex**70** while retaining highly diatropic characteristics exhibited NIR absorption.

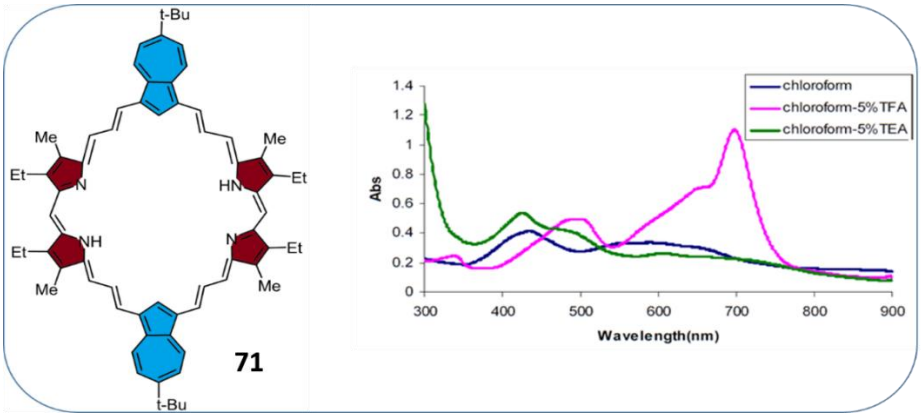

Figure 1.49, Azulene incorporated expanded vinylogous carbaporphyrin

Azulene incorporated expanded vinylogous carbaporphyrin **71** was reported by Lash and co-worker is nonaromatic in nature. Addition of TFA led to C-protonation to form a tetracationic species and exhibits strong band at 698 nm and weaker absorptions at 339 and 499 nm.[78]

1.6. Bridge Porphyrinsoids:

The chemistry of expanded porphyrins is interesting topic because of their unique properties. One of the most interesting properties is the model of aromaticity. Expanded porphyrins such as sapphyrins, rubyrins, and hexaphyrins exhibits aromaticity. However due to structural distortion expanded prphyrins do not stay in molecular plan results lost their aromaticity. Introducing spacer linkers such as phenylene, thiophene, pyrrole, dithienothiophene, azulene inside the macrocycle have been challanging to scientist as spacer group devide the macrocycle known as bridge porphyrinoids. The conjugation path can go through either the spacer or through the periphery of a macrocycle. For this reason, it is possible to have dual-potential electronic properties and two aromatic pathways that operate independently, which we term as 'dual aromaticity'. The first phenylene bridge porphyrinoids was reported by Osuka and co-worker. T. K Chandrasekher and co-workers reported dithienothiophene bridge porphyrinoids that exhibits baird type

aromaticity in the triplet state. All types of literature known as bridge porphyrinoids are discussed in chapter **5**.

1.7. Scope of the thesis

The design and synthesis of such molecules which exhibits adoptive aromaticity with NIR absorption is challenging due to their potential application in chemistry and biology. Aromatic compounds having absorptions and emissions in the red or near-infrared (NIR) region are capable materials for a broad range of applications such as photodynamic therapy dyes, semiconductors in light-emitting diodes, photo-sensitizers in solar cells and microscopic imaging agents. Porphyrins are biologically active 18 π aromatic ligands. Compare to porphyrin, carbaporphyrins are highly aromatic and exhibits red-shifted absorption. The aim of the thesis is to design and synthesized of new NIR absorptive aromatic carbaporphyriods. In chapter 3, I have synthesized core modified 18π doubly N-confused porphyrins, which exhibiting aromaticity with NIR absorption. In chapter 4 I have synthesized 26 π core modified vinylogous azulisapphyrin, which exhibiting adoptive aromatic with NIR absorption. In Chapter 5 I have synthesized core modified azulene bridge porphyrinoid, which exhibiting adoptive aromaticity with NIR absorption.

1.8. References

1. (a) H. Nakazumi and M. Matsuoka., *Chem. Rev.,* 1992, **92**, 1197-1226; (b) C. Jiao and J. Wu, *Curr. Org. Chem.,* 2010, **14**, 2145-2168; (c) Z. Sun, J. Wu, *Aust. J. Chem.,* 2011, **64**, 519-528; (d) A. Muranaka, M. Yonehara and M. Uchiyama, *J. Am. Chem. Soc.* 2010, **132**, 7844-784; (e) G. M. Fischer, E. Daltrozzo and A. Zumbusch, *Angew. Chem. Int. Ed.,* 2011, **50**, 1406-1409 (f) G. Kubheka J.Mack, T. Nyokong and Z. Shen, *Molecules,* 2020, **25**, 3689 (1-14); (g) D. Zhang, *Int. J. Nanomedicine,* 2021, **16**, 4901–4911. (h) P. Liu, X. Mu, X. D. Zhang and D. Ming, *Bioconjugate Chem*. 2020, **31**,260-275.
2. (a) Y. Wang and X. P. Yan, *Chem. Commun*., 2013, **49**, 3324–3326;(b) Y. Ma, Y. Zhang and W. W. Yu, *J. Mater. Chem. C*, 2019, **7**, 13662—13679.
3. N. Venkatachalam, Y. Saito, and K. Soga, *J Am Ceram Soc* ,2009,**92**, 1006–1010.
4. M. Wainwright, *Color. Technol.,* **2010**, *126*, 115–126.
5. M. Pawlicki, H. A. Collins, R. G. Denning and H. L. Anderson, *Angew. Chem., Int. Ed.,* 2009, **48**, 3244–3266.
6. G. Qian, Z. Zhong, M. Luo, D. Yu, Z. Zhang, Z. Y. Wang and D. Ma, *Adv. Mater*., 2009, **21**, 111–116.
7. P. A. Bouit, D. Rauh, S. Neugenbauer, J. L. Delgado, E. D. Piazza, S. Rigaut, O. Maury, C. Andraud, V. Dyakonov and N. Martin, *Org. Lett*., 2009, **24**, 4806–4809.
8. D Dahal, L McDonald, S Pokhrel, S Paruchuri and M Konopka Y. Pang *Chem. Commun.*, 2019,**55**, 13223-13226.
9. N. Ishikawa and Y. Kaiz, *J. Porphyrins Phthalocyanines*, 1999, **3**, 514–524.
10. H. Lee, J. C. Mason and S. Achilefu, *J. Org. Chem*., 2006, **71**, 7862–7865.
11. A. Loudet and K. Burgess, Chem. Rev., 2007, **107,** 4891–4932.
12. (a) A. Mishra, R. K. Behera, P. K. Behera, B. K. Mishra and G. B. Behera, *Chem. Rev*., 2000, **100**, 1973– 2011; (b) A. Samanta, M. Vendrell, R. Das and Y. T. Chang, *Chem. Commun*., 2010, **46**, 7406–7408; (c) D. P. Pantoja, R. Donoso, L. Agulló, M Córdova, M Seeger, D. H. Pieper and B. González, *Environmental Microbiology* , 2012, **14**. 1091-1117.

13. (a) H. Xiang, J Cheng, X. Ma, X. Zhou and J. J. Chruma, *Chem. Soc. Rev.,* 2013, **42**, 6128-6185; (b) F Ding, Y. Zhan, X. Lu and Y. Sun, *Chem Sci*., 2018, **9**, 4370-4380.
14. H. Jia, J. Ding, A. Hauser, S. Decurtins S. X Liu, *Asian J. Org. Chem.,* 2014, **3**, 198 – 202.
15. G. Brocks, A. Tol, *J. Phys. Chem.* 1996, **100**, 1838 –1846.
16. Q. Zhang, X. Liu, F.Jiao, S. Braun,M Javad J, X. Crispin, T. Ederth and M. Fahlman, *J. Mater. Chem. C*, 2017,**5**, 275-281.
17. Q. Gang and W Z Yuan, *Chem. Asian J*. 2010, **5**, 1006 – 1029.
18.. A. Aouchiche, S. Djennane and A. Boucekkine, *Synth. Met*., 2004, **140**, 127 –133.
19. Y. Yamashita, K. Ono, M. Tomura and S. Tanaka, *Tetrahedron* 1997, **53**, 10169 – 10178.
20. T. M. Krygowski and M. K. Cyrański, *Chem. Rev.,* 2001**, 101***,* 1385-1419.
21. P. v. R. Schleyer, C. Maerker, A. Dransfeld, H. Jiao and N. J. R. van Eikema Hommes, *J.Am. Chem. Soc.,* 1996, **118**, 6317-6318
22. D. Geuenich, K. Hess, F. Köhler and R. Herges, *Chemical reviews* 2005, **105**, 3758-3772.
23. T. M. Krygowski and M. K. Cyrański, *Chem. Rev.,* 2001**, 101***,* 1385-1419.
24. L. M. Tolbert, *Acc. Chem. Res*.,1992, **25**, 561 –568.
25. R. C. Fortenberry, C. M. Novak, T. J. Lee, P. P. Bera and J. E. Rice, *ACS Omega,* 2018, **3**,16035−16039.
26. J. Mack, *Chem. Rev.,* 2017, **117**, 3444−3478.
27. T. K. Chandrashekar, and S. Venkatraman*, Acc. Chem. Res.*,2003, **36**, 9, 676–691.
28 A. Jasat and D.Dolphin, *Chem. Rev.*,1997, **97**, 2267–2340.
29. E.D. Sternberg, D. Dolphin, C. Brückner, *Tetrahedron*, 1998, **54**, 4151-4202 and references therein; (b) R. K. Pandey and G. Zheng, Porphyrins as Photosensitizers in Photodynamic Therapy In The Porphyrin Handbook, Kadish, K. M.; Smith, K. M.; Guilard, R. Eds.; Academic Press: New York, 2000, Vol. **6**, pp. 55-124. (c) R. Bonnett, *Chem. Soc. Rev*., 1995, **24**, 19-33.
30. N. Tsolekile S. Nelana and O. S. Oluwafemi, *Molecules* ,2019, **24**, 2669-2684.

31. D. Howard, S. Sebastian, Q. V.C. Le, B. Thierry and I. Kempson *Int. J. Mol. Sci.,* 2020, **21**, 579-602.
32. K. S. Suslick, C.T. Chen, G. R. Meredith and L.T. Cheng, *J. Am. Chem. Soc.*, 1992, **114**, 6928–6930.
33. T. Higashino, H. Nakatsuji, R. Fukuda, H. Okamoto, H. Imai; M. Hassid, T. Murakami and H. Imahori, *ChemBioChem.,* 2017, **18**, 951 – 959.
34. (a) J. Sankar, S. Mori, S. Saito, H. Rath, M. Suzuki, Y. Inokuma, H. Shinokubo, K. S. Kim, Z. S. Yoon, J. Y. Shin, J. M. Lim, Y. Matsuzaki, O. Matsushita, A. Muranaka, N. Kobayashi, D. Kim, and A. Osuka *J Am Chem, Soc*., 2008, **130**, 13568–13579; (b) M. Alonso, P. Geerlings, and F. D. Proft *Chem. Eur. J.,* 2013, **19**, 1617 – 1628.
35. T. Tanaka, T. Sugita, S. Tokuji, S. Saito and A. Osuka *Angew Chem Int Ed*, 2010, **49**, 9488-9491.
36. A. Srinivasan, V. G. Anand, S. J. Narayanan, S. K. Pushpan, M. R. Kumar and T. K. Chandrashekar *J. Org. Chem*, 1999, **64**, 8693-8697.
37. S. K. Pushpan, A. Srinivasan, V. G. Anand, S. Venkatraman, T. K. Chandrashekar, B. S. Joshi, R. Roy and H. Furuta, *J. Am. Chem. Soc.,* 2001, **123**, 5138-5139.
38. K. S, Kim , ZS, Yoon, A B, Ricks , JY, Shin, S, Mori, J, Sankar, S, Saito , YM, Jung, MR, Wasielewski, A, Suka and D, Kim, *J. Phys. Chem. A,* 2009, **113**, 4498–4506.
39. (a) J. Y. Shin, J. M. Lim, Z. S. Yoon, K. S. Kim, M. C. Yoon, S. Hiroto, H. Shinokubo, S. Shimizu, A. Osuka and D. Kim, J. *Phys. Chem. B,* 2009*,* **113***,* 5794–5802*;* (b) K. Naoda, H. Mori, J. Oh, K. H. Park, D. Kim, and A. Osuka, *J. Org. Chem.* 2015, **80**, 11726–11733.
40. W. Y. Cha, T. Yoneda, S Lee, J. M. Lim, A. Osuka and D. Kim, *Chem. Commun.*, 2014, **50**, 548-550.
41. (a) J. L. Sessler and R. A. Miller, *Biochem. Pharmacol.* 2000, **59**, 733–739; (b) S. W. Young, F. Qing, A. Harriman, J. L. Sessler, W. C. Dow, T. D. Mody, G. W. Hemmi, Y. P. Hao, R. A. Miller, *Proc. Natl. Acad. Sci. U.S.A.* 1996, **93**, 6610–6615; (c) W. A. Reiter, A. Gerges, S. Lee, T. Deffo, T. Clifford, A. Danby, K. Bowman-James, *Coord.*

Chem. Rev. 1998, **174**, 343–359; (d) S.Mori and A. Osuka, *J. Am. Chem. Soc.,* 2005, **127**, 8030-8031.

42. A. Tsuda and A. Osuka, *Science,*2001. **293**, 79–82.
43. (a) A. Tsuda, A. Nakano, H. Furuta, H. Yamochi and A. Osuka, *Angew.Chem., Int. Ed.,* 2000, **39**, 558-561; (b) A. Tsuda, H. Furuta and A. Osuka, *Angew. Chem., Int. Ed.,* 2000, **39**, 2549-2552; (c)A. Tsuda, H. Furuta and A. Osuka, *J. Am. Chem. Soc.,* 2001, **123**, 10304-10321.
44. T. Tanaka, N. Aratani, J. M. Lim, K. S. Kim, D. Kim and A. Osuka, *Chem. Sci*., 2011, **2**, 1414–1418.
45. Y. Saegusa, T. Ishizuka, K. Komamura, S. Shimizu, H. Kotani, N. Kobayashi and T. Kojim, Phys. *Chem. Chem. Phys.,* 2015, **17**, 15001-15011.
46. (a) T. D. Lash and D. T. Richter, *J. Am. Chem. Soc.,* 1998, **120**, 9965-9966; (b) D. T. Richter and T. D. Lash, Tetrahedron *Lett*., 1999, **40**, 6735–6738; (c) D. T. Richter and T. D. Lash, *J.Org. Chem.,* 2004, **69**, 8842-8850.
47. P. K Panda, Y. J. Kang and C.-H. Lee, *Angew. Chem., Int. Ed.,* 2005, **44**, 4053–4055.
48. D. G. Cho, P. Plitt, S. K. Kim, V. Lynch, S. J. Hong, C.-H. Lee and J. L. Sessler, *J. Am. Chem. Soc.,* 2008, **130**, 10502–10503
49. S. Y. Kee, J. M. Lim, S. J Kim, J. Yoo, J. S. Park, T. Sarma, V. M. Lynch, P. K. Panda, J. L. Sessler, D. Kim and C.-H. Lee, *Chem. Commun.,* 2011, **47**, 6813–6815.
50. T. Sarma and P. K. Panda, *Chem. - A Eur. J.*, 2011, **17**, 13987–13991.
51. M. Ishida, S. J. Kim, C. Preihs, K. Ohkubo, J. M. Lim, B. S. Lee, J. S. Park, V. M. Lynch, V. V. Roznyatovskiy, T. Sarma, P. K. Panda, C. H. Lee, S. Fukuzumi, D. Kim and J. L. Sessler, *Nat. Chem.*, 2013, **5**, 15–20.
52. (a). D. Wu, A. B. Descalzo, F. Weik, F. Emmerling, Z. Shen, X. Z. You and K. Rurack, *Angew. Chem. Int. Ed.*, 2008, **47**, 193–197; (b). J.Tian L. Ding, H. J. Xu, Z. Shen, H. Ju, L. Jia, L. Bao and J. S. Yu, *J. Am. Chem. Soc*., 2013, **135**, 18850–18858.
53 (a) T. K. Chandrashekar, V. Prabhuraja, S. Gokulnath, R. Sabarinathana and A. Srinivasan, *Chem. Commun.,* 2010, **46**, 5915–5917; (b) G. Karthik, A. Srinivasan and T. K. Chandrashekar, *Org. Lett.,* 2014, **16**, 3472–3475; (c) G. Karthik, J. M. Lim,

A. Srinivasan, C. H. Suresh, D. Kim and T K. Chandrashekar, *Chem. Eur. J.,* 2013, **19**, 17011–17020; (d) G. Karthik, A. Srinivasan, C. H. Suresh and T. K. Chandrashekar
Chem. Commun., 2014, **50**, 12127−12130; (e) A. Ghosh, A. Chaudhary, A. Srinivasan, C. H. Suresh and T. K. Chandrashekar, *Chem. Eur. J*., 2016, **22**, 3942−3946; (f) A. Ghosh, A. Srinivasan, C. H. Suresh, and T. K. Chandrashekar, *Chem. Eur. J*., 2016, **22**, 11152−11155; (g)S. Dash, A. Ghosh and T. K. Chandrashekar, *J. Porphyrins Phthalocyanines* 2019; **23**: 2-7

54. H. Rath, A. Mallick. T. Ghosha and A. Kalita, *Chem. Commun.,* 2014, **50**, 9094-9096.

55. A. Mallick, J. Oh, D. Kim and H. Rath, *Chem. Eur. J.,* 2016, **22**, 8026-8031.

56.. *A.* Mallick, J. Oh, M. A. Majewski, M. Stępien,´ D. Kim and H. Rath, *J. Org. Chem* 2017, **82**, 556−566.

57.(a) H. Furuta, T. Asano and T. Ogawa*. J. Am. Chem. Soc*., 1994, **116**, 767-768;(b) P. J. Chmielewski, L. Latos-Grażyński, L. Rachlewicz and T. Głowiak, *Angew. Chem., Int. Ed. Engl.* 1994*,* **33**, 777-779

58. H. Maeda, Y. Ishikawa, T. Matsuda, A. Osuka and H. Furuta *J. Am. Chem. Soc.* 2003, **125**, 11822-11823.

59. M. Toganoh and H. Furuta, Chem. *Lett.* 2019, **48**, 615–622.

60. H. Furuta, T. Ishizuka, A.Osuka and T. Ogawa, *J. Am. Chem. Soc.*, 1999, **121**, 2945–2946.

61. M. Toganoh, T. Ishizukaa and H. Furuta, *Chem. Commun*., 2004, 2464–2465.

62. M. Toganoh, T. Kimura, H. Uno and H. Furuta, *Angew. Chem. Int. Ed.,* 2008, **47**, 8913 –8916

63. H. Furuta and A. Osuka, *Angew. Chem. Int. Ed.,* 2001, **40**, 619-621.

64. M. Toganoh, A. Sato and H. Furuta, *Angew. Chem., Int. Ed.,* 2011, **50**, 2752-2755.

65. M. Toganoh, H. Matsuo, A. Sato and H. Furuta, *Chem. Eur. J.,* 2016, **22**, 8316-8322.

66. T. D. Lash, *Eur. J. Org. Chem.*, 2007, **2007**, 5461−5481.

67. T. D. Lash and S. T. Chaney, *Angew.Chem. Int. Ed. Engl.,*1997, **36**, 839-840.

68. S. Venkatraman, V. G. Anand, V. PrabhuRaja, H. Rath, . Sankar, T. K. Chandrasekar W. Teng and K. R. Senge, *Chem. Commun.,* 2002, **38**, 1660−1661.

69. (a) N. Sprutta and M. Świderska, *J. Am. Chem. Soc*, 2005, **127**, 13108-13109; (b) N. Sprutta, M. Siczek , L. L. Grażyński, M. Pawlicki, L. Szterenberg and T.Lis, *J. Org. Chem.* 2007, **72**, 9501-9509.
70. K. C. Sahoo**,** M. Sangeetha**,** D. Usharani and H. Rath, *J. Porphyrins Phthalocyanines* 2019; **23**: 1–10.
71. K. Kurotobi, K. S. Kim, S. B. Noh, D. Kim and A. Osuka, *Angew. Chem., Int. Ed*., 2006, **45**, 3944-3947.
72. D. T. Richter and T. D. Lash, *J. Org. Chem.,* 2004, **69**, 8842–8850.
73. M. J. Białek and L. L. Grażyński, *Chem. Commun.,* 2018, **54**, 1837-1840.
74. G. Qian, Z. Zhong, M. Luo, D. Yu, Z. Zhang, Z. Y. Wang and D. Ma, *Adv. Mater*., 2009, **21**, 111–116
75. S. Beckmann, T. Wessel, B. Franck, W. Hönle, H. Borrmann and H.-G. von Schnering, *Angew.Chem., Int. Ed. Engl.,*1990, **29**, 1395-1397.
76. C. Eickmeier and B. Franck, *Angew. Chem. Int. Ed. Engl.,*1997, **36**, 2213-2215
77. L. Xu ,G. M. Ferrence and T. D. Lash, *Org. Lett.,*2006, **22**, 5113–5116
78. Z. Zhang ,G. M. Ferrence and T. D. Lash,*Org. Lett*., 2009, **11**, 1249– 1252.

General Experimental Methods and Techniques

Chapter 2

2.1. Introduction

This chapter deals with the chemicals used for synthesis and the synthetic methods employed to obtain appropriate precursors for macrocycles described in **Chapters 3**, **4** and **5**. Instruments utilized for the characterization of the macrocyclic compounds are also described briefly.

2.2. Chemicals for Syntheses

Pyrrole and *N*-methyl pyrrole were procured from Sigma Aldrich chemicals USA, was distilled before use. Deuterated solvents (chloroform-*d,* dichloromethane-d_2, acetonitrile-d_3, water-d_2 and dimethyl formamide-d_6) for NMR measurements were used as received. Benzoyl chloride, 4-fluorobenzoyl chloride, 2,6-difluobenzoyl chloride, 2,3,4,5,6-pentafluorobenzoyl chloride, anhydrous aluminium chloride, lithium aluminium hydride, *N,N′*-dimethylformamide, copper acetate, palladium chloride, zinc acetate, nickel acetate, trifluoroacetic acid (TFA), and *p*-touluenesulphuric acid were procured from Sigma-aldrich and Merck Pvt. Ltd. Anhydrous ammonium chloride, sodium chloride, sodium bicarbonate, sodium sulphate and calcium chloride were obtained from Merck chemicals, Germany. THF, DMF, DMSO, acetone, CH_2Cl_2, $CHCl_3$, $C_2H_4Cl_2$ and CH_3CN were distilled, dried and deoxygenated *via* usual procedure before use. Air sensitive materials and stock solutions were handled and prepared in glove box. Other reactions were carried out under argon atmosphere and a work-up procedure was done at ambient conditions. Aluminum oxide (basic and neutral), silica gel (100-200 mesh), silica gel for PTLC were purchased from Merck chemicals, India.

2.3. Physico-chemical techniques

Instruments used for the characterization and evaluation of spectroscopic data are discussed below. Electronic absorption spectra were measured with a PerkinElmer Lambda 950 UV-vis-NIR spectrophotometer with a quartz cuvette of

path length 1cm. ^{1}H NMR, ^{13}C and 2D NMR spectra were recorded on a Bruker AV 300 MHz, 400 MHz and 500 MHz spectrometer and chemical shifts were reported as the delta scale in ppm relative to $CHCl_3$ (δ = 7.26 ppm), CH_2Cl_2 (δ = 5.32 ppm), DMSO-d_6 (δ = 2.50 ppm) and CH_3CN (δ = 1.94 ppm) as internal reference for ^{1}H NMR. MALDI-TOF MS data were recorded using Bruker Daltonics flex Analyser and ESI HR-MS data were recorded using Waters QTOF Micro YA263 spectrometer. Cyclic voltammetric studies were carried out on Bioanalytical Systems EC epsilon. A three-electrode system consisting of a Platinum (Pt) working electrode, a commercially available saturated Ag/AgCl electrode, reference electrode and a Pt mesh counter electrode were used. The reference electrode was separated from the bulk of solution by a fritted glass bridge filled with the solvent/supporting electrolyte mixture. Half wave potentials were measured as the average of anodic and cathodic peak potentials.

2.4. Theoretical Calculation:

Quantum mechanical calculations were carried out for macrocycles reported in **Chapter 3** with Gaussian 09 program suite.[3] Geometry optimizations were performed by density functional theory (DFT) and a time-dependent (TD)-DFT method, respectively, with B3LYP, employing a basis set consisting of 6-31g** for all atoms. The X-ray crystallographic structures were used as initial geometries for geometry optimization. The nucleus-independent chemical shift (NICS)[4] values also were obtained with the gauge including atomic orbital (GIAO) method. For the anisotropy of the induced current density (ACID)[5] calculation, we employed the continuous set of gauge transformation (CSGT) method.

Theoretical calculations of free base conformers and reduced congeners in **Chapter 3** were optimized using density functional theory (DFT) with Becke's three-parameter hybrid exchange functional and the Lee-Yang-Parr correlation functional (B3LYP)[6] and 6-31G(d,p) basis set [7] for all the atoms (B1). Nature of these

optimized geometries as a local minima were confirmed by harmonic vibrational frequency calculations at the same level of theory.

2.5. Synthesis of Precursor Compounds

2.5.1. Synthetic Scheme

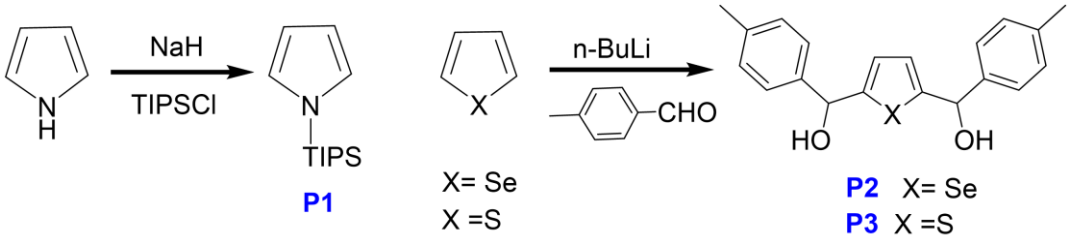

Scheme 2.1

2.5.1.1. Synthesis and characterization

1-(triisopropylsilyl)-1H-Pyrrole (**P1**). To a suspension of sodium hydride (60% dispersion in oil, 1.520 g, 31.68 mmol) in tetrahydrofuran (50 mL) was slowly added pyrrole (1.934 g, 28.8 mmol) at 0°C. The mixture was stirred at the same temperature for 1.5 hours. To the mixture was slowly added triisopropylsilyl chloride (5.552 g, 28.8 mmol) at 0°C. The resulting mixture was stirred at the same temperature for another 1.5hours. To the reaction mixture was added ice-water. It was extracted with diethyl ether. The extract was washed with water, dried over anhydrous sodium sulfate, and concentrated under reduced pressure to give of 1-(triisoppropylsilyl) pyrrole as yellow oil. Rf 0.8 (Hexane). Yield: 6.3 g (99%).

^{1}H NMR (500 MHz, $CDCl_3$, 300K, δ [ppm]): 6.80 (t, 2H); 6.32 (t, 2H); 1.10 (d, Methyl); 1.47 (septet, methine CH). **^{13}C NMR (125 MHz, $CDCl_3$, 300K, δ [ppm]):** 11.73; 17.81; 110.034; 124.01. HR-ESI-TOF MS (m/z): 224.21[M+ H] $^{+}$(223.11 calc. for $[C_{13}H_{25}NSi]^{+}$).

2, 5 -Bis(p-tolylhydroxymethyl) selenophene (**P2**).To a solution of selenophene (1 g, 7.6 mmol) in 45 mL of n-hexane containingN,N',N,N- tetramethylenediamine (2.87 mL, 19.08 mmol) under argon atmosphere, n-butyl lithium (12.7 mL,19.08 mmol) was added slowly and was stirred at room temperature for two hours and later refluxed for two hours.Thereaction was then allowed to attain room temperature. *p*-Tolylaldehyde (2.24 mL, 19.08 mmol) was dissolved in 25 mL oftetrahydrofuran (THF) and was added drop wise to the reaction mixture in ice-cold condition. After the addition, the reaction mixture was allowed to attain the room temperature and was stirred for an additional two hours. The reaction was quenched with saturated ammonium chloride solution and was stirred for half an hour. This was then extracted with ether or ethyl acetate (100 mL). The organic layers were combined and was washed with brine and dried over anhydrous sodium sulphate. The crude product obtained on evaporation of the solvent was recrystallized from toluene. The solid obtained was identified as **P2**.Yield: 1.6 g (57%).

^{1}H NMR (400 MHz, $CDCl_3$, 300 K, δ [ppm]): 2.34 (s, 3H); 5.89 (s, 1H); 6.84 (s, 1H); 7.15 (d, 1H, J= 10.4 Hz); 7.30 (d, 1H, J = 10.8 Hz); **^{13}C {^{1}H} NMR (100 MHz, $CDCl_3$, 300 K, δ [ppm])**: 21.29; 74.32; 126.20; 126.31; 129.36; 137.87; 140.62; 155.95. HR-ESI-TOF MS (m/z): 395.16 $[M^{+}Na]^{+}$(372.06. calc. for $[C_{20}H_{20}O_2Se]^{+}$).

2, 5–Bis(p-tolylhydroxymethyl) thiophene(**P3**): Thiophene (1.9 mL, 23.7 mmol), N, N, N′, N′ tetramethylenediamine (9 mL,59.42 mmol) in dry n-hexane (40 mL), n-butyl lithium (38 mL, 59.42 mmol) and *p*-Tolylaldehyde (7.0 mL, 59.42 mmol) in 20mL THF under similar reaction conditions as mentioned above gave diol**10**. Yield: 4.5g (59%).

^{1}H NMR (400 MHz, $CDCl_3$, 300 K, δ [ppm]): 2.347(s, 3H); 5.8 (s, 1H); 6.67 (d, 1H, J= 3.2 Hz); 7.15(d, 1H, J= 8 Hz); 7.29(d, 1H, J= 10 Hz). **^{13}C NMR (100 MHz, $CDCl_3$, 300 K, δ [ppm]**): 21.11; 72.35; 124.18; 126.18; 129.14; 137.66; 139.99; 148.21. HR-ESI-TOF MS (m/z): 347.23 $[M+Na]^{+}$(324.12 calc. for $[C_{20}H_{20}O_2S]^{+}$).

2.5.1.2. Mass spectra:

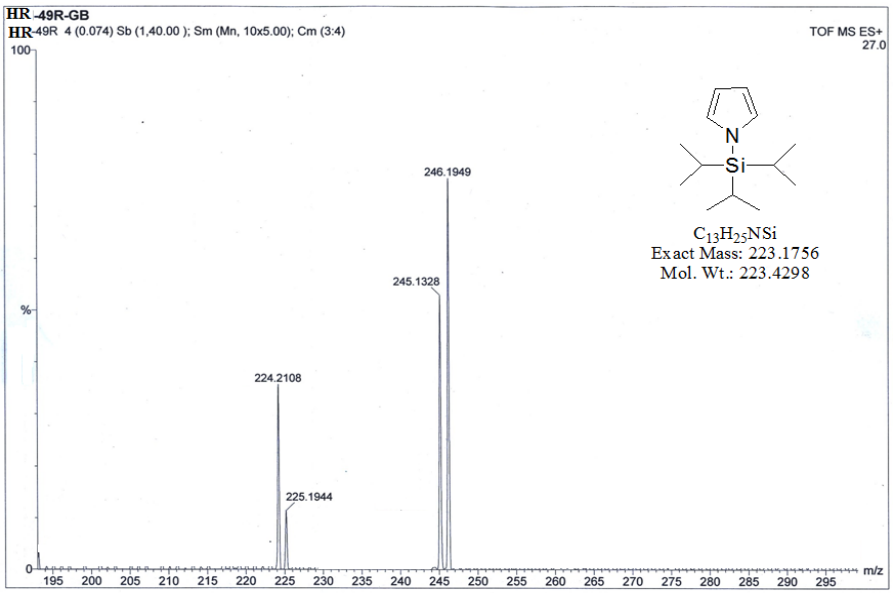

Figure 2.1. MS Spectra of **P1**

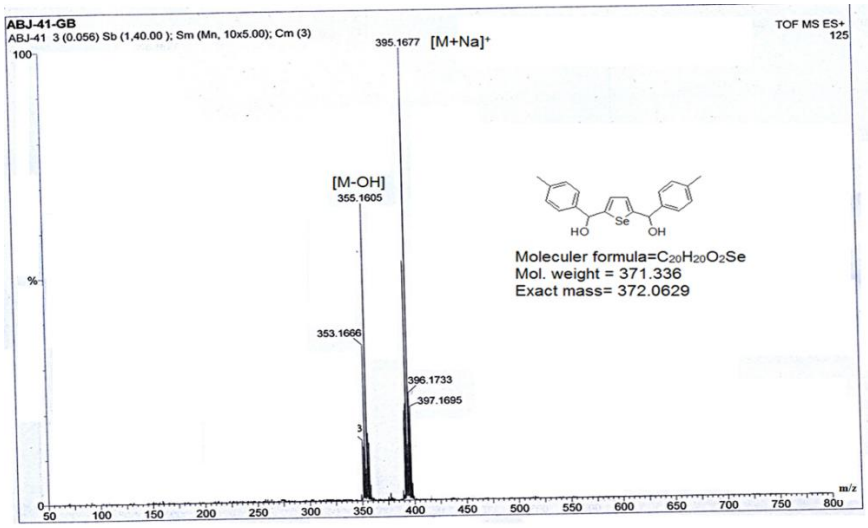

Figure 2.2. MS Spectra of **P2**

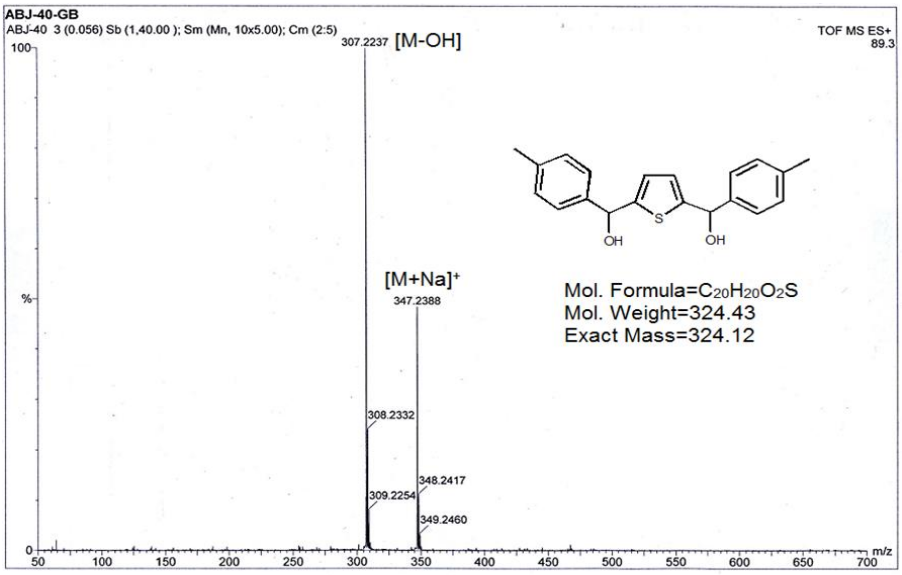

Figure 2.3. MS Spectra of **P3**

2.5.1.3. NMR Spectra:

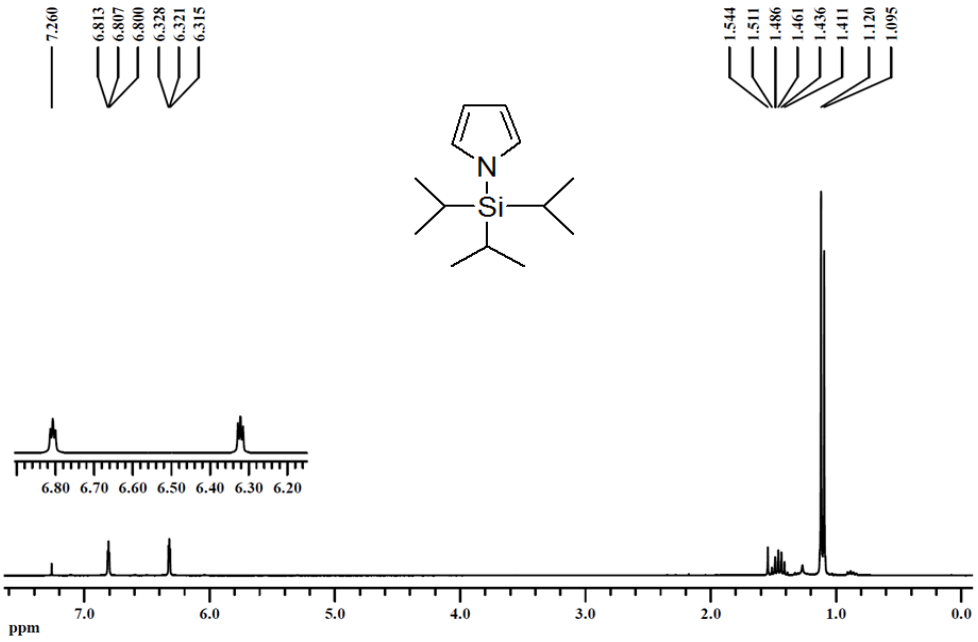

Figure 2.4. ^{1}H NMR Spectrum of **P1** in $CDCl_3$ at RT

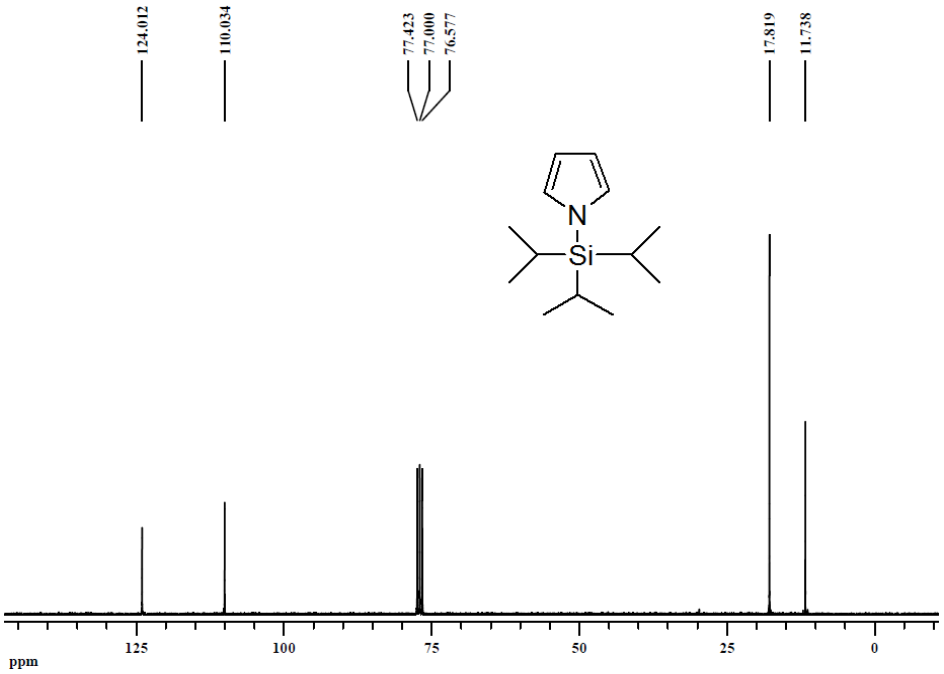

Figure 2.5. ^{13}C NMR Spectrum of **P1** $CDCl_3$ at RT

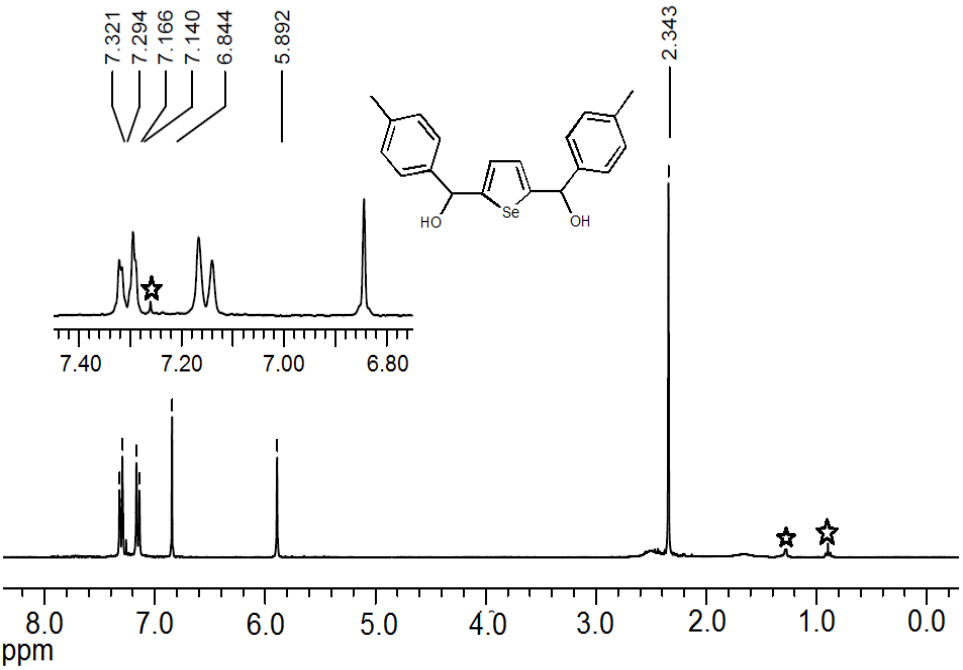

Figure 2.6. ^{1}H NMR Spectrum of **P2** $CDCl_3$ at RT

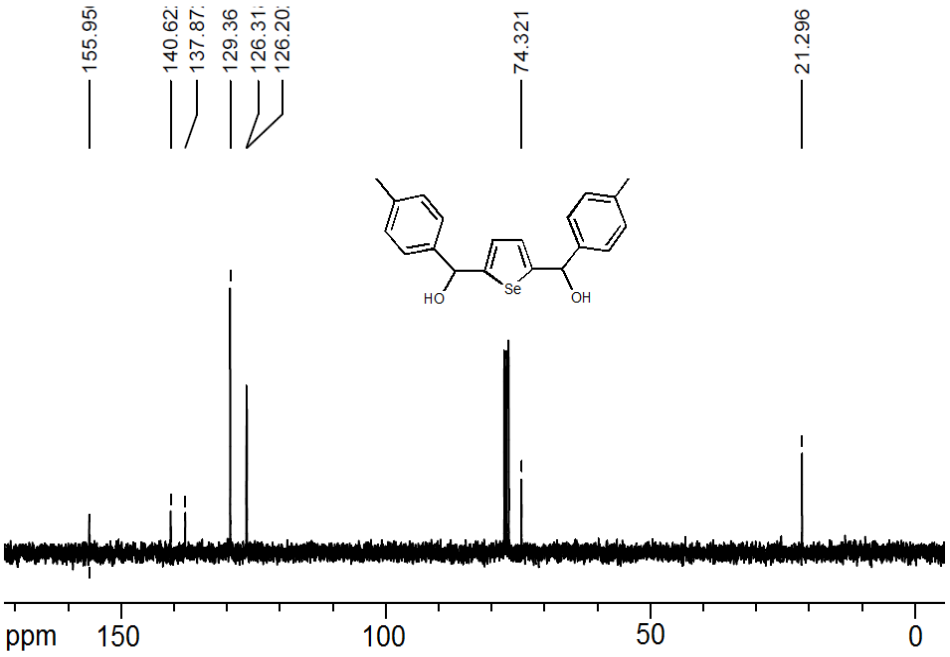

Figure 2.7. ^{13}C NMR Spectrum of **P2** in $CDCl_3$ at RT

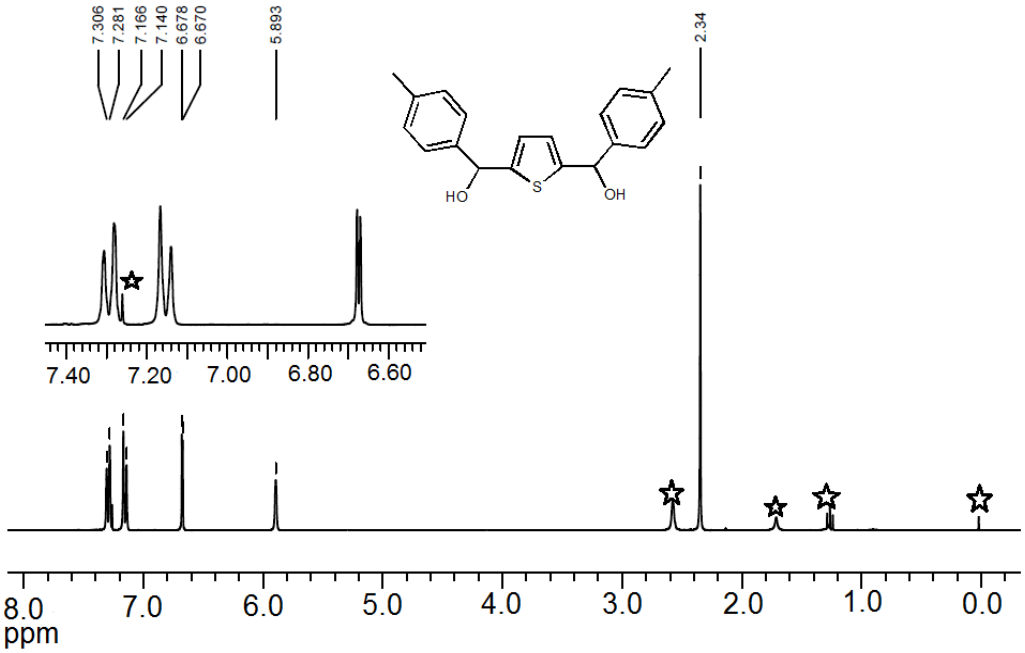

Figure 2.8. ^{1}H NMR Spectrum of **P3** in $CDCl_3$ at RT

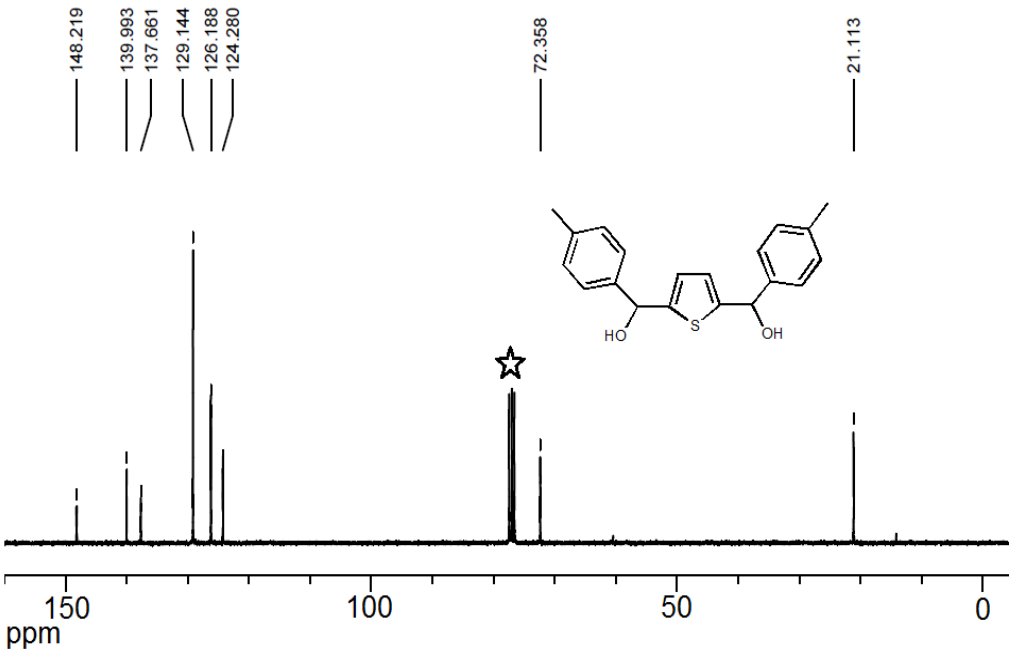

Figure 2.9. ^{13}C NMR Spectrum of **P3** in $CDCl_3$ at RT

2.6.2. Synthesis of Precursor Compounds

2.6.2.1. Synthetic Scheme

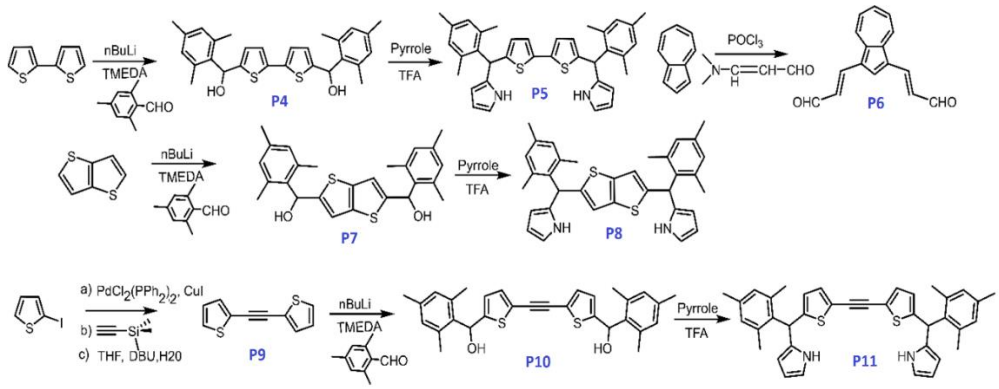

Scheme 2.2

[2,2'bithiophene]5,5'diylbis(mesitylmethanol) (**P4**): To a solution of 2,2'-bithiophene (0.5g, 3 mmol) in 20 mL of n-hexane containingN, N,N ,N-tetramethylenediamine (1.35 mL, 9.02 mmol) under argon atmosphere, n-butyl lithium(1.6 M) (5.6 mL,9.02 mmol) was added slowly and was stirred at room temperature for two hours and later refluxed for two hours.Thereaction was then allowed to attain room temperature. Mesitaldehyde (1.33 mL, 9.02 mmol) was dissolved in 20 mL oftetrahydrofuran (THF) and was added drop wise to the reaction mixture in ice-cold condition. After the addition, the reaction mixture was allowed to attain the room temperature and was stirred for an additional two hours. The reaction was quenched with saturated ammonium chloride solution and was stirred for half an hour. This was then extracted ethyl acetate (100 ml). The organic layers were combined and was washed with brine and dried over anhydrous sodium sulphate. The crude product obtained on evaporation of the solvent was recrystallized from toluene. The solid obtained was identified as **P4** Yield ~910 mg (57%).

^{1}H NMR (300 MHz, $CDCl_3$, 300 K, δ [ppm]): 2.28 (s, 6H); 2.33 (s, 12H); 6.39 (br, 2H); 6.51 (m, 2H); 6.86 (s, 4H); 6.91 (d, 2H, J = 10.4 Hz); 7.30 (d, 1H, J= 10.8 Hz); **^{13}C NMR** (75 MHz, $CDCl_3$, 300 K, δ [ppm]): 20.62; 21.02; 69.45; 123.17; 124.4; 130.28; 135.52; 136.97; 137.07; 137.87; 146.52. HRMS (ESI) m/z: $[M- OH]^+$Calcd for $C_{28}H_{29}OS_2$ 445.1563; Found 445.1558.

5,5'-bis(mesityl(1H-pyrrol-2-yl) methyl)-2,2'-bithiophen (**P5**): Compound P4 (1g, 2.16 mmol) was dissolved in pyrrole (30mL, 0.432 mol). The solution was stirred for 45 min under nitrogen atmosphere atroom temperature. Trifluoroacetic acid (0.1 mL,) was added and stirred for 1 h. The reaction mixture was quenched by dichloromethane; product was neutralized by NaOH (aq) solution, extracted by dichloromethane, dried over Na_2SO_4, and dried in rotary evaporator to give yellow oil. The crude product was purified by silica gechromatography using ethyl

acetate–hexane (10:90) solution. Compound P5 was obtained as light yellow foam. Yield 0.604 g (50%).

^{1}H NMR (300 MHz,$CDCl_3$, 300 K, δ [ppm]): 2.14(s, 12H,-Me); 2.28(s, 6H, -Me); 6.02(s, 2H,-CH); 6.10(brs, 2H, β-H of pyrrole); 6.16(dd, 2H, β-H of pyrrole); 6.67(d, 2H, J = 4.5, β-H of pyrrole); 6.71(d, 2H, of thiophene); 6.87 (s, 4H,–CH); 6.91 (d, 2H, β-H of thiophene); 7.86(brs, 2H, -NH). **^{13} C NMR** (75 MHz, CDCl3, 300 K, δ [ppm]): 20.95; 29.45; 40.66; 107.13; 108.67; 116.51; 122.76; 126.30; 130.51; 131.94; 135.58; 136.28; 136.94; 137.54. HRMS (ESI) m/z: $[M+H]^+$Calcd for $C_{36}H_{37}N_2S_2$ 561.2398; Found 561.7377.

(2E,2'E)-3,3'-(azulene-1,3-diyl)diacrylaldehyde (**P6**) : Phosphorus oxychloride (0.45) was added dropwise to a stirred solution of azulene (200 mg; 1.56 mmol) and 3-dimethylaminoacrolein (90%; 0.5 mL; 5.15 mmol) in dichloroethane (40 mL) while maintaining the temperature below 10°C. The resulting solution was stirred under refluxed overnight. The next day, 2.5 M sodium hydroxide solution (20 mL) was added and the biphasic mixture stirred for an additional 10 min. After cooling to room temperature, the mixture is diluted with chloroform and washed with water. The solvent was removed on a rotary evaporator, initially using aspirator pressure and then an oil pump. The residue was run through a silica column eluting with chloroform to give the stretched dialdehyde **P6** as a dark powder. Yield 0.310 mg (42%).

^{1}H NMR (500 MHz, $CDCl_3$, 300 K, δ [ppm]): 6.87 (2H, dd); 7.57 (t,); 8.03 (d, 2H J = 15.5 Hz), 8.53(s , 1H); 8.64 (d, 2H, J = 10 Hz), 9.79 (2H, d, J = 7.5 Hz). **^{13} C NMR (75 MHz, CDCl3, 300 K, δ [ppm]):** 31.06; 125.23 127.59 ;128.62; 133.96; 135.15; 141.05; 142.47; 142.77; 193.47. HRMS (ESI) m/z: $[M+H]^+$Calcd for $C_{16}H_{13}O_2$ 237.091; Found 237.0916.

Synthesis of (**P7**): To a 250 mL round-bottomed flask equipped with a magnetic bar, thieno [3, 2-b] thiophene (1 g, 7.13 mmol) was placed followed by dry THF (40 mL).

The reaction mixture was stirred under inert atmosphere. N, N, N′, N′-Tetramethyl ethylenediamine (3.2 mL, 0.021 mol) was added followed by stirring for half an hour at room temperature. Afterward, n-BuLi in hexane (1.6 M) (13.04 mL, 0.021 mol) was added through rubber septa dropwise, yellow turbidity started forming. The reaction mixture was stirred at room temperature for 2 hours and then heated to 66°C for 1 hour. The reaction mixture was brought room temperature after which it was brought to ice cold temperature. At ice-cold temperature, Mesitaldehyde (2.62 mL, 0.017 mol) in dry THF (40 mL) was then added dropwise to the reaction mixture, the reaction mixture was stirred for 2 hours. The reaction mixture was quenched by saturated NH_4Cl (aq) solution, product was extracted by diethyl ether, dried over Na_2SO_4. The crude product was precipitated out by hexane and purified by silica gel column chromatography using ethyl acetate-hexane (1:4) solution. The solvent was evaporated and light yellow solid was obtained. Yield 2.09 g (67%). R_f 0.2 (Hexane/EtOAc = 9:1).

^{1}H NMR (500 MHz, $CDCl_3$, 300 K, δ[ppm]): 2.28 (s, 6H); 2.33 (s, 12H); 6.46 (s, 2H); 6.71 (s, 2H); 6.87 (s, 4H). **^{13}C NMR (125 MHz, $CDCl_3$, 300 K, δ[ppm]):** 20.66, 29.84, 69.82, 116.41, 130.92, 135.36, 137.02, 137.92, 138.30, 148.88. HR-ESI-TOF MS (*m/z*) 459.02 $[M + Na]^+$ (436.63. calc. for $[C_{26}H_{28}O_2S_2]^+$).

Synthesis of (**P8**): Compound **P7** (1g, 2.29 mmol) was dissolved in pyrrole (15 mL, 0.19 mol). The solution was stirred for 45 minutes under nitrogen atmosphere at room temperature. Trifluoroacetic acid (0.05 mL, 0.22 mmol) was added and stirred for 1 hour. The reaction mixture was quenched by dichloromethane; product was neutralized by NaOH (aq) solution, extracted by dichloromethane, dried over Na_2SO_4 and dried in rotary evaporator to give yellow oil. The crude product was purified by silica gel chromatography using 10% ethylacetate-hexane mixture. Compound **P8** was obtained as light yellow foam. Yield 0.702 g (57%). R_f 0.3 (Hexane/EtOAc = 4:1). **^{1}H NMR (500 MHz, $CDCl_3$, 300K, δ[ppm]):** 2.03 (s, 6H, -Me); 2.29-2.35 (s, 12H, -Me); 4.24 (s, 2H,-CH); 6.03 (br, 1H, β-H of pyrrole); 6.13 (s, 1H, β-H of

thienothiophene); 6.23 (d, 1H, J = 4.5 Hz, β-H of pyrrole); 6.30 (d, 1H, J = 4.5 Hz; β-H of pyrrole); 6.54 (br, 1H, β-H of pyrrole); 6.69 (s, 1H, β-H of thienothiophene); 6.70-6.71 (m, 1H, β-H of pyrrole); 6.72-6.73 (m, 1H, β-H of pyrrole); 6.86 (s, 2H, Mesityl-CH); 6.92 (s, 2H, Mesityl-CH); 7.99 (br, 1H, -NH); 8.50 (br, 1H, -NH). **^{13}C NMR (125 MHz, $CDCl_3$, 300 K, δ[ppm]):** 20.15, 20.74, 20.97, 21.11, 22.90, 30.85, 41.24, 107.47, 108.56, 109.26, 109.43, 117.01, 117.47, 118.91, 124.71, 126.35, 129.29, 130.68, 133.32, 134.03, 135.96, 136.44, 136.52, 136.87, 137.00, 137.15, 137.18, 137.53, 145.55. HRMS (m/z) 534.4229 [M^+] (534.78 calc. for $C_{34}H_{34}N_2S_2$).

2-(2-(Thiophene-2-yl)ethynyl)thiophene (**P9**). To an oven-dried 25 mL round-bottom flask were added $Pd(PPh_3)_2Cl_2$ (67.4 mg, 6 mol %), CuI (30.5 mg, 10 mol %), and 2-iodothiophene (0.17 mL, 1.6 mmol), and the flask was purged with argon. Argonpurged anhydrous toluene (8 mL) and 1,8-diazabicyclo[5.4.0]- undec-7-ene (1.43 mL, 6 equiv) were added successively by a syringe. Ice-chilled trimethylsilylethyne (104.5 μL, 0.50 equiv) was then added by a syringe, followed immediately by distilled water (11.5 μL, 40 mol %). The reaction flask was covered by aluminum foil and stirred for 18h at room-temperature (RT). Then, the reaction mixture was partitioned in ethyl ether and distilled water (50 mL each). The organic layer was washed with 10% HCl (3 × 75 mL) and saturated aqueous NaCl (75 mL) and dried over $MgSO_4$. The crude product was purified by silica gel column chromatography using ethyl acetate− hexane (0.1:99.9) solutionYield: 130.9 mg, 86%, mp 98−100 °C.

^{1}H NMR (500 MHz, $CDCl_3$) δ 7.27−7.31 (m, 4H), 7.00−7.02 (m, 2H). **^{13}C NMR (100 MHz, $CDCl_3$)** δ 132.2, 127.7, 127.2, 123.0, 86.3. HRMS (ESI-TOF) (m/z): [M+ Na]$^+$ calcd for $C_{10}H_6S_2$ 212.9911; Found 189.9951.

2,5-Bis(mesitylhydroxymethyl)-1,2-Di(thiophen-2-yl)- ethyne **(P10).** To a 250 mL round-bottomed flask equipped with a magnetic bar, 6 (1.354 g, 7.13 mmol) was placed followed by dry THF (40 mL). The reaction mixture was stirred under inert

atmosphere. N, N, N, N-Tetramethyl ethylenediamine (3.2 mL, 0.021 mol) was added followed by stirring for half an hour at room temperature. Afterward, n-BuLi in hexane (1.6 M) (13.04 mL, 0.021 mol) was added through rubber septa dropwise, yellow turbidity started forming. The reaction mixture was stirred at room temperature for 2 h and then heated to 66 °C for 1 h. The reaction mixture was brought to room temperature after which it was brought to ice cold temperature. At ice cold temperature, mesitaldehyde (2.62 mL, 0.017 mol) in dry THF (40 mL) was then added dropwise to the reaction mixture, the reaction mixture was stirred for 2 h. The reaction mixture was quenched by saturated NH_4Cl (aq) solution, product was extracted by diethyl ether, dried over Na_2SO_4. The crude product was precipitated out by hexane and purified by silica gel column chromatography using the mixture of ethyl acetate–hexane (20:80) solution. The solvent was evaporated and light yellow solid was obtained.

Yield 2.30 g (67%). mp 135–137 °C. **^{1}H NMR (500 MHz, $CDCl_3$, 300 K, δ [ppm]):** 1.65 (brs, 2H); 2.28 (s, 6H); 2.31 (s, 12H); 6.39 (s, 2H); 6.52 (d, 2H, J = 3.5 Hz); 6.86 (s, 4H); 7.05 (d, 2H, J = 3.5 Hz).
^{13}C NMR (125 MHz, $CDCl_3$, 300 K, δ [ppm]): 20.3, 20.8, 69.3, 86.4, 122.2, 123.5, 130.0, 131.9, 135.3, 136.7, 137.8, 150.2. HRMS (ESI-TOF) m/z: [M+ Na]+ calcd for $C_{30}H_{30}O_2S_2$ 469.1269.1585; found 469.1272.

2-(Mesityl(1H-pyrrole-2-yl)methyl) 1,2-Di(thiophen-2- yl)ethyne-5-yl)methyl)-1H-pyrrole **(P11).** Compound **P10** (1.11 g, 2.29 mmol) was dissolved in pyrrole (15 mL, 0.19 mol). The solution was stirred for 45 min under nitrogen atmosphere at room temperature. Trifluoroacetic acid (0.05 mL, 0.22 mmol) was added and stirred for 1 h. The reaction mixture was quenched by dichloromethane; product was neutralized by NaOH (aq) solution, extracted by dichloromethane, dried over Na_2SO_4, and dried in rotary evaporator to give yellow oil. The crude product was purified by silica gel

chromatography using ethyl acetate–hexane (10:90) solution. Compound 8 was obtained as light yellow foam. Yield 0.760 g (57%).

^{1}H NMR (500 MHz,$CDCl_3$, 300 K, δ [ppm]): 2.11(s, 12H,-Me); 2.28(s,6H, -Me); 6.06(s, 2H,-CH); 6.13(brs, 2H, β-H of pyrrole); 6.17(s, 2H, β-H of pyrrole); 6.66(d, 2H, J = 4.5, β-H of pyrrole); 6.74(d, 2H, J = 4.5, β-H of thiophene); 6.87 (s, 4H, –CH); 7.06 (d, 2H, β-H of thiophene); 7.84(brs, 2H, -NH). **^{13}C NMR (125 MHz, $CDCl_3$, 300 K, δ [ppm]):** 20.7, 40.6, 86.2, 107.0, 108.5, 116.5, 121.4, 125.6, 130.4, 131.4, 131.6, 135.2, 136.9, 137.3, 148.2. HR-ESI-TOF MS (m/z): Found 584.7821[M+] (Calcd 584.23 for $[C_{38}H_{36}N_2S_2]+$).

2.5.2.2. Mass spectra:

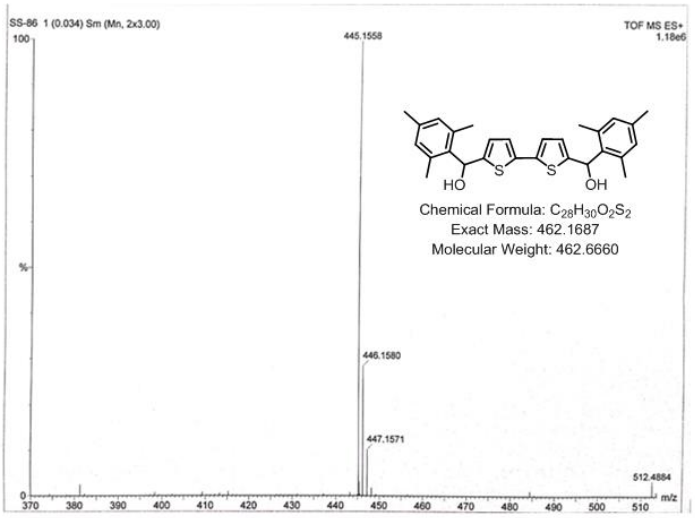

Figure 2.10. MS Spectrum of **P4**

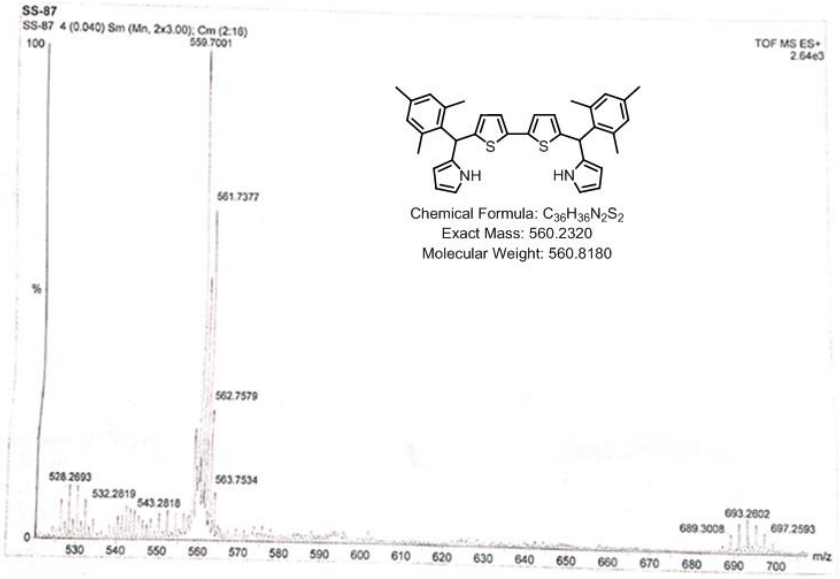

Figure 2.11. MS Spectrum of **P5**

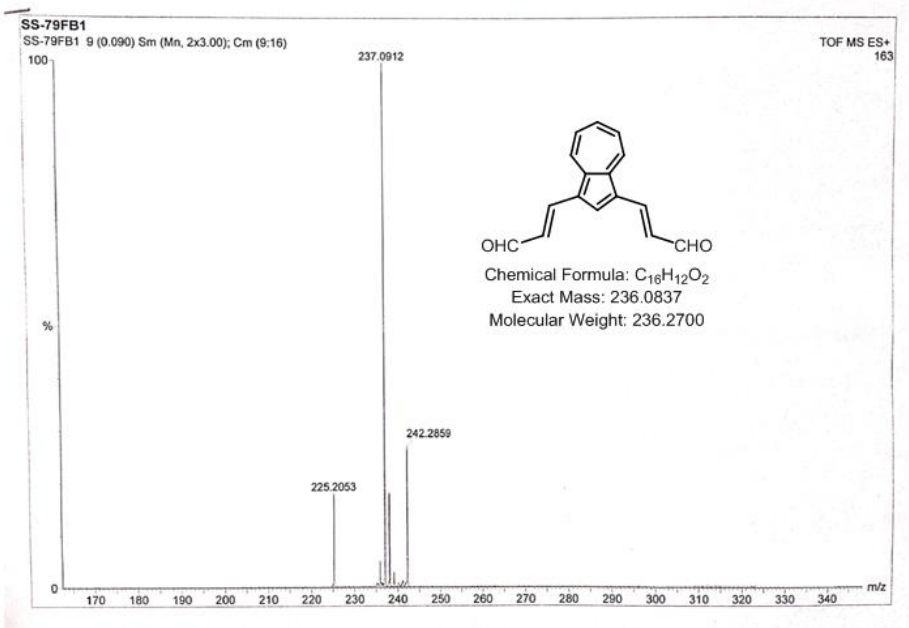

Figure 2.12. MS Spectrum of **P6**

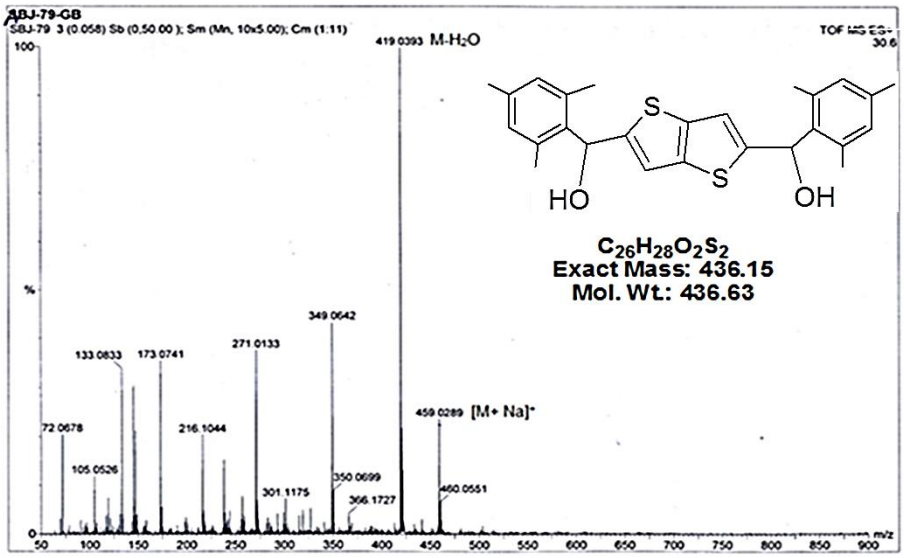

Figure 2.13. MS Spectrum of **P7**

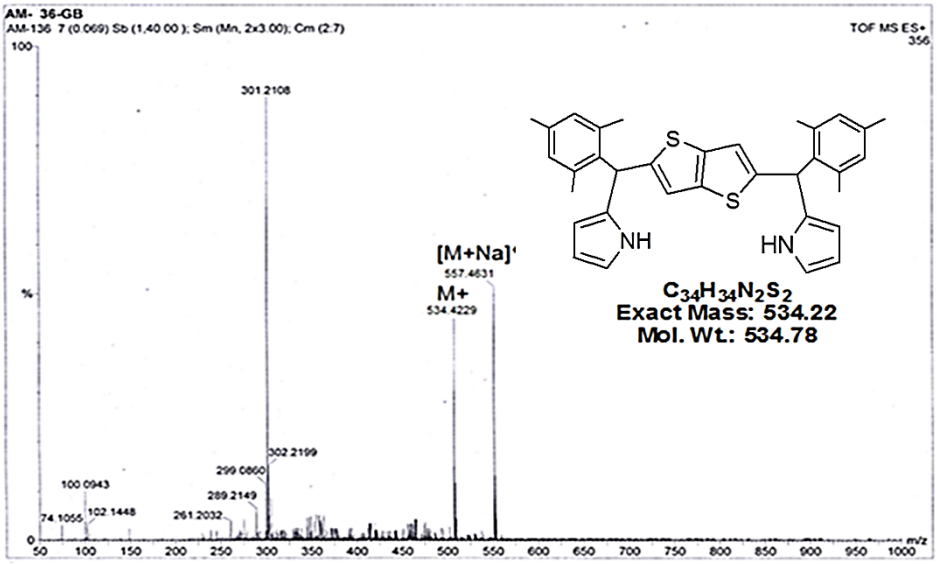

Figure 2.14. MS Spectrum of **P8**

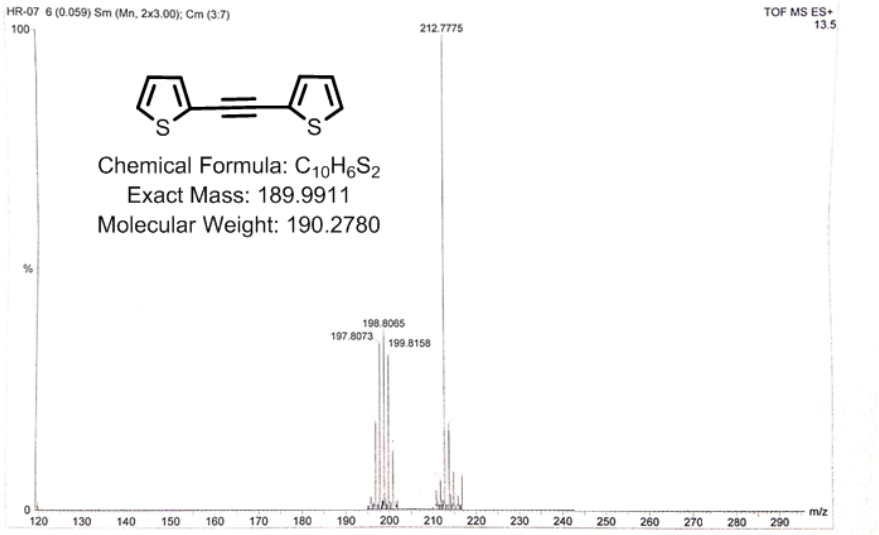

Figure 2.15. MS Spectrum of **P9**

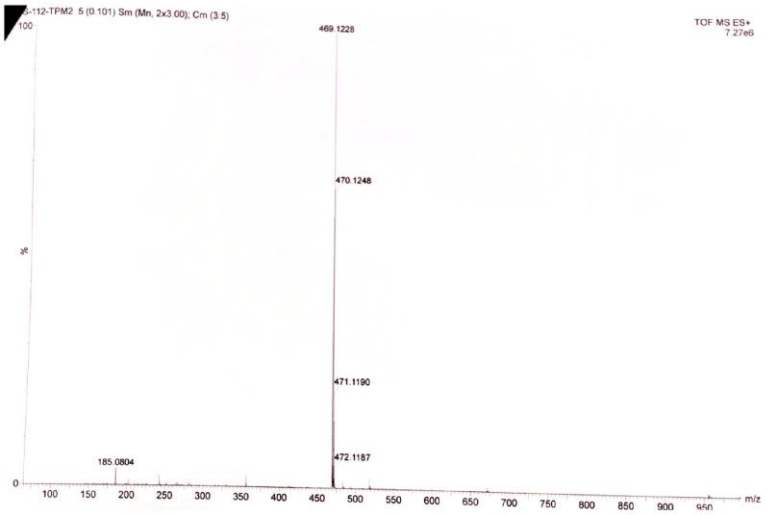

Figure 2.16. MS Spectrum of **P10**

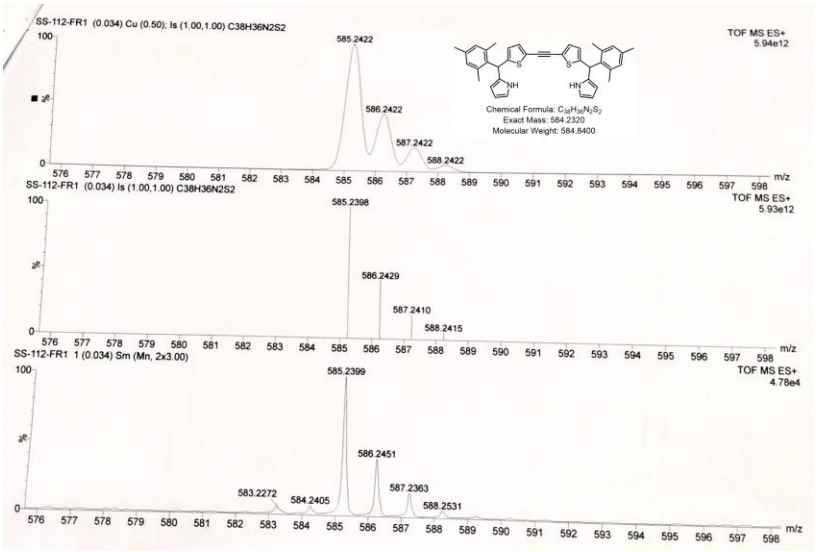

Figure 2.17. MS Spectrum of **P11**

2.5.2.3 NMR Spectra:

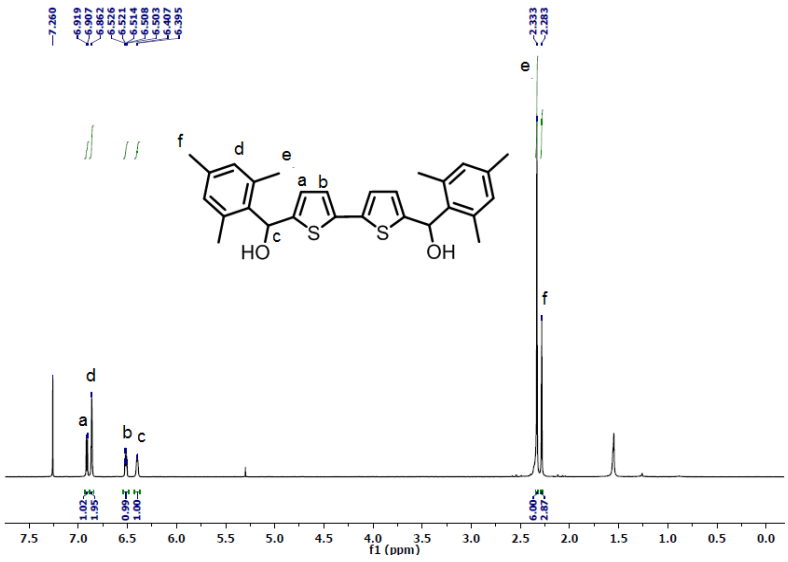

Figure 2.18. ^{1}H NMR Spectrum of **P4** in $CDCl_3$ at RT

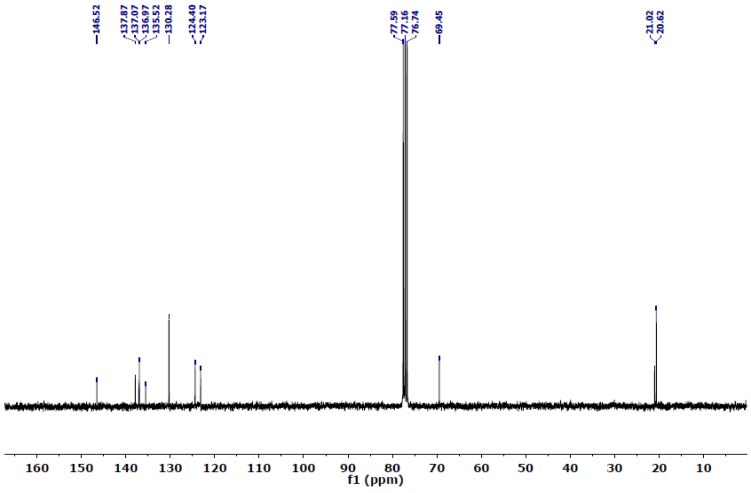

Figure 2.19. ^{13}C NMR Spectrum of **P4** in $CDCl_3$ at RT

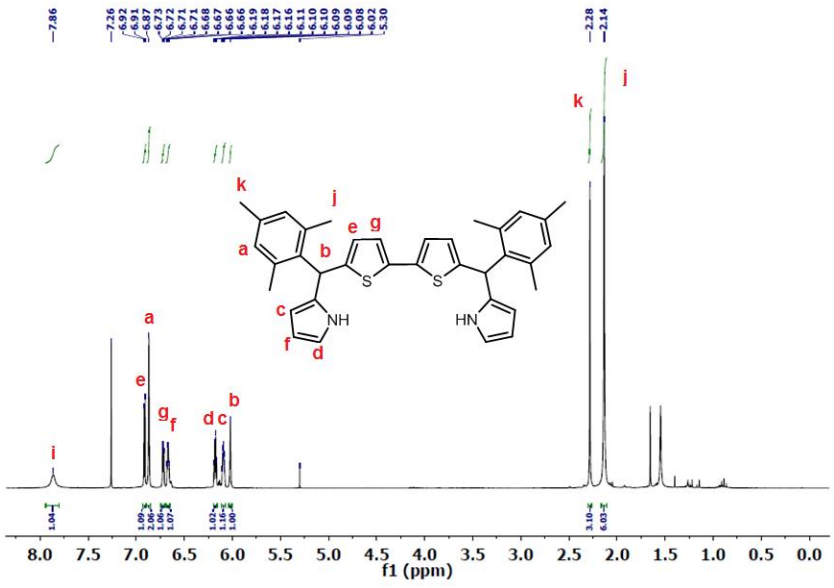

Figure 2.20. ^{1}H NMR Spectrum of **P5** in $CDCl_3$ at RT

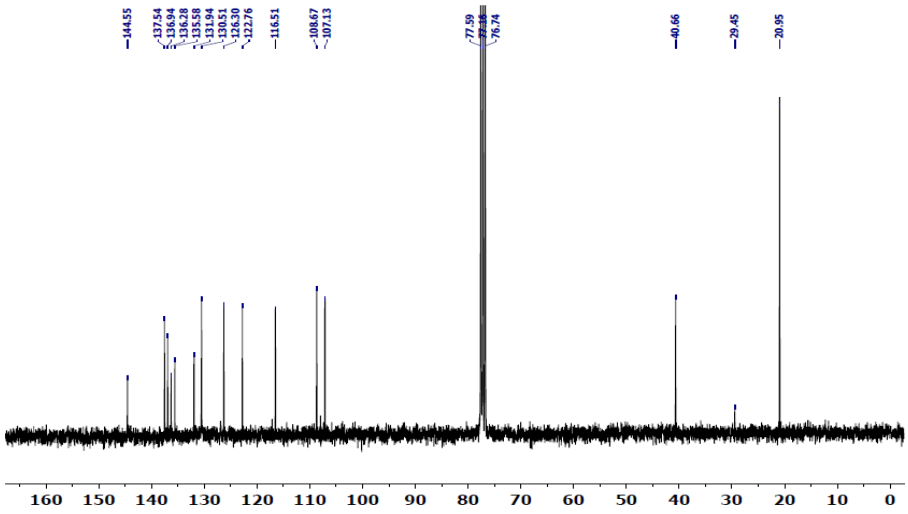

Figure 2.21. ^{13}C NMR Spectrum of **P5** in $CDCl_3$ at RT

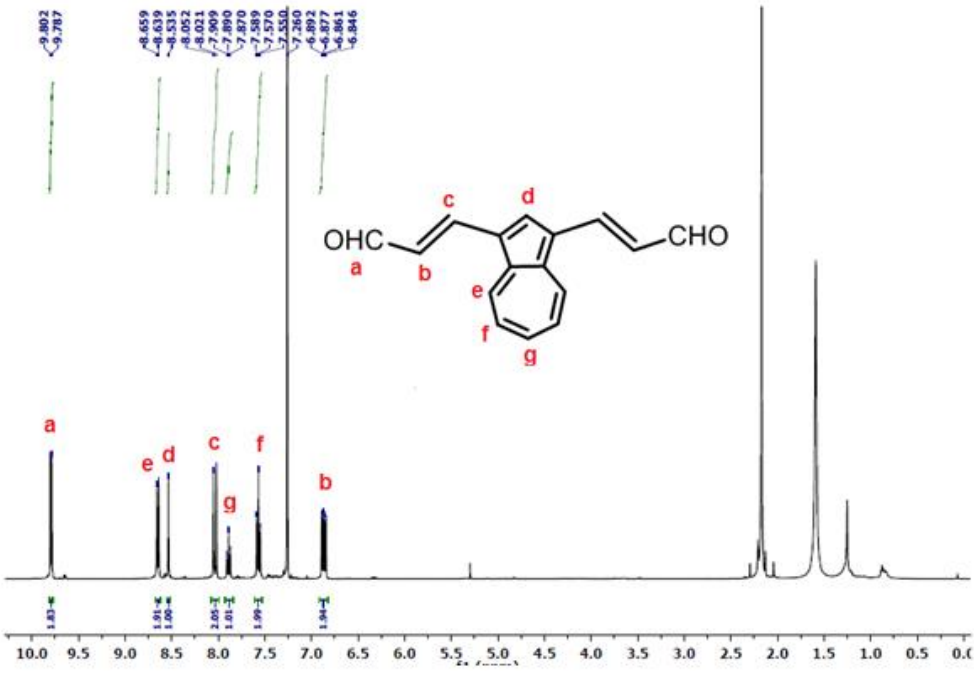

Figure 2.22. ^{1}H NMR Spectrum of **P6** in $CDCl_3$ at RT

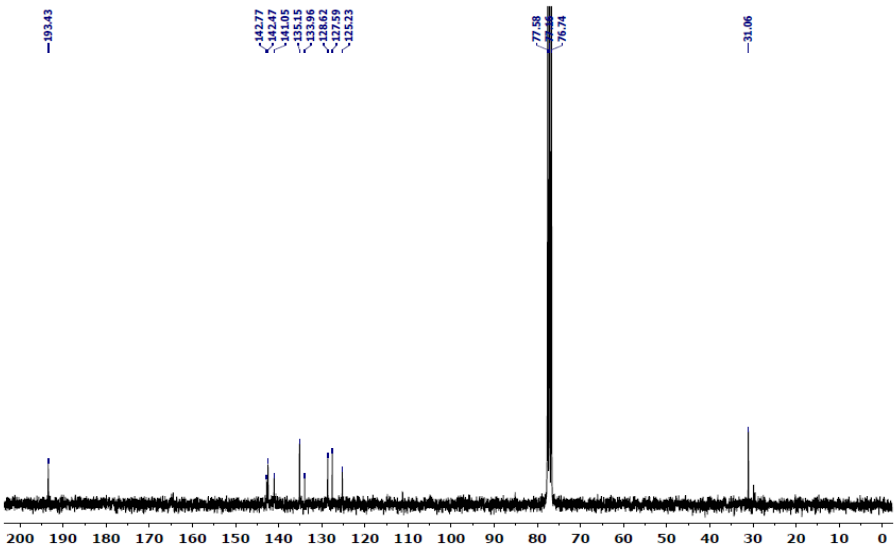

Figure 2.23. ^{13}C NMR Spectrum of **P6** in $CDCl_3$ at RT

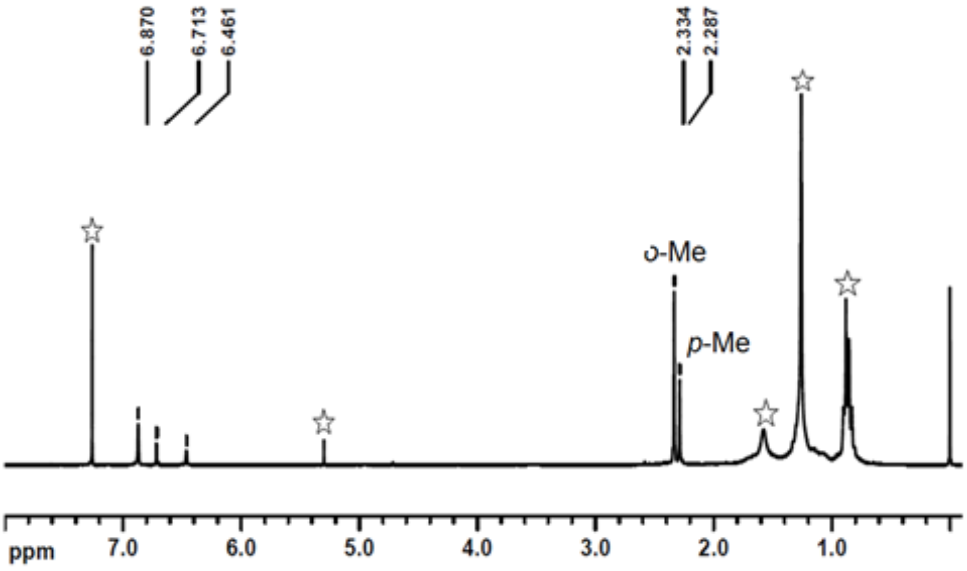

Figure 2.24. ^{1}H NMR Spectrum of **P7** in $CDCl_3$ at RT

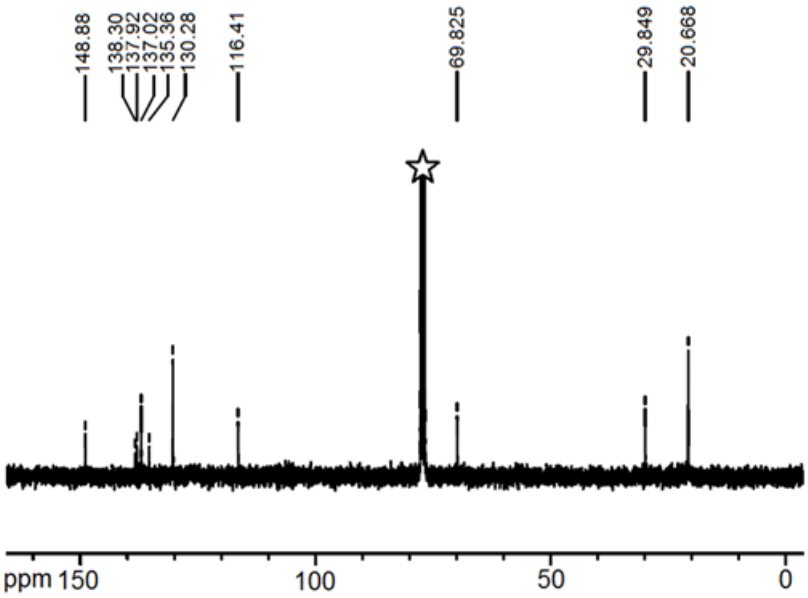

Figure 2.25. ^{13}C NMR Spectrum of **P7** in $CDCl_3$ at RT

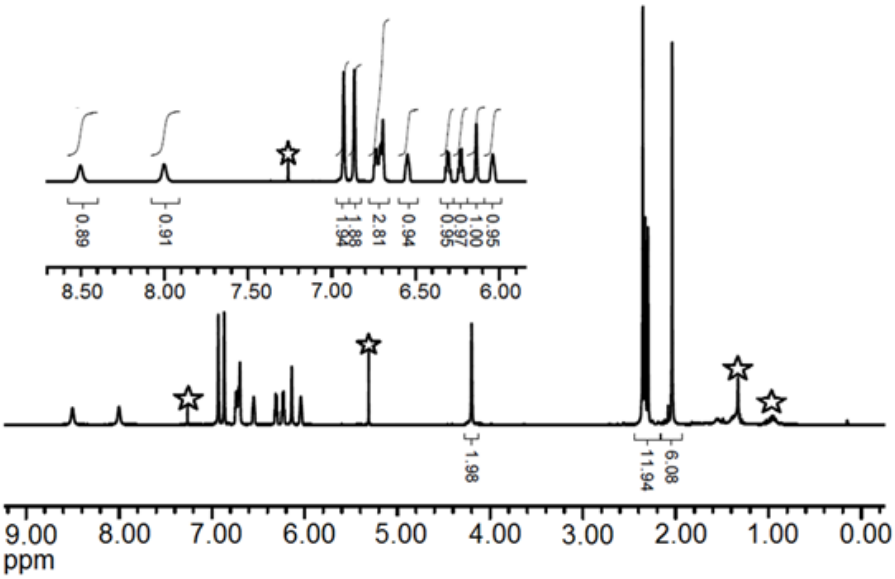

Figure 2.26. ^{1}H NMR Spectrum of **P8** in $CDCl_3$ at RT

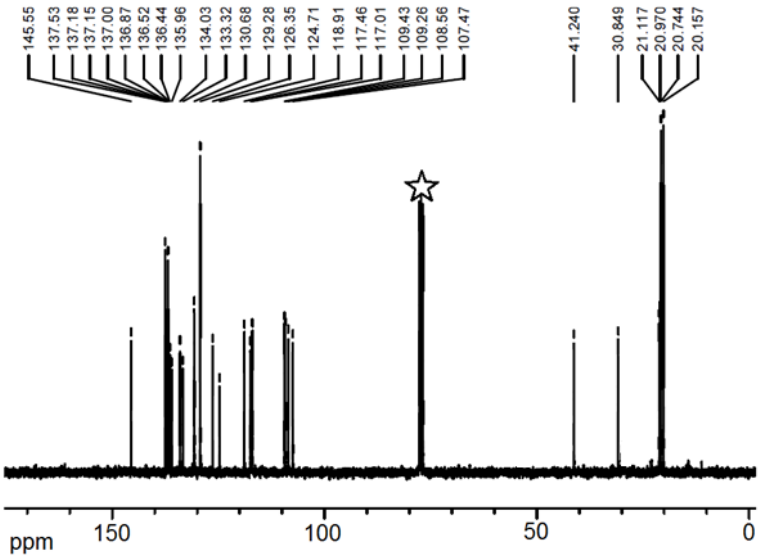

Figure 2.27. ^{13}C NMR Spectrum of **P8** in $CDCl_3$ at RT

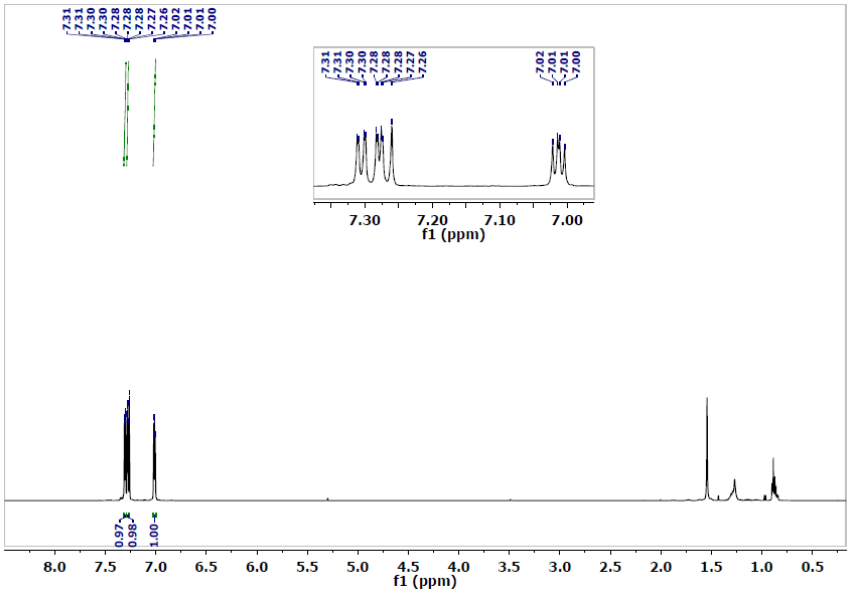

Figure 2.28. ^{1}H NMR Spectrum of **P9** in $CDCl_3$ at RT

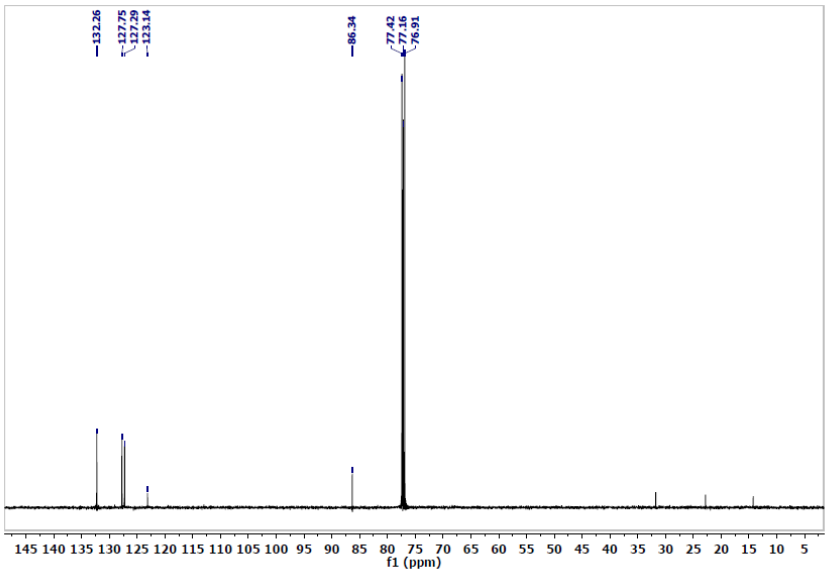

Figure 2.29. ^{13}C NMR Spectrum of **P9** in $CDCl_3$ at RT

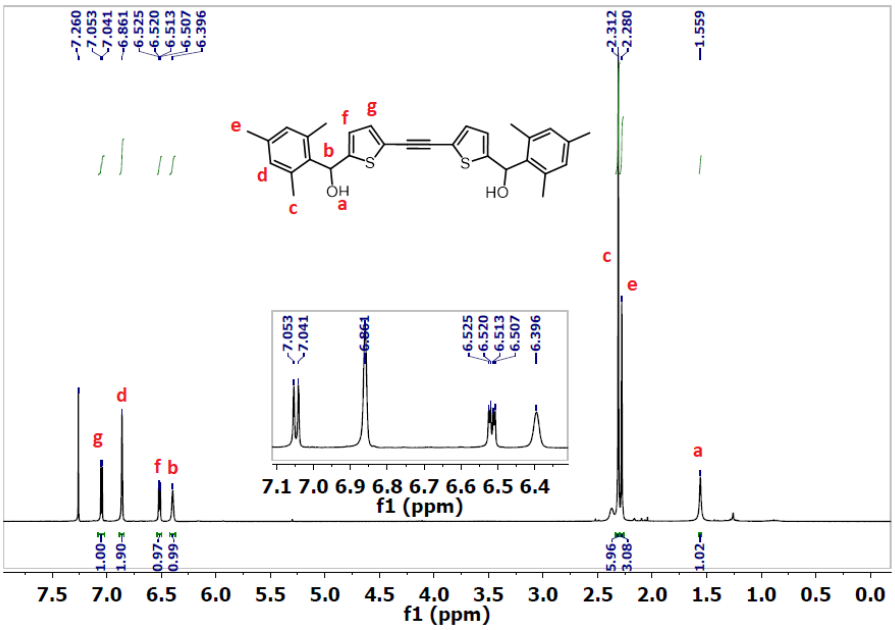

Figure 2.30.^{1}H NMR Spectrum of **P10** in $CDCl_3$ at RT

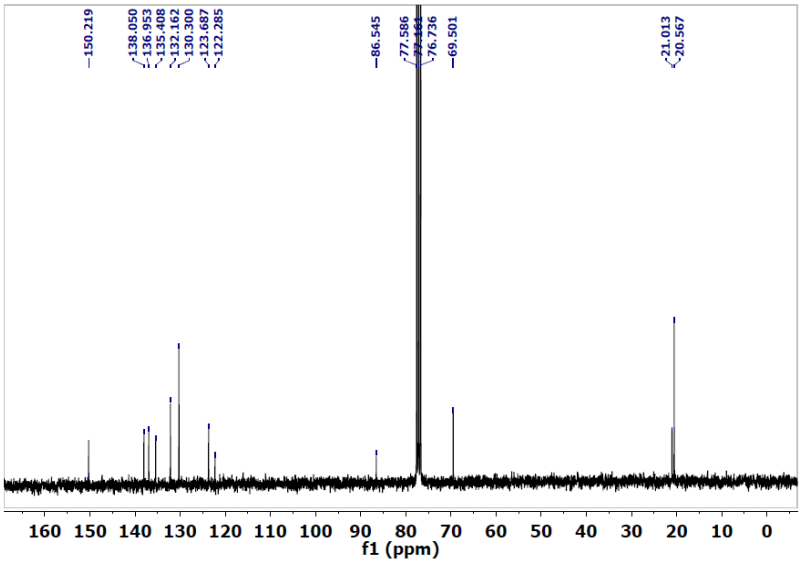

Figure 2.31. ^{13}C NMR Spectrum of **P10** in $CDCl_3$ at RT

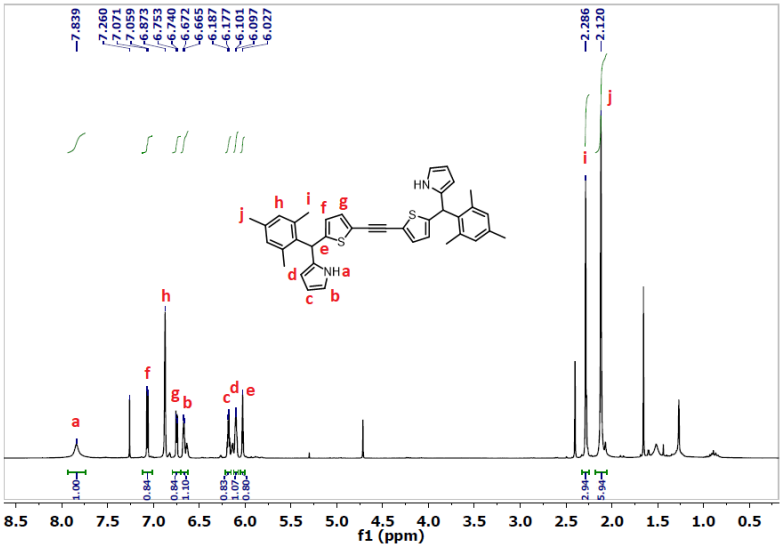

Figure 2.32. ^{1}H NMR Spectrum of **P11** in $CDCl_3$ at RT

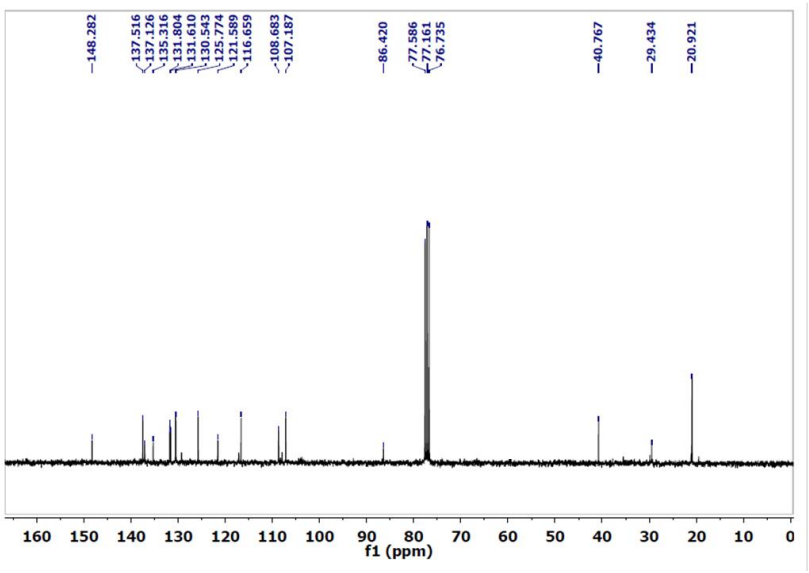

Figure 2.33. ^{13}C NMR Spectrum of **P11** in $CDCl_3$ at RT

2.6. References:

1 T. Schulz, K. Meindl, D. Leusser, D. Stern, J. Graf, C. Michaelsen, M. Ruf, G. M. Sheldrick abd D. Stalke, *J. Appl. Crystallogr.,* 2009, **42**, 885-891.

2 (a)A. L. J. Spek, *J. Appl. Crystallogr.,* 2003, **36**, 7-13; (b)A. L. Spek, *Acta Crystallogr. Sect. D. Biol. Crystallogr.* ,2009, **65**, 148-155.

3 M. J. Frisch, G. W. Trucks, H. B. Schlegel, G. E. Scuseria, M. A. Robb, J. R. Cheeseman, G. Scalmani, V. Barone, G. A. Petersson, H. Nakatsuji, X. Li, M. Caricato, A. V. Marenich, J. Bloino, B. G. Janesko, R. Gomperts, B. Mennucci, H. P. Hratchian, J. V. Ortiz, A. F. Izmaylov, J. L. Sonnenberg, Williams, F. Ding, F. Lipparini, F. Egidi, J. Goings, B. Peng, A. Petrone, T. Henderson, D. Ranasinghe, V. G. Zakrzewski, J. Gao, N. Rega, G. Zheng, W. Liang, M. Hada, M. Ehara, K. Toyota, R. Fukuda, J. Hasegawa, M. Ishida, T. Nakajima, Y. Honda, O. Kitao, H. Nakai, T. Vreven, K. Throssell, J. A. Montgomery Jr., J. E. Peralta, F. Ogliaro, M. J. Bearpark, J. J. Heyd, E. N. Brothers, K. N. Kudin, V. N. Staroverov, T. A. Keith, R. Kobayashi, J. Normand, K. Raghavachari, A. P. Rendell, J. C. Burant, S. S. Iyengar, J. Tomasi, M. Cossi, J. M. Millam, M. Klene, C. Adamo, R. Cammi, J. W. Ochterski, R. L. Martin, K. Morokuma, O. Farkas, J. B. Foresman and D. J. Fox, Wallingford, CT, 2016.

4 (a)P. v. R. Schleyer, C. Maerker, A. Dransfeld, H. Jiao and N. J. R. van Eikema Hommes, *J. Am. Chem. Soc.* 1996, **118**, 6317-6318; (b)K. Wolinski, J. F. Hinton and P. Pulay, *J. Am. Chem. Soc.,* 1990, **112**, 8251-8260; (c)F. J. London, *Phys. Radium,* 1937, **8**, 397-409.

5 (a)T. A. Keith and R. F. W. Bader, *Chem. Phys. Lett.,* 1993, **210**, 223-231; (b)J. R. Cheeseman, G. W. Trucks, T. A. Keith and M. J. Frisch, *J. Chem. Phys.,* 1996, **104**, 5497-5509; (c)D. Geuenich, K. Hess, F. Köhler and R. Herges, *Chem. Rev.* 2005, **105**, 3758-3772.

6 (a)C. Lee, W. Yang and R. G. Parr, *Phys. Rev. B,* 1988, **37**, 785-789; (b)A. D. Becke, *J. Chem. Phys.,* 1993, **98,** 1372-1377.

7 (a)G. A. Petersson and M. A. Al-Laham, *J. Chem. Phys.,* 1991, **94**, 6081-6090; (b)a. Petersson, A. Bennett, T. G. Tensfeldt, M. A. Al-Laham, W. A. Shirley and J. Mantzaris, *J. Chem. Phys.,* 1988, **89**, 2193-2218.

NIR Absorbing Dithia/Diselena DiCarbaporphyrinoids with adoptive Aromaticity

Chapter 3

3. Abstract

Doubly confused porphyrin (N_2CP) holds two confused pyrrole rings in the cyclic structure. Here two hitherto unknown highly stable thiophene and selenophene analogs of *trans*-Doubly mutant [18] π-conjugated heteroannulenes have been unambiguously synthesized and characterized. These two heteroannues are highly aromatic with the observation of inner ring protons resonating in the upfield zone and outer ring protons resonating in the deshielded zone in accordance with the electronic absorption spectra that exhibited sharp Soret band and well defined Q-type bands in the Vis-NIR region. These aromatic compounds are synthesized in a one-step reaction of the acid catalyst condensation reaction of 2, 5-bis(p-tolylhydroxymethyl)thiophene/2,5-bis(p-tolylhydroxymethyl)selenophene with N-protected TIPS pyrrole followed by oxidation with chloranil. In-depth solution state spectroscopic measurements and DFT level theoretical calculations strongly conclude the adoptive aromaticity with strong NIR absorption of these new macrocycles.

3.1. Introduction

Porphyrins and porphyrin isomers have attracted considerable attention due to their versatile structures and anticipated properties such as catalysis, coordination chemistry, sensor development, cancer treatment, nanotechnology, and molecular-scale information storage.[1a-e] In 1994, Furuta and Latos-Grazynski's groups independently reported a new type of porphyrin isomer, N-confused porphyrin (NCP). NCP has the same backbone structure as porphyrin (1,1,1,1). However, NCP has a "confused pyrrole," which is a pyrrolic moiety at the α -and β-

positions linked to the surrounding *meso*-carbons. As a consequence, NCP comprises a NNNC in the center and an N atom pointing outwards. NCP is expected to exhibit different coordination modes from those of normal porphyrins.[2]

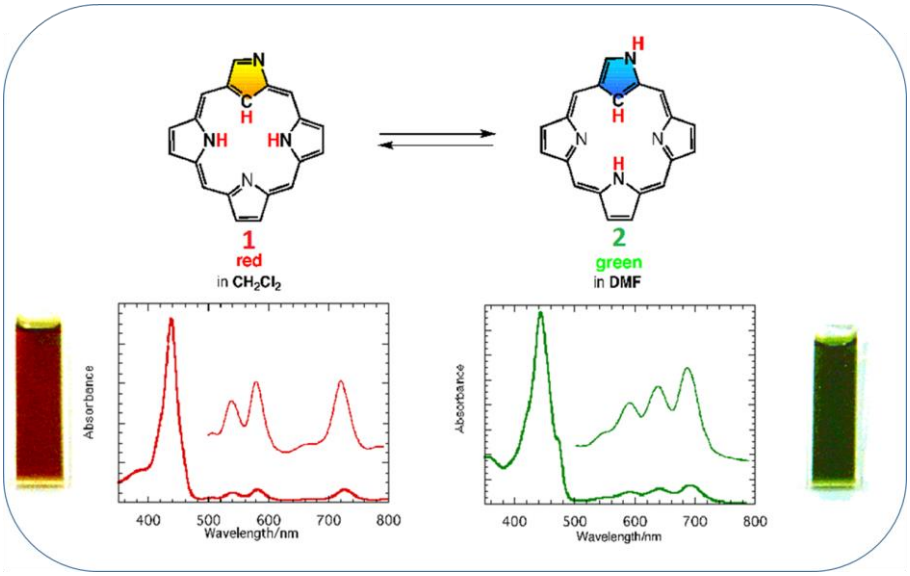

Figure 3.1. Uv-Vis of N–confused porphyrin

NCP exhibits NH tautomerism in solution depending on the accepting ability of the solvent. The peripheral nitrogen and internal nitrogen atoms are involved in NCP tautomerism, and two kinds of tautomers are detected through spectroscopic methods. There are three hydrogen atoms in the nucleus of one form of tautomer (NCP-3H), and the other has two core hydrogen atoms and one peripheral nitrogen hydrogen atom (NCP-2H). Both structures were elucidated by X-ray diffraction analyses. NCP-3H is primarily observed in non-polar solvents, while NCP-2H is strongly stabilized by the hydrogen bonding interaction at the periphery of the NH moiety in polar solvents, such as DMF and acetone. These two tautomers show different aromaticity, photochemical properties, and so on.[3]

Doubly N-confused porphyrins, where two pyrrole units are connected to the *meso*-carbons at the α- and β-positions.[4] Doubly N-confused porphyrin (N_2CP) is of

particular interest because there are exist two inner core carbon and two nitrogen atoms that can be used for metal coordination and two outer peripheral nitrogen atoms for the interaction with the external ions or molecules.

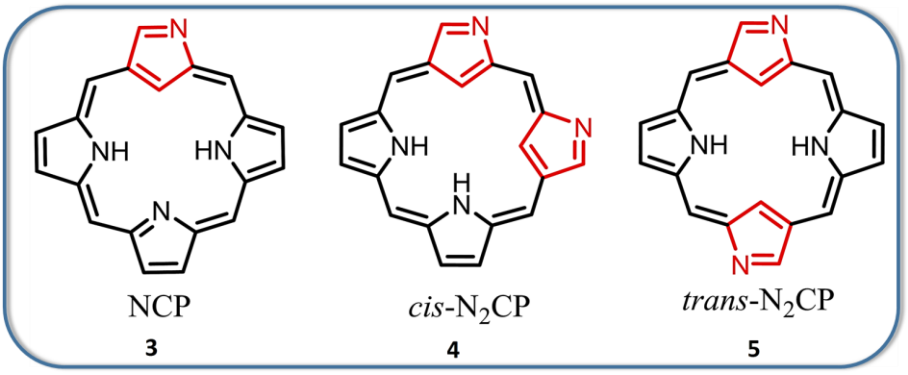

Scheme 3.1. Porphyrin isomers.

Their remarkable ability to act as tetracoordinate ligands to form transition metal complexes inside the porphyrin cavity involving a metal-carbon bond has resulted in the development of simple and organometallic divalent/trivalent complexes with metal-carbon bonds.[5] The possible stabilization of higher oxidation states of metals by doubly N-confused porphyrins has been reported by Furuta et.al.[4]. They reported *cis*-doubly N-confused porphyrin (N_2CP) **6** as shown in Scheme 3.2[6] which stabilized the metal in a higher oxidation state having rare Ag(III) **7** and Cu(III) metal complexes **8** Both the complexes are diamagnetic and have square-planar coordination with two sets of metal-carbon bonds.

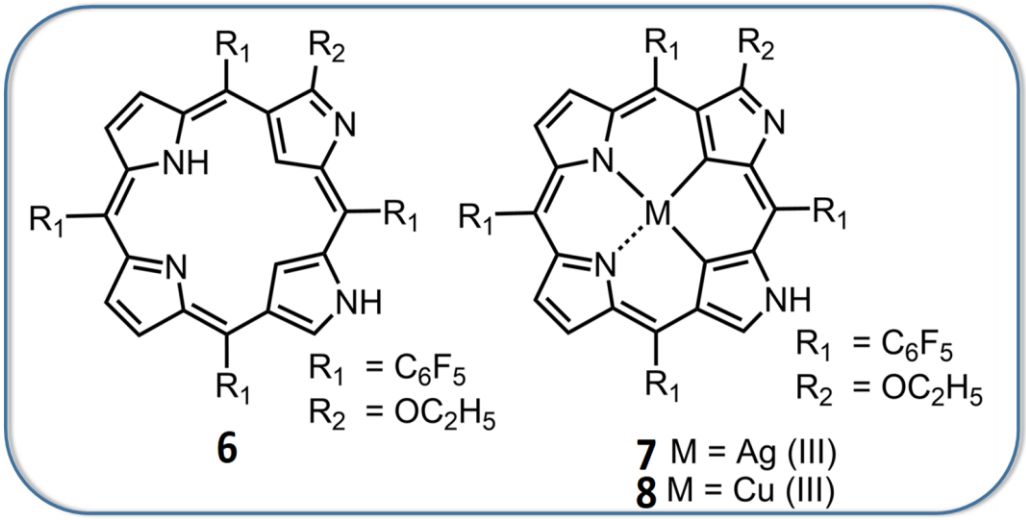

Scheme 3.2 Metal complex of N-confused porphyrin.

The same group also reported *trans*-N_2CP from N-confused N-fused porphyrin. Treatment of N-confused N-fused porphyrin NCFP with KOH/EtOH followed by ring-opening reaction

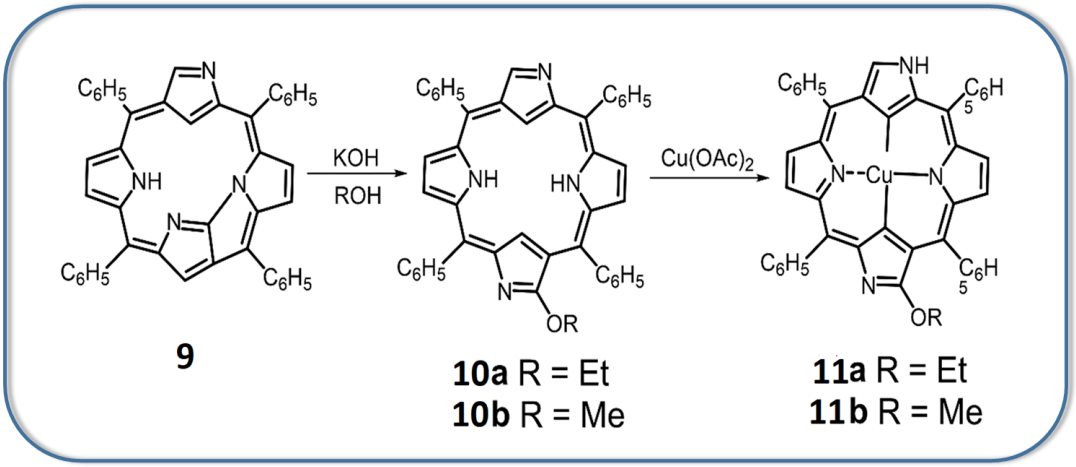

Scheme 3.3. *Trans*-Doubly N-confused isophlorin.

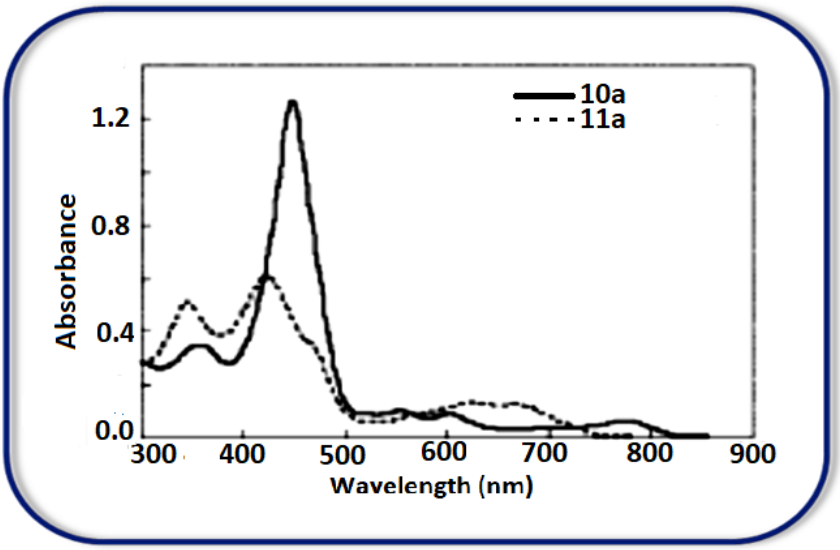

Figure 3.2. Uv-Vis-NIR spectra of **10** and **11**

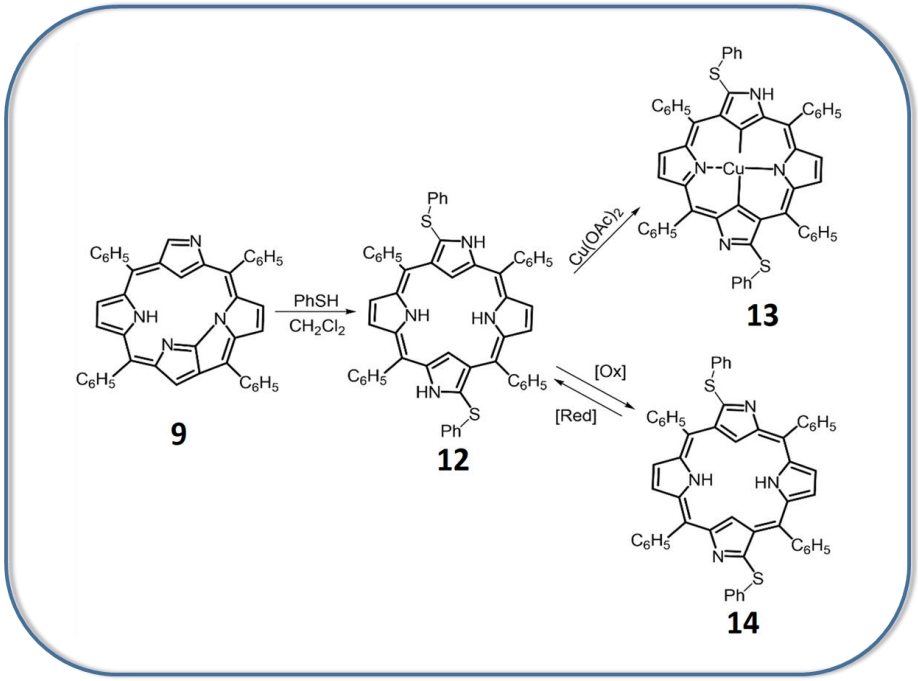

Scheme 3.4. *Trans*-doubly N-confused isophlorin with phenylthiol group.

In addition, *trans*-doubly N-confused isophlorin was reported by Furuta and co-workers from N-fused porphyrin **12** bearing phenylthio groups at the α position of

pyrrole. Oxidized product of the macrocycle gave trans-doubly N-confused Porphyrin **14**. This macrocycle stabilized the Cu in +3 oxidation state **13**.[7]

3.2. Results and discussion

3.2.1. Synthesis

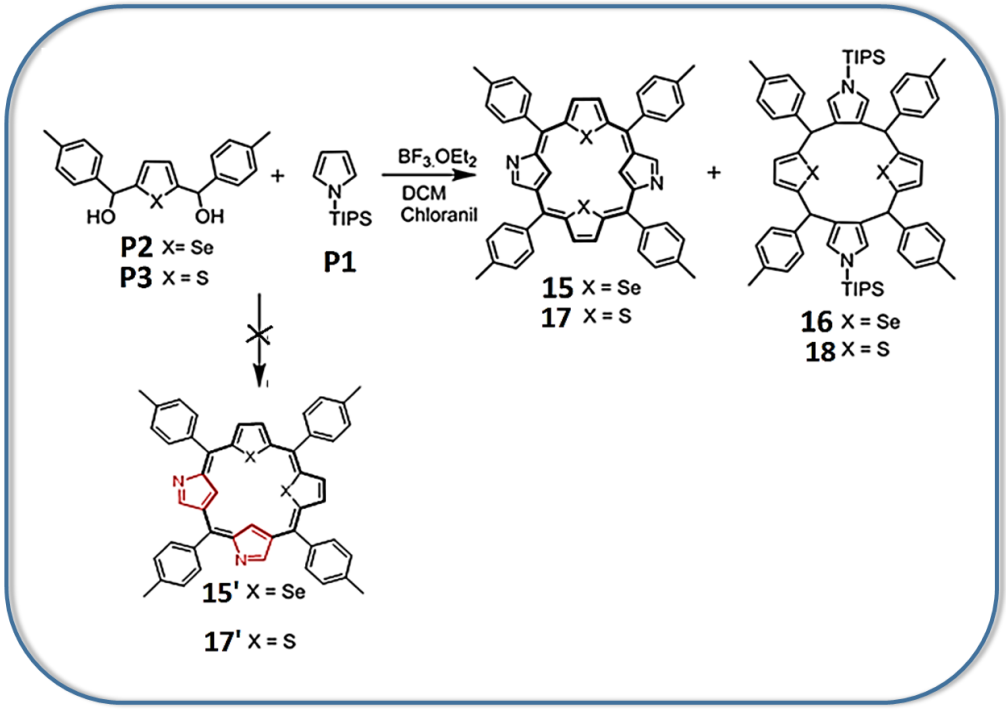

Scheme 3.5. Synthesis of dithia/diselena*Trans*-doubly N-confused porphyrinoids.

The targeted synthesis of the hitherto unknown trans-doubly N-confused dithia/diselena porphyrins **15/17**. Acid-catalyzed conventional oxidative condensation of N-TIPS pyrrole **P1**[8] and 2,5-bis(p-tolylhydroxymethyl)selenophene **P2** 2, 5-bis(p-tolylhydroxymethyl)thiophene **P3** [8](1: 1 molar ratio) using $BF_3{\cdot}OEt_2$ and subsequent chloranil oxidation have led to the isolation of meso-aryl substituted *trans*-doubly N-confused porphyrins **15** and **17** as major products and their corresponding *meso* saturated heterocyclic macrocycles **16** and **18** with unconventional β, β-pyrrole connectivities as byproducts in meager yields. The best

yields of macrocycles **15** and **17** have been obtained with 0.1 equiv. of the Lewis acid as the catalyst. Column chromatographic separation over basic alumina followed by repeated silica gel (200–400 mesh) chromatographic separation and preparative thin-layer chromatography (PTLC) afforded **15** and **17** in yields of 30% and 20% as air-stable dark green and green solids, respectively, while macrocycles **16** and **18** were obtained as yellow sticky products in negligible amounts. It is to be emphasized that all the four macrocycles reported in this manuscript do not have any precedence in the literature (**Scheme 3.5)** depicts the possibilities of reactive intermediates formed in situ during the progress of the reaction leading to the isolation of **15**, **16** **17** and **18**.

It is pertinent to highlight that cis-doubly N-confused porphyrins **15′** and **17′** (**Scheme 3.5**) are most unstable thermodynamically owing to the bigger size of Se/S and lone pair– lone pair electronic repulsions of the two adjacent selenium atoms and/or sulfur atoms.

3.2.2. Absorption spectroscopy and Mass spectrometry:

The new macrocycles have been thoroughly characterized via various spectroscopic and in-depth theoretical analyses. Macrocycles **15** and **17**exhibited the parent ion peak at m/z 801 and 705 under positive-mode MALDI-TOF mass spectrometry. On the other hand, macrocycles **16** and **18** exhibited the parent ion peak at m/z 1117.4658 and 1023.5532, respectively, under positive-mode ESI-TOF mass spectrometry. The fully conjugated aromatic nature of macrocycles **15** and **17**, both for the free bases under neutral conditions and the dications upon protonation, is supported by the UV-vis-NIR spectral pattern (**Fig.3.3**). As expected for aromatic porphyrins,[9] the electronic absorption spectrum of the free base form of **15** comprises a sharp Soret band at 484 nm and well-defined Q-type bands at 562 and 618 nm and a broad band at 807 nm tailing up to 1020 nm. Macrocycle **17** exhibits an exactly similar UV-vis-NIR spectral pattern to the Soret band at 461 nm along

with well-defined Q-type bands at 542 and 586 nm, respectively, and a broad band at 798 nm tailing up to 1050 nm, whereas all aza *trans* double N-confused porphyrins [10]absorb only up to 850 nm.

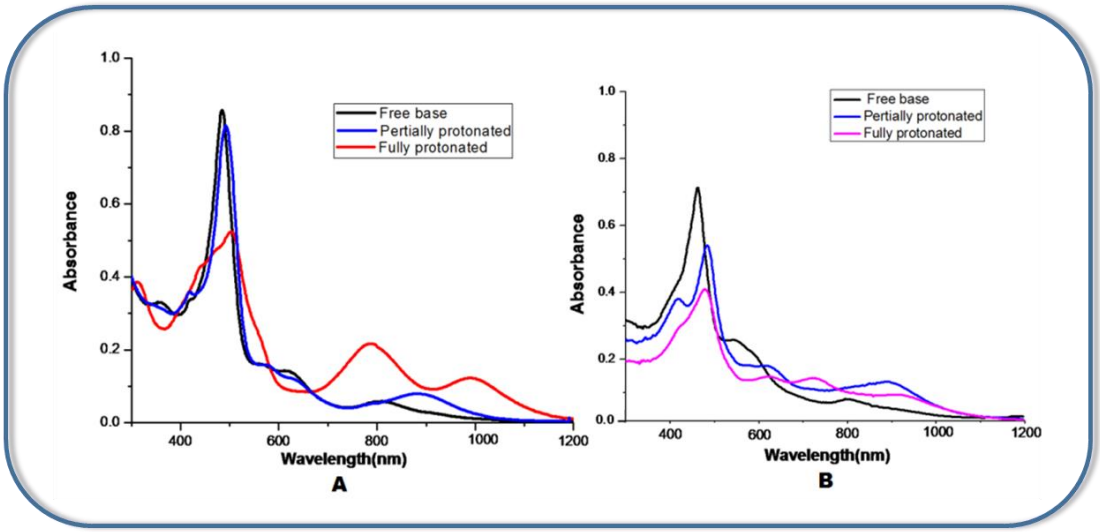

Figure 3.3. Uv-Vis-NIR spectra of **15** and **17**

The bathochromic shift observed in macrocycle **15** compared to **17** is a mere consequence of a smaller size of sulfur compared to selenium.[11] Upon protonation, both the macrocycles exhibit a 20–25 nm redshift in the Soret band region while more intense and red-shifted Q-type bands have been observed, clearly typifying the porphyrinic nature of these macrocycles with aromaticity. Titration of **15** and **17** with trifluoroacetic acid has been performed to isolate the protonated form completely (**Fig. 3.4** and **Fig. 3.6**). Contrarily, the macrocycles **16** (**Fig. 3.5**) and **18**(**Fig**. **3.7**) exhibited only a single absorption band at 439 nm and 431 nm respectively, concluding nonaromaticity in these macrocycles with lack of π-conjugation.

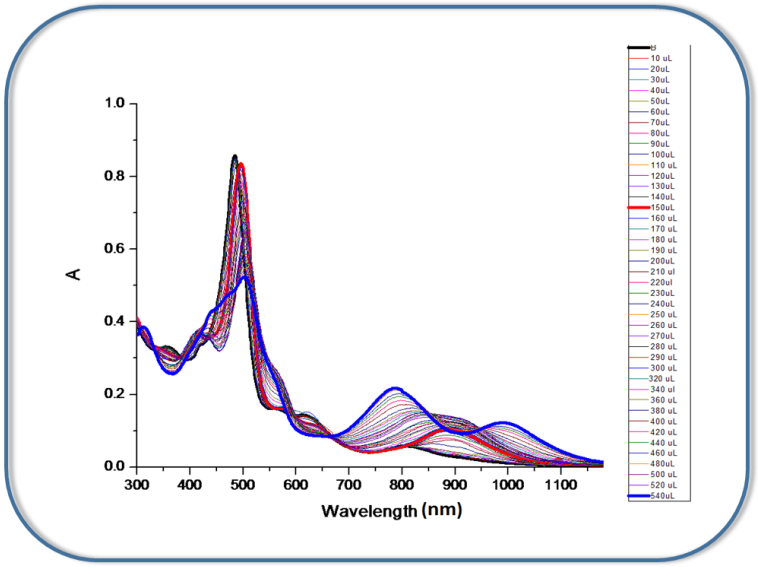

Figure 3.4. Acid titration UV-vis-NIR Spectra of **15** in (TFA/CH_2Cl_2)

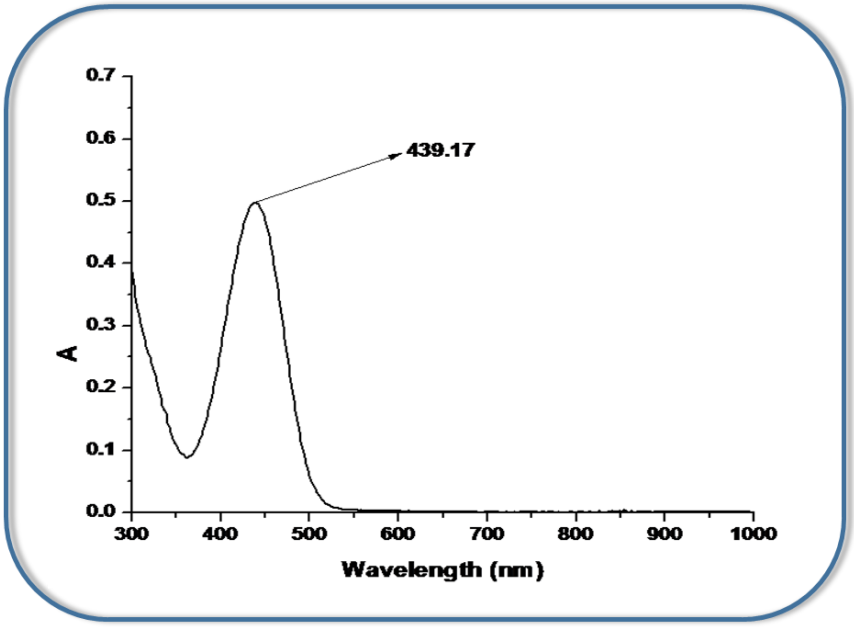

Figure 3.5 Uv-Vis spectrum of **16**

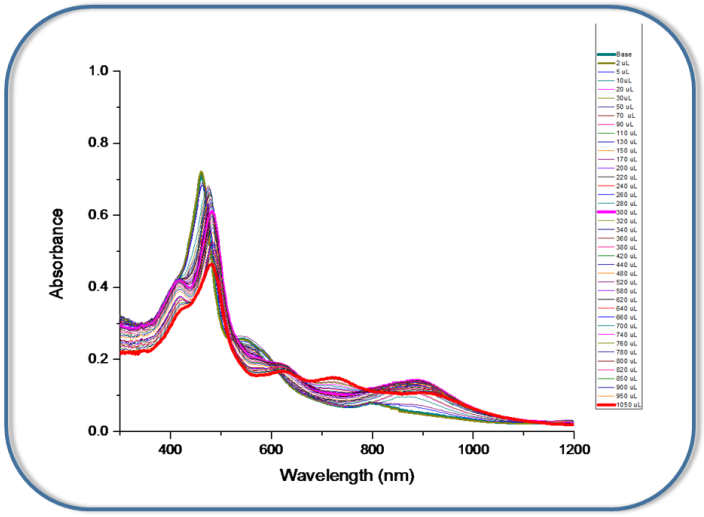

Figure3.6. Acid titration UV-vis-NIR Spectra of **17** in (TFA/CH_2Cl_2)

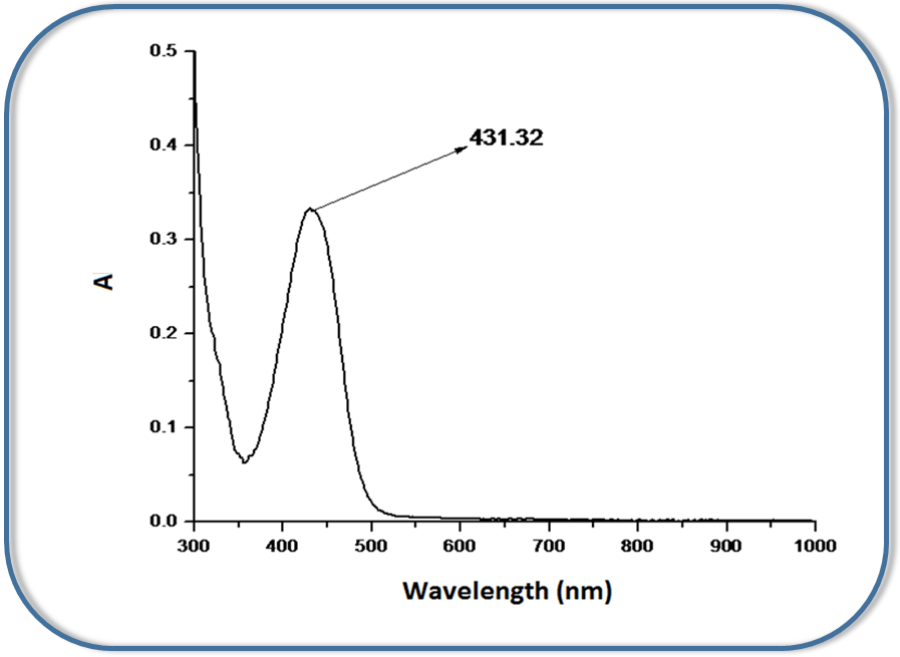

Figure 3.7 Uv-Vis- spectrum of **18**

3.2.2. ^{1}H NMR Study

In conjunction with the electronic absorption spectral patterns, ^{1}H NMR spectroscopic analysis of macrocycles **15** and **17** revealed the presence of an apparent sustained diamagnetic ring current ascribable to the aromatic macrocycle through an [18]π electronic delocalization motif in the free base forms. Due to the characteristic diatropic ring current effect of the macrocycle, the protons inside the macrocycle resonate in the upfield region and the protons on the periphery resonate in the deshielded region.[12]

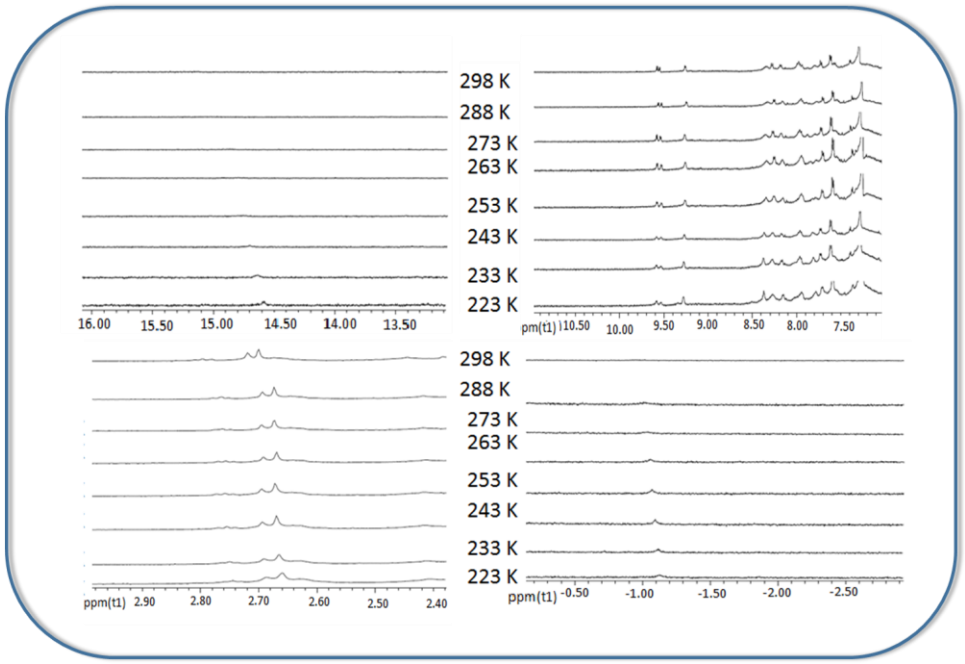

Figure 3.8. Variable temperature ^{1}H NMR Spectra of free base **17** in $CDCl_3$

These later revealed the typical downfield resonances of the outer α-pyrrolic protons and the upfield resonance of the inner β-pyrrolic protons. For both macrocycles **15** and **17**, we could not observe well-split peaks in the ^{1}H-NMR spectra at room temperature owing to macrocyclic fluxionality as a consequence of unconventional α,β connectivities of the pyrrole rings. Only, upon lowering the

temperature to 253 K for **17** (**Fig. 3.8**) and 223 K for **17**, we could observe additional peaks in the most deshielded and in the most shielded region accounting for external ∝-CH and internal β-CH protons of N-confused pyrrole rings respectively.

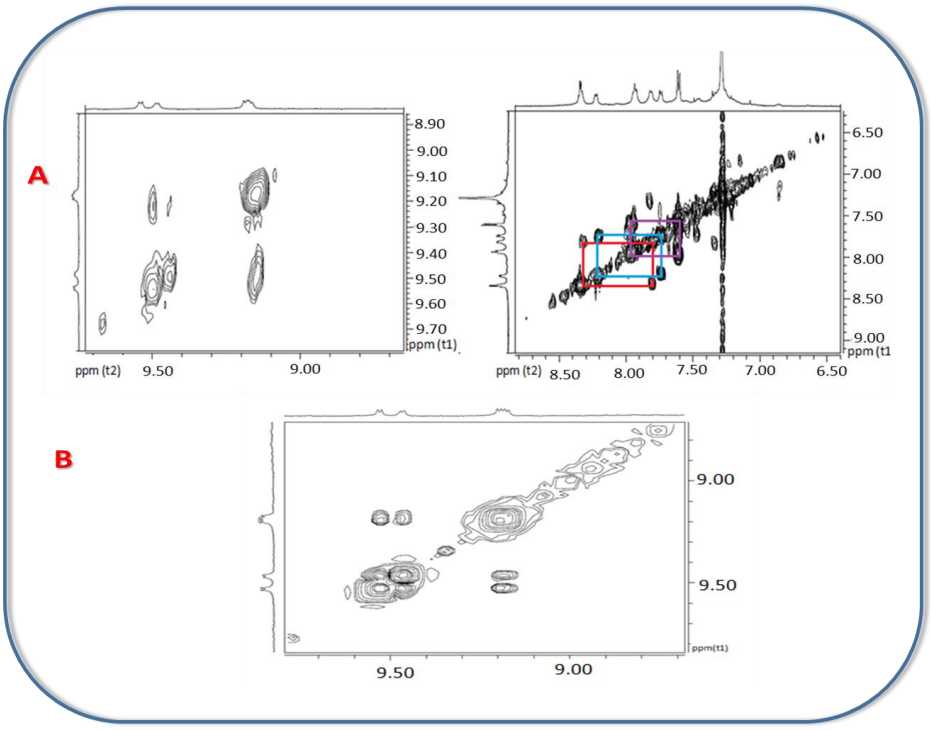

Figure 3.9. 1H -1H 2D COSY NMR spectra of **15** in CDCl3 (A: 298 K; B: 253 K)

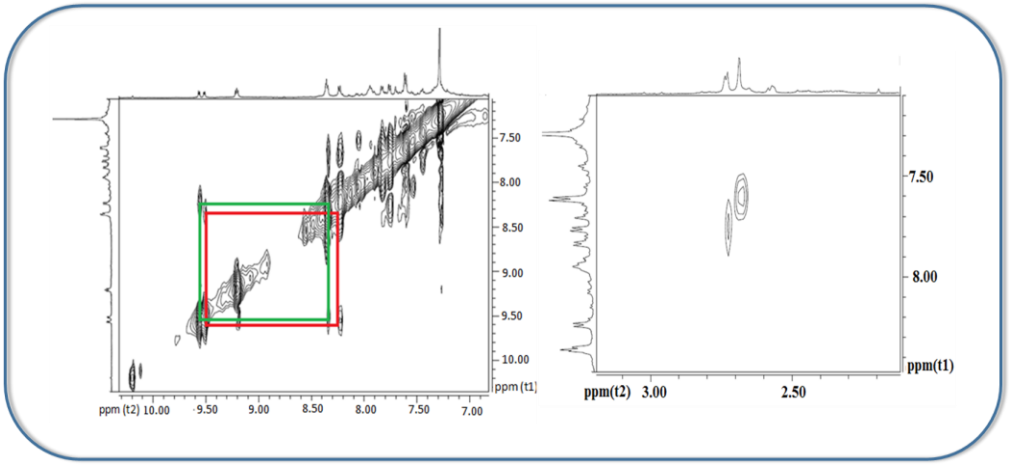

Figure 3.10. 1H -1H 2D ROESY NMR spectra of **15** in $CDCl_3$ at 298 K

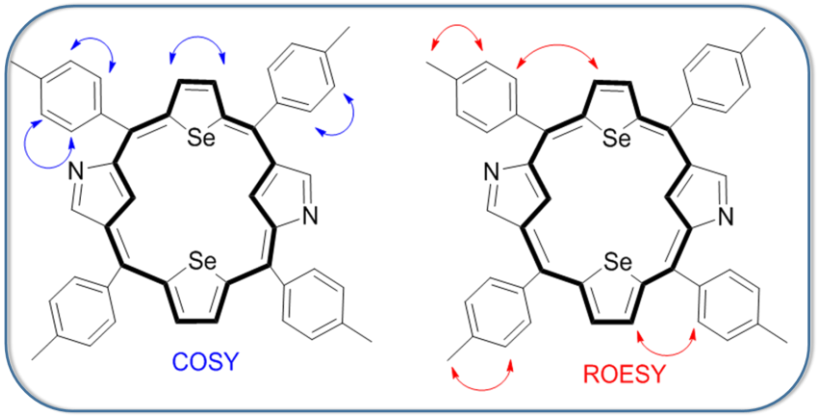

Figure 3.11. Various Scalar and Dipolar couplings observed in **15 in** $CDCl_3$

At 298 K, the observation of two sharp singlets at δ = 2.68 and 2.70 ppm for **15** assignable for the methyl signals of *meso*-tolyl substituents clearly justify the presence of two magnetically non-equivalent *meso*-tolyl substituents. In the 2D ROESY spectra of **15** at 298 K, the two sets of correlations between the peaks at δ = 7.60 and 2.68 ppm and between the peaks at δ = 7.74 and 2.70 ppm clearly indicated that the signals at δ = 7.60 and 7.74 ppm correspond to the m-CH protons of the *meso*-tolyl substituents (**Fig. 3.10**). Furthermore, in the 2D COSY spectra (**Fig. 3.9A**), the correlations between the signals at 7.60 ppm and 7.92 ppm and between the signals at 7.74 ppm and 8.20 ppm reveal the later signals as the *o*-CH protons of the same *meso*-tolyl substituent.

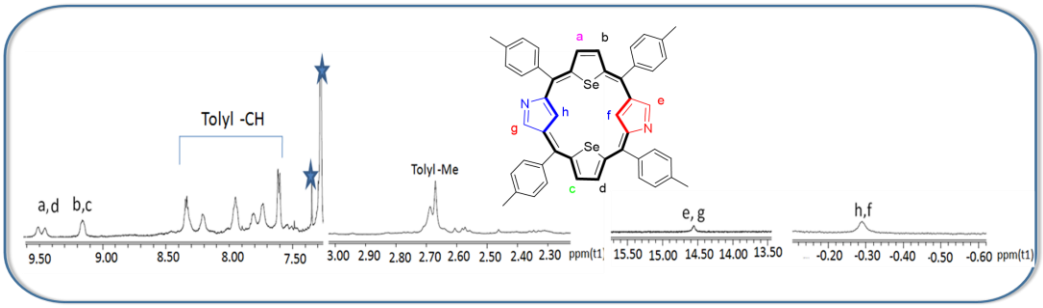

Figure **3.12**. Completely assigned 1H NMR spectra of **15** in $CDCl_3$

There are additional correlations between peaks at δ = 8.34 and 7.81 ppm and δ = 7.92 and 8.20 ppm. In the 2D COSY spectra at 253 K (**Fig. 3.9B**), two correlations in the deshielded region between the doublets at δ = 9.55 and 9.22 ppm and between the doublets at 9.48 ppm and 9.19 ppm indicate the magnetically non-equivalent nature of the two selenophene rings with the observation of four β-CH protons. The final assignment of selenophene β-CHs has been further confirmed from the observation of the two sets of cross-peaks between a pair of signals at δ = 9.55 and 8.34 ppm and the second pair of signals at δ = 9.48 and 8.20 ppm in the 2D ROESY spectra at 298 K (**Fig. 3.10**).

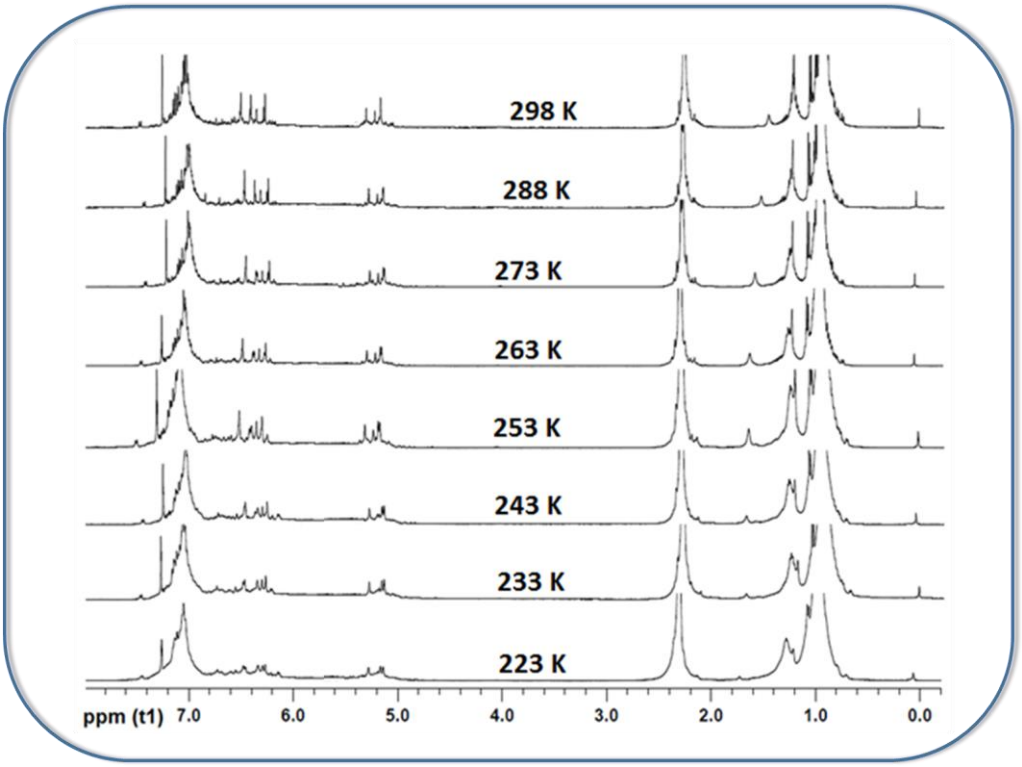

Figure 3.13. Variable temperature ^{1}H NMR Spectra of free base **16** in $CDCl_3$

At 253 K, the observation of a singlet in the highly deshielded region at ca. δ = 14.56 ppm (2H outer pyrrole α-H) and another singlet in the up-field region at ca. δ = −0.29 ppm (2H, inner pyrrole β-H) with Δδ = 14.85 ppm for **15** (**Fig. 3.12**) and

Δδ = 15.65 ppm for **17**(**Fig. 3.20–3.21**) (difference in the chemical shift value of the most deshielded and the most shielded protons),[13] clearly indicate the strong aromatic nature of **15** and **17** in the free base form. The observation of a single signal for both outer α-CHs in the most deshielded region and a single signal in the shielded zone for both inner β-CHs of the N-confused pyrrole rings could be due to the fact that both these rings are deviated from the mean macrocyclic plane (defined through four meso-carbon atoms) to the same extent on both sides and hence experience the macrocyclic diamagnetic ring current to an equal extent in the solution state. The ^{1}H NMR spectral patterns for macrocycles **16** (**Fig.3.14-3.19**) and **18** (**Fig**. **3.22–3.28**) clearly reveal the presence of four meso-CH protons with a lack of π-conjugation in line with their UV-vis spectral patterns.

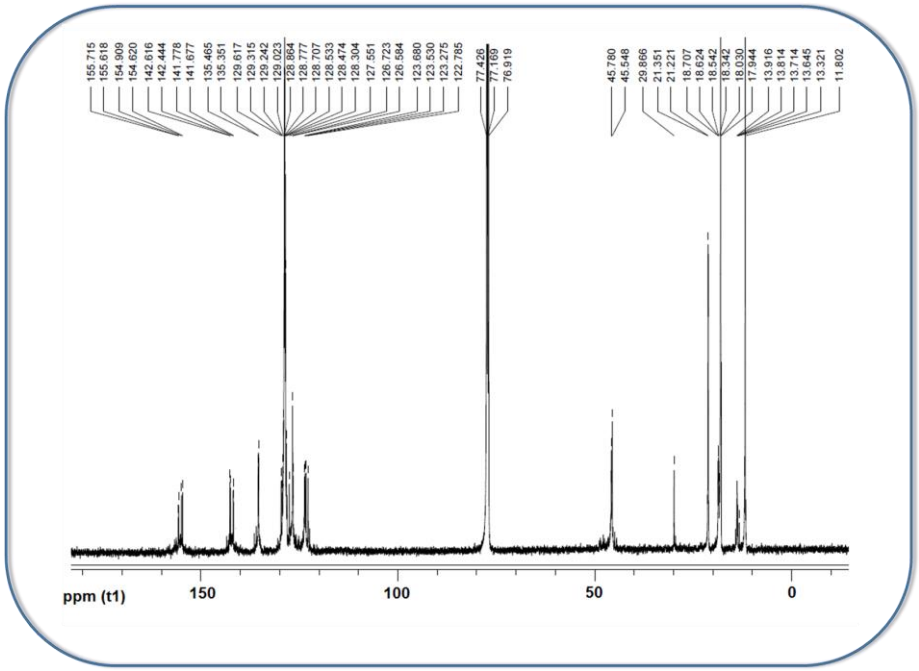

Figure 3.14. ^{13}C NMR Spectra of Free base **16** in $CDCl_3$ at 298 K

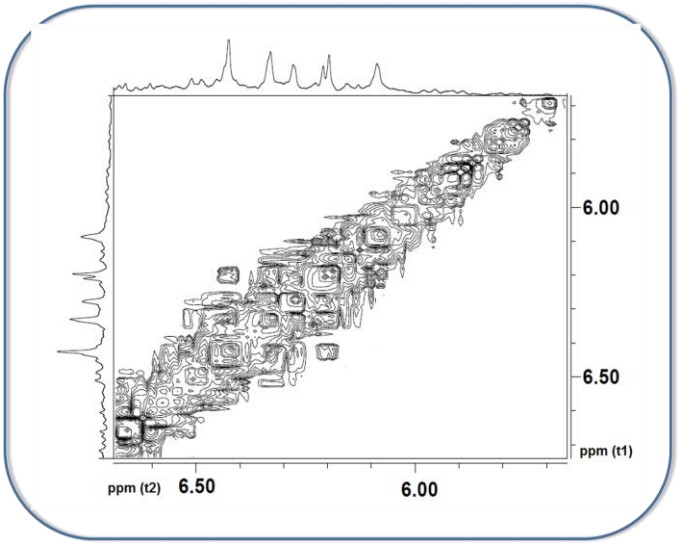

Figure 3.15. .^{1}H -^{1}H 2D COSY Spectra of free base **16** at 298 K

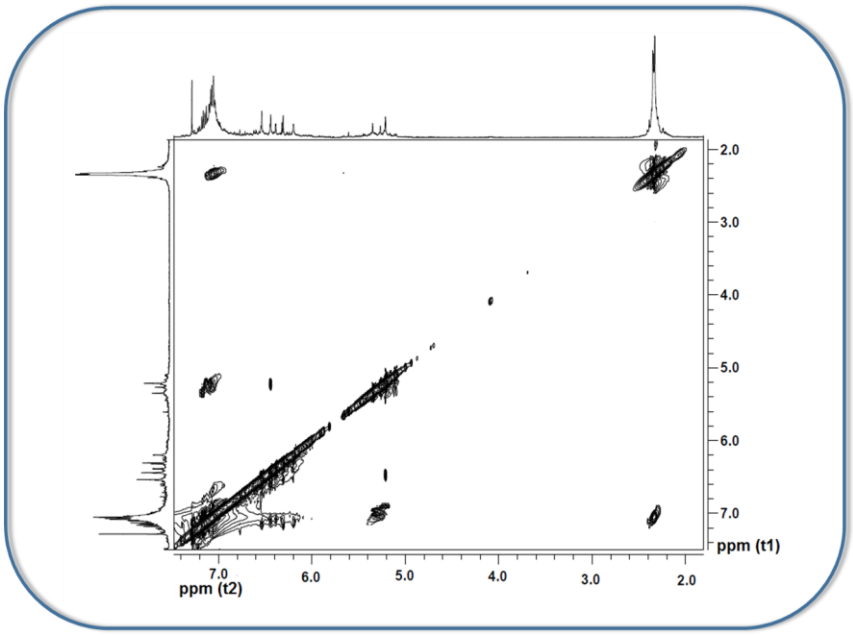

Figure 3.16 .^{1}H -^{1}H 2D ROESY Spectra at 298 K of free base **16**

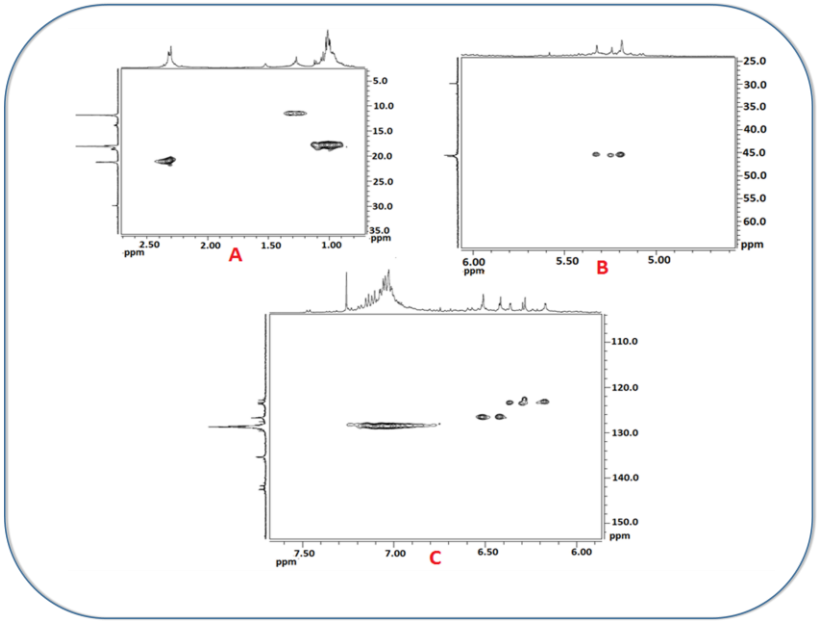

Figure 3.17 .^{1}H -^{13}C HSQC Spectra of free base **16** at 298 K

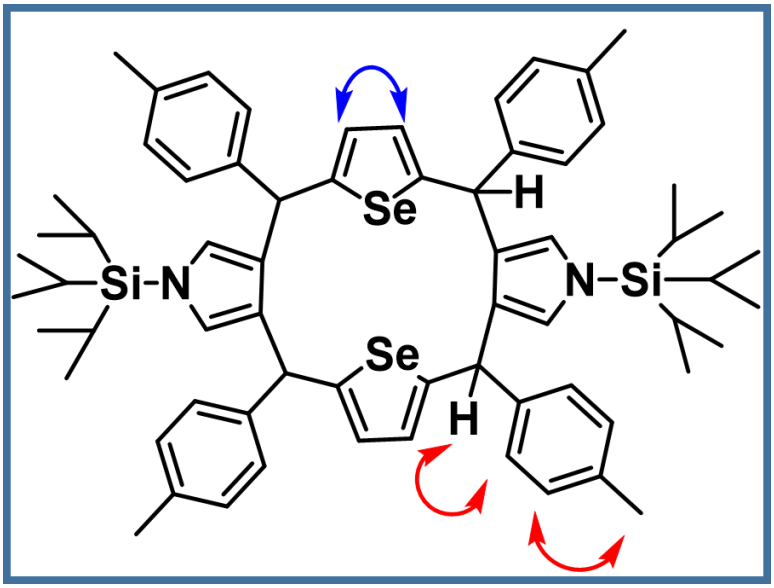

Figure 3.18. Various Scalar and Dipolar Couplings observed for free base **16**

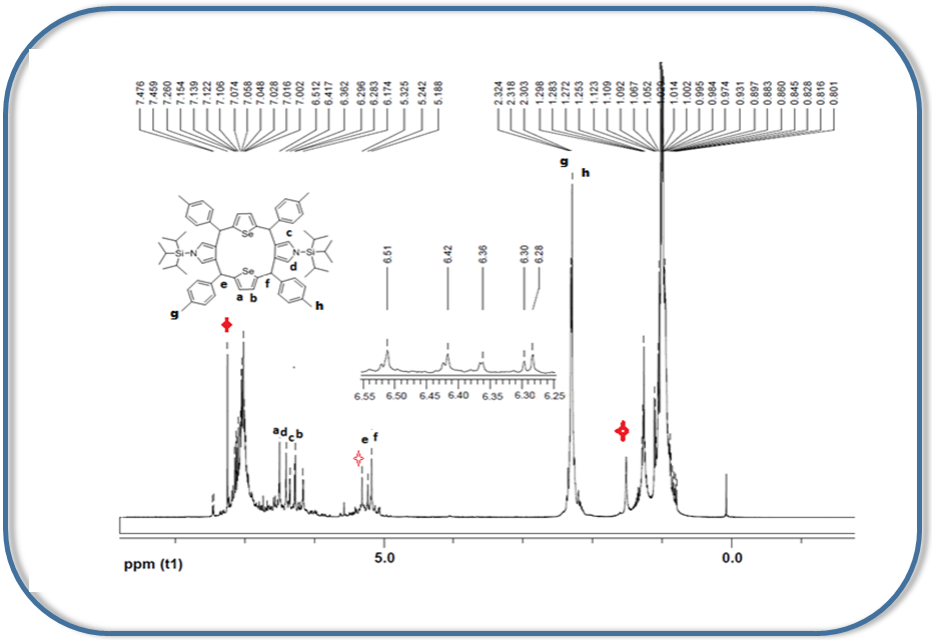

Figure 3.19. Completely assigned ^{1}H NMR Spectra of free base **16** in $CDCl_3$

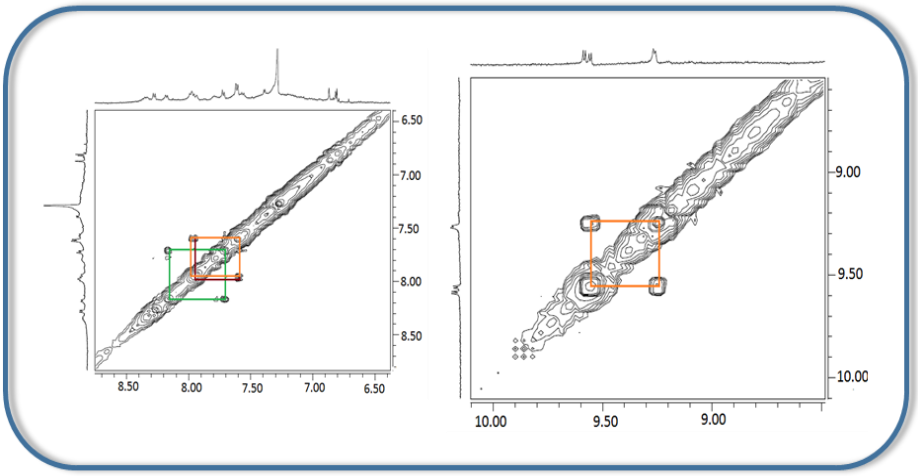

Figure 3.20. ^{1}H -^{1}H 2D COSY Spectra at 298 K of free base **17**

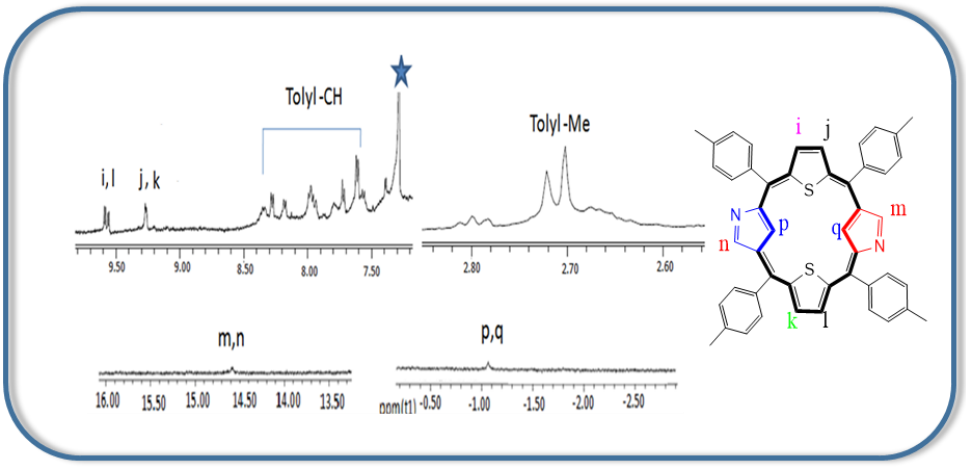

Figure 3.21. Complete assignment of ^{1}H NMR Spectra of free base **17**

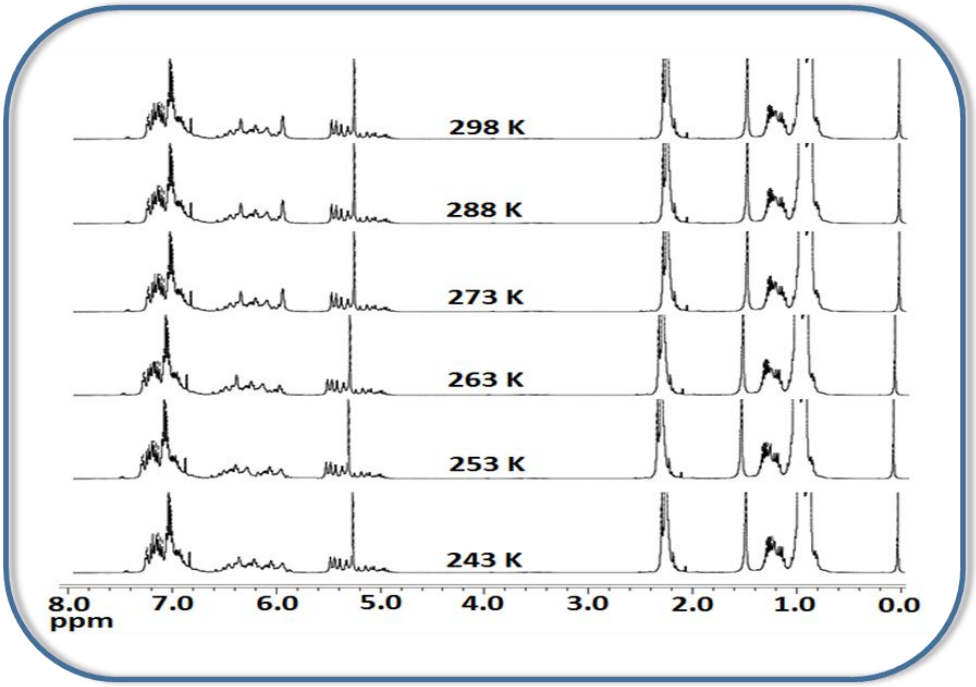

Figure 3.22. Variable temperature ^{1}H NMR Spectra of freebase **18** in CD_2Cl_2

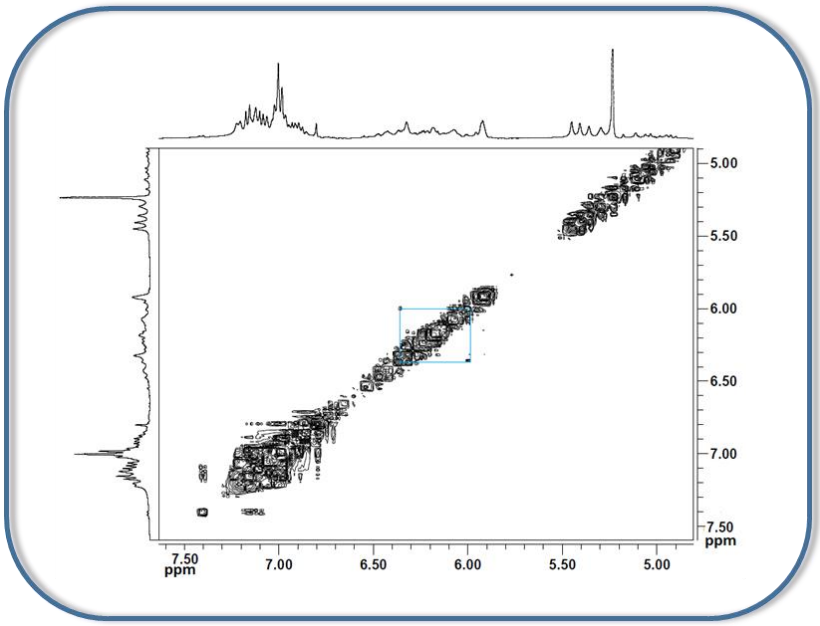

Figure 3.23. ^{1}H -^{1}H 2D COSY Spectra at 298 K of free base **18**

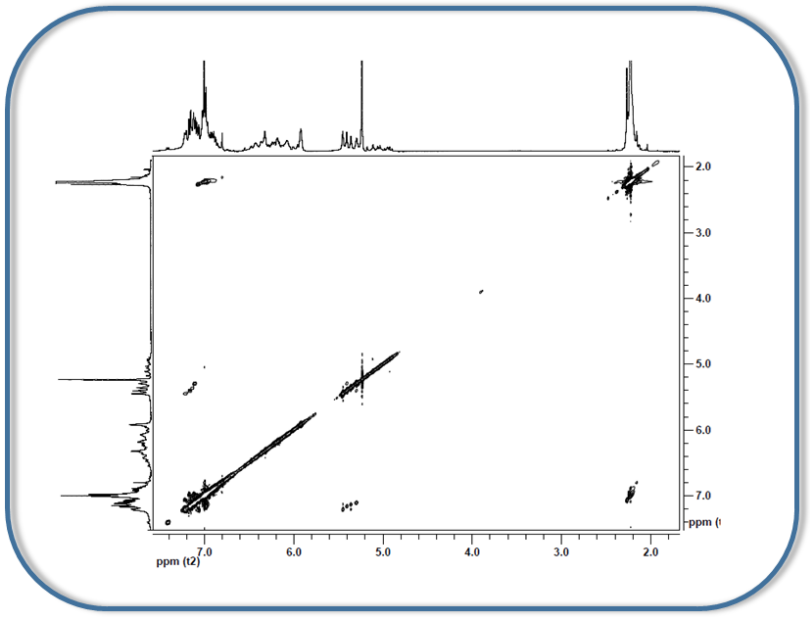

Figure3.24. ^{1}H -^{1}H 2D ROESY Spectra at 298 K of free base **18**

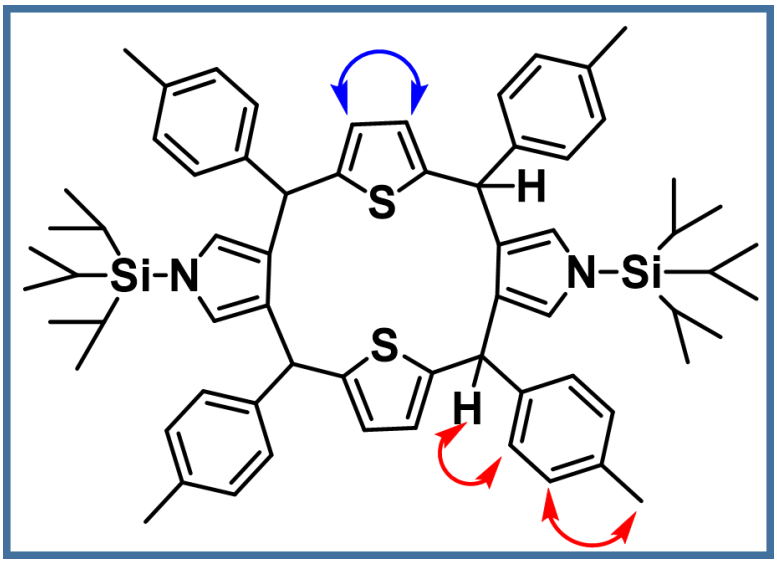

Figure 3.25. Various Scalar and Dipolar couplings of Free base of **18**

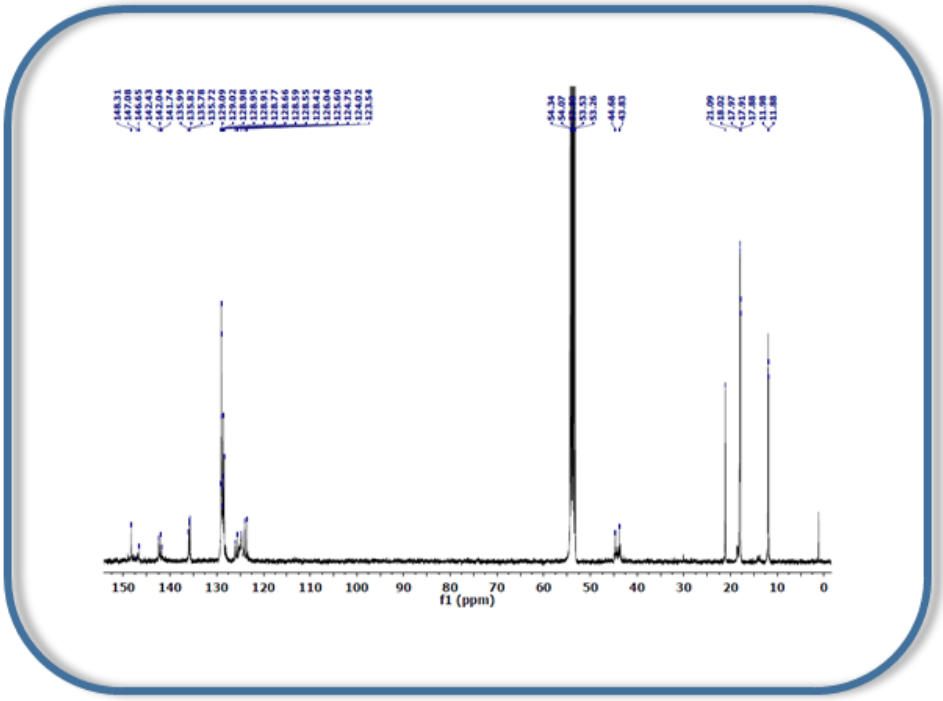

Figure 3.26. ^{13}C NMR Spectra of Free base **18**in CD_2Cl_2

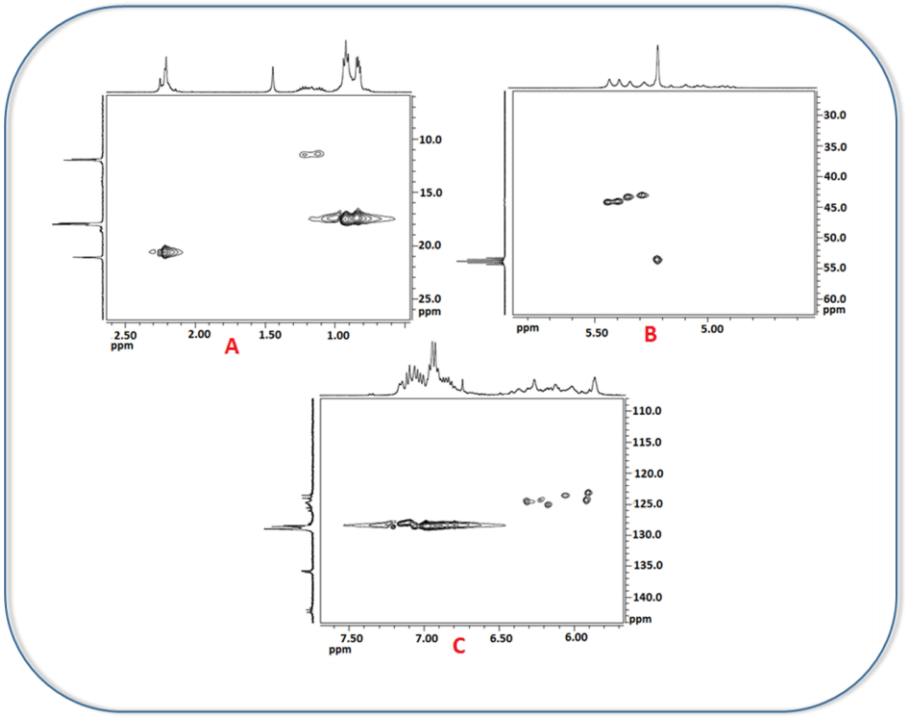

Figure 3.27 .^{1}H -^{13}C 2D HSQC Spectra at 298 K of free base **18**

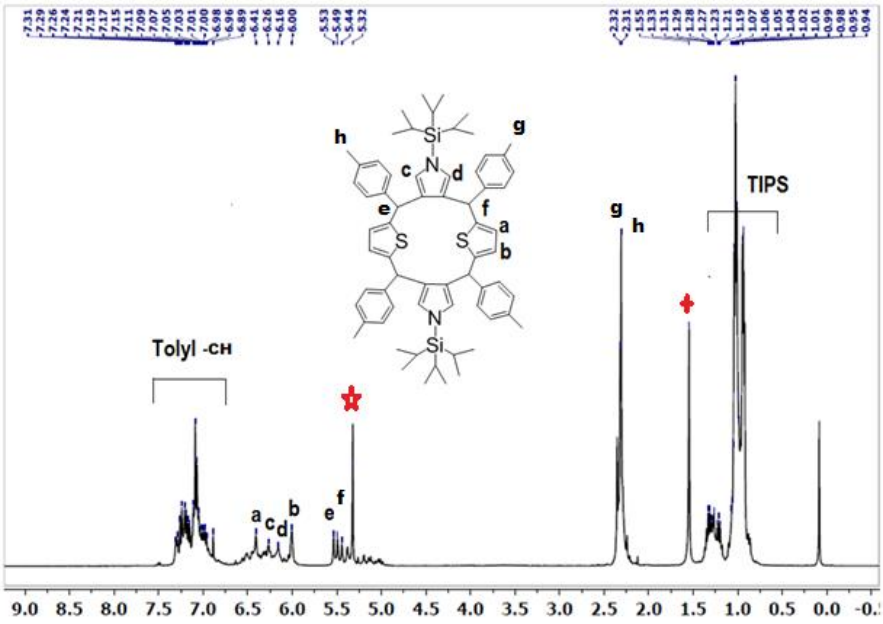

Figure 3.28. Complete assignment of ^{1}H NMR Spectra of Free base **18** in $CDCl_3$

3.2.3. Cyclic voltammetry and FMO

The electronic properties of the new macrocycles have been probed with cyclic voltammetry and differential pulse voltammetry in dichloromethane using tetrabutylammonium hexafluorophosphate as the supporting electrolyte. Macrocycle **15** exhibited one quasi reversible oxidation couple at 1.09 V followed by two irreversible oxidation peaks at 1.28 V and 1.53 V, while there were three irreversible reduction peaks (−0.60 V, −0.83 V, and −1.05 V) with the HOMO–LUMO energy gap of 1.69 V (**Fig**. **3.29**). The electrochemical behavior and the HOMO–LUMO energy gap value of **15** are in trend with the doubly N-confused porphyrin.[14] and macrocycle **16** exhibited one irreversible reduction peak -0.914 and three irreversible oxidation peaks (1.263V, 1.507V and 1.683V) with HOMO-LUMO energy gap 2.17 V. For macrocycle **17**, electrochemical studies could not be carried out due to low solubility.

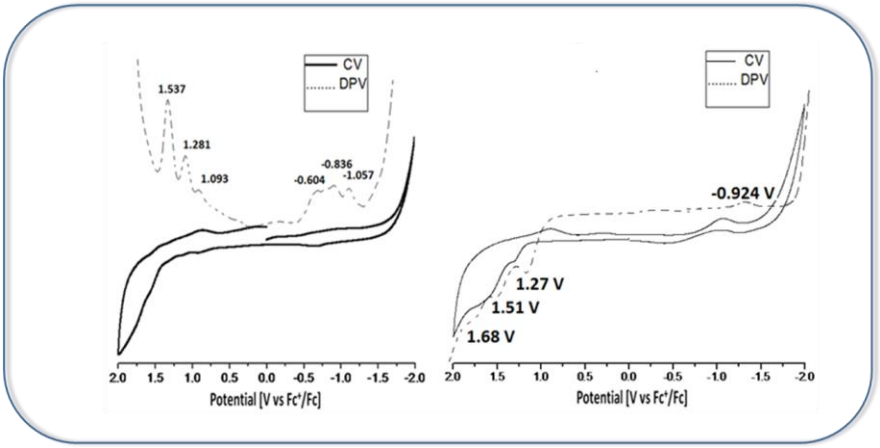

Figure 3.29. Cyclic Voltammogram of free base**15** (left) and **16** (right)

For macrocycles **15/17** and **16/18**, failure to obtain a good single crystal suitable for X-ray diffraction in the free base form and/or the protonated form forced us to resort to geometry optimization based on ^{1}H NMR spectra to arrive at the proposed structure of the macrocycles based on the density functional theory (DFT)-

formalism.[15] **Fig**. **3.30** summarizes all plausible conformers for macrocycles **15** and **17**. It is to be noted that compared to diselena/dithia porphyrins (Se_2TTP/ S_2TTP),[16] the corresponding singly-N-confused porphyrins (Se_2CTTP/S_2CTTP)[17] are energetically higher by 14–16 kcal mol−1 (**Fig. 3.31**) and on a similar note, the diselena/dithia doubly N-confused porphyrins (**15**/**17**) are found to be energetically higher by 14–16 kcal mol^{-1} compared to their singly N-confused isomers (Se_2CTTP/S_2CTTP) (**Fig. 3.31**); this is in line with the fact that multiple N-confusion leads to a significant loss of thermodynamic stability.[18]

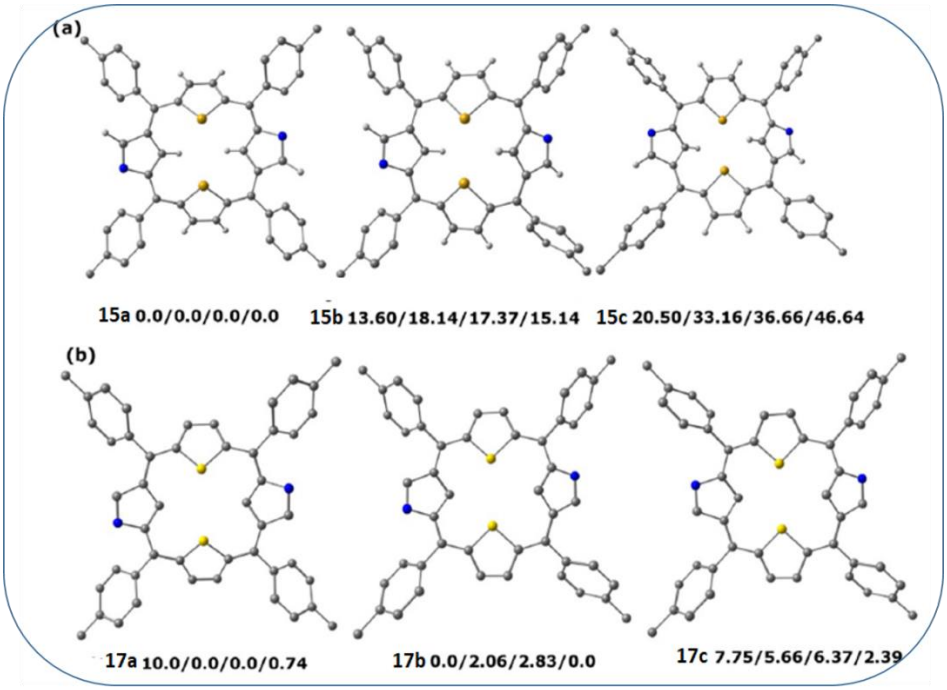

Figure 3.30. Plausible conformers of **15** (a) and **17** (b). The relative free energies (ΔG, kJ/mol) of conformers are obtained at B1b/B1c/B2/B2a level of theories. For the sake of calrity, the hydrogen atoms are omitted.

The most stable optimized structures of free bases **15** and **17** showed near planar geometries without any ring inversion and the mean plane deviation (MPD) values of N-confused pyrrole rings with respect to four *meso* carbon atoms are 25.29 and 25.84 Å. The anti-conformation of N-confused porphyrins **15** and **17** are more

stable compared to the syn-conformation obtained at lower and higher basis sets, with dispersion including the WB97XD functional[19] and B3LYP functional[20] (**Fig. 3.30**.)

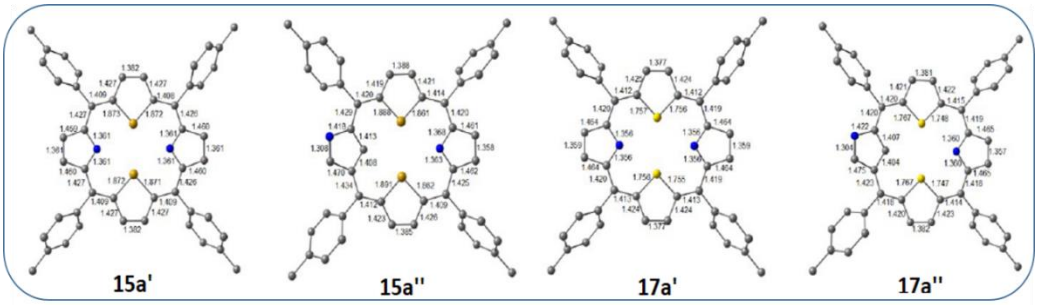

Figure **3.31**. Key bond lengths for the free base form of Diselena porphyrin (Se2TTP, **15a'**), Diselena singly Nconfused porphyrin (Se2CTTP, **15a''**). The relative free energies (ΔG, kJ/mol) of **15a'** and **15a''** are 30.09 and 16.89 kcal/mol lower than Diselena doubly N-confused porphyrin, **15a**. Dithia porphyrin (S2TTP, **17a'**) and Dithia singly N-confused porphyrin (S2CTTP, **17a''**) are 30.01 and 14.67 kcal/mol lower than Dithia doubly N-confused porphyrin **17a** at B1b level of theory. For the sake of calrity, the hydrogen atoms are omitted.

A plausible reason for the stability of the anti-conformation of *trans*-doubly N-confused porphyrins **15** and **17** is due to the minimization of steric repulsions between N-confused pyrrole inner β-CHs with the selenium and sulfur lone pair electrons. To gain an insight into the origin of intense NIR absorption bands of **15** and **17**, we performed time-dependent (TD)-DFT[21] calculations at the B3LYP-6-311+G (d) level of theory. The simulated UV-vis-NIR spectra in the presence of dichloromethane for **15** and **17** were found to coincide with the steadystate absorption spectra (**Fig.3.44,3.47, Table3.1, 3.4**). On the basis of calculations, the electronic vertical transitions corresponding to the Soret-like band and the Q type band observed in the steady-state absorption spectra of **15** and **17** mainly involve HOMO−3, HOMO−1, HOMO to LUMO and LUMO+1 orbitals that correspond o lone

pair orbital of Se/N, a1u, a2u and eg type orbitals (**Table3.1, 3.4, Fig.3.3),** While the N-confused pyrrole rings and thiophene/selenophene rings results in mixing of π CH and lone pair orbitals of S/Se to a1u and a2u orbitals and breaks the symmetry of TTP that results in the splitting of Q bands that are red-shifted further in comparison to Se_2TTP/S_2TTP.

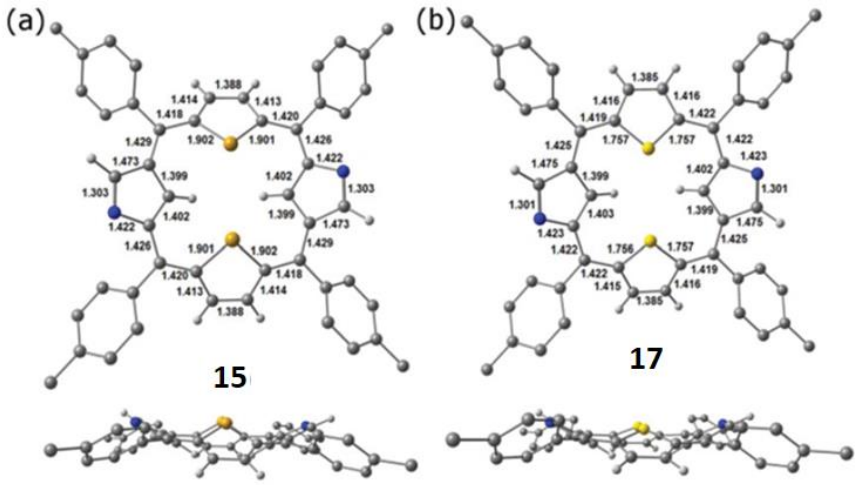

Figure **3.32**. Optimized structure and key bond length parameters of **15** (a: top view, side view) and **17** (b: top view, side view) at B3LYP/6-311+G (d) level of theory. Hydrogen atoms are omitted for clarity.

The band in the NIR region is the Q type band originating due to the S0–S1 transition of the lone pair orbital of Se/S with an a2u type orbital to eg orbital of **15/17**. These orbitals are all characterized by delocalized π-electron densities through an 18π electronic circuit. On a similar note, upon protonation, the number of bands in the visible and NIR region mainly involves delocalized π orbitals summarizes(**Fig.3.45,3.46, Table3.2,-3.3, Table3.5,-3.6**). **Fig. 3.33** all plausible conformers for macrocycles **16** and **18**. The most stable optimized structure of free bases **16** and **18** (**Fig. 3.34**) showed highly puckered geometry where the selenophene/thiophene rings are stacked one over the other and TIPS-pyrrole rings are the backbone to the ladder-like structure. Additionally, the TD-DFT absorption

spectra are in accordance with the steady state absorption for **16** and **18** (**Fig.3.50,3.51, Table3.7,-3.8)**

. The aromaticity of **15** and **17** has been well supported by the NICS (0) value[22] at the centre of the macrocycles as −8.67 ppm and −8.19 ppm respectively obtained with gauge independent atomic orbital (GIAO) method based on the optimized geometries (**Fig. 3.37**).

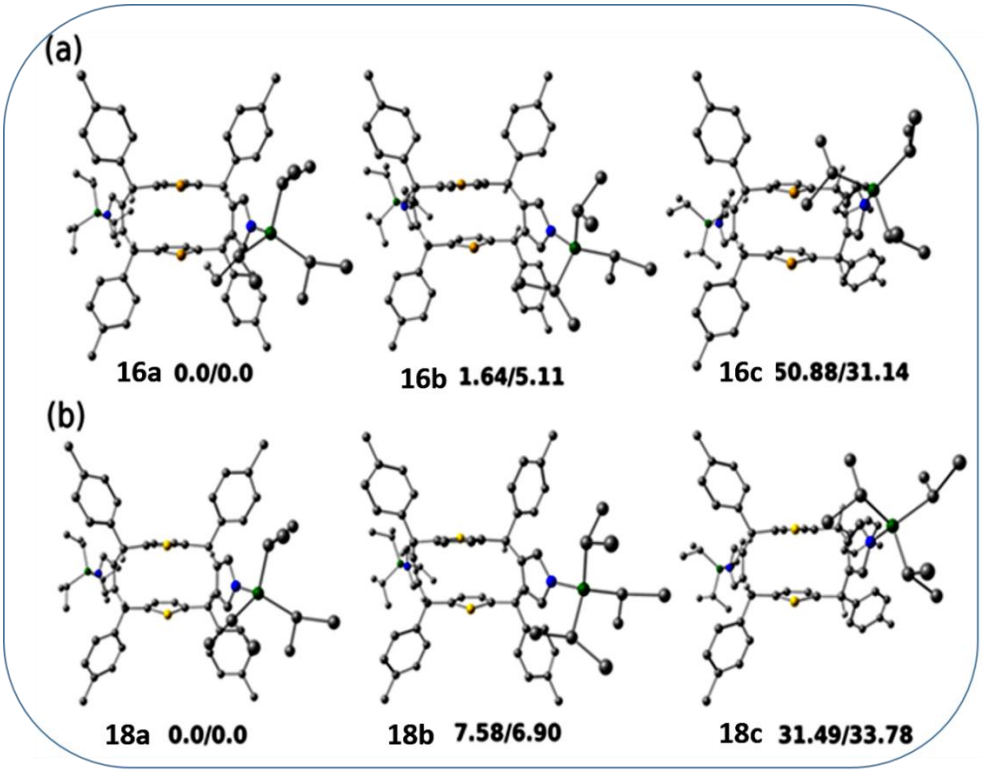

Figure 3.33. Plausible conformers of **16** and **18**. The relative free energies (ΔG, kJ/mol) of conformers are obtained at B1b/B1c/B2/B2alevel of theories

Furthermore, the calculated Anisotropy of the Current-Induced Density (ACID)[23] plots also strongly support the aromaticity of these macrocycles. In the ACID plot (**Fig. 3.35**), the distinct clockwise ring current visualized the aromatic nature of both macrocycles **15** and **17**. Most importantly, the calculated HOMA (Harmonic Oscillator Model of Aromaticity) values of free bases **15** and **17** are 0.808

and 0.813, respectively (**Fig. 3.36**), indicating the aromatic nature of both the macrocycles.[24]

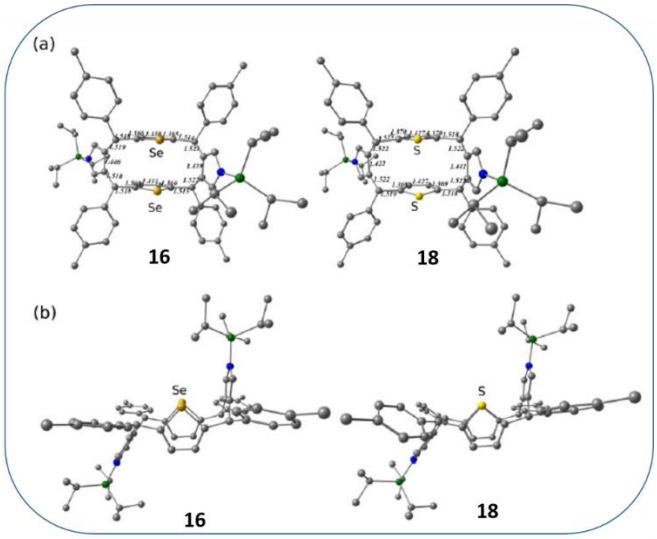

Figure 3.34. (a) Top view of optimized geometries and key bond lengthparameters (Å) of free base form of **16** and **18** at **B1**b level of theory. (b) Side view of free base form of **16** and **18**. For the sake of clarity the hydrogen atoms are not shown here.

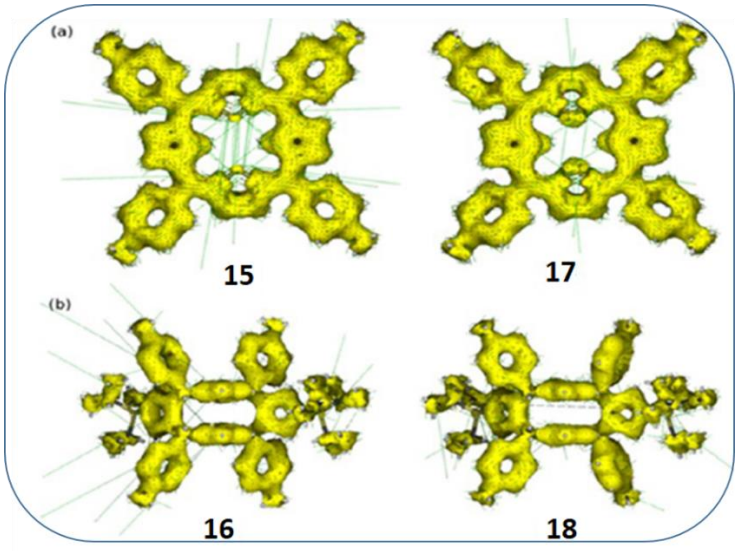

Figure 3.35. AICD plots of the free base form of (a) **15**, **17** (b) **16, 18** at **B1b** level of theory

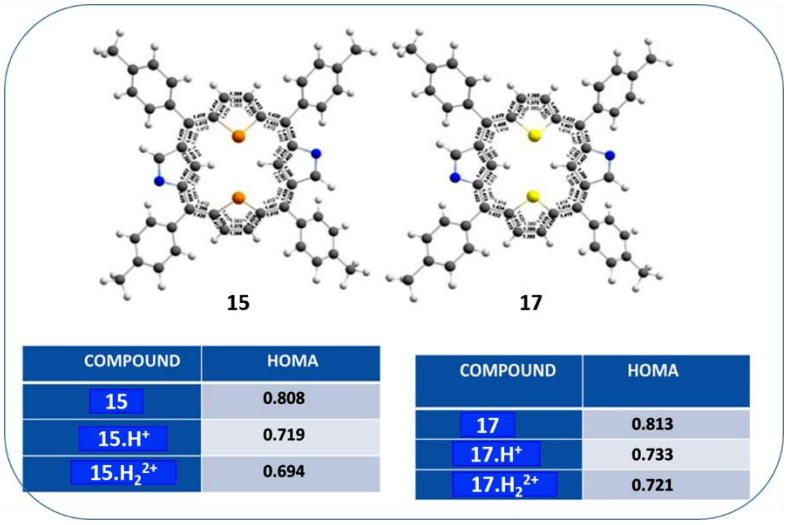

COMPOUND	HOMA
15	0.808
15.H⁺	0.719
15.H_2^{2+}	0.694

COMPOUND	HOMA
17	0.813
17.H⁺	0.733
17.H_2^{2+}	0.721

Figure 3.36. Optimized geometries and key bond length parameters (Å) of **15** and **17** in freebase form, protonated and doubly protonated forms at B3LYP/6-311+G* level of theory.

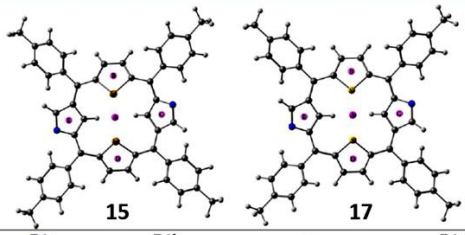

15	B1c	B1b	17	B1c	B1b
A(-5)	-2.415	-2.321	A(-5)	-2.529	-2.401
A(-4)	-3.538	-3.417	A(-4)	-3.705	-3.532
A(-3)	-5.176	-5.027	A(-3)	-5.387	-5.158
A(-2)	-7.166	-7.024	A(-2)	-7.344	-7.098
A(-1)	-8.578	-8.568	A(-1)	-8.551	-8.367
A(0)	-8.503	-8.671	A(0)	-8.289	-8.190
A(1)	-7.252	-7.458	A(1)	-8.387	-8.406
A(2)	-5.876	-5.816	A(2)	-6.920	-6.751
A(3)	-4.374	-4.111	A(3)	-4.863	-4.654
A(4)	-3.015	-2.823	A(4)	-3.275	-3.122
A(5)	-2.065	-1.928	A(5)	-2.065	-2.103
B	-14.90	-16.01	B	-14.94	-16.06
C	3.527	3.239	C	3.940	3.701
D	-14.90	16.01	D	14.96	-16.04
E	3.527	-3.239	E	3.939	3.702

Figure 3.37. NICS value of free base form of **10** and **12** at B1c [B3LYP/6-311+G(d)] and B1b [B3LYP/6-31G(d,p)]level of theory. A represents the center of macrocycle ring including all the core atoms. While the value in theparenthesis represent the position of dummy atom above and below the plane in angstroms. B and D represents centerof thioselenium/thiosulfur rings. C and E represent the Nconfused pyrrole rings.

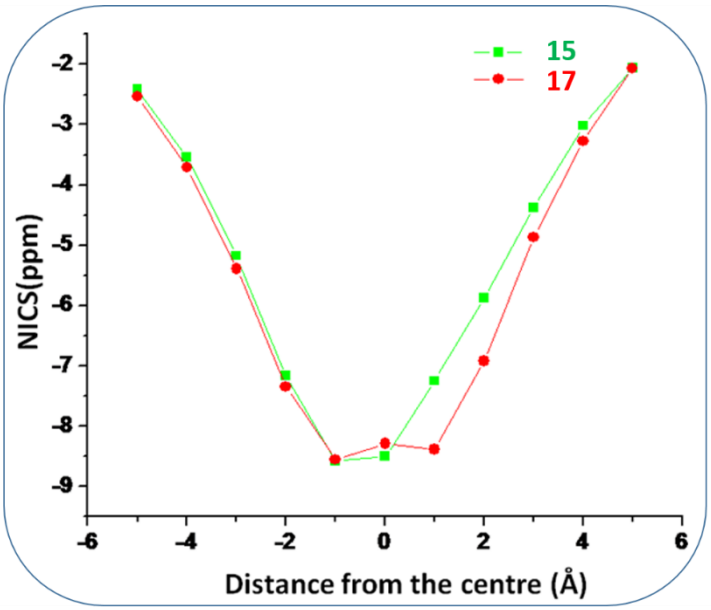

Figure 3.38. The plot of chemical shift *vs* distance of probe for **15** and **17**

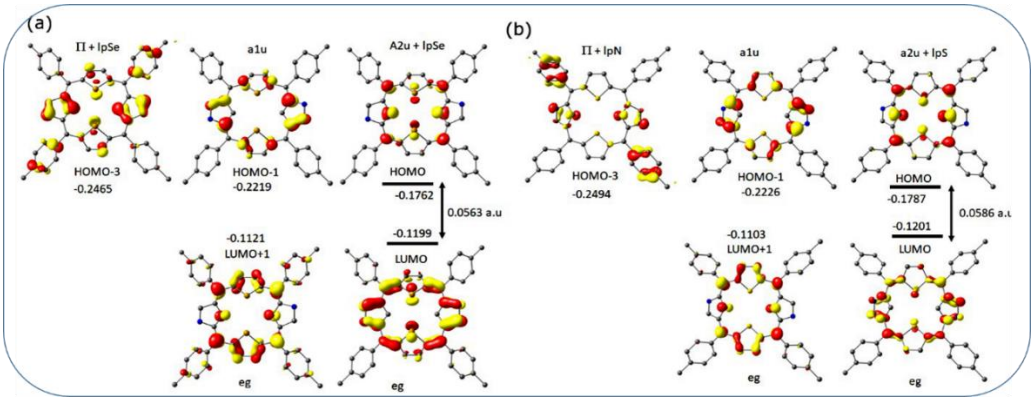

Figure 3.39. Frontier molecular orbitals for DFT optimized structures of (a) **10** and (b) **12,** at B3LYP/6-311+G (d) level of theory in presence of solvent. The HOMO and LUMO orbitals and the energy gap is also mentioned in a.u.

3.3. Conclusion and Future aspects:

In conclusion, syntheses of heteroatom-containing *trans*-Doubly mutant heteroannulenes and *meso*-saturated heterocyclic macrocycles with strong NIR absorption have been achieved for the very first time in high yields by use of appropriate precursors. The exclusive product formation under specific catalytic

conditions in high yields, complete structural characterization using 1D, 2D NMR, UV-Visible spectroscopy, cyclic voltammetry and in-depth theoretical analysis are the highlights in this chapter. NIR-absorbing/-emitting systems are of current scientific interest owing to their biomedical applications such as photodynamic therapy dyes, tissue diagnostics and microscopic imaging agents. We strongly hope that the availability of multigram quantities of these new core modified trans-doubly N-confused porphyrins will allow further exploitation of rich chemistry in terms of their coordination behavior towards transition metals and their use as catalysts for organic transformations. Such thriving research is currently under progress from our laboratory.

3.4. Experimental Section

General Synthetic Procedure for Compound 15 and 16.

Under nitrogen atmosphere and in dark condition a solution of 186 mg of compound **P2** (0.5 mmol), 1-(triisoppropylsilyl) pyrrole1 23μL(0.5 mmol) **P1** and boron trifluoride diethyl etharate(11μL) in 250 mL dry dichloromethane was stirred for 1hour. Then, chloranil (307 mg, 1.25 mmol) was added and opened to air and the mixture was refluxed for another 1 hour. The solvent was removed under reduced pressure and the compound was filtered by basic alumina column followed by repeated silica gel column chromatography in the mixture of 20% dichloromethane - hexane solution the compound **16** was obtained and with 50% dichloromethane - hexane solution the compound **15** was obtained. After recrystallization, the compound **15** and **16** were obtained as dark greenish crystal and yellow amorphous compound respectively.

Compound **15:** Yield. ~ 32mg (8 %).^{1}H NMR (500 MHz, $CDCl_3$, 298 K, δ[ppm], TMS): 2.68-2.70(s, tolyl Me); 7.60-8.34 (d, 16H, tolyl-CH); 9.16 (d, 1H, selenophene β-H , ^{3}J =5 Hz); 9.18 (d, 1H, selenophene β-H , ^{3}J =6 Hz); 9.48 (d, 1H, selenophene β-H , ^{3}J =4.5

Hz); 9.53 (d, 1H, selenophene β-H , ^{3}J =5Hz) ^{1}H NMR (500 MHz, $CDCl_3$, 243 K δ[ppm], TMS): -0.29 (brs, 2H,inner pyrrole β-H); 14.56 (brs, 2H, outer pyrrole α-H);. MALDI-TOF MS (m/z): 801.571 (800.1202 calc. for $[C_{48}H_{36}N_2Se_2]^+$). UV-Vis (CH_2Cl_2, λ [nm], (ϵ [$M^{-1}cm^{-1}$]), 298K): 484.62,(1.61x10^4); 562.38 (3.2 x10^3); 616.38 (2.8 x10^3); 804.61 (1.17 x10^3); [(UV-VIS [CH_2Cl_2, 10% TFA/CH_2Cl_2, λ [nm],(ϵ [$M^{-1}cm^{-1}$]), 298K)]: 502.91 (1.04 x10^4);788.45 (4.35 x10^3) ; 991.92 (2.45 x10^3).

Compound **16:** Yield. ~56mg (10%).HRMS (m/z):1118.898 (1118.4347 calc. for $[C_{66}H_{82}N_2Se_2Si_2]^+$); UV-Vis ($CH_2Cl_2$, λ [nm], (ϵ [$M^{-1}cm^{-1}$]), 298K): 439.17(1.45 x103). NMR (500 MHz, $CDCl_3$, 298 K, δ[ppm], TMS):6.98-7.13 (m, 16H, tolyl-CH); 6.51 (brs, 2H, selenophene β-H); 6.41 (s, 2H, α-H of TIPS- Pyrrole); 6.36 (s, 2H, α-H of TIPS-Pyrrole); 6.28 (d, 2H, selenophene β-H ^{3}J =6.5 Hz); 5.24 (s, 2H, *meso*-CH); 5.18 (s, 2H, *meso*-CH); 2.32(s, 6H, tolyl Me); 2.30(s, 6H, tolyl Me); 1.27-1.28 (m, 6H, TIPS–CH);0.92-1.12(m,36H,TIPS-CH_3).
^{13}CNMR(125MHz,$CDCl_3$,δ[ppm]):11.80,13.21,13.64,13.71,13.81,13.91,17.94,18.03, 18.34,18.54,18.62,18.70,21.22,21.35,29.86,45.54,45.78,45.82,122.78,123.27,123.53,123.68,126.58,126.72,127.55,128.30,128.47,128.53,128.77,128.86,129.02,129.24,129.31,129.61,133.35,133.46,141.67,141.77,142.44,142.61,154.62,154.90,155.61, 155.71.

General Synthetic Procedure for Compound 17 and 18.

Under nitrogen atmosphere and in dark condition a solution of 162.2 mg of compound **P3** (0.5 mmol), 1-(triisoppropylsilyl) pyrrole **P1** 123μL (0.5 mmol) and boron trifluoride diethyl etharate(11μL) in 250 mL dry dichloromethane was stirred for 1hour. Then, chloranil (307 mg, 1.25 mmol) was added and opened to air and the mixture was refluxed for another 1 hour. The solvent was removed under reduced compound was filtered by basic alumina column followed by repeated silica gel column chromatography in the mixture of 30% dichloromethane - hexane solution the compound **18** was obtained and with 70% dichloromethane - hexane solution

the compound **17** was obtained. After recrystallization, the compound **17** and **18** were obtained as dark greenish crystal and yellow amorphous compound respectively.

Compound **17**: Yield. ~35mg (~10%).^{1}H NMR (500MHz, $CDCl_3$, 298K, δ [ppm], TMS): 2.70-2.72 (s, tolyl Me); 7.60-8.35 (d, 16H, tolyl-CH); 9.26-9.27 (d, thiophene β-H ,^{3}J =5.5 Hz); 9.53 (d, 1H, thiophene β-H ,^{3}J=4.5 Hz); 9.55 (d, 1H, thiophene β-H ,^{3}J=5 Hz); ^{1}H NMR (500 MHz, $CDCl_3$, 243 K δ [ppm], TMS): -01.09 (brs, 2H,inner pyrrole β-H); 14.56 (brs, 2H, outer pyrrole α-H);.**MALDI-TOFMS** (m/z):705.646 (704.2320 Calc. for $[C_{48}H_{36}N_2S_2]^+$). UV-vis (CH_2Cl_2, λ [nm], (ϵ [$M^{-1}cm^{-1}$]), 298K): 461.31,(1.31x10^4); 542.47 (5.1x10^3); 586.81 (4.06 x10^3); 798.61 (1.6x10^3); [(UV-VIS [CH_2Cl_2, 10% TFA/CH_2Cl_2, λ [nm],(ϵ [$M^{-1}cm^{-1}$]), 298K)]: 477.33 (8.2x10^3);625.73 (2.96 x10^3); 724.63 (2.756 x10^3) ; 914.07(1.7 x10^3).

Compound **18**: Yield. ~ 51mg (~10 %).HRMS of 10(m/z):1022.513 (1022.55 Calc. For [$C_{66}H_{82}N_2S_2Si_2]^+$). UV-Vis (CH2Cl2, λ [nm], (ϵ [$M^{-1}cm^{-1}$]), 298K): 431.3(1.5 x10^3).^{1}H NMR (400 MHz, $CDCl_3$, 298 K, δ [ppm], TMS):6.89-7.31 (m, 16H, tolyl-CH); 6.41 (brs, 2H, thiophene β-H); 6.26 (s, 2H, α-H of TIPS- Pyrrole); 6.16 (s, 2H, α-H of TIPS- Pyrrole); 6.0 (brs, 2H, thiophene β-H); 5.53 (s, 2H, *meso*-CH); 5.49 (s, 2H, *meso*-CH); 2.31 (s, 6H, tolyl Me); 2.32(s, 6H, tolyl Me); 1.19-1.33 (m, 6H, TIPS-CH); 0.94-1.07(m,36H,$TIPSCH_3$).^{13}C{^{1}H}100MHz,$CDCl_3$,δ[ppm]):11.68,11.73,11.87,13.88,17.88,18.02,18.61,22.59,22.85,43.95,44.74,122.97,123.37,123.92,124.09,124.43,124.57,124.73,124.90,125.54,126.01,126.39,127.97,128.05,128.18,128.43,128.53,128.67,129.00,145.18,145.65,147.74,148.38.

Characterization Data

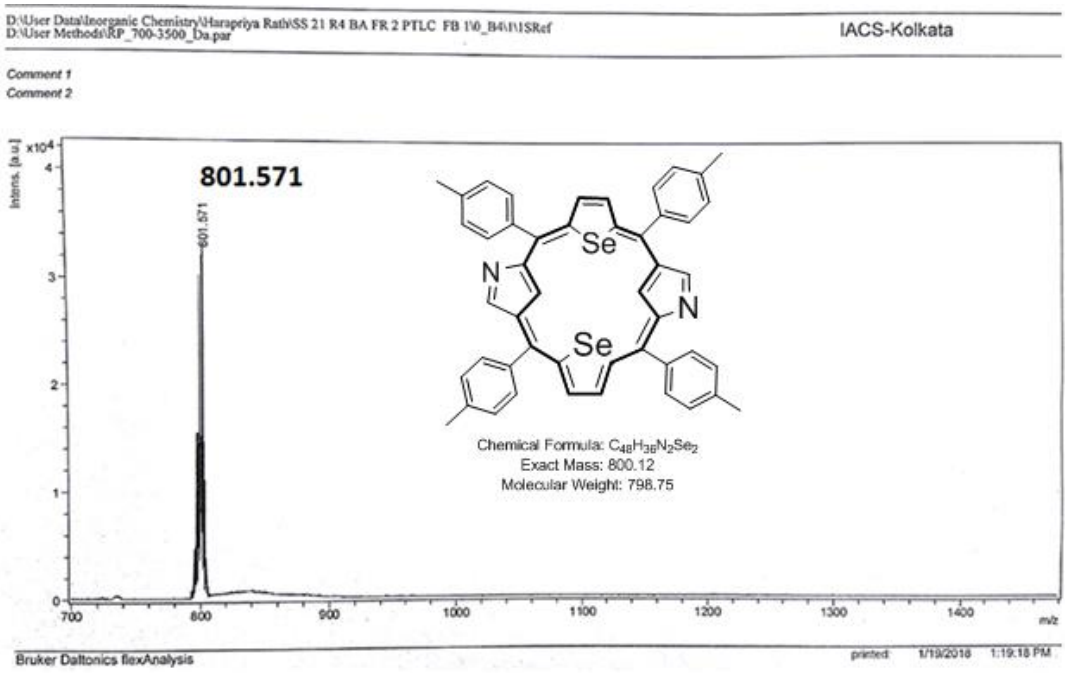

Figure 3.40. MALDI-TOF MS Spectra of **17**

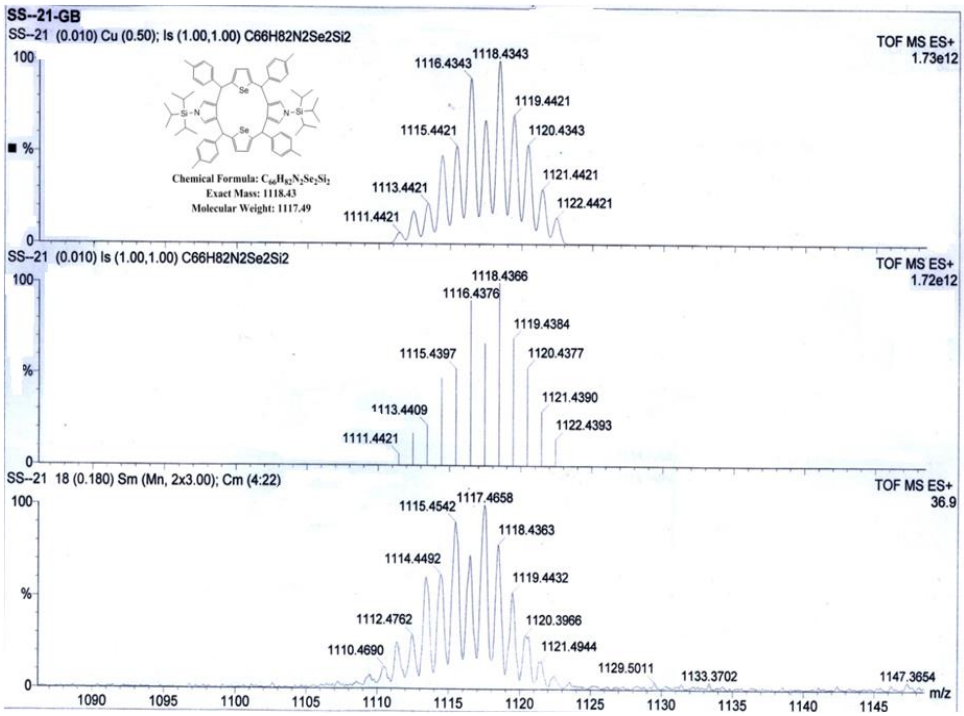

Figure 3.41. HR-MS data of **16**

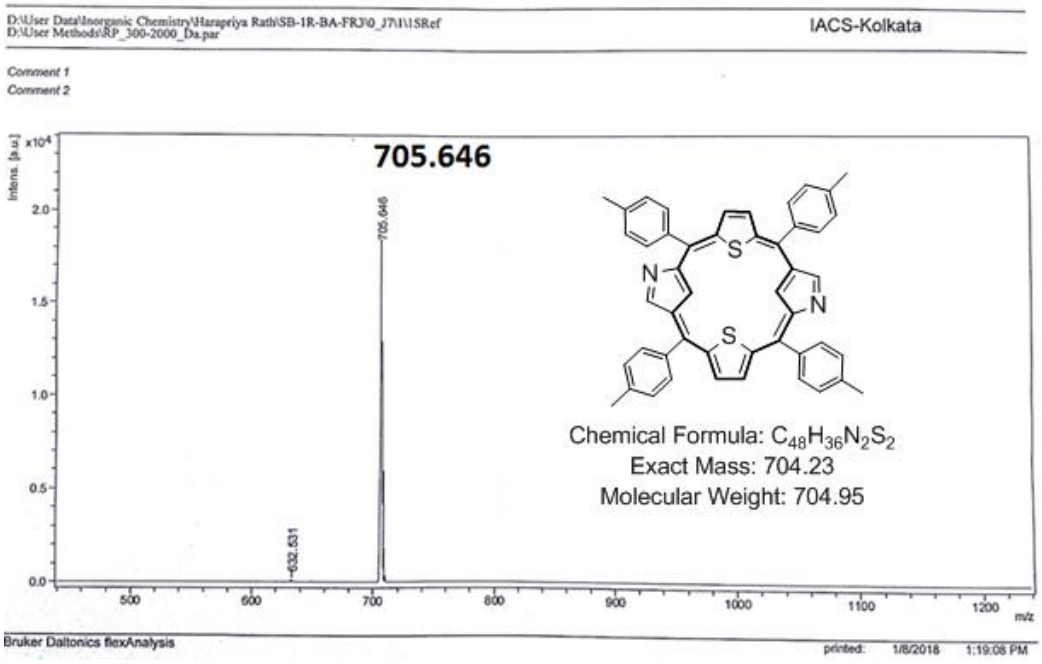

Figure 3.42. MALDI-TOF MS Spectra of **17**

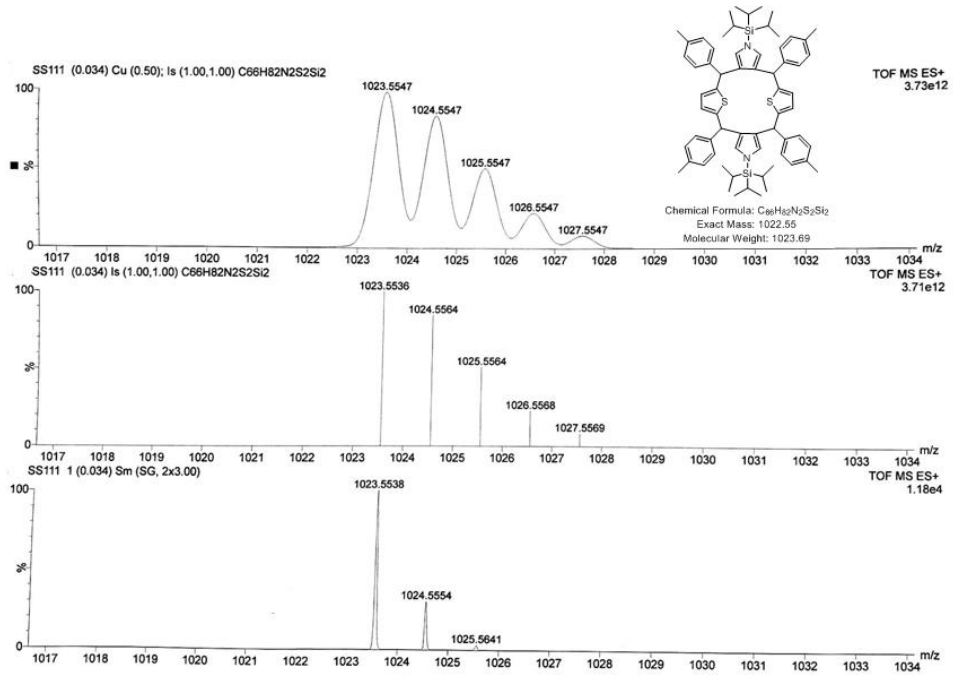

Figure 3.43. HR-MS Spectra of **17**

3.5. Theoretical Study

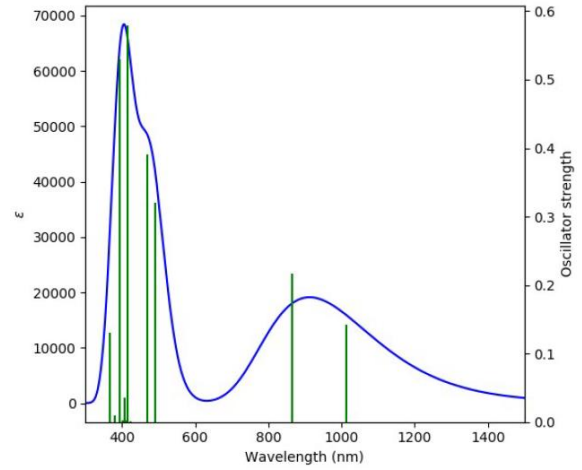

Figure 3.44. TD-DFT absorption spectrum of free base form of **15** at B3LYP/6-311+G* (B1c) level of theory and the corresponding electronic transitions are shown in the table below. Note that we observe lone pair orbital of Selenium transition to eg orbitals. Mixing of these orbitals in a2u orbitals too.

Table 3.**1**. Summary of UV-vis spectral data of free base form of **15**

No.	Energy (cm-1)	Wavelength (nm)	Oscillator. Strength	Symmetry	Major contributions
1	9864.161	**1013.771**	**0.1418**	**Singlet-A**	**HOMO->LUMO (93%)**
2	**11545.83**	**866.1138**	**0.216**	**Singlet-A**	**HOMO->L+1 (93%)**
3	19082.27	524.0466	0.0001	Singlet-A	HOMO->L+2 (94%)
4	**20405.83**	**490.0561**	**0.3195**	**Singlet-A**	**H-1->LUMO (45%), H-1->L+1 (39%)**
5	**21292.23**	**469.6549**	**0.3905**	**Singlet-A**	**H-1->LUMO (45%), H-1->L+1 (44%)**
6	22384.31	446.7416	0.0003	Singlet-A	H-5->LUMO (20%), H-2->LUMO (76%)
7	23565.1	424.3563	0.0008	Singlet-A	H-4->LUMO (48%), HOMO->L+3 (33%)
8	23843.36	419.4039	0.0002	Singlet-A	H-5->LUMO (15%), H-4->L+1 (32%), H-2->L+1 (37%)
9	**24018.38**	**416.3477**	**0.5795**	**Singlet-A**	**H-3->LUMO (85%)**
10	24188.57	413.4184	0.0025	Singlet-A	H-4->LUMO (20%), H-4->L+1 (21%), HOMO->L+3 (43%)
11	24546.68	407.3871	0.0355	Singlet-A	H-6->LUMO (77%), H-3->L+1 (10%)
12	24753.16	403.9889	0.0002	Singlet-A	H-5->LUMO (29%), H-2->L+1 (43%)
13	24884.62	401.8546	0.0023	Singlet-A	H-5->LUMO (20%), H-4->LUMO (19%), H-4->L+1 (34%)
14	**25466.96**	**392.6657**	**0.5299**	**Singlet-A**	**H-3->L+1 (81%)**
15	26152.53	382.3722	0	Singlet-A	H-7->LUMO (18%), H-5->L+1 (68%)
16	26317.87	379.9699	0.0094	Singlet-A	H-6->L+1 (54%), HOMO->L+4 (40%)
17	26575.97	376.2798	0	Singlet-A	H-8->LUMO (35%), H-7->LUMO (29%), H-5->L+1 (10%)
18	27128.46	368.6166	0.0002	Singlet-A	H-8->LUMO (36%), H-7->LUMO (42%)
19	27158.3	368.2115	0.0358	Singlet-A	H-6->L+1 (29%), HOMO->L+4 (48%)
20	27322.84	365.9942	0.1308	Singlet-A	H-9->LUMO (80%)

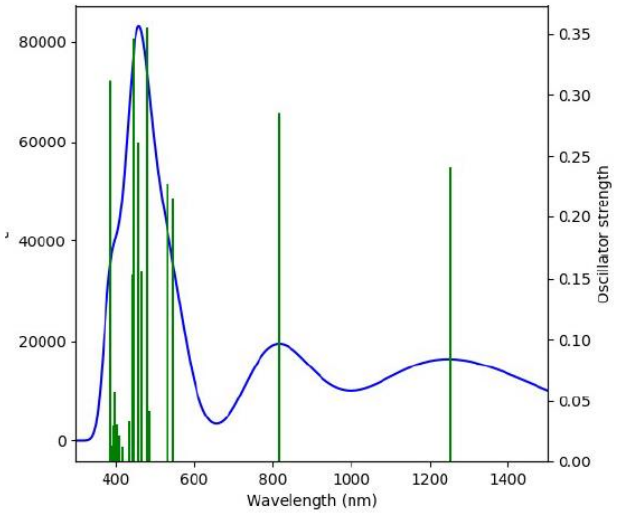

Figure 3.45. TD-DFT absorption spectrum of patially protonated form of **15** at B3LYP/6-311+G* (B1c) level of theory and the corresponding electronic transitions are shown in the table below.

Table 3.2. Summary of UV-vis spectral data of partially protonated form of **15**

No.	Energy (cm-1)	Wavelength (nm)	Oscillator. Strength	Symmetry	Major contributions
1	8142.167	1228.174	0.1706	Singlet-A	HOMO->LUMO (102%)
2	**12499.17**	**800.0529**	**0.1755**	**Singlet-A**	**HOMO->L+1 (89%)**
3	**16948.13**	**590.0357**	**0.1216**	**Singlet-A**	**H-1->LUMO (81%)**
4	18798.36	531.9612	0.0133	Singlet-A	H-2->LUMO (13%), HOMO->L+2 (76%)
5	19131.47	522.699	0.0388	Singlet-A	H-3->LUMO (15%), H-2->LUMO (58%), HOMO->L+2 (10%)
6	20006.58	499.8355	0.1705	Singlet-A	H-4->LUMO (15%), H-3->LUMO (61%)
7	20826.04	480.1681	0.1354	Singlet-A	H-6->LUMO (16%), H-4->LUMO (63%)
8	21091.4	474.1269	0.0881	Singlet-A	H-5->LUMO (82%)
9	**21520.49**	**464.6735**	**0.333**	**Singlet-A**	**H-6->LUMO (61%), H-4->LUMO (10%)**
10	**21984.25**	**454.871**	**0.296**	**Singlet-A**	**H-6->LUMO (10%), H-1->L+1 (58%)**
11	22394.79	446.5324	0.1351	Singlet-A	H-7->LUMO (73%), H-1->L+1 (10%)
12	22876.3	437.1336	0.0146	Singlet-A	H-11->LUMO (10%), H-8->LUMO (67%)
13	23269.9	429.7397	0.0262	Singlet-A	H-9->LUMO (79%)
14	24265.19	412.113	0.0133	Singlet-A	H-11->LUMO (57%), H-10->LUMO (12%), H-8->LUMO (14%)
15	24459.57	408.8379	0.0655	Singlet-A	H-2->L+1 (77%)
16	24626.53	406.0662	0.0067	Singlet-A	H-11->LUMO (16%), H-10->LUMO (75%)
17	24949.15	400.8153	0.2342	Singlet-A	H-3->L+1 (60%), HOMO->L+3 (25%)
18	25196.76	396.8764	0.0042	Singlet-A	H-12->LUMO (33%), HOMO->L+3 (43%)
19	25313.71	395.0428	0.0241	Singlet-A	H-13->LUMO (18%), H-12->LUMO (34%), H-5->L+1 (13%), H-3->L+1 (15%)
20	25584.71	390.8584	0.025	Singlet-A	H-12->LUMO (13%), H-6->L+1 (29%), H-4->L+1 (14%)

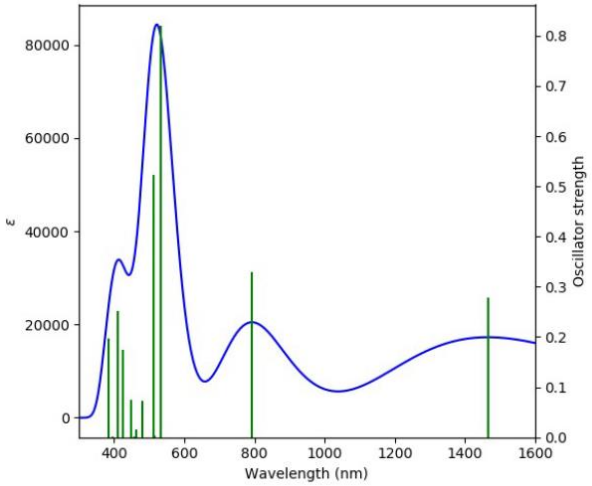

Figure 3.46. TD-DFT absorption spectrum of fully protonated form of **15** at B3LYP/6-311+G* (B1c) level of theory and the corresponding electronic transitions are shown in the table below.

Table 3.3. Summary of UV-vis spectral data of fully protonated form of **15**

No.	Energy (cm-1)	Wavelength (nm)	Oscillator. Strength	Symmetry	Major contributions
1	**7051.705**	**1418.097**	**0.2169**	**Singlet-A**	**HOMO->LUMO (108%)**
2	**12795.18**	**781.5443**	**0.2015**	**Singlet-A**	**HOMO->L+1 (89%)**
3	16565.82	603.6525	0	Singlet-A	H-2->LUMO (15%), HOMO->L+2 (83%)
4	18258.78	547.6817	0.0009	Singlet-A	H-2->LUMO (81%), HOMO->L+2 (12%)
5	18450.74	541.9837	0.6542	Singlet-A	H-4->LUMO (13%), H-1->LUMO (78%)
6	18753.2	533.2424	0.2381	Singlet-A	H-4->LUMO (78%)
7	18798.36	531.9612	0.0014	Singlet-A	H-6->LUMO (15%), H-3->LUMO (78%)
8	19381.5	515.9559	0.0551	Singlet-A	H-5->LUMO (92%)
9	19756.55	506.1612	0.0018	Singlet-A	H-8->LUMO (23%), H-6->LUMO (66%)
10	19962.22	500.9462	0	Singlet-A	H-8->LUMO (74%), H-6->LUMO (17%)
11	19998.52	500.0371	0.0282	Singlet-A	H-7->LUMO (87%)
12	**20388.89**	**490.4632**	**0.0026**	**Singlet-A**	**H-9->LUMO (99%)**
13	22026.19	454.0049	0.3215	Singlet-A	H-10->LUMO (80%)
14	23379.59	427.7234	0.0139	Singlet-A	H-11->LUMO (85%), H-1->L+1 (11%)
15	24550.71	407.3202	0.0001	Singlet-A	H-12->LUMO (85%), H-2->L+1 (10%)
16	24699.92	404.8596	0	Singlet-A	H-2->L+1 (39%), HOMO->L+3 (41%)
17	24733.8	404.3051	0.1249	Singlet-A	H-11->LUMO (12%), H-4->L+1 (29%), H-1->L+1 (50%)
18	25079.81	398.7271	0.0002	Singlet-A	H-3->L+1 (67%)
19	25230.64	396.3436	0.3679	Singlet-A	H-4->L+1 (64%), H-1->L+1 (30%)
20	25778.29	387.9234	0	Singlet-A	H-9->L+1 (27%), H-8->L+1 (37%), H-6->L+1 (10%), H-3->L+1 (22%)

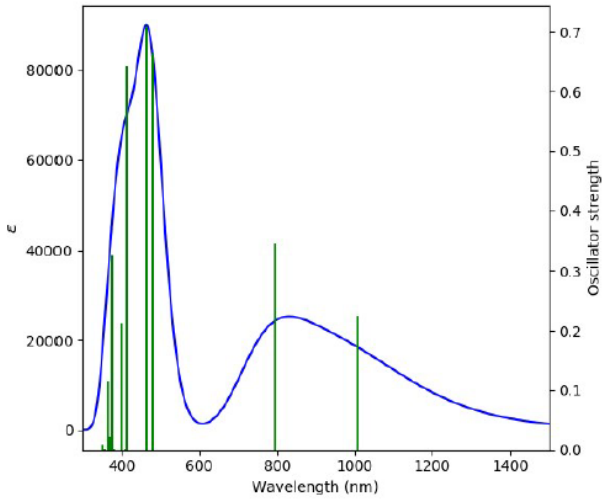

Figure 3.47. TD-DFT absorption spectrum of free base form of **17**at B3LYP/6-311+G* (B1c) level of theory and the corresponding electronic transitions are shown in the table below.

Table3. 4. Summary of UV-vis spectral data of free base form of **17**

No.	Energy (cm-1)	Wavelength (nm)	Oscillator. Strength	Symmetry	Major contributions
1	**10292.44**	**971.5868**	**0.1453**	**Singlet-A**	**HOMO->LUMO (93%)**
2	**12729.85**	**785.5553**	**0.2352**	**Singlet-A**	**HOMO->L+1 (91%)**
3	20381.63	490.6379	0.0001	Singlet-A	HOMO->L+2 (91%)
4	21070.43	**474.5988**	**0.391**	Singlet-A	H-3->LUMO (10%), H-1->LUMO (47%), H-1->L+1 (35%)
5	**22027.81**	**453.9716**	**0.5381**	**Singlet-A**	**H-1->LUMO (41%), H-1->L+1 (47%)**
6	22479.48	444.8502	0.0001	Singlet-A	H-4->LUMO (20%), H-2->LUMO (74%)
7	24088.55	415.1349	0.0004	Singlet-A	H-4->LUMO (64%), H-2->LUMO (16%)
8	**24397.46**	**409.8787**	**0.4707**	**Singlet-A**	**H-3->LUMO (80%)**
9	25073.36	398.8297	0.2966	Singlet-A	H-5->LUMO (74%)
10	25098.36	398.4324	0.0002	Singlet-A	H-2->L+1 (81%)
11	25808.13	387.4748	0.0001	Singlet-A	H-4->L+1 (14%), HOMO->L+3 (74%)
12	26354.97	379.435	0.2411	Singlet-A	H-3->L+1 (87%)
13	26536.45	376.8402	0.0008	Singlet-A	H-9->LUMO (12%), H-7->LUMO (45%), H-4->L+1 (10%)
14	26755.02	373.7616	0	Singlet-A	H-7->LUMO (15%), H-4->L+1 (54%), HOMO->L+3 (12%)
15	27197.82	367.6765	0	Singlet-A	H-6->LUMO (77%), H-4->L+1 (12%)
16	27323.64	365.9834	0.0462	Singlet-A	H-5->L+1 (68%), HOMO->L+4 (21%)
17	27405.11	364.8955	0.1766	Singlet-A	H-8->LUMO (74%)
18	28071.32	356.2355	0.0887	Singlet-A	H-8->L+1 (13%), H-5->L+1 (19%), HOMO->L+4 (59%)
19	28176.98	354.8997	0.0001	Singlet-A	H-9->LUMO (66%), H-7->LUMO (19%)
20	28643.17	349.1234	0.0014	Singlet-A	HOMO->L+5 (90%)

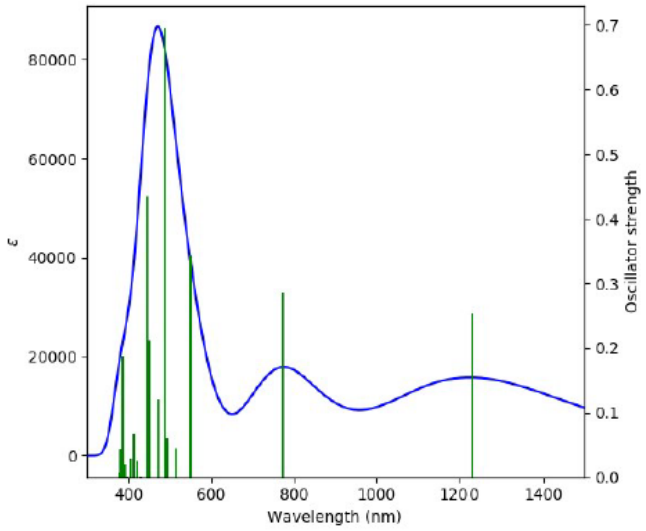

Figure 3.48. TD-DFT absorption spectrum of partially protonated form of **17** at B3LYP/6-311+G* (B1c) level of theory and the corresponding electronic transitions are shown in the table below.

Table 3.5. Summary of UV-vis spectral data of partially protonated form of **17**

No.	Energy (cm-1)	Wavelength (nm)	Oscillator. Strength	Symmetry	Major contributions
1	8286.54	1206.776	0.1768	Singlet-A	HOMO->LUMO (101%)
2	**13045.21**	**766.5648**	**0.1652**	**Singlet-A**	**H-1->LUMO (13%), HOMO->L+1 (83%)**
3	16565.01	603.6819	0.0982	Singlet-A	H-2->LUMO (14%), H-1->LUMO (73%)
4	18658.02	535.9624	0.03	Singlet-A	H-3->LUMO (75%)
5	19353.27	516.7085	0.0776	Singlet-A	H-4->LUMO (27%), H-3->LUMO (11%), H-2->LUMO (41%), HOMO->L+2 (10%)
6	19436.35	514.4999	0.0354	Singlet-A	H-4->LUMO (11%), H-1->L+1 (12%), HOMO->L+2 (68%)
7	20425.18	489.5917	0.1246	Singlet-A	H-5->LUMO (69%)
8	21013.97	475.8739	0.6506	Singlet-A	H-5->LUMO (14%), H-4->LUMO (45%), H-2->LUMO (21%)
9	**21765.68**	**459.4389**	**0.1058**	**Singlet-A**	**H-6->LUMO (84%)**
10	21950.38	455.573	0.2662	Singlet-A	H-8->LUMO (24%), H-1->L+1 (49%)
11	22497.22	444.4993	0.1381	Singlet-A	H-8->LUMO (62%), H-1->L+1 (20%)
12	22710.96	440.316	0.0324	Singlet-A	H-7->LUMO (85%)
13	24150.66	414.0674	0.0447	Singlet-A	H-11->LUMO (23%), H-9->LUMO (59%)
14	24339.39	410.8566	0.0085	Singlet-A	H-12->LUMO (10%), H-11->LUMO (25%), H-10->LUMO (46%), H-9->LUMO (13%)
15	24471.67	408.6358	0.0268	Singlet-A	H-12->LUMO (13%), H-11->LUMO (35%), H-10->LUMO (20%), H-9->LUMO (12%), H-2->L+1 (12%)
16	24569.26	407.0126	0.013	Singlet-A	H-2->L+1 (71%)
17	24850.75	402.4024	0.1197	Singlet-A	H-12->LUMO (13%), H-3->L+1 (68%)
18	25076.58	398.7784	0.047	Singlet-A	H-12->LUMO (46%), H-10->LUMO (11%), H-3->L+1 (24%)
19	25622.62	390.2801	0.0278	Singlet-A	H-13->LUMO (26%), H-4->L+1 (67%)
20	26175.11	382.0423	0.0044	Singlet-A	H-13->LUMO (23%), H-5->L+1 (39%), HOMO->L+3 (21%)

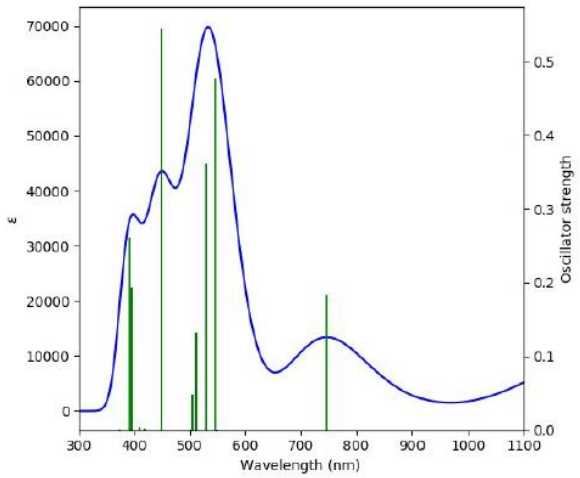

Figure3.49. TD-DFT absorption spectrum of fully protonated form of **17** at B3LYP/6-311+G* (B1c) level of theory and the corresponding electronic transitions are shown in the table below.

Table 3.6. Summary of UV-vis spectral data of fully protonated form of **25**

No.	Energy (cm-1)	Wavelength (nm)	Oscillator. Strength	Symmetry	Major contributions
1	7167.043	1395.276	0.2216	Singlet-A	HOMO->LUMO (107%)
2	13379.12	747.433	0.1844	Singlet-A	H-1->LUMO (11%), HOMO->L+1 (85%)
3	17019.91	587.5471	0	Singlet-A	H-2->LUMO (28%), HOMO->L+2 (70%)
4	18232.16	548.4813	0.0005	Singlet-A	H-2->LUMO (68%), HOMO->L+2 (24%)
5	18296.69	546.547	0.4776	Singlet-A	H-4->LUMO (33%), H-1->LUMO (62%)
6	**18784.65**	**532.3495**	**0**	**Singlet-A**	**H-5->LUMO (21%), H-3->LUMO (71%)**
7	18899.18	529.1234	0.3608	Singlet-A	H-9->LUMO (10%), H-6->LUMO (10%), H-4->LUMO (47%), H-1->LUMO (21%)
8	**19515.39**	**512.4161**	**0.1319**	**Singlet-A**	**H-6->LUMO (86%)**
9	19565.4	511.1064	0.0005	Singlet-A	H-5->LUMO (74%), H-3->LUMO (20%)
10	19796.07	505.1507	0.0488	Singlet-A	H-7->LUMO (84%)
11	19945.28	501.3716	0.0005	Singlet-A	H-8->LUMO (95%)
12	22323.01	447.9683	0.5457	Singlet-A	H-9->LUMO (75%)
13	**23935.31**	**417.7928**	**0.0022**	**Singlet-A**	**H-10->LUMO (90%)**
14	24382.95	410.1227	0.0003	Singlet-A	H-12->LUMO (87%)
15	24445.05	409.0807	0.0037	Singlet-A	H-11->LUMO (53%), H-4->L+1 (10%), H-1->L+1 (32%)
16	25263.7	395.8248	0	Singlet-A	H-3->L+1 (12%), H-2->L+1 (74%), HOMO->L+3 (10%)
17	25344.36	394.5651	0.1937	Singlet-A	H-11->LUMO (16%), H-4->L+1 (24%), H-1->L+1 (57%)
18	25536.32	391.5991	0.2614	Singlet-A	H-11->LUMO (29%), H-4->L+1 (61%)
19	25566.97	391.1297	0.0001	Singlet-A	H-3->L+1 (84%)
20	26843.74	372.5263	0.0013	Singlet-A	H-5->L+1 (92%)

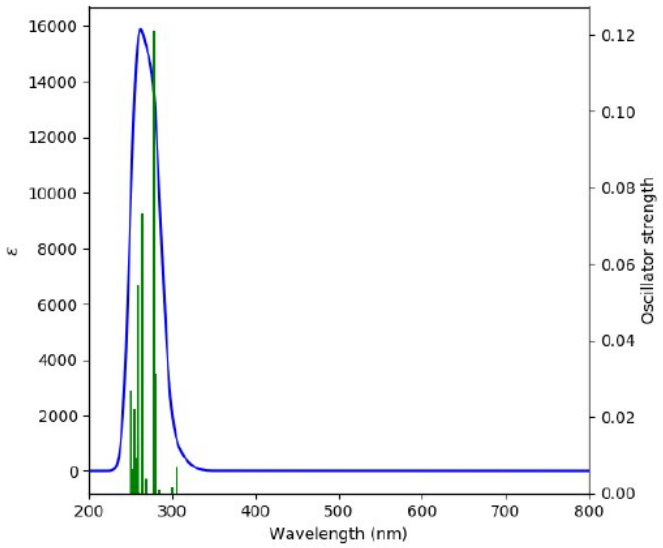

Figure 3.50. TD-DFT absorption spectrum of free base form of **16** at B3LYP/6-311+G* (B1c) level of theory and the corresponding electronic transitions are shown in the table below.

Table 3.7. Summary of UV-vis spectral data of free base form of **16**

No.	Energy (cm-1)	Wavelength (nm)	Oscillator Strength	Symmetry	Major contributions
1	32685.62	305.945	0.0068	Singlet-A	H-1->LUMO (19%), HOMO->LUMO (79%)
2	33288.92	300.4002	0.0016	Singlet-A	H-1->LUMO (79%), HOMO->LUMO (19%)
3	35055.28	285.2638	0.0009	Singlet-A	H-2->LUMO (97%)
4	35842.47	278.9986	0.0313	Singlet-A	H-4->LUMO (31%), H-3->LUMO (65%)
5	**35923.93**	**278.3659**	**0.1212**	**Singlet-A**	**H-4->LUMO (65%), H-3->LUMO (30%)**
6	37349.92	267.7382	0.0038	Singlet-A	HOMO->L+2 (27%), HOMO->L+3 (18%), HOMO->L+10 (13%)
7	37599.15	265.9635	0	Singlet-A	H-1->L+2 (28%), H-1->L+3 (13%), H-1->L+5 (13%), H-1->L+10 (15%), HOMO->L+2 (15%)
8	37947.58	263.5214	0.0734	Singlet-A	HOMO->L+1 (87%)
9	38422.64	260.2632	0.0002	Singlet-A	HOMO->L+2 (22%), HOMO->L+3 (60%)
10	38639.6	258.8018	0.0144	Singlet-A	H-5->LUMO (15%), H-1->L+1 (17%), HOMO->L+4 (50%)
11	38725.1	258.2305	0.0543	Singlet-A	H-1->L+1 (44%), HOMO->L+4 (26%)
12	38798.49	257.742	0.0092	Singlet-A	H-1->L+3 (10%), HOMO->L+5 (42%)
13	38812.21	257.6509	0.0057	Singlet-A	H-5->LUMO (65%), H-1->L+1 (24%)
14	39188.87	255.1745	0.0222	Singlet-A	H-1->L+2 (11%), H-1->L+3 (13%), HOMO->L+7 (46%)
15	39242.91	254.8231	0.0025	Singlet-A	H-1->L+2 (24%), H-1->L+3 (18%), HOMO->L+6 (11%), HOMO->L+7 (22%)
16	39256.62	254.7341	0.003	Singlet-A	H-1->L+4 (14%), HOMO->L+6 (42%), HOMO->L+7 (17%)
17	39440.51	253.5464	0.0028	Singlet-A	H-1->L+4 (52%), HOMO->L+6 (21%)
18	39601.82	252.5136	0.0063	Singlet-A	H-1->L+3 (20%), H-1->L+5 (47%)
19	39641.34	252.2619	0.0005	Singlet-A	H-1->L+4 (11%), HOMO->L+8 (50%)
20	39891.38	250.6808	0.0268	Singlet-A	H-1->L+6 (77%)

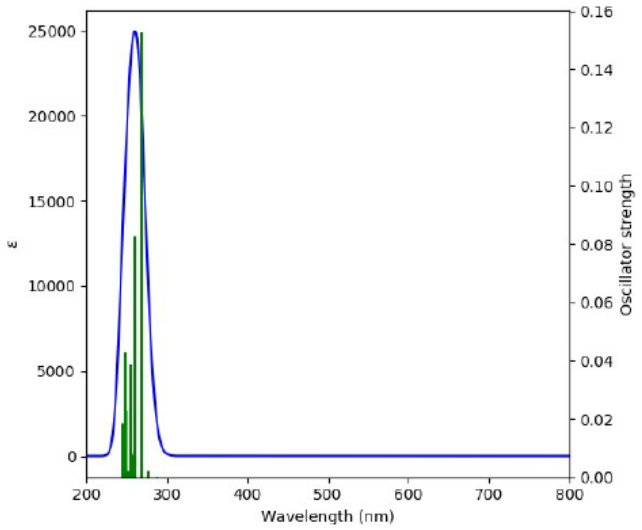

Figure 3.51 TD-DFT absorption spectrum of free base form of **18** at B3LYP/6-311+G* (B1c) level of theory and the corresponding electronic transitions are shown in the table below

Table3 8. Summary of UV-vis spectral data of free base form of **18**

No.	Energy (cm-1)	Wavelength (nm)	Osc. Strength	Symmetry	Major contribs
1	34726.2	287.967	0.0002	Singlet-A	HOMO->LUMO (97%)
2	**36068.31**	**277.2517**	**0.0021**	**Singlet-A**	**H-1->LUMO (98%)**
3	**37282.17**	**268.2247**	**0.1527**	**Singlet-A**	**H-2->LUMO (85%)**
4	**37340.24**	**267.8076**	**0.004**	**Singlet-A**	**H-3->LUMO (90%)**
5	38423.45	260.2578	0.0828	Singlet-A	HOMO->L+1 (52%), HOMO->L+2 (21%)
6	38503.3	259.718	0.0524	Singlet-A	HOMO->L+1 (29%), HOMO->L+2 (23%), HOMO->L+3 (30%)
7	38680.74	258.5266	0.0076	Singlet-A	H-1->L+2 (14%), HOMO->L+2 (33%), HOMO->L+3 (41%)
8	38871.08	257.2606	0.0007	Singlet-A	H-1->L+1 (12%), HOMO->L+4 (68%)
9	39144.51	255.4637	0.0083	Singlet-A	H-1->L+4 (10%), HOMO->L+5 (54%)
10	39230.81	254.9017	0.0223	Singlet-A	HOMO->L+7 (19%), HOMO->L+8 (50%)
11	39246.94	254.7969	0.0035	Singlet-A	HOMO->L+7 (47%), HOMO->L+8 (20%)
12	39267.1	254.6661	0.0387	Singlet-A	H-1->L+6 (12%), HOMO->L+6 (61%)
13	39747.81	251.5862	0.002	Singlet-A	H-4->LUMO (82%)
14	40071.24	249.5556	0.0022	Singlet-A	H-5->LUMO (21%), H-1->L+1 (31%), HOMO->L+9 (15%)
15	40226.1	248.5948	0.0231	Singlet-A	H-3->L+3 (14%), H-1->L+2 (18%), H-1->L+3 (37%)
16	40411.6	247.4537	0.043	Singlet-A	H-1->L+1 (11%), H-1->L+4 (22%), HOMO->L+9 (23%)
17	40465.64	247.1232	0.0102	Singlet-A	H-5->LUMO (38%), H-3->L+2 (10%)
18	40487.42	246.9903	0.0113	Singlet-A	H-5->LUMO (15%), H-3->L+2 (22%), H-1->L+2 (22%)
19	40571.3	246.4796	0.0177	Singlet-A	H-3->L+1 (42%), H-1->L+5 (11%), H-1->L+7 (11%)
20	40762.45	245.3238	0.0184	Singlet-A	H-1->L+5 (25%), H-1->L+8 (11%)

	B1 (B3LYP/6-31G)			B1a (WB97XD/6-31G)		
	E	E+ZPE	G	E	E+ZPE	G
15a	-6758.09684	-6757.39743	-6757.48265	-6757.48833	-6756.77843	-6756.86387
15b	-6758.08597	-6757.38497	-6757.47003	-6757.47568	-6756.76520	-6756.84966
15c	-6758.08073	-6757.37917	-6757.46515	-6757.46916	-6756.75794	-6756.84293
	B1b (B3LYP/6-31G(d,p))			B1c (B3LYP/6-311+G(d))		
	E	E+ZPE	G	E	E+ZPE	G
15a	-6759.0606	-6758.36787	-6758.45312	-6763.72248	-6763.02307	-6763.10829
15b	-6759.0573	-6758.36365	-6758.44792	-6763.71733	-6763.01632	-6763.10138
15c	-6759.053	-6758.35948	-6758.44533	-6763.71124	-6763.00968	-6763.09566
	B2 (B3LYP/6-311G(d,p))			B2a(B3LYP/def2TZVP)		
	E	E+ZPE	G	E	E+ZPE	G
15a	-6763.779697	-6763.08029	-6763.15524	-6764.07448	-6763.37508	-6763.46030
15b	-6763.774834	-6763.07383	-6763.15889	-6764.07047	-6763.36946	-6763.45453
15c	-6763.767119	-6763.06557	-6763.14089	-6764.05811	-6763.35655	-6763.44253
	B1c (B3LYP/6-311+G(d))			B2 (B3LYP/6-311G(d,p))		
	E	E+ZPE	G	E	E+ZPE	G
16a	-8051.90238	-8050.58841	-8050.71230	-8056.76765	-8055.45368	-8055.57757
16b	-8051.90265	-8050.58840	-8050.71167	-8056.7666	-8055.45235	-8055.57562
16c	-8051.88386	-8050.57028	-8050.69292	-8056.75665	-8055.44307	-8055.56571
	B1 (B3LYP/6-31G)			B1a (WB97XD/6-31G)		
	E	E+ZPE	G	E	E+ZPE	G
17a	-2756.06442	-2755.36222	-2755.44548	-2755.37717	-2754.66531	-2754.74891
17b	-2756.06309	-2755.36058	-2755.44406	-2755.37361	-2754.66147	-2754.74484
17c	-2756.05893	-2755.35664	-2755.44259	-2755.36947	-2754.65774	-2754.73883
	B1b (B3LYP/6-31G(d,p))			B1c (B3LYP/6-311+G(d))		
	E	E+ZPE	G	E	E+ZPE	G
17a	-2756.66826	-2755.97288	-2756.05189	-2757.07502	-2756.37282	-2756.456075
17b	-2756.66800	-2755.97256	-2756.05570	-2757.07432	-2756.37181	-2756.455289
17c	-2756.66400	-2755.96890	-2756.04894	-2757.07026	-2756.36798	-2756.45392
	B2 (B3LYP/6-311G(d,p))			B2a(B3LYP/def2TZVP)		
	E	E+ZPE	G	E	E+ZPE	G
17a	-2757.13244	-2756.4302	-2756.51349	-2757.36368	-2756.66148	-2756.74473
17b	-2757.13149	-2756.429	-2756.51245	-2757.36404	-2756.66153	-2756.74501
17c	-2757.12741	-2756.4251	-2756.51107	-2757.36016	-2756.65787	-2756.74382
	B1c (B3LYP/6-311+G(d))			B2 (B3LYP/6-311G(d,p))		
	E	E+ZPE	G	E	E+ZPE	G
18a	-4049.49104	-4048.17641	-4048.30497	-4050.12861	-4048.81397	-4048.30497
18b	-4049.48998	-4048.17522	-4048.30208	-4050.12780	-4048.81304	-4048.30208
18c	-4049.48235	-4048.16740	-4048.29298	-4050.11905	-4048.80410	-4048.29298

Table 3.9. Total energies and with zero point energy and free energy correction (a.u) for plausible conformers of compounds **15**, **16**, **17** and **18** at **B1**, **B1a**, **B1b**, **B1c, B2** and **B2a** level of theory.

Compound	B1b		B2	
	(ΔE+ZPE)	ΔG	ΔE+ZPE	ΔG
16a	0.00	0.00	0.00	0.00
16b	0.03	1.64	3.49	5.11
16c	47.60	50.88	27.85	31.14
18a	0.00	0.00	0.00	0.00
18b	3.11	7.58	2.44	6.90
18c	23.61	31.49	25.91	33.78

Table 3.10. Relative energies of **16** and **18** including zero point energy (ΔE+ZPE) and Gibbs free energy (ΔG) in kJ/mol at **B1**b and **B2** level of theory

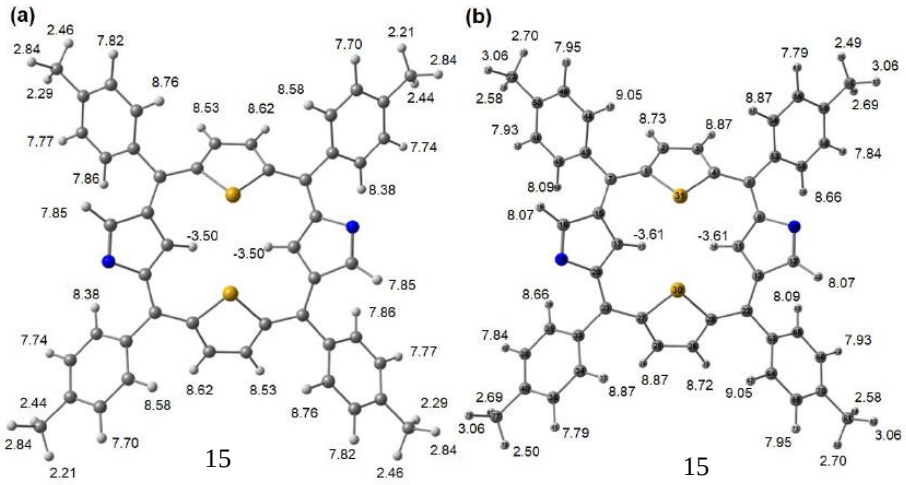

Figure 3.52. Calculated 1H-NMR chemical shift values of **15** at B1b and B1c level of theory

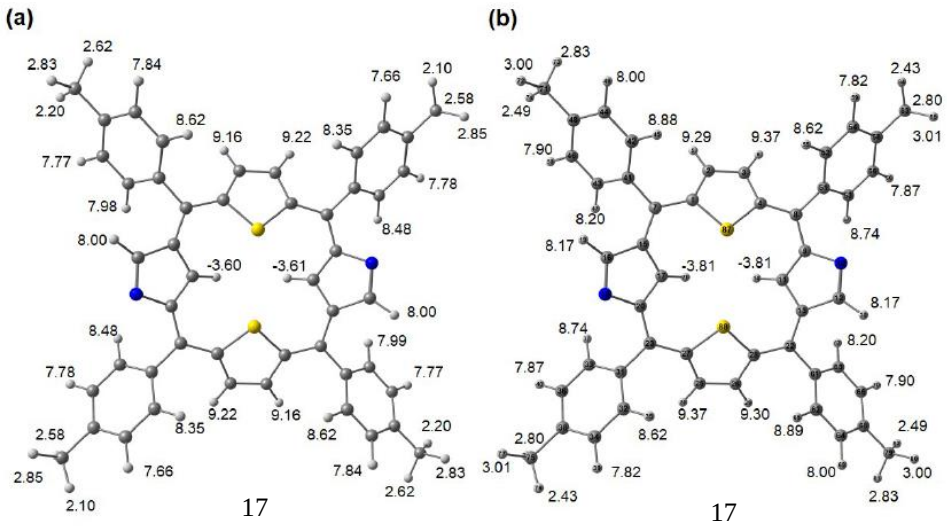

Figure 3.53. Calculated ^{1}H-NMR chemical shift values of 17 at B1b and B1c level of theory

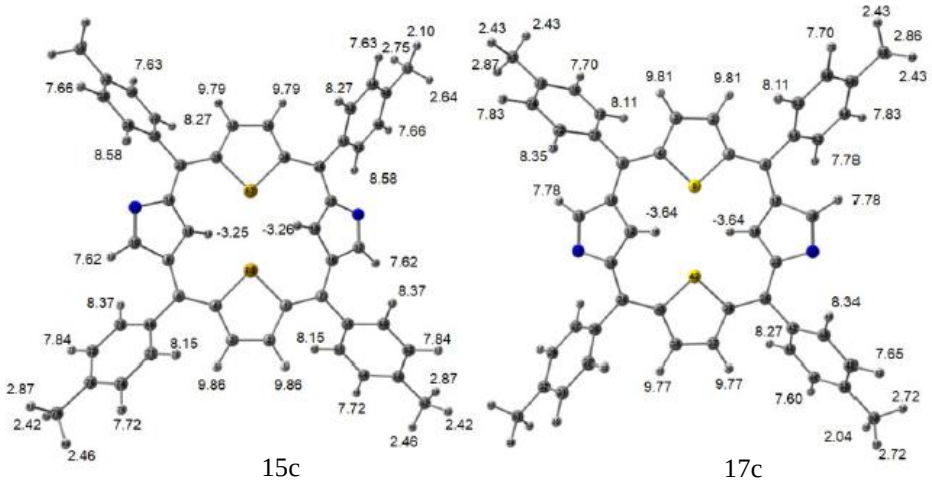

Figure 3.54. Calculated ^{1}H-NMR chemical shifts of **15c and 17c** at B3LYP/6-31G(d,p), B1b level of theory.

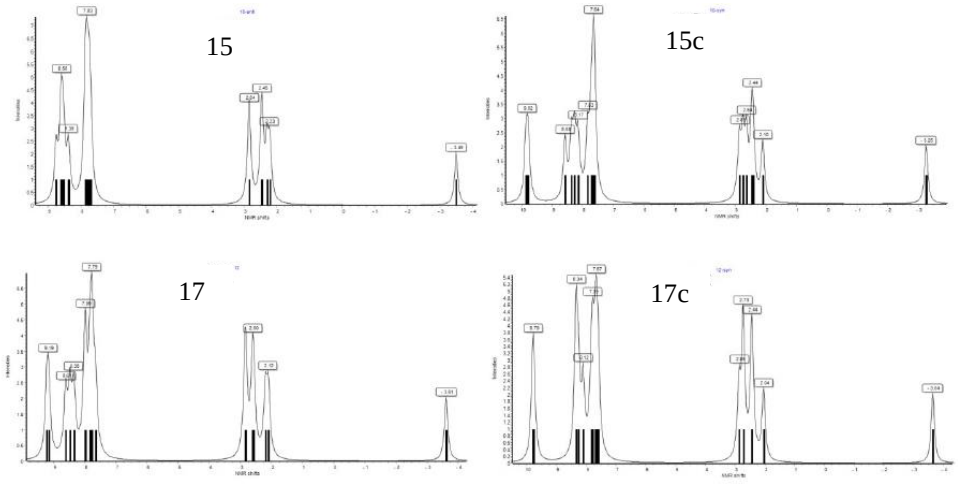

Figure 3.55. Calculated ^{1}H-NMR spectral pattern of **15, 15c, 17** and **17c** at B3LYP/6-31G(d,p), B1b level of theory.

3.6. References

1. (a) Won, D.; Lee, J. S.; Ba, Q.; Cho, Y. J.; Cheong, H. Y.; Choi, S.; Kim, C. H.; Son, H. J.; Pac, C. and Kang S.O. *ACS Catal.,*2018**, 8***,* 1018-1030; (b) Ding, Y., Zhu, W.H.; Xie and Y. Analogues.*Chem. Rev.,* 2017, **117**, 2203-2256; (c), F. Schmitt, P. Govindaswamy, ,G. S. Fink, W. H. Ang, P. J. Dyson, L. J. Jeanneret and B. Therrien, *J. Med. Chem*., 2008, **51***,* 1811-1816; (d) H. Tanaka, T. Ikeda, M. Takeuchi, K. Sada, ,S Shinkai and T. Kawai, *,ACS.Nano.,* 2011, **5***,* 9575-9582; (e), D. T. Gryk, C. Clausen, K. M. Roth, N. Dontha, D. F. Bocian, W. G. Kuhr and J. S Lindsey. *J. Org. Chem.,* 2000, **65**, 7345-7355.
2. (a) H. Furuta, T. Asano and T. Ogawa*. J. Am. Chem. Soc*., 1994 **116**, 767-768; (b) P. J. Chmielewski, L. Latos-Grażyński, L. Rachlewicz and T. Głowiak, *Angew. Chem., Int. Ed. Engl.* 1994*,* **33**, 777-779
3. M. Toganoh and H. Furuta, *Chem. Commun*., 2012, **48***,* 937–954
4. (a) H. Furuta, , H. Maeda and A. Osuka, *J. Am. Chem. Soc.,* 2000*,* **122***,* 803-807; (b) J. Yan, M. Takakusaki, Y. Yang, S. Mori, B. Zhang, Y. Feng, M. Ishida and H. Furuta., *Chem. Commun.,* 2014**, 50**, 14593-14596; (c) H. Maeda, , A. Osuka and H. Furuta, *J. Am. Chem. Soc.,* 2003*,* **125***,* 15690-15691;(d), H. Furuta, H. Maeda and A. Osuka,*J. Org. Chem.,*2000, **65**, 4222-4226.
5. (a) L**.** Szterenberg, and L. Latos-Grażyński., *Inorg.Chem*., 1997, **36**, 6287**-**6291; (b) P.J. Chemielewski, L. Latos-Grażyński, and T. Glowiak, *J. Am. Chem. Soc.,*1996, **118**, 5690**-**5692. (c) P. J. Chmielewski, L. Latos-Grażyński and I. Schmidt, *Inorg.Chem.,* 2000*,* **39***,* 5475-5482; (d) H. Furuta, T. Ogawa, Y. Uwatoko and K Araki, *Inorg.Chem*. 1999, **38**, 2676**-**2682; (e), H. Furuta**,** N. Kubo, T. Ishizuka, A. Osuka, H. Nanami and T. Ogawa, *Inorg.Chem*., 2000, **39**, 5424-5425; (f) H. Furuta**,** H. Maeda, A. Osuka, M. Yasutak, T. Shinmyozu and Y. Ishikawa**,** *Chem. Commun*., 2000, 1143-1144.
6. H. Furuta, H. Meada and A. Osuka, *J. Am. Chem. Soc.,* 2000, **122***,* 803-807

7. J. Yan, M. Takakusaki, Y. Yang, S. Mori, B. Zhang, Y. Feng, M. Ishida, H. Furuta *Chem. Commun.,* **2014**, *50*, 14593-14596
8. A. Mallick and H. Rath, *Chem. – Asian J*., 2016, **11**, 986-990.
9. M. J**.** Gouterman, *Mol. Spectrosc*., 1963, **11**, 108-127.
10. H. Maeda, A. Osuka and H. Furuta, *J. Am. Chem. Soc.,* 2003, **125**, 15690-15691.
11. S. K. Pushpan, A. Srinivasan, V. G. Anand, T. K. Chandrashekar,A. Subramanian, R. Roy, K. Sugiura and Y. Sakata, *J. Org. Chem*., 2001, **66**, 153-161.
12. E. Z. Hückel, *Physics*, 1931, **70**, 204-286.
13. B. Franck and A. Nonn, *Angew. Chem., Int. Ed*., 1995, **34**, 1795-1811.
14. N. Halder, M. Sangeetha, D. Usharani, and H. Rath, *J. Org. Chem.,* 2020, **85**, 2059-2067.
15. M. J. Frisch, et al., Gaussian 16 (A.03), Gaussian, Inc., Wallingford CT, 2016.
16. T. Kaur, W.-Z. Lee and M. Ravikanth, *Inorg. Chem*., 2016, **55**, 5305-5311.
17. N. Sprutta and L. Latos-Grażyński, Org. Lett., 2001, **3**, 1933-1936.
18. (a) H. Furuta, H. Maeda and A. Osuka, *J. Org. Chem*., **2000**, *65*, 4222-4226.;(b) H. Furuta, H. Maeda, A. Osuka, *J. Org. Chem*., 2001, **66**, 8563-8572.
19. J.-D. Chai and M. Head-Gordon, *Phys. Chem. Chem. Phys.,* 2008, **10**, 6615-6620.
20. (a) A. D. Becke, *J. Chem. Phys.,* 1992**, 96**, 2155-2160; (b) A. D. Becke, *J. Chem. Phys*., 1993, **98**, 5648-5654.
21. (a) C. Adamo, D. Jacquemin, *Chem. Soc. Rev.,* 2013, **42**, 845-856.;(b) G. Scalmani, M. J. Frisch, B. Mennucci, J. Tomasi and R. Cammi V. Barone, *J. Chem. Phys.,* 2006, **124**, 0941071.
22. P. v. R. Schleyer, C. Maerker, A. Dransfeld, H. Jiao and N. J. R. V. E. Hommes, *J. Am. Chem. Soc.,* 1996, **118**, 6317-6318.
23. D. Geuenich, K. Hess, F. Köhler and R. Herges, *Chem. Rev.,* 2005, **105**, 3758-3772.
24. T. M. Krygowski and M. K. Cyrański, *Chem. Rev.,* 2001, **101**,1385-1420.

NIR Absorbing monocarba Vinylogous porphyrinoids with adoptive Aromaticity

4. Abstract

Hückel aromatic dithia [26] core modified expanded azuliporphyrinoid (1.3.3.1.0) has been synthesized following literature known acid catalyzed condensation protocol. Whereas incorporation of bithiophene moiety has led to charge separated resonance delocalized tropylium cation surmising the aromatic nature of the this carbaporphyrinoid with the observation of inner ring protons resonating in the upfield zone and outer ring protons resonating in the deshielded zone in accordance with the electronic absorption spectra that exhibited splited Soret band and well defined Q-type bands in the vis-NIR region. In situ the azulene seven member ring was constracted to acelyted derivative of six member moity which gave a new type of aromatic carbaporphyrinoid with NIR absorption. Contrarily, swiping the bithiophene moiety with fused thieno [2,3, b] thiophene has anticipated the obvious antiaromatic nature of the corresponding azuliporphyrinoid (1.3.3.1.0) with the observation of inner ring protons resonating in the deshielded zone and outer ring protons resonating in the up zone in accordance with the electronic absorption spectra that exhibited Soret band and a stretch Q-type band in NIR region. The spectroscopic preclusion of aromaticity/antiaromaticity has been well supported by DFT level theoretical calculation and solid state X-ray crystal structural proof wherever possible.

Chapter 4

4.1. Introduction

Aromaticity is a fundamental concept in chemistry that explains molecular stability and their reactivity. According to Hückel's rule, cyclic conjugation, planarity and (4n + 2)π-electrons in the conjugation path way are the essential factors required to define aromaticity of a compound.[1] Expanded porphyrins, which contain more than four pyrrole rings connected by *meso*-methine bridges have come to the forefront in the research field of aromaticity for the study of both Hückel and Möbius aromaticity. Since their molecular topologies can be easily interchanged and controlled by various external stimuli such as metal coordination,[2] temperature control,[3] and protonation[4].

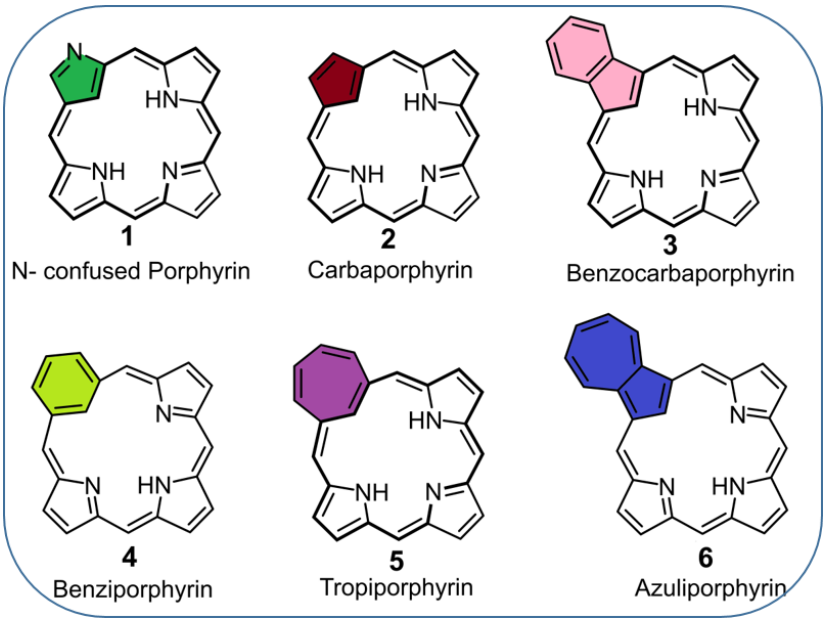

Figure 4.1. Literarure known carbaporphyrin

Modifications of porphyrinoid core, which involves the replacement of one[5] or more[6] of the nitrogen atoms by CH unit, have led to a new class of macrocycles known as carbaporphyrinoids. They can be classified as monocarbaporphyrins, opp-dicarbaporphyrins , adjdicarbaporphyrins , tricarbaporphyrins, and

tetracarbaporphyrinoid.[7] Carbaporphyrins[8], benziporphyrins,[9] tropiporphyrins,[10] and azuliporphyrins[11] are the true conjugated monocarbaporphyrinoids.[12] Azuliporphyrins, first reported in 1997 by Lash and coworkers, are a class of carbaporphyrins where azulene is incorporated into the macrocyclic framework (Figure 4.2).

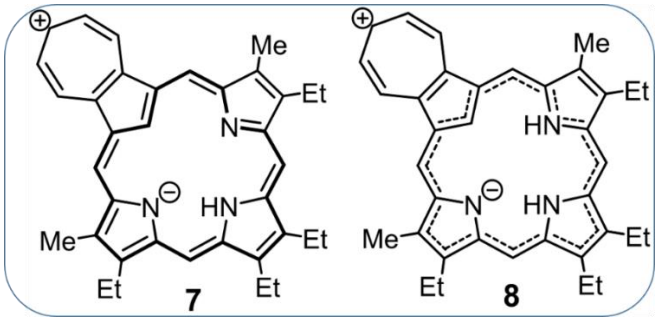

Figure 4.2. Charge Seperated Azuliporphyrin

Spectroscopic properties reveal that these type of macrocycles show borderline porphyrin aromaticity with dipolar canonical forms making important contributions and their aromatic character usually increases upon protonation.[11] Azuliporphyrins exhibit unusual reactivity, can act as trianionic ligands as well as dianionic ligands, can also stabilize unusual oxidation states of metals such as silver(III), form stable organometallic complex with Ni(II), Pd(II), Pt(II), Ru(II), Rh(III), Ir(III), and undergo oxidative metalation with copper(II) salts (Figure 4.3).[13]

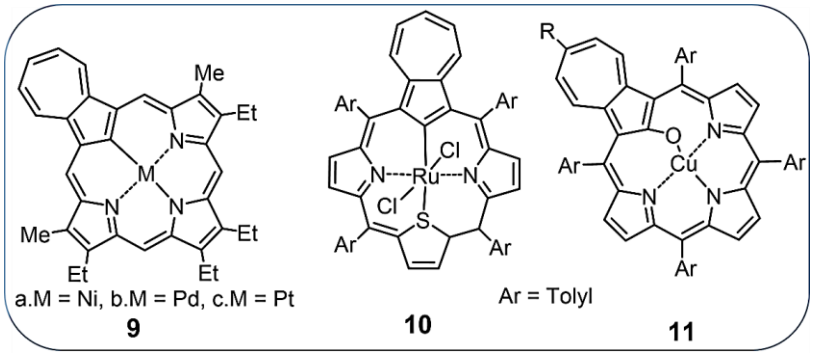

Figure 4.3. Metal complexes of azuliporphyrins

Both the electronic structure and the aromaticity can be further altered by replacing one or more nitrogen atoms inside the core by heteroatoms, such as S or Se, and are termed as core modified azuliporphyrins (Figure 4.4)[14]

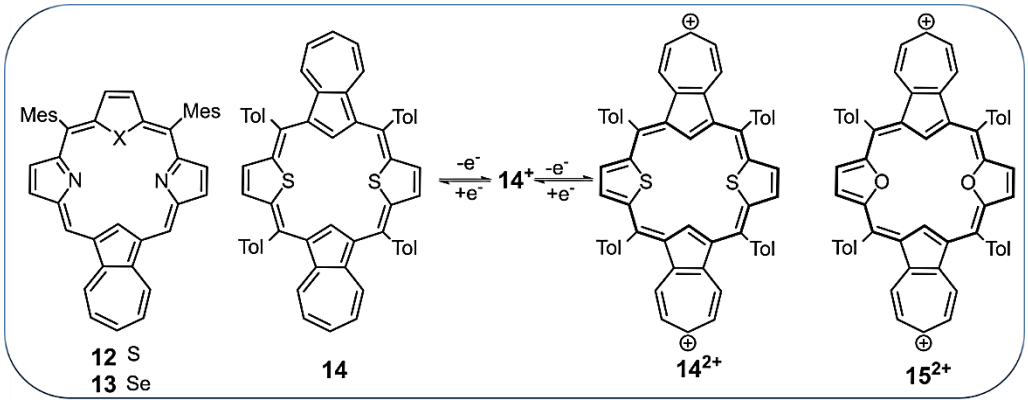

Figure 4.4.Core modified azuliporphyrin

Sapphyrin is the simplest possible expanded porphyrin with 22π electrons. The existence of sapphyrins was noted serendipitously by Woodward and coworkers[15] during their efforts to synthesize vitamin B_{12}, although the synthesis of azasapphyrins was reported much later. Woodword named these pentapyrrolic compounds as sapphyrins because of their intense blue-colored crystals

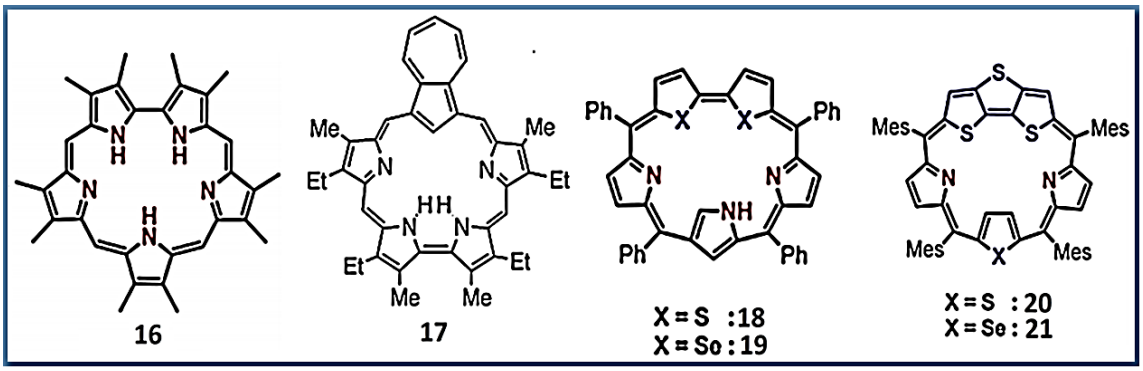

Figure 4.5. Literature known modified-sapphyrins

Sapphyrins is the first reported example of a class of macmcycles that has come to be known in general terms as “expanded porphyrins”. Sapphyrin have potential application, anion binding, photodynamic therapy (PDT),photodynamic inactivation (PDI), and magnetic resonance imaging (MRI).[16] The first carbasapphyrin was reported by T. D. Lash and co worker.The free base carbasapphyrins were unstable but the monoprotonated hydrochloride salts could easily be isolated and characterized. Carbasapphyrins retain a strong diatropic ring current due to the presence of 22π electron delocalization pathways and exhibiting NIR absorption. [17] N-Confused Expanded Porphyrin: First Example of a Modified Sapphyrins with an Inverted N-Confused Pyrrole Ring **18** and **19** were synthesized by Tavarekere K. Chandrashekar and co-worker exhibiting NIR absorption.[18] In continuation *meso*-Aryl Core-Modified Fused Sapphyrins **20** and **21** were synthesized by the same group which exhibited NIR absorption with adoptive aromaticity in free base as well as in their protonated form.[19]

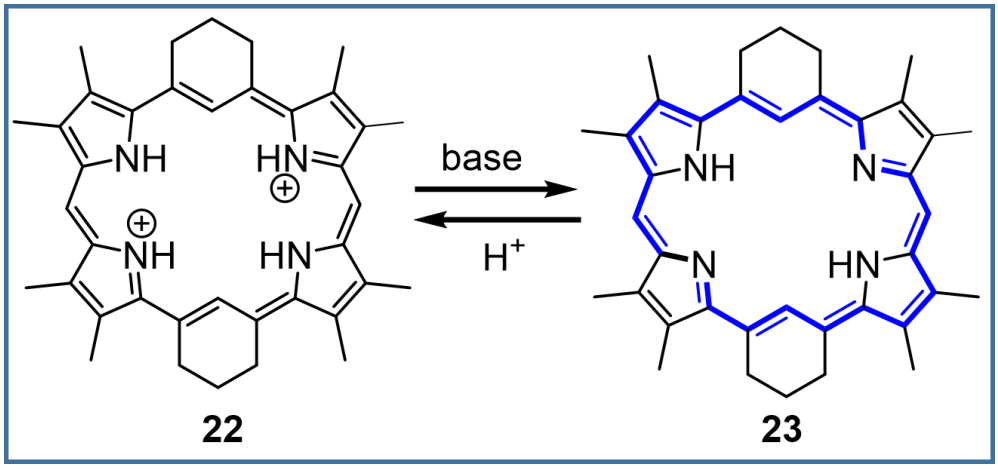

Figure 4.6. Vinylogousporphyrins

Vinylogousporphyrins are annulene-like systems with extended π-conjugation pathways that could be used both to explore the limits of aromaticity and antiaromaticity. Due to strong red-shifted absorption spectra, vinylogous porphyrins are attractive as potential sensitizers for use in various light-based therapeutic

applications. They have been found potential application in Photosensitizers in photodynamictherpy.[20] Vinylogous porphyrin systems exhibits unusual E-Z isomerization in the presence of $PdCl_2$ resulting in new class of *cis–trans* interconvertible isomers, with diverse structural and electronic properties.[21] *Cis-trans* isomarisation are induced by light,[22]heat, solvent,[23] their tautomer.[24] Molecules exhibiting such phenomena find potential application as optical memories and switches at the molecular level.[25]

First vinylogous porphyrin, 22π-electron [1,3,1,3] platyrin **22** was reported by Berger and LeGoff.[26] Upon deprotonation of **23** gave the corresponding free base **22** (Figure 4.6). The free base **23** is unstable but its dication species **22** is stable and aromatic with NIR absorption. In continuation, macrocycle **24** (the protonated form of **25**), reveals a strong diamagnetic ring current effect. [27]

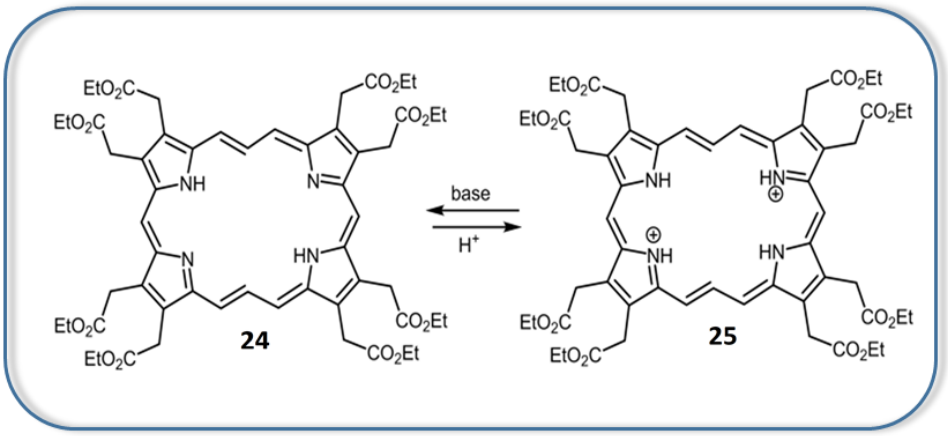

Figure 4.7. Vinylogousporphyrins

First member in this series of tetravinylogous porphyrins was synthesized by Franck and Gosmann in 1986, via a biomimetic sequence analogous to porphyrin biosynthesis.[28] This expanded porphyrin exhibits a remarkably strong diatropic ring-current effect. The aromatic porphyrin like nature of **26** is manifested in its absorption spectrum by the presence of an

intense Soret band at 546 nm and a remarkably intense long wave absorption at 783 nm with a shoulder at 830 nm. Photophysical studies of this 26π system of **26** have served to identify as a potential candidate for application in PDT.

In continuation the electronic absorption of furan analog of aromatic octaethyl-[26] porphyrin-(3.3.3.3) **27** exhibited a strong Soret band at 525 nm and Q bands at higher wavelength.[29]

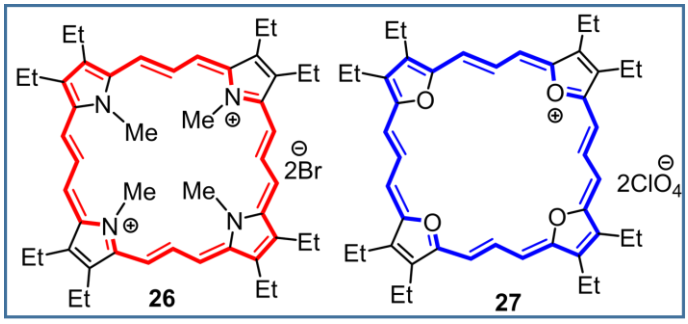

Figure 4.8. Tetravinylogous porphyrins

The aromatic octavinylogous [34]porphyrin-(5.5.5.5) system **29** was synthesized by Knfibel and Franck in 1988.[30] The [34] porphyrin **29**, which forms deep blue (λmax = 664 nm) solutions, exhibited an extraordinarily large ring-current effect in the 'H NMR spectrum.

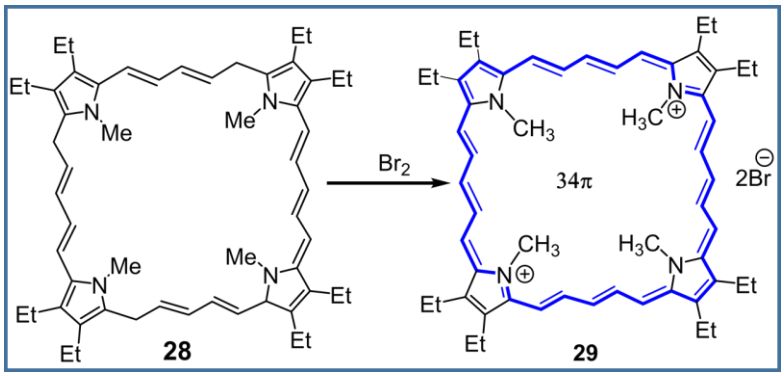

Figure 4.9. Octavinylogous [34]porphyrin-(5.5.5.5)

Chapter 4

Azulene incorporated expanded carbaporphyrinoids continue to be synthesized for studying their interesting photophysical property of free base and their metal complex[31]. In this chapter I have synthesized NIR absorptive aromatic (anti-aromatic) core modified vinylogous azulisapphyrins (1.3.3.1.0).

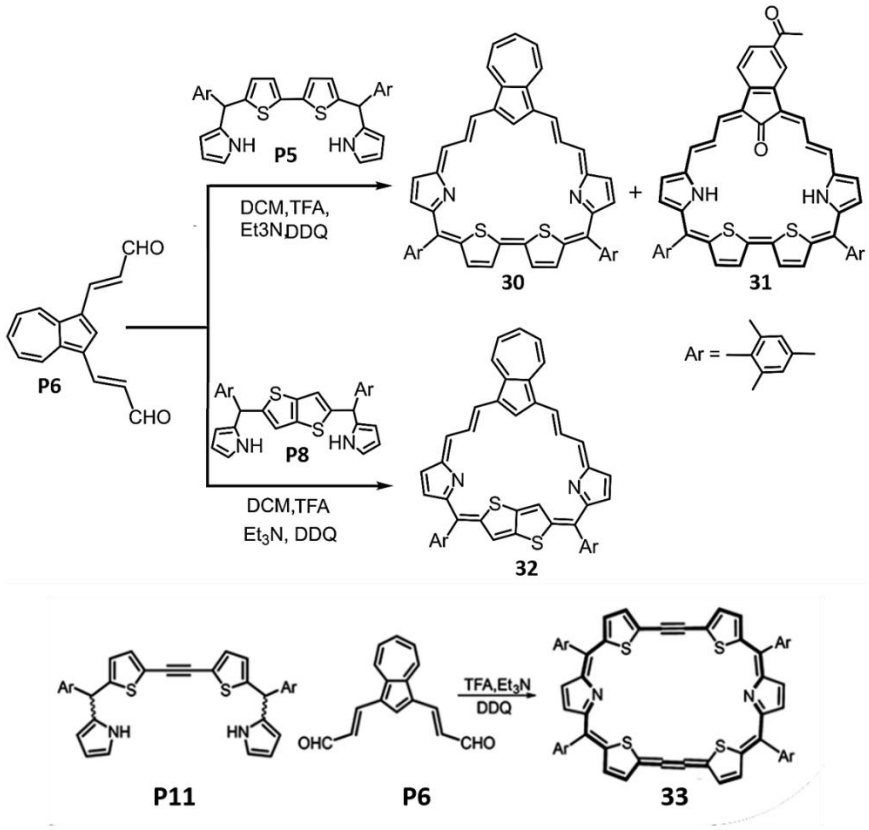

Scheme 4.1. [4 + 1] Acid-Catalyzed Condensation of core modified carbapo rphyrinoid **30,31, 32** and **33**

4.2. Result and Discussion

As outlined in Scheme 4.1, a [4 + 1] acid-catalysed MacDonald type oxidative condensation, i.e. the reaction of tetrapyrrane **P5** with azulene-1,3-bis-acrylaldehyde **P6** in methylene chloride using trifluoroacetic acid (TFA) as the catalyst followed by oxidation with DDQ, led to the exclusive isolation of carbasapphyrins **30** and **31**. Column chromatographic separation over basic alumina followed by repeated silica

gel (200–400 mesh) chromatographic separation and preparative thin layer chromatography (PTLC) techniques led to the isolation of **30** in 20% yield as a violet solid, while **31** was obtained as a shining green solid in ~30% yield.

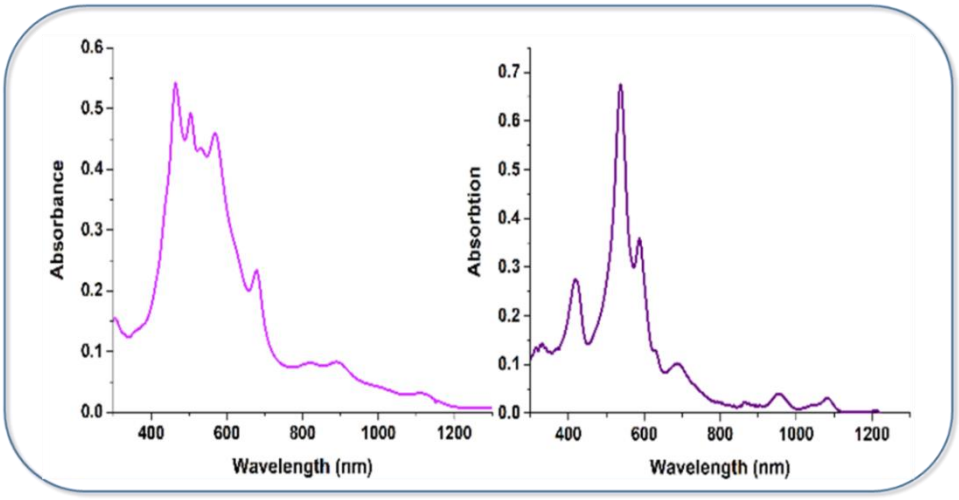

Figure 4.10. UV-vis-NIR Spectrum of 30 (left) & 31 (right) in CH_2Cl_2

The structures of these new macrocycles were precluded by various spectroscopic analyses. The heteroannulenes **30**, and **31**, and exhibited parent ions peaks at m/z 759.2867 and 789.2608, respectively, in ESI-TOF mass spectrometer accounting for their compositions. (Fig. 4.45, Fig. 4.46). The presence of a C=O group has been confirmed by the transitions at 1685 cm^{-1} for **31** in the IR spectrum. The elemental composition of **32** has been confirmed by MALDI-TOF spectral analysis with m/z value at 732.781. The electronic absorption spectral patterns of **30**and **31** (Fig. 4.10) with strong Soret band(s) and well-defined Q-type bands along with NIR absorption beyond 1000 nm engender typical porphyrinic nature[32] that would be expected for highly delocalized, conjugated systems potentially corresponding to aromatic [26] system. The electronic absorption spectra of the macrocycle **30** in the free base exhibited exhibited split Soret bands at 464, 504 and 531 nm followed by multiple Q-bands at 678, 817, 889 and 1111 nm respectively. That indicates the tropylium character of **30"** plays an important role in the aromatization of the molecule.[8] While Carbasapphyrin **31** exhibited split Soret bands at 537 and 587 nm along with Q-type

bands at 992 and 1082 nm. Under these premises, porphyrinoid **30** can be surmised as **30**" with π-electron communication mediated by charge separated dipolar resonance form while **31** could exist as the enol tautomers **31**"-1 and **31**"-2 (Scheme 2).

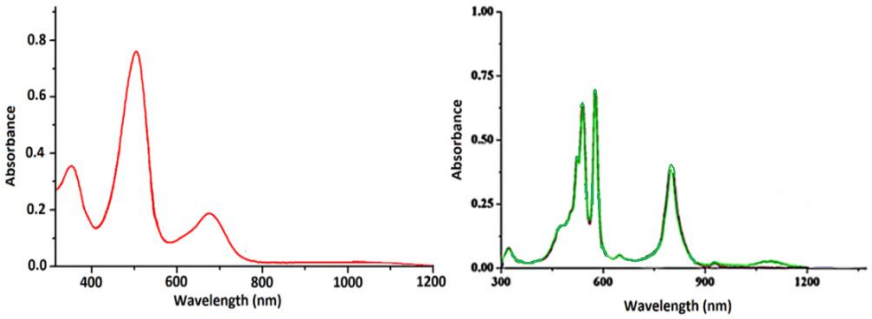

Figure 4.11. UV-vis-NIR Spectrum of 32 (left) & 33 (right) in CH_2Cl_2

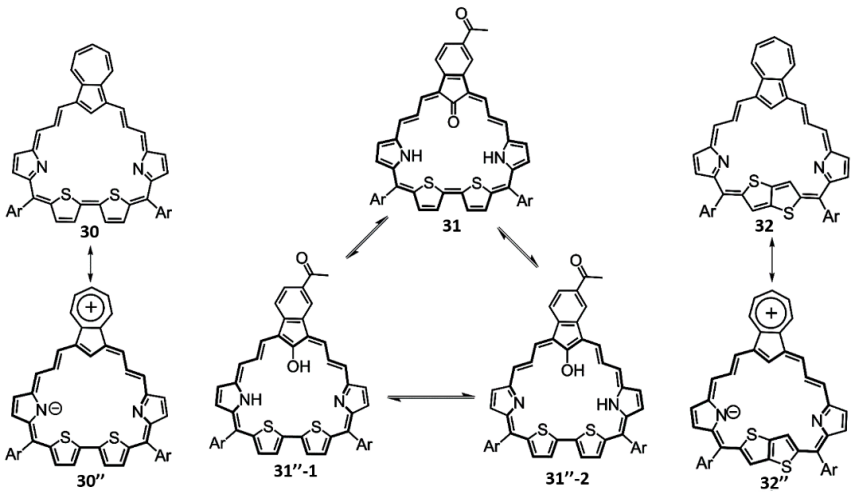

Scheme 2. Charge separated Dipolar resonance structure of **30** and **32**and enol-tautomers of **31.**

The formation of macrocycle **31** was confirmed by solid state single crystal X-ray diffraction analysis. Slow evaporation of diethyl ether–dichloromethane solutions of **31** resulted in X-ray quality single crystals. [33] The diffraction-based X-ray crystal structure of **31** happened to be planar (Fig. 4.13 D). The solid-state X-ray crystal structure reveals macrocyclic π-conjugation with a 28π electron path. While the seven

membered ring of azulene has been transformed into an acetylated benzene ring, the five membered ring is with a ketone group. The carbonyl group of the acetyl substituent is disordered over two sites in 1 : 3 ratio and the terminal C28 atom (Fig. 4.12) resides on the mirror plane (space group Pnma), and hence treated with a fixed occupancy of 0.5 (0.25 for each disordered part). Based on the in-depth spectroscopic analyses and DFT level theoretical studies, we interpret **31** to exist as its enol tautomers **31 ″-1** and **31 ″-2**, accounting for its aromaticity

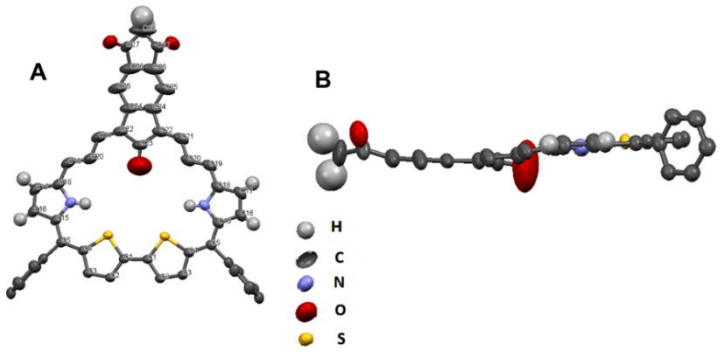

Figure 4.12 X-ray crystal structure of **31** (A: Top view, B: side view). The thermal ellipsoids are scaled to 50% probability level

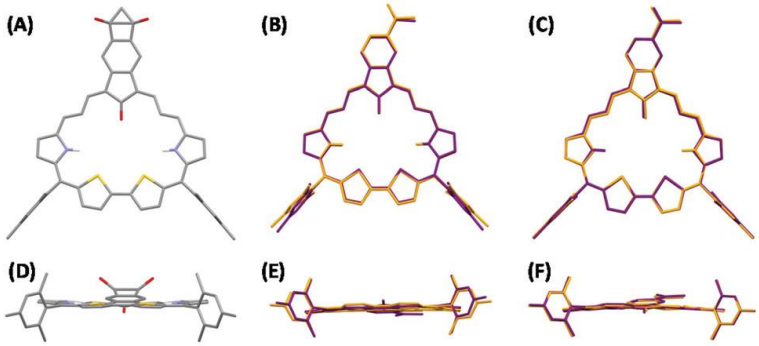

Figure 4.13. Molecular structure of **31** determined by X-ray crystallographic analysis. (A: top view, D: side view), structure overlay between XRD (purple) and computed (orange) structures (B: top view, E: side view), C: structure overlay between **31''-1** (purple) and **31''-2** (orange) optimized structures (C: top view, F: side view). Solvent molecules and hydrogen atoms are omitted (except for NHs) for clarity

NMR analyses reveal the features of aromaticity for both **30** and **31**. The diatropic ring current of the macrocycles clearly distinguished the protons present in the core and on the periphery of the macrocycle. All the protons present in the cavity of the

macrocycles resonate in the up-field region, while the signals for the periphery protons are strongly deshielded due to the ring current effect of the macrocycle. The explicit assignment of individual proton signals is based on 2D homo and hetero correlations More precisely, for **30**, upon lowering the temperature to 223 K, the most shielded triplet at 1.03 ppm resonated at 0.12 ppm, while the most deshielded doublets at 9.61 and 10.1 ppm were further deshielded to 9.78 and 10.26 ppm (Fig. 4.14). The two sets of doublets at 10.26 and 9.78 ppm correlating with each other (Fig. 4.15) and exhibiting correlation with the triplet at 0.61 ppm in the COSY spectra at 263 K (Fig. 4.16) unambiguously confirm the doublets as external bridging methines (a and b) while the triplet as internal bridging CH (c). The observed Δδ value[34] (difference in the chemical shift between inner NH/CH and outer NH/CH protons in the 1H NMR spectrum) of 9.65 ppm for **30** concludes substantial diamagnetic ring current in the macrocycle. The fully assigned ^{1}H NMR spectrum of **30**, shown in Fig. 4.19-4.20 (Fig. 4.21A′), strongly supports the charge-separated dipolar resonance structure **30** (Scheme 2) ascribable to aromaticity through a [26]π electronic delocalization motif.

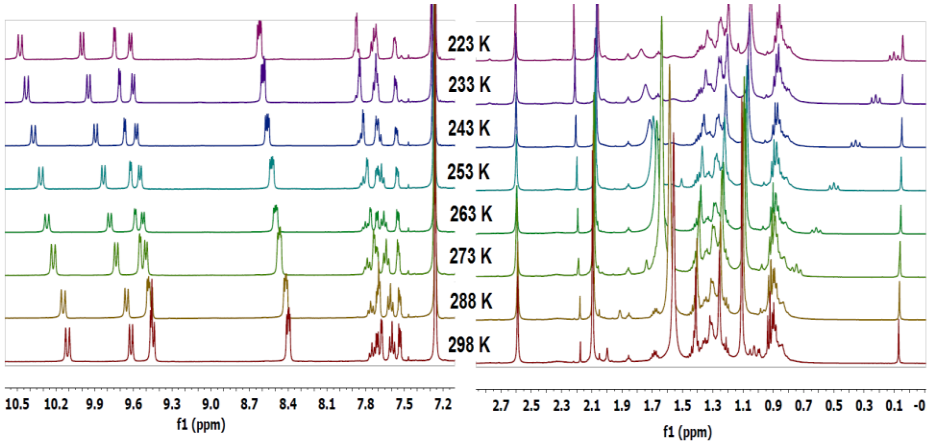

Figure 4.14. Variable temperature ^{1}H NMR Spectra of free base 30 in $CDCl_3$

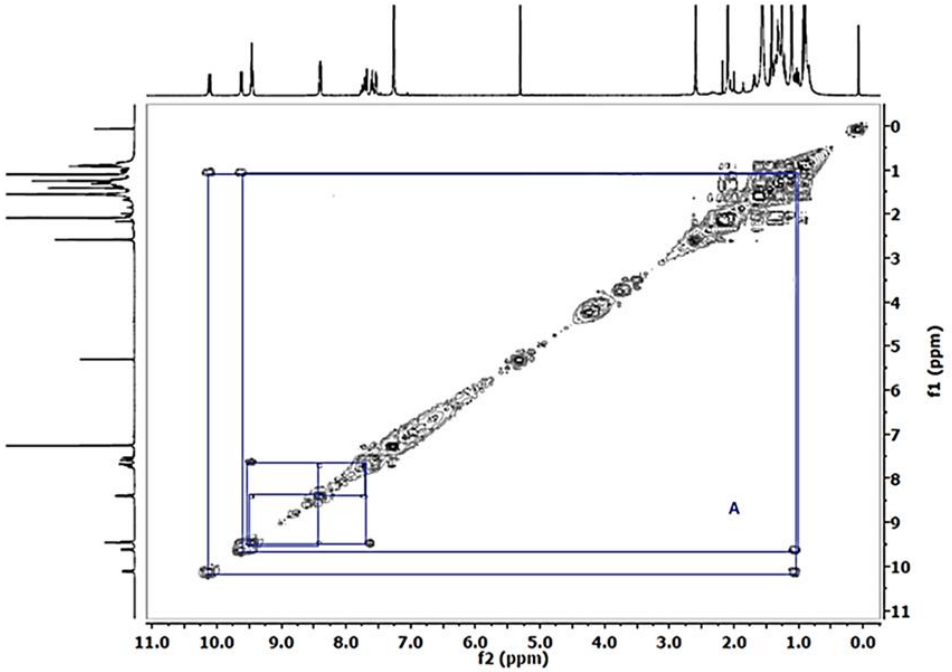

Figure 4.15.^{1}H-^{1}H COSY spectrum of free base 30 in $CDCl_3$ (A: 298 K)

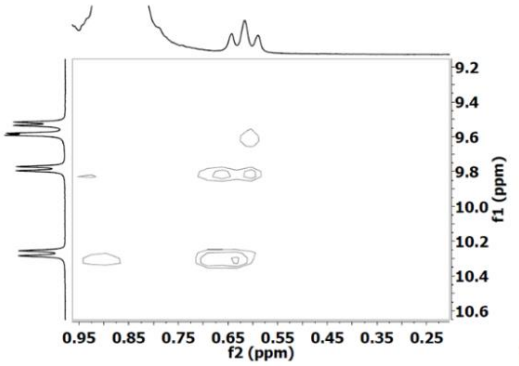

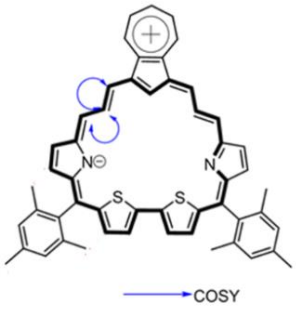

^{1}H ppm	^{1}H ppm
10.26 (d)	0.61 (t)
9.78 (d)	0.61(t)

Figure 4.16: ^{1}H -^{1}H 2D COSY NMR spectra of **30** in $CDCl_3$ at 263 K

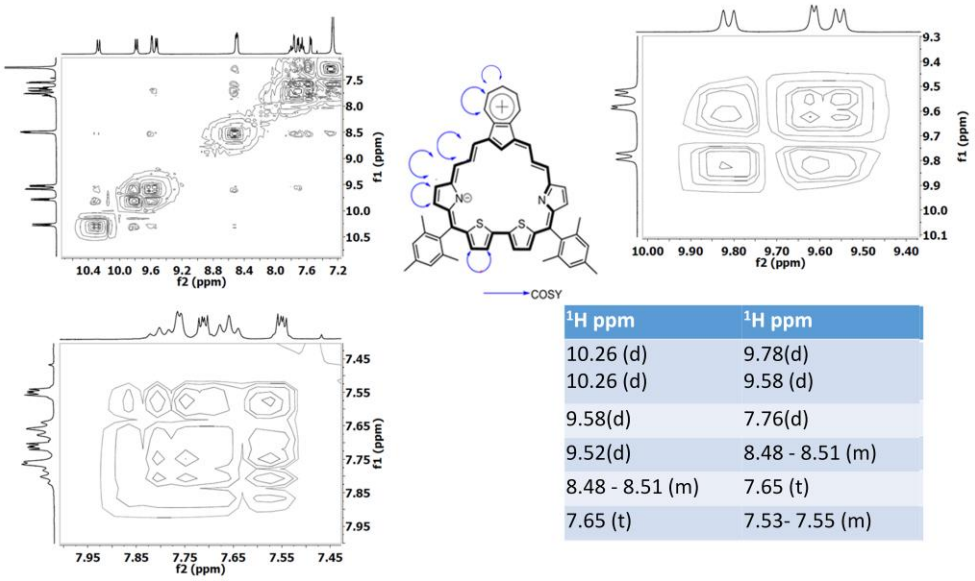

^{1}H ppm	^{1}H ppm
10.26 (d) 10.26 (d)	9.78(d) 9.58 (d)
9.58(d)	7.76(d)
9.52(d)	8.48 - 8.51 (m)
8.48 - 8.51 (m)	7.65 (t)
7.65 (t)	7.53- 7.55 (m)

Figure 4.17. ^{1}H-^{1}H COSY spectra of free base 30 in $CDCl_3$ at 263 K

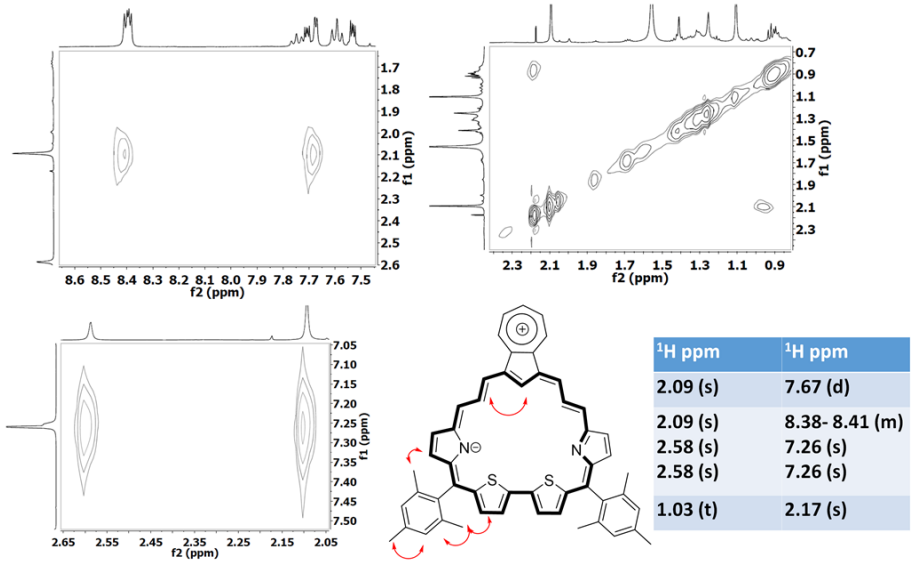

^{1}H ppm	^{1}H ppm
2.09 (s)	7.67 (d)
2.09 (s) 2.58 (s) 2.58 (s)	8.38- 8.41 (m) 7.26 (s) 7.26 (s)
1.03 (t)	2.17 (s)

Figure 4.18: ^{1}H -^{1}H 2D ROESY NMR spectra of **30** in $CDCl_3$ at 298 K

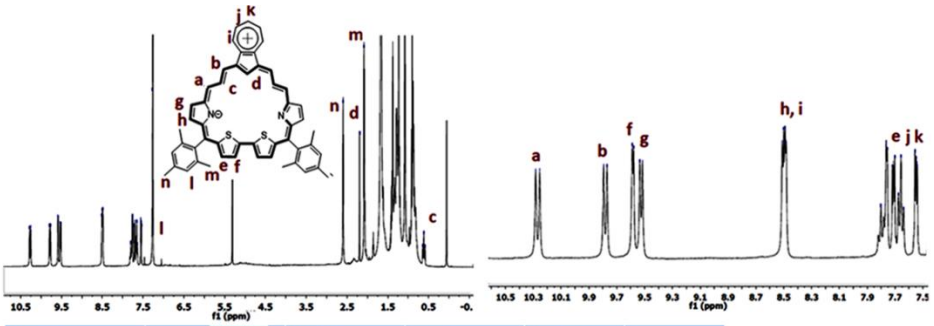

Position	ppm	Position	ppm	Position	ppm
a	10.26 (d)	g	9.52 (d)	l	7.26
b	9.78 (d)	h, i	8.48-8.51 (m)	m	2.07
c	0.61 (t)	j	7.65 (t)	n	2.59
d	2.19 (s)	k	7.53-7.55 (m)		
e	7.76 (d)				
f	9.58 (d)				

Figure 4.19. Complete ^{1}H NMR spectral assignment of **30** in $CDCl_3$ at 263 K

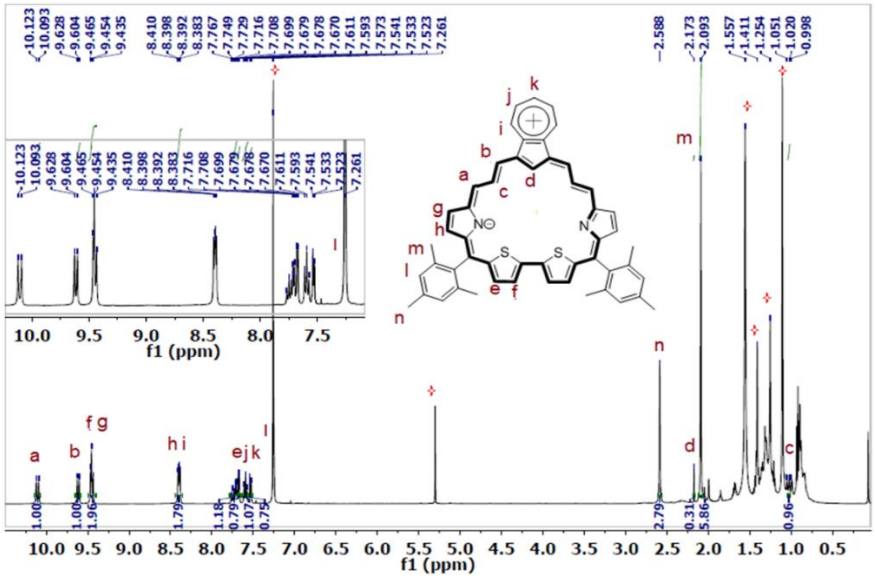

Figure 4.20: Complete ^{1}H NMR spectral assignment of **30** in $CDCl_3$ at 263 K

For **31**, 1H NMR spectra revealed many signals compared to **30** in the entire region. However, based on 2D homo and hetero correlations (Fig. 4.22–4.28), it was possible to assign each individual peak and postulate the existence of enol form **31″** as two equilibrating NH tautomers **31″**-1 and **31″**-2 each with an intrinsic asymmetry.

The observed Δδ value[33] of 14.83 ppm for **31**″ reveals a sustained diatropic ring current in the macrocycle. Though acquisition of **31**″-1 and **31**″-2 as two NH tautomers (Scheme 2) could be expected for **31**″, however given the broadening of the peaks in the spectral pattern, **31** could exist in isoenergetic enol forms **31**″-1 and **31**″-2 through a [26]π electronic delocalization motif in solution. Fig. 4.21B′ shows the partial ^{1}H NMR spectra of **31**″, while (Fig. 4.28) shows each individual peak assignment. The sparingly soluble nature of **31** in a high boiling deuterated solvent made it difficult to record variable high temperature ^{1}H NMR spectra at lower temperature (Fig.4.14); however no drastic change was visible nor any shift in the ppm values for the signals. This supports the existence of the isoenergetic tautomers **31**″-1 and **31**″-2 in solution.

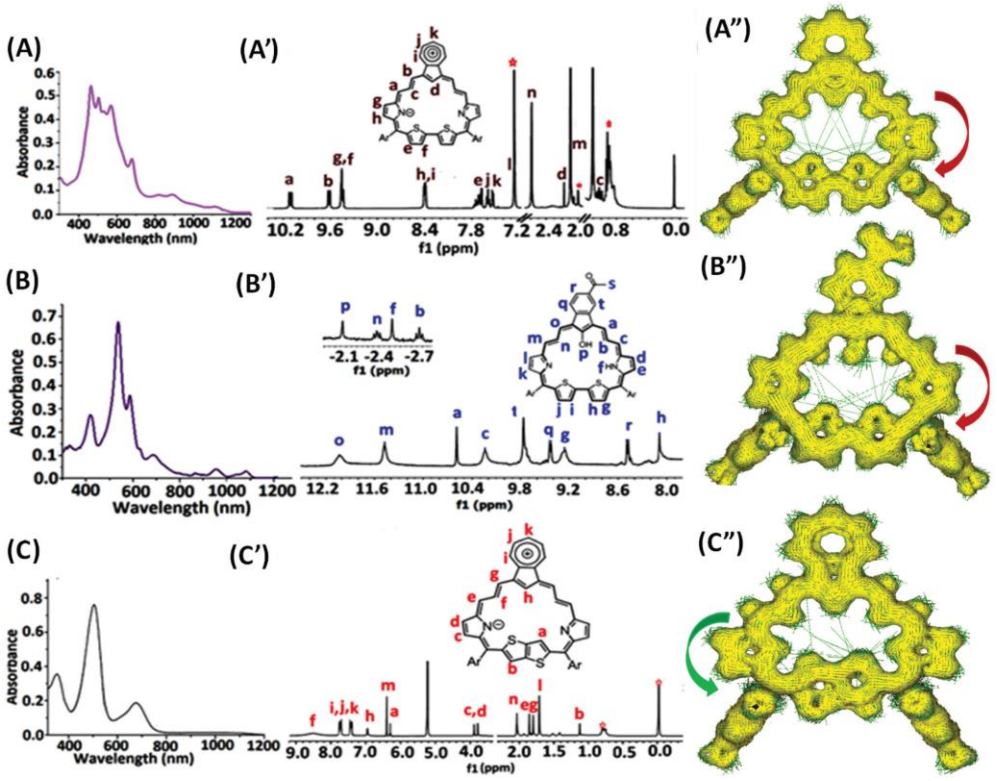

Figure 4.21 UV-vis-NIR absorption spectra of **30** (A), **31** (B), and **32** (C) in CH_2Cl_2 at 298 K. ^{1}H-NMR Spectra of **30**'' as a free base in $CDCl_3$ at 263 K (A'),**31**'' in CD_2Cl_2 at 298 K (B') and **32**'' as a free base in CD_2Cl_2 at 298 K (C'). AICD plots of **30** (A''), **31**'' (B'') and **32** (C'').

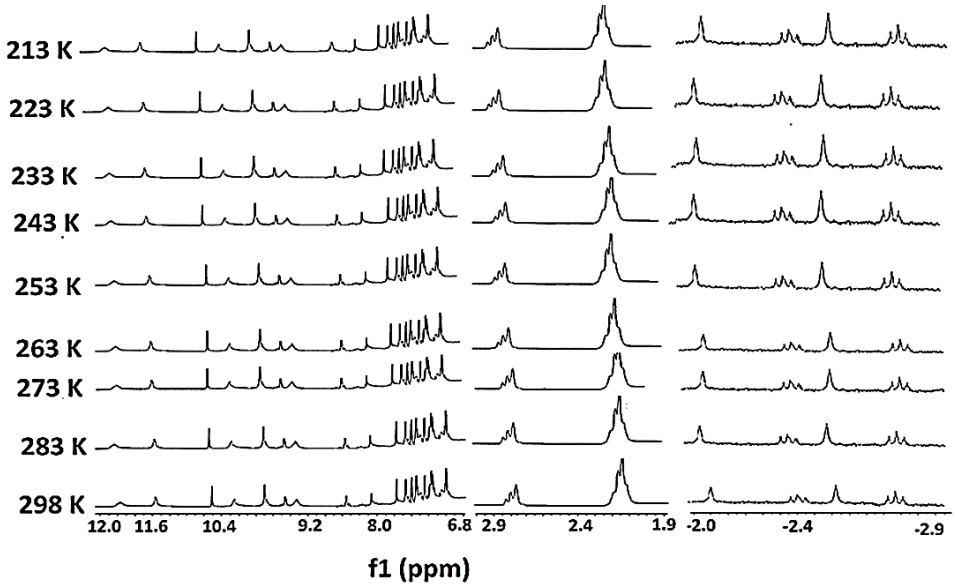

Figure 4.22. Low VT ^{1}H NMR spectra of **31''** in CD_2Cl_2

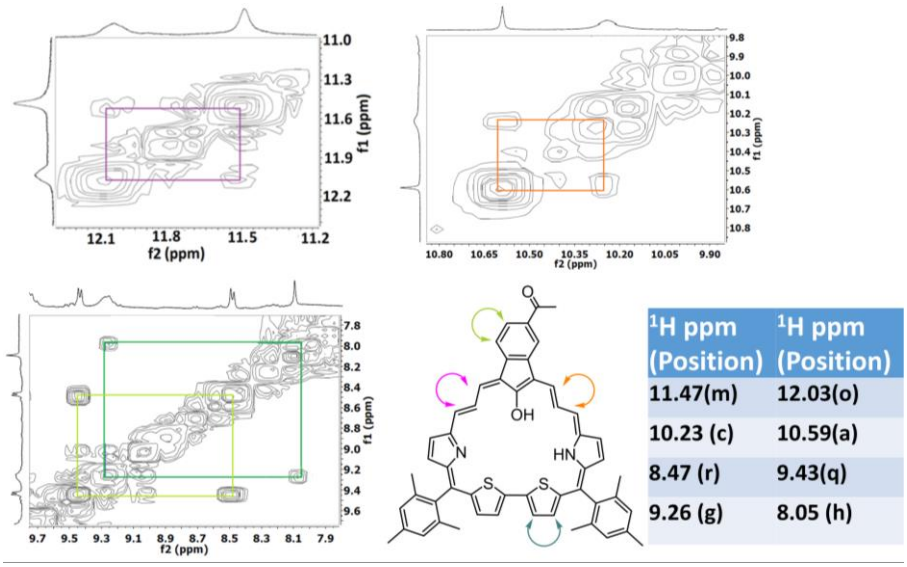

^{1}H ppm (Position)	^{1}H ppm (Position)
11.47(m)	12.03(o)
10.23 (c)	10.59(a)
8.47 (r)	9.43(q)
9.26 (g)	8.05 (h)

Figure 4.23: ^{1}H -^{1}H 2D COSY NMR spectra of **31''** in CD_2Cl_2 at 298 K

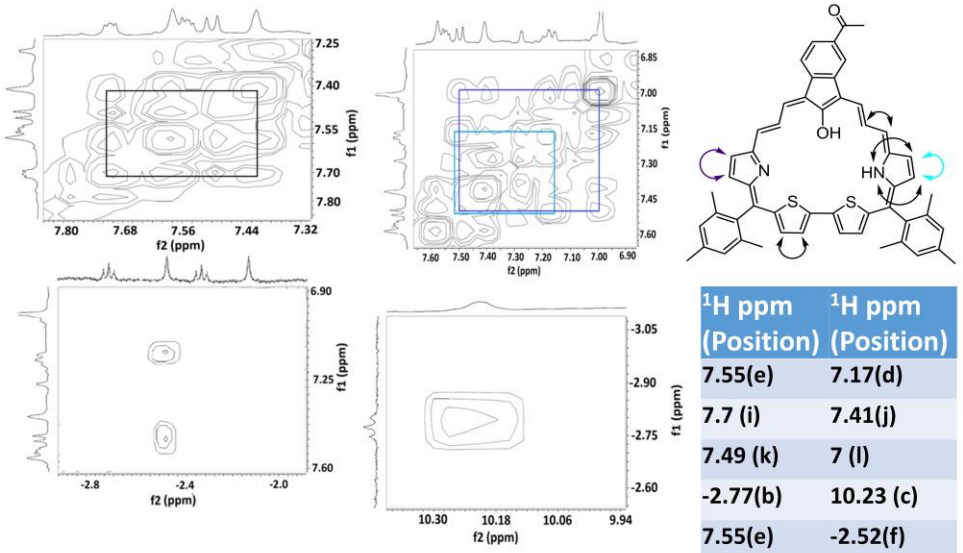

^{1}H ppm (Position)	^{1}H ppm (Position)
7.55(e)	7.17(d)
7.7 (i)	7.41(j)
7.49 (k)	7 (l)
-2.77(b)	10.23 (c)
7.55(e)	-2.52(f)
7.17(d)	-2.52(f)

Figure 4.24: ^{1}H -^{1}H 2D COSY NMR spectra of **31"** in CD_2Cl_2 at 298 K

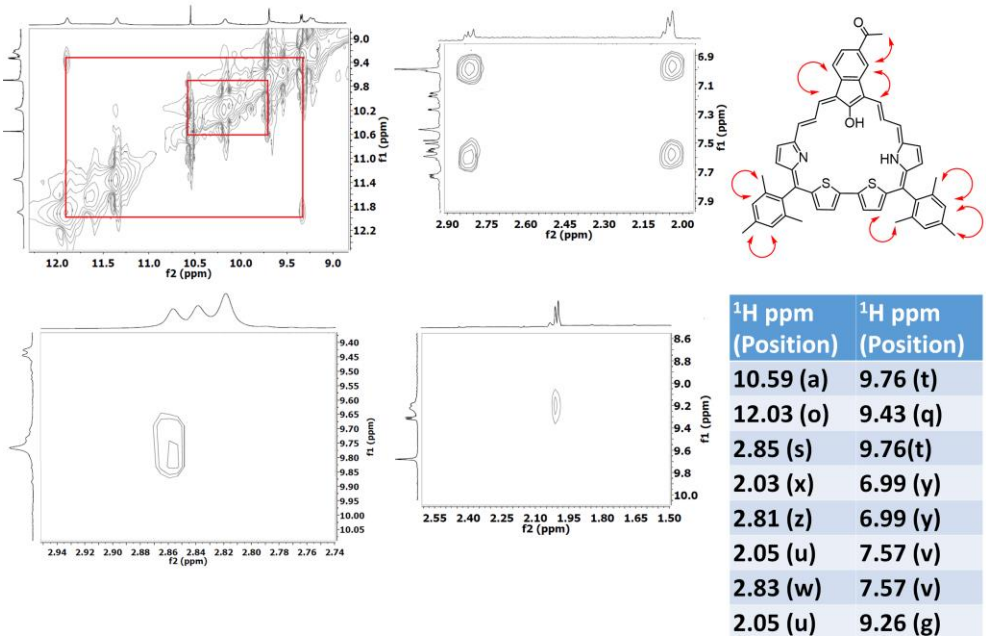

^{1}H ppm (Position)	^{1}H ppm (Position)
10.59 (a)	9.76 (t)
12.03 (o)	9.43 (q)
2.85 (s)	9.76(t)
2.03 (x)	6.99 (y)
2.81 (z)	6.99 (y)
2.05 (u)	7.57 (v)
2.83 (w)	7.57 (v)
2.05 (u)	9.26 (g)

Figure 4.25. ^{1}H -^{1}H 2D ROESY NMR spectra of **31"** in CD_2Cl_2 at 298 K

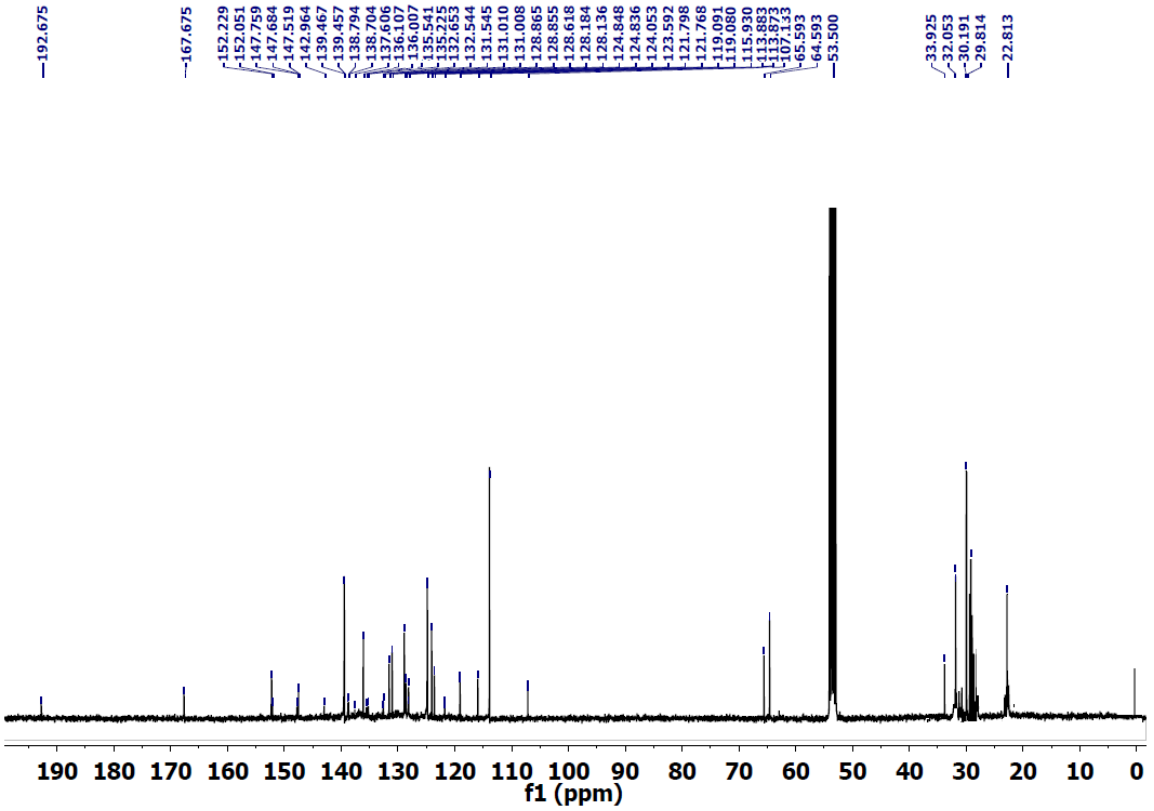

Figure 4.26: ^{13}C NMR spectra of **31"** in CD_2Cl_2 at 298 K

In order to understand the effect of the type of precursor in modulating the formation of highly aromatic and NIR absorptive porphyrinoids **30″/31″**, we reacted pyrromethane **P8** with **P6**, as shown in Scheme 1. Surprisingly, under similar reaction conditions to those for **30/31**, we anticipated macrocycle **32** as the sole product (Scheme 1) in 25% yield, while acidolysis of pyrromethane **P11** (Scheme S1) has led to the formation of enthynylene-cumulene conjugated [30] porphyrinoid **33**.[35] The elemental composition of **32** has been confirmed by MALDI-TOF spectral analysis with the m/z value at 732.781 (Fig. 4.47). The steady state electronic absorption spectra of **32** exhibit the Soret band at 511 nm, and a Q-type broad band centred at

658 nm with a weak band stretched up to 1200 nm (Fig. 4.21C and Fig.4.11), thus indicating porphyrin nature with antiaromaticity. [36]

Well resolved ^{1}H-NMR peaks were obtained at ambient temperature for **32**. Intriguingly, though a highernumber of signals are expected in the ^{1}H NMR spectrum based on the lower symmetry of the macrocycle **32**, experimentally we did not anticipate such observation even after lowering the temperature. The low temperature ^{1}H NMR spectral patterns of **32** (Fig. 4.29) revealed structural rigidity with a near planar macrocyclic framework lacking conformational fluxionality. The characteristic paratropic ring current effect leads the protons inside the macrocycle to resonate in the deshielded region while leading the protons on the periphery to resonate in the up-field region.[37] The ^{1}H-NMR spectral pattern of **32** at 298 K revealed sharp singlets at 6.9, 6.3 and 6.4 ppm while a broad peak at 8.5 ppm. Based on COSY correlations (Fig. 4.30), the singlet at 6.4 ppm has been assigned to *m*-CHs of the *meso*-mesityl ring, while the singlets at 1.75 and 2.05 ppm correspond to *o* and *p*-methyl CHs, respectively. Two sets of broad peaks at 1.78 ppm and 1.88 ppm correlating with each other and correlating with the broad peak at 8.5 ppm indicated the former peaks to be from outer meso-CHs while the latter to be from inner CHs.

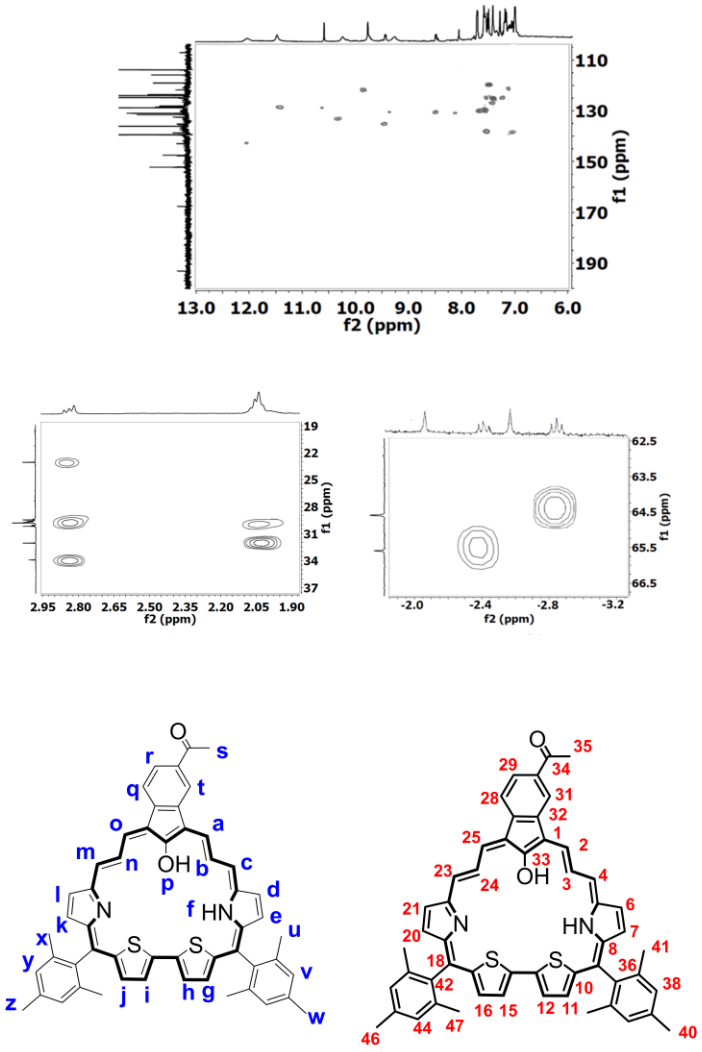

^{1}H ppm (Position)	^{13}C ppm(Position)
10.59 (a)	128.85 (2)
-2.77 (b)	64.59 (3)
	147.75(1)
10.23 (c)	132.54 (4)
	128.18 (5)
7.17 (d)	124.83 (6)
7.55 (e)	119.08 (7)
-2.52 (f)	
9.26 (g)	131.54 (11)
	128.13 (8)
	135.22 (10)
8.05 (h)	131.01 (12)
	132.65 (13)
	135.54 (14)
7.7 (i)	131 (15)
7.41 (j)	124.05 (16)
	136 (17)
	121.79(19)
7.49 (k)	123.59 (20)
7 (l)	124.84 (21)
	128.86(22)
11.47 (m)	128.61 (23)
-2.38 (n)	65.59 (24)
^{1}H ppm (Position)	^{13}C ppm(Position)
12.03 (o)	142.96 (25)
-2.07 (p)	
	147.68(26)
	152.05(27)
9.43 (q)	136.1 (28)
8.47 (r)	138.7 (29)
	167.97(30)
	152.22(32)
	107.13(33)
	192.67(34)
2.85 (s)	33.92 (35)
9.76 (t)	121.76 (31)
2.83 (u)	22.81 (41)
7.57 (v)	138.79 (38)
2.05 (w)	29.81 (40)
2.81 (x)	30.19 (47)
6.99 (y)	139.45 (44)
2.03 (z)	22.81 (46)

Figure 4.27: HSQC NMR spectra of **31"** in CD_2Cl_2 at 298 K

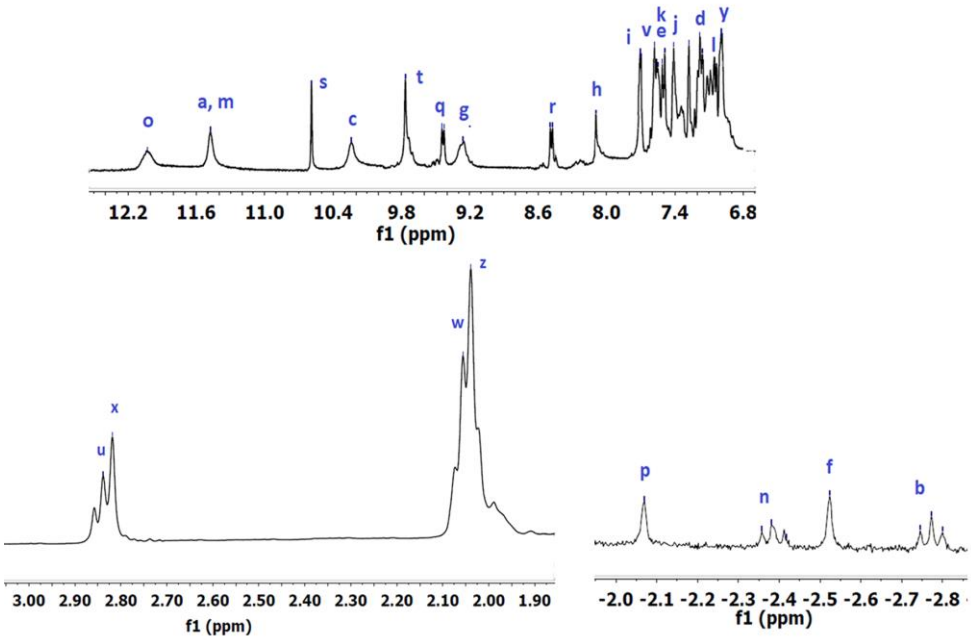

Figure 4.28: Complete ^{1}H NMR spectral assignment of **31"** in CD_2Cl_2 at 298 K

Furthermore, the broad peak at 8.5 ppm exhibiting dipolar coupling in the 2D ROESY spectra (Fig. 4.31) with the singlet at 6.9 ppm clearly reveals the latter peak to be from inner CH of the azulene five membered ring. The singlet at 6.3 ppm exhibiting no correlation with any signals in the 2D COSY and ROESY spectra has been unambiguously assigned to the inner CH of the thienothiophene ring, while the singlet at 1.1 ppm correlating with the o-methyl peak at 1.75 ppm in the 2D ROESY spectra (Fig. 4.31) strongly revealed the former to be from outer CH of the thienothiophene ring. The outer β-CH protons of noninverted pyrrole rings have been assigned to doublets at 3.8 and 3.9 ppm based on the COSY spectra. Based on the observed spectral pattern, **32** could exhibit the antiaromatic nature[37] through the dipolar resonance structure **32″** (Scheme 2) via a 24 π conjugation pathway. (Fig. 4.21C′) depicts the ^{1}H NMR spectra of **32″**.

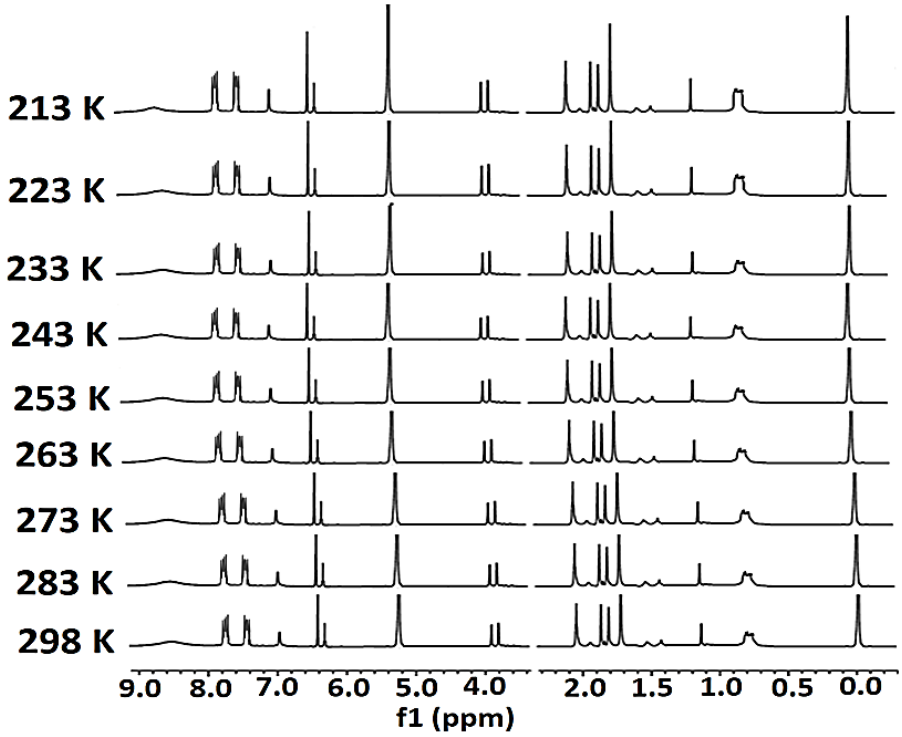

Figure 4.29: Low VT ^{1}H NMR spectral pattern of **32**in CD_2Cl_2

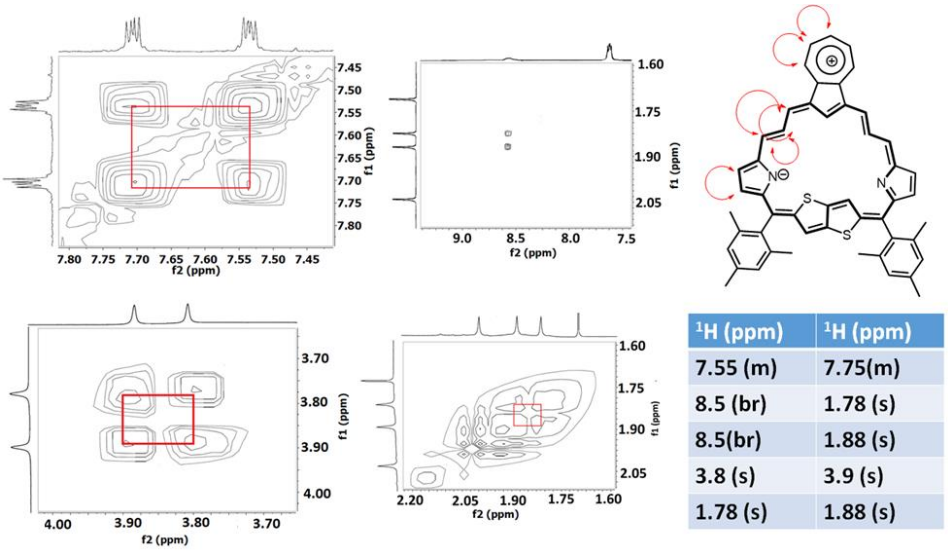

^{1}H (ppm)	^{1}H (ppm)
7.55 (m)	7.75(m)
8.5 (br)	1.78 (s)
8.5(br)	1.88 (s)
3.8 (s)	3.9 (s)
1.78 (s)	1.88 (s)

Figure 4.30: ^{1}H -^{1}H 2D COSY NMR spectra of **32** in CD_2Cl_2 at 298 K

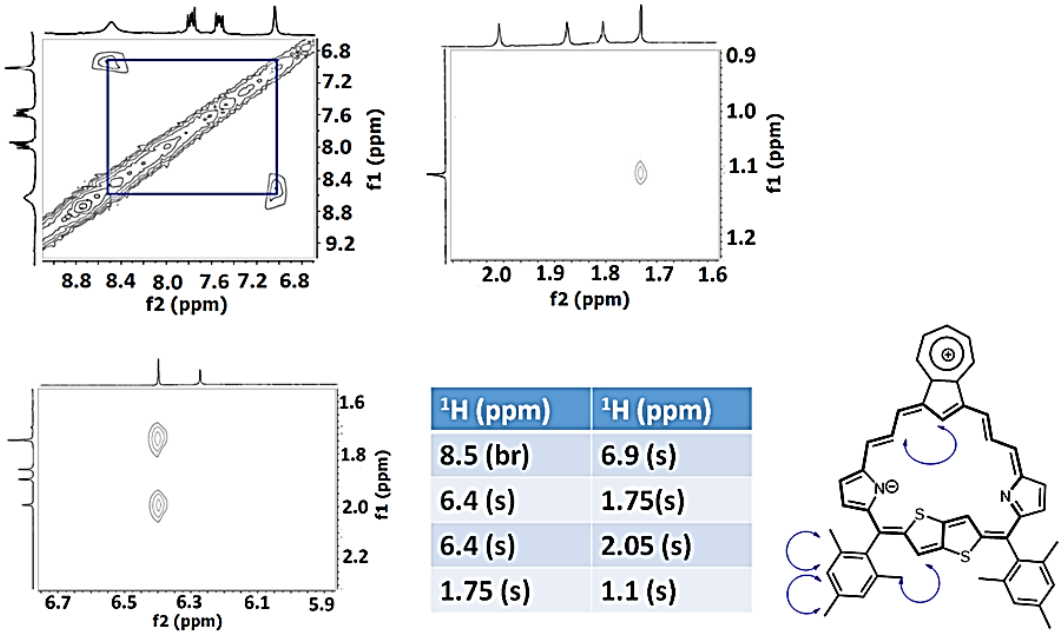

^{1}H (ppm)	^{1}H (ppm)
8.5 (br)	6.9 (s)
6.4 (s)	1.75(s)
6.4 (s)	2.05 (s)
1.75 (s)	1.1 (s)

Figure 4.31: ^{1}H -^{1}H 2D ROESY NMR spectra of **31** in CD_2Cl_2 at 298 K

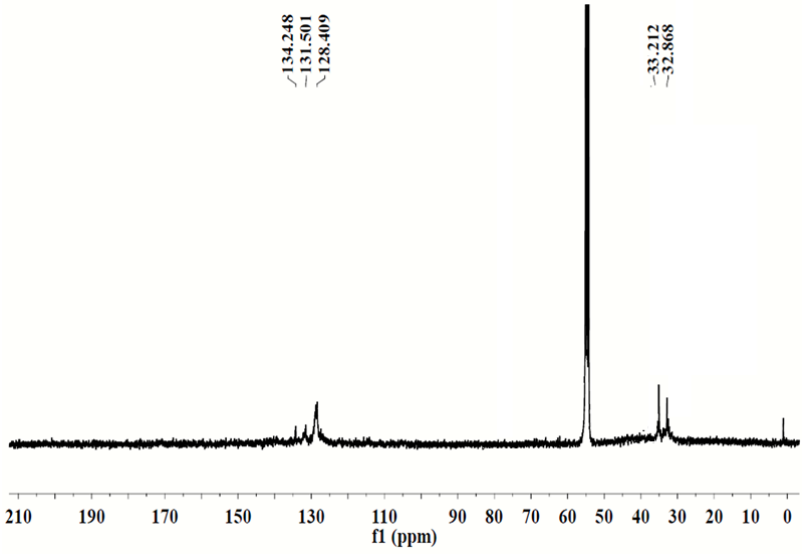

Figure 4.32: ^{13}C NMR spectra of **32** in CD_2Cl_2 at 298 K

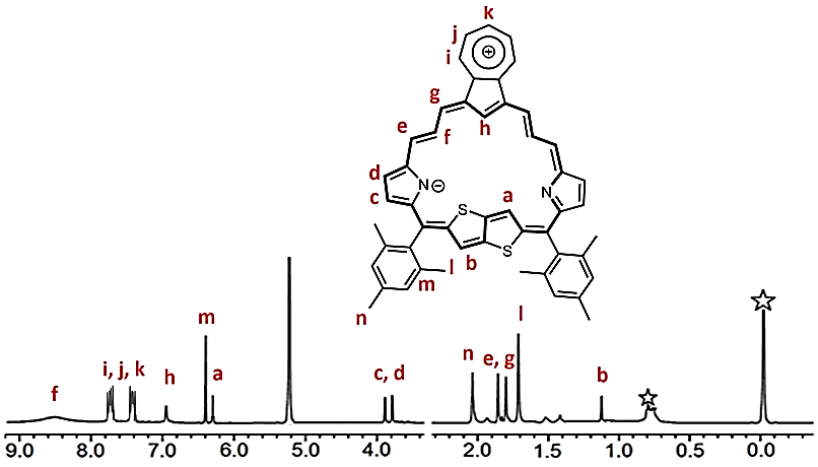

Figure 4.33: Complete ^{1}H NMR spectral assignment of **32** in CD_2Cl_2 at 298 K

Though crystallographic data for **30** and **32** are lacking, based on the density functional theory (DFT) calculations at the B3LYP/6-31G (d,p) level,[38] the keto–enol tautomer **31″** of **31** (we could not optimize the structure of **30″** and **32″** due to the charge separated dipolar resonance nature) has been postulated in addition to the conformational isomerism of **30**, **31**, **31″** and **32**. Isomer **31″**-2 of **31** is more stable than isomer **31″**-1 by a margin of 10.2 kJ mol^{-1}. There is no notable deviation in the structures between **31″**-1 and **31″**-2 (Fig. 4.52, 4.53 and Fig. 4.21C). In all the cases (**30**, **31**, **31″**-1, **31″**-2 and **32**), the conformations with inverted thiophene rings are found to be thermodynamically less stable (Table 4) and the most stable structures exhibit strictly planar geometries without any ring inversion (Fig. 4.49–4.68). This is in line with the NMR spectroscopic observations. The C–C (1.38 to 1.48 Å), C–S (1.77–1.78 Å) and C–N bond lengths (1.36–1.39 Å) of **30**, **31**, **31″**-1, **31″**-2 and **32** are within the single- and double-bond limits (Fig. 4.52), indicating enhanced delocalization of π-electrons throughout the macrocycles. The LUMO levels are nearly identical in all cases (Fig. 4.70) The HOMO levels are destabilized from **30** to **31** due to the presence of acetyl, keto and enol groups and imino/amino type pyrrole rings. Compared to the keto form (**31**), the HOMO and LUMO levels of the enol forms (**31″**-1 and **31″**-2) are

destabilized by 0.27 eV (**31**″-1), 0.25 (**31**″-2) [HOMO], and 0.07 eV (**31**″-1), 0.06 eV (**31**″-2) [LUMO], respectively, resulting in a narrow HOMO– LUMO gap (1.60 eV) for the keto form (**31**). The HOMO–LUMO gap for the enol form **31**″-1 and **31**″-2 is 1.79 and 1.78 eV, respectively (Fig. 4.34).

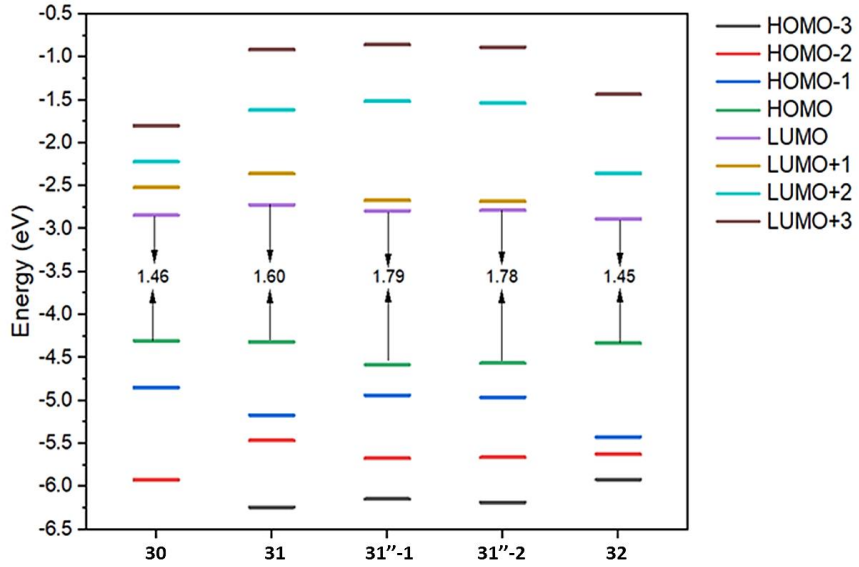

Figure 4.34 FMO energy levels of **30, 31, 31**"-**1, 31**"-**2** and **32** at the B3LYP/6-31G (d, p) level

Table 1. The calculated nucleus-independent chemical shifts (NICS) values for **30, 31, 31"-1, 31"-2** and **32**

Distance (Å)	**30**	**31**	**31"-1**	**31"-2**	**32**
-8	-0.923	-0.261	-1.772	-1.767	0.735
-7	-1.203	-0.330	-2.347	-2.342	1.033
-6	-1.582	-0.419	-3.150	-3.148	1.490
-5	-2.088	-0.527	-4.270	-4.275	2.203
-4	-2.734	-0.647	-5.791	-5.812	3.317
-3	-3.484	-0.743	-7.730	-7.776	5.002
-2	-4.206	-0.724	-9.898	-9.973	7.278
-1	-4.730	-0.421	-11.769	-11.882	9.460
0	-4.929	-0.078	-12.511	-12.653	10.299
1	-4.730	-0.439	-11.738	-11.836	9.309
2	-4.207	-0.768	-9.915	-9.964	6.995
3	-3.485	-0.798	-7.744	-7.781	4.781
4	-2.735	-0.696	-5.780	-5.813	3.190
5	-2.088	-0.566	-4.243	-4.272	2.138
6	-1.582	-0.447	-3.120	-3.144	1.459
7	-1.203	-0.351	-2.320	-2.338	1.021
8	-0.923	-0.275	-1.751	-1.764	0.733

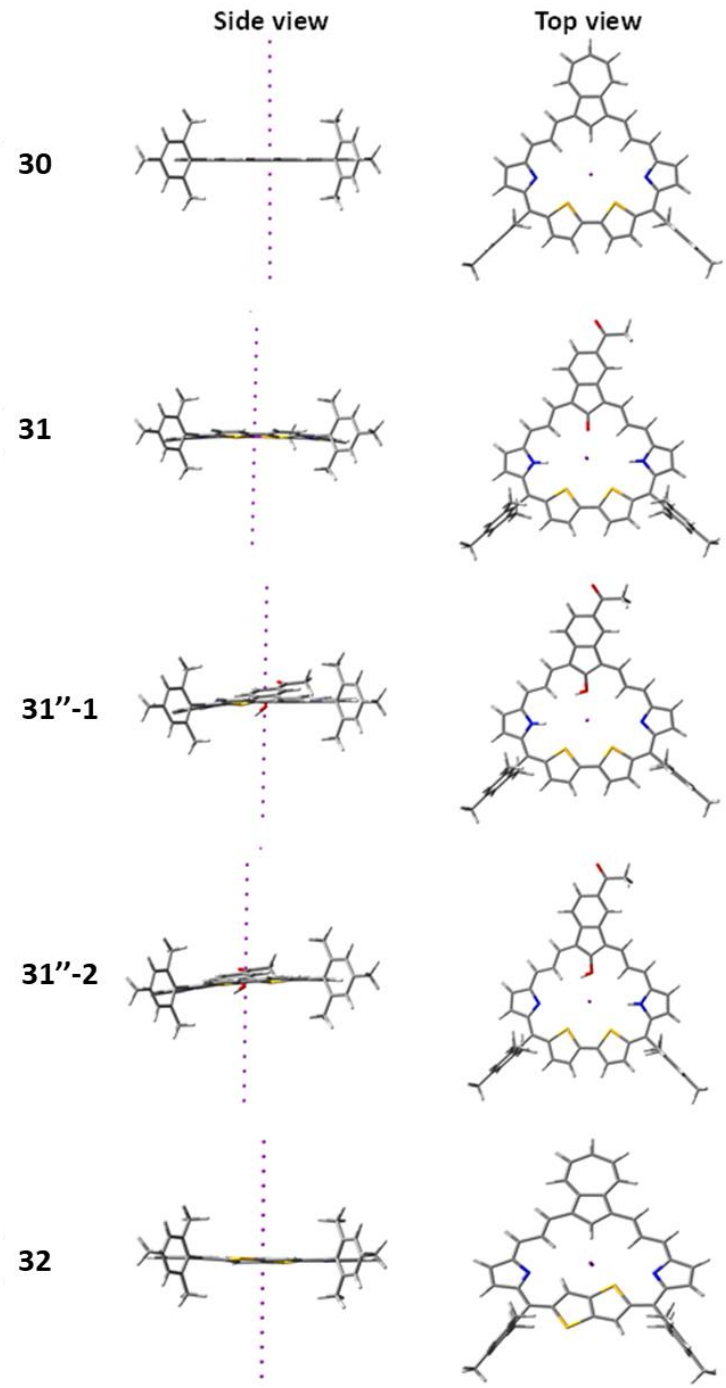

Figure 4.35 The centres of macrocycles **30**, **31**, **31**”-**1, 31**”-**2** and **32** for the NICS values were designated at the non-weighted mass of π conjugation pathway of the macrocycles

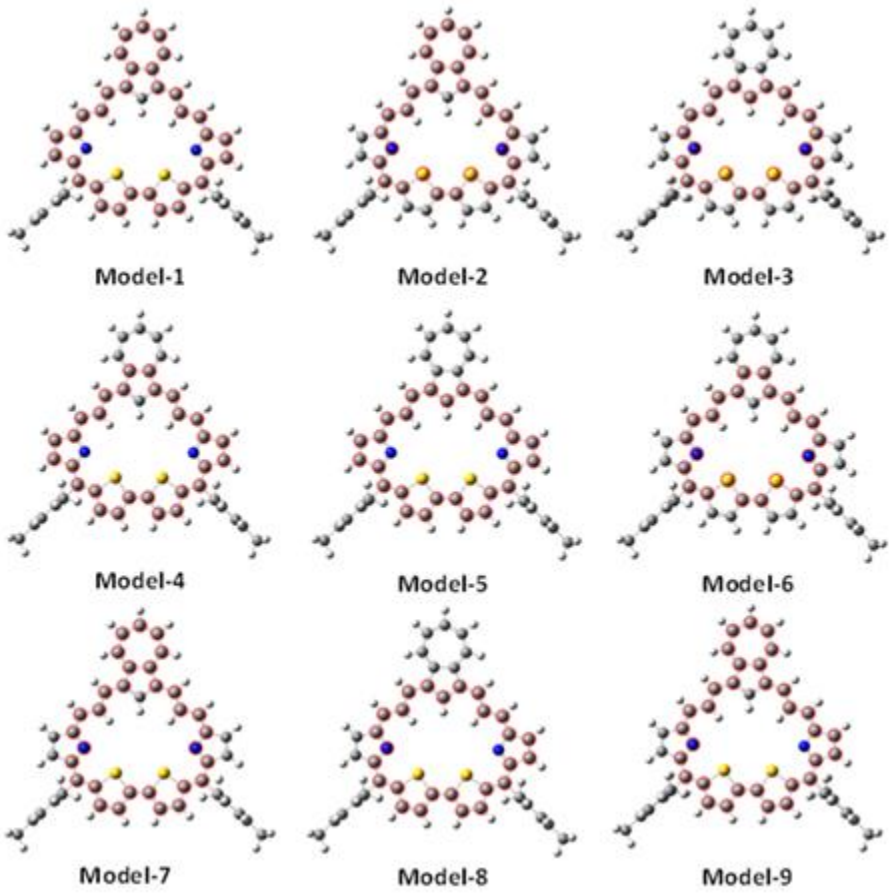

Figure 4.36 The different delocalization paths of macrocycles used to calculate HOMA values

Table 2. Harmonic oscillator model of aromaticity (HOMA) values for **30, 31, 31**" and **32**

Delocalization paths	**30**	**31**	**31"-1**	**31"-2**	**32**
Model-1	0.633	0.723	0.708	0.710	0.450
Model-2	0.729	0.602	0.677	0.679	0.671
Model-3	0.709	0.437	0.762	0.762	0.623
Model-4	0.501	0.682	0.665	0.668	0.246
Model-5	0.595	0.605	0.785	0.787	0.350
Model-6	0.595	0.534	0.623	0.623	0.498
Model-7	0.807	0.693	0.794	0.787	0.629
Model-8	0.697	0.583	0.794	0.881	0.569
Model-9	0.717	0.709	0.712	0.787	0.629

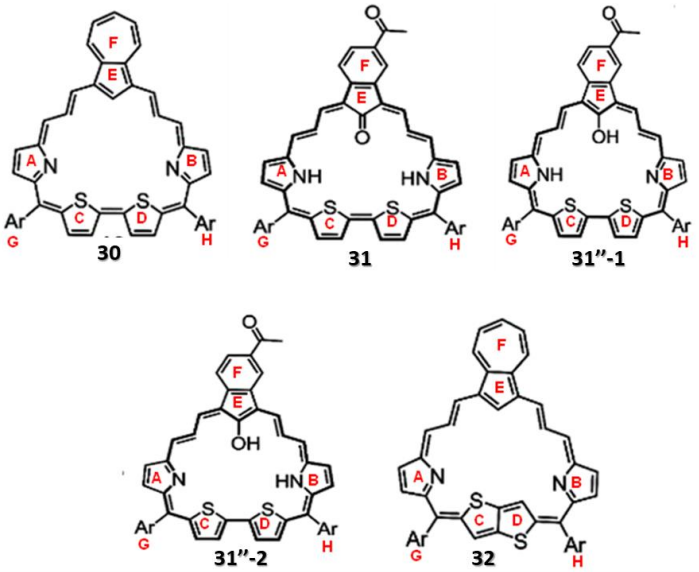

Figure 4.37 Representation of individual rings used to calculated NICS, HOMA and *H* indices

The 7-membered azulene ring and thiophene ring contribute significantly to the HOMO and LUMO of **30** and **32**, resulting in narrower HOMO–LUMO gaps (1.46 eV and 1.45 eV) than those for the other macrocycles (Fig. 4.34). The structures **31**″-1 and **31**″-2 were optimized based on the crystal structure of **31**, and the UV-vis-NIR absorptions were calculated by TD-DFT.[39] While the bands in the region 464–569 nm for **30** originate from the HOMO–2 → LUMO, HOMO–1 → LUMO+2 and HOMO → LUMO+3 transitions with π → π* character (~90%), the Q-band in the region at 889 nm corresponds to the promotion of an electron from HOMO → LUMO with significant π → π* character (94%). Based on the energy minimized structure of **31**, the Soret band and Q-type bands could be as assigned to transitions mainly from HOMO–2 → LUMO+1 (86%) and HOMO → LUMO (95%), respectively, with significant π → π* character (Tables 9). In the case of **31**″-1 and **31**″-2, Soret and Q-type bands originate from HOMO–2 → LUMO+1 (41–88%) and HOMO →LUMO (62–73%), respectively.

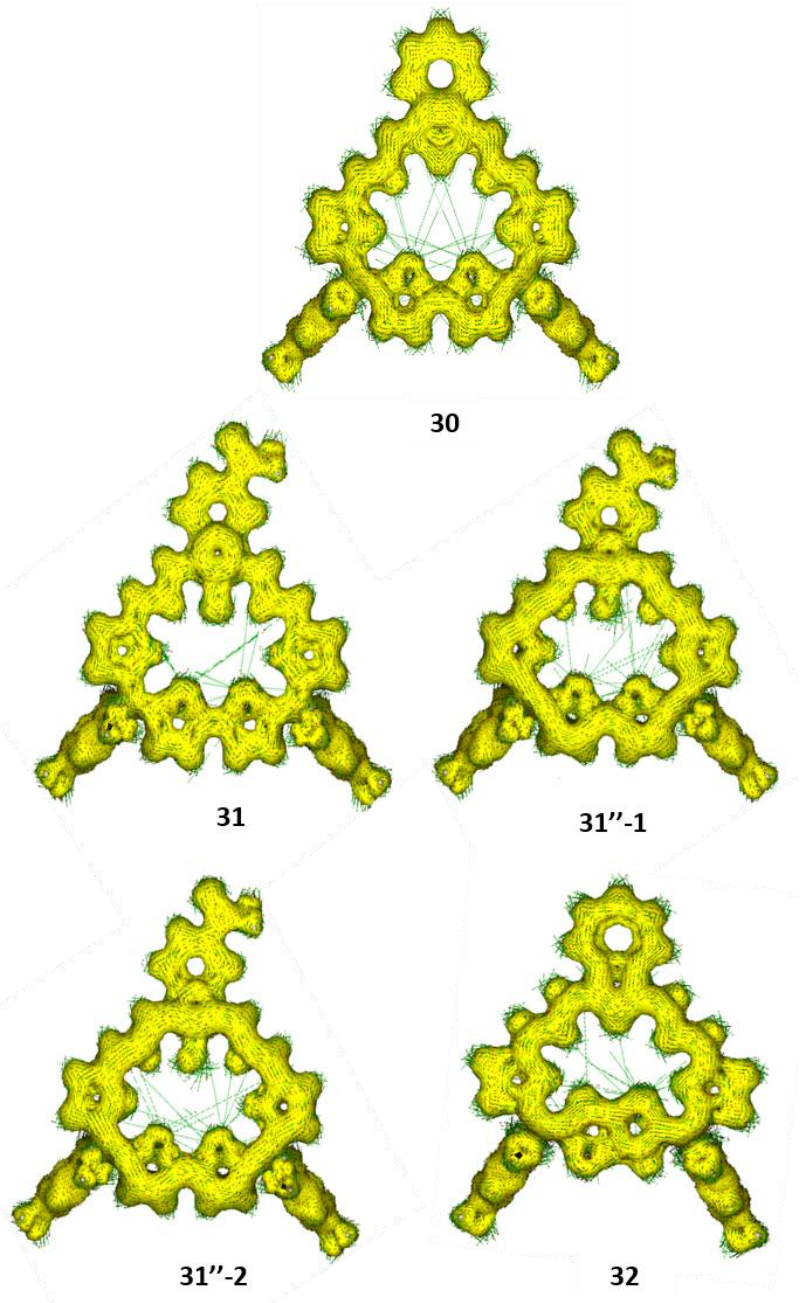

Figure 4.38 The Anisotropy of Induced Current Density (AICD) plot of **30**, **31**, **31**"-**1, 31**"-**2** and **32** at B3LYP-6-31G(d,p) level of theory. A continuous clock-wise ring current along the macrocycle indicating the aromatic nature of macrocyles in **30**, **31**, **31**"-**1, 31**"-**2** and continuous anti clock-wise ring current along the macrocycle indicating the anti-aromatic nature of macrocyle in **32**

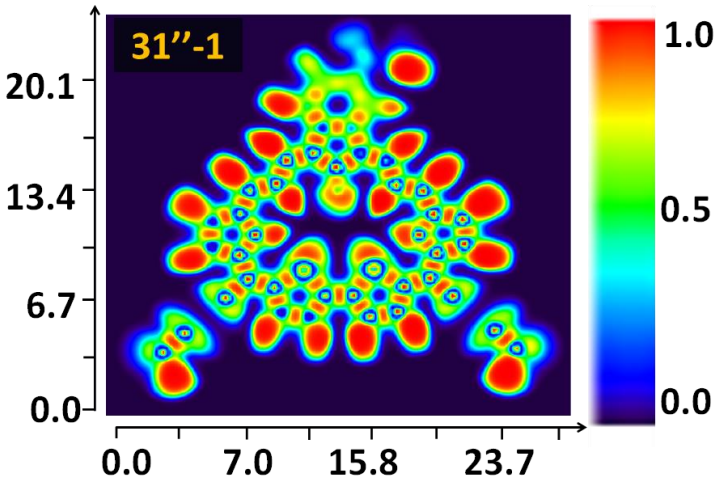

Figure 4.39 Colour-filled map of the electron localization function of **31**''-**1** at the B3LYP/6-31G (d,p) level

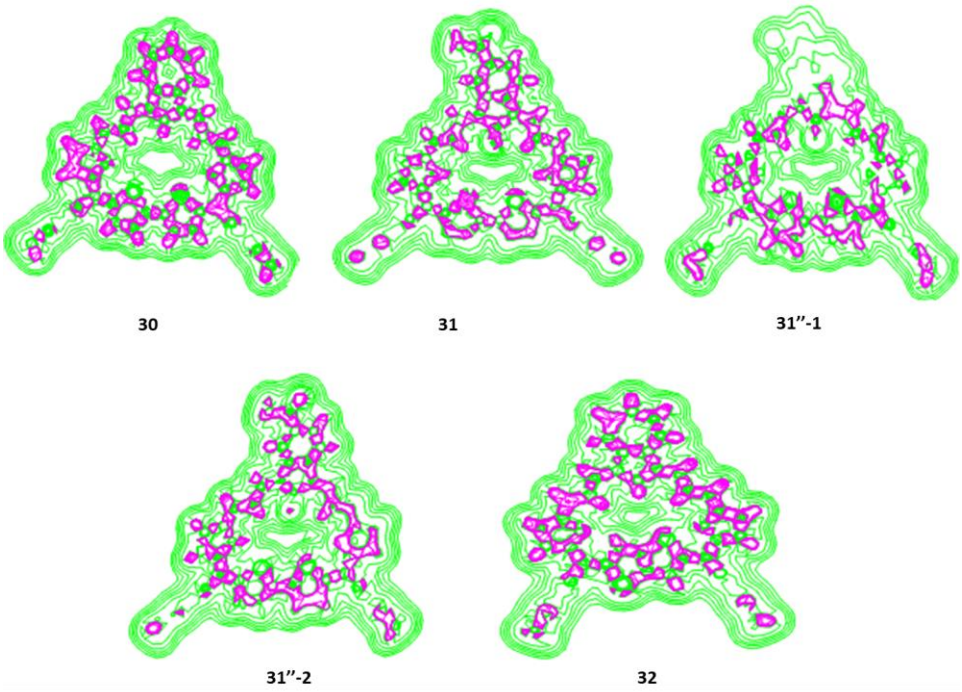

Figure 4.40 The Contour line diagram of the Laplacian of electron density along the macrocycle plane. Solid green lines indicate charge depletion [$\nabla^2_{\rho(r)}$>0] and solid gray lines indicate charge concentration [$\nabla^2_{\rho(r)}$<0]

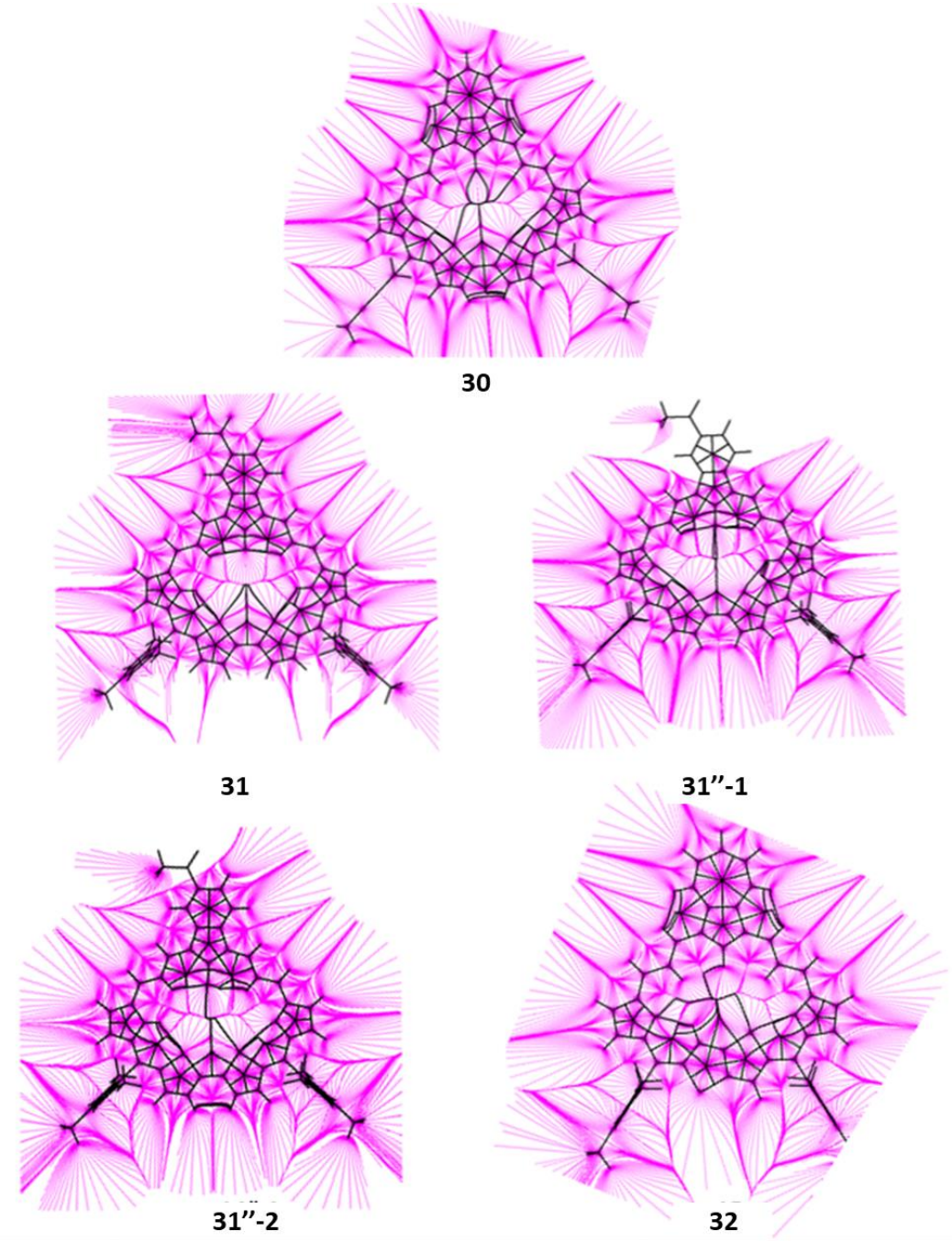

Figure 4.41 The Gradient vectors of the macrocycles computed at B3LYP/6-31G (d,p) level

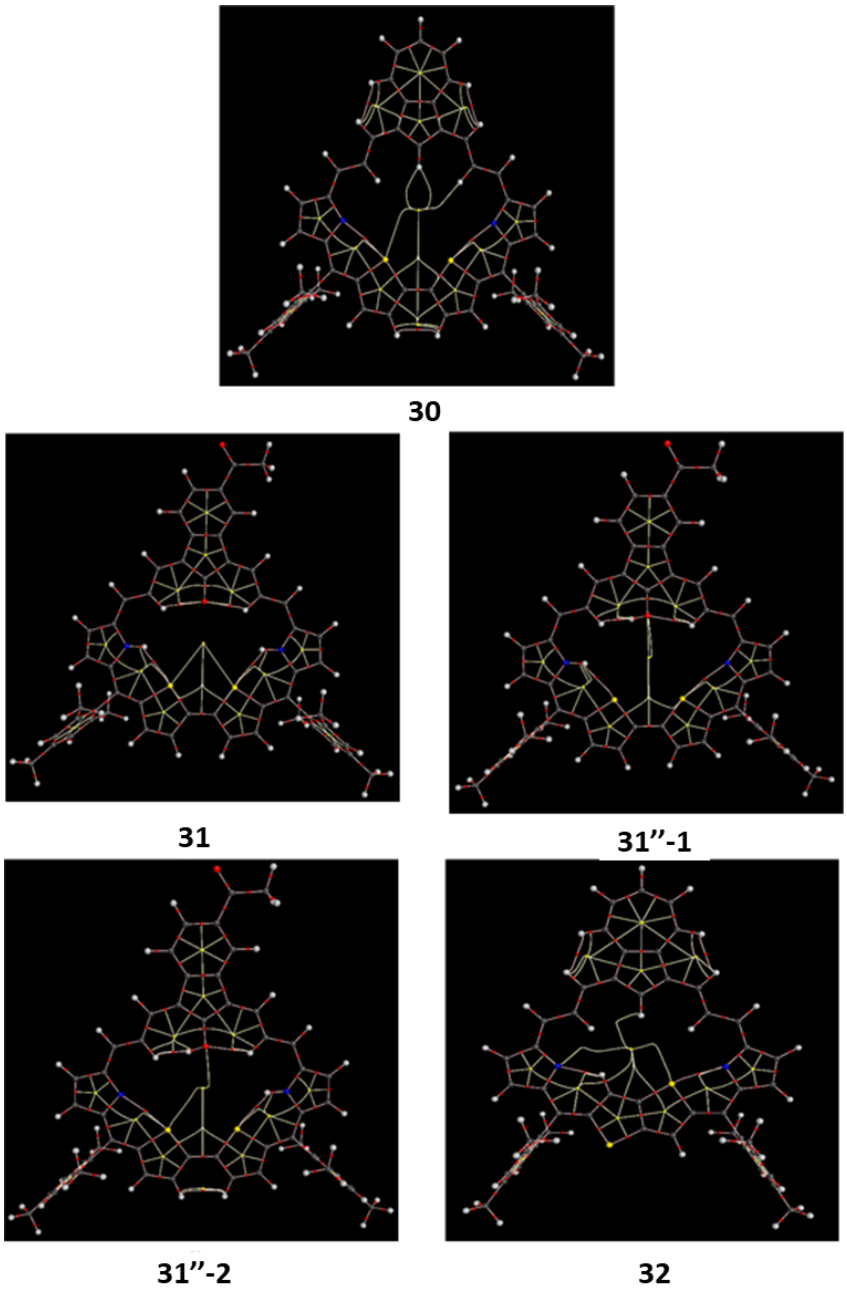

Figure 4.42 Molecular graph of **30**, **31**, **31”-1, 31”-2** and **32**. Solid lines indicate bond paths and large circles correspond to attractors, small red ones to bond critical points (BCPs), yellow ones to ring critical points (RCPs)

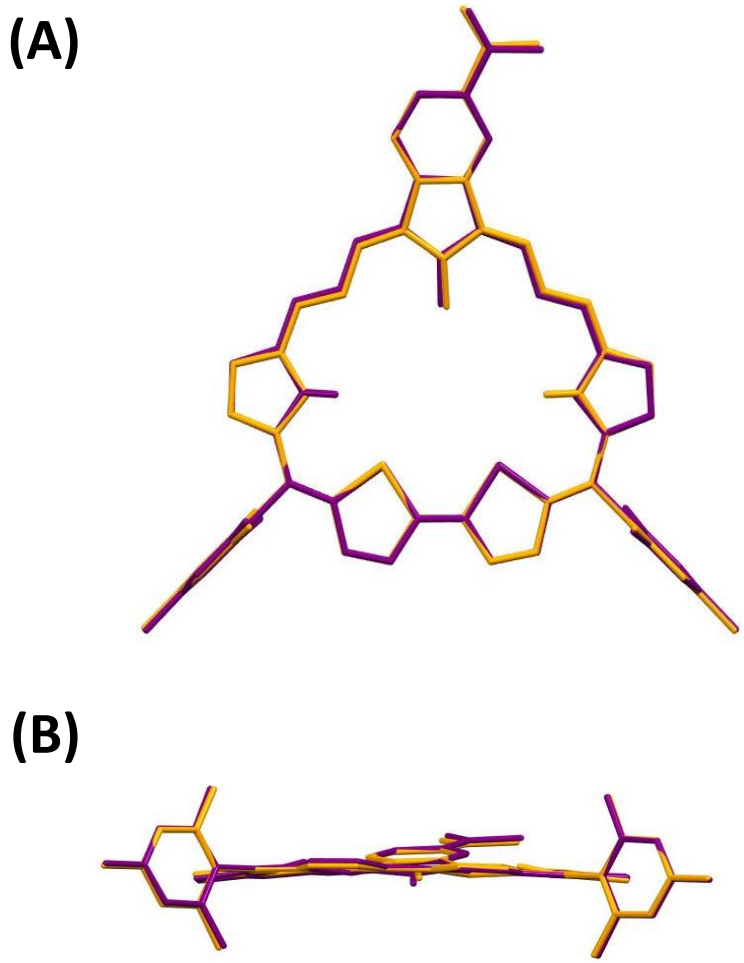

Figure 4.43 Structure overlay between **31**''**-1** (purple) and **31**''**-2** (yellow) of optimized structures (A: top view, B: side view)

The experimental Soret and Q-type absorption bands predicted at 511 nm and 658 nm for **32** originate from the HOMO–3 → LUMO, HOMO → LUMO (~83%, 47%), HOMO–2 → LUMO+3 (44%), and HOMO → LUMO+1 (88%) transition with significant π → π* character, whereas the weak stretched band (1200 nm) originates exclusively from HOMO → LUMO (99%) (Table 13).

Furthermore, the aromaticity (anti-aromaticity) of all the macrocycles is supported by the anisotropy of the induced current density (ACID)[40] plots. The distinct

diatropic (clockwise) ring currents of **30** (Fig. 4.21A″), **31**, **31**″, **31**″-1 and **31**″-2 (Fig. 4.21B″) strongly reveal the aromatic nature (Fig. 4.72). However, the current density vectors plotted onto the ACID isosurface of **32**(Fig. 4.21C″ and Fig. 4.38) indicate a strong paratropic ring current in the macrocycle, confirming anti-aromaticity. The NICS[41] values computed at the non-weighted mass of π-conjugation of the macrocycles confirmed the planar geometry of the macrocycles (NICS values above and below the rings are nearly identical).

The HOMA (harmonic oscillator model of aromaticity)[42] values have been calculated considering several possible delocalization pathways within the macrocycle (Fig. 4.36). For **30**, based on the most favourable delocalization pathway, the calculated HOMA value is 0.807, while the HOMA value of **31** (0.583) is lower than that of **31**″-1 (0.794) and **31**″-2 (0.881), indicating the highly aromatic nature of **31**″-1 and**31**″-2 (Table 2). The very low HOMA values for **32** (0.246–0.671) compared to other macrocycles indicates anti-aromaticity (Table 4). The positive energy density (H) values analysed by the RCP (ring critical point) also support these findings (Table 8)

A topographical analysis for an ELF (electron localization function) has also been carried out (Fig. 4.44). The high electron localisation confirms the presence of shared electron bonding (Fig. 4.44). The Laplacian function ∇ρ(r)2 contour plot through the macrocycle plane shows that the valence shell charge concentration (VSCC) zone is diffused over the entire macrocycles in **31**″-1 and **31**″-2. This indicates that there is charge transfer throughout the macrocycles confirming the extended delocalization. The contour plot of **32** has no such VSCC covering the entire macrocycle, indicating a lack of extended charge transfer in the macrocycle. The path lengths through the macrocycle are bifurcated equally by the bond critical points (BCPs), which is clearly inferred from the presence of zero-flux surfaces (or interatomic surfaces (IAS)) in **30**, **31**, and **31**″-1 and **31**″-2, while the presence of zero-flux surfaces is not bifurcated equally in the macrocycle 15 (Fig. 4.44).

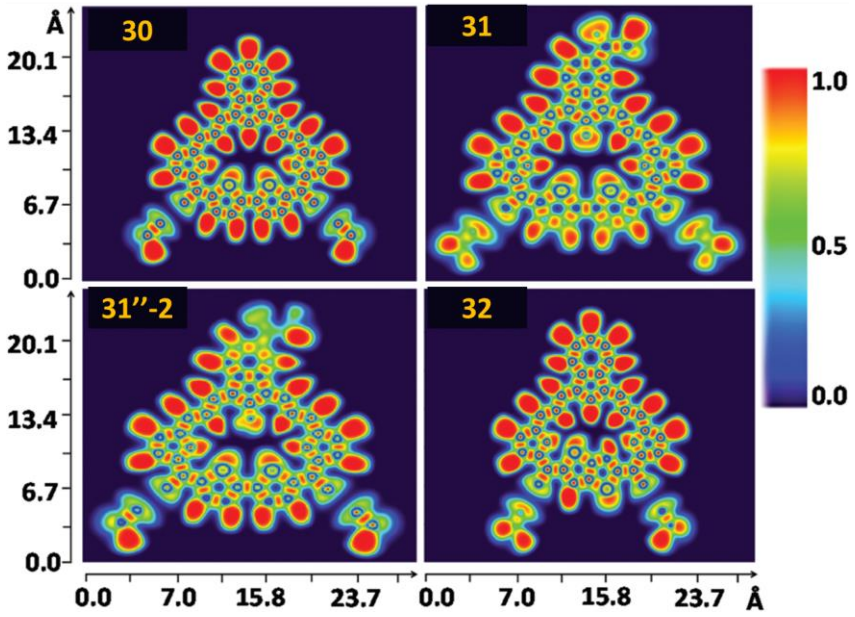

Figure 4.44 Colour-filled map of the electron localization function at the B3LYP/6-31G (d,p) level. The bonds are described by orange localization domains. The blue and dark blue regions exhibit a decrease of the electron localisation function.

4.3. Conclusion

In conclusion, acid-catalyzed condensation of tetrapyrrane **P5** with azulene-1,3-bis-acrylaldehyde **P6** using TFA as catalyst followed by oxidation with DDQ gave an unusual tropylium-fused vinylogous carbaporphyrinoid **30**. Under oxidative condition it converts to fully conjugated vinylogous benzocarbaporphyrinoid **31**. Contrarily, swiping the bithiophene moiety with fused thieno [2,3, b] thiophene has anticipated the obvious anti aromatic nature of the corresponding azuliporphyrinoid (1.3.3.1.0) **32**. The UV-vis spectra of **30** and **31''** indicates porphyrinic nature with aromaticity and exhibiting NIR absorption. The new macrocycles have large cavity that may be utilised as a receptor. These vinylogous carbasapphyrins exhibiting NIR absorption beyond 1100 nm in their neutral form may find application in bio-imaging and other related applications.

4.4 Crystallographic Data

Table **3**

Parameters	31
Chemical formula	$C_{53}H_{44}N_2O_2S_2$
Formula weight	805.2922
Temperature	100 K
Crystal system	orthorhombic
Space group	P n m a
a (Å); α (°)	22.5989(8); 90
b (Å); β(°)	20.6160(7); 90
c (Å); γ (°)	9.7234(3); 90
V (Å3); Z	4530.1(3); 4
ρ (calc.) mg m-3	1.153
μ(Mo Kα) mm-1	0.157
2θmax (°)	54.14°
R(int)	3.42%
Completeness to θ	99.4
Data / param.	5132/284
GOF	1.060
R1 [F>4σ(F)]	7.08%
wR2 (all data)	19.83%
max. peak/hole (e.Å-3)	0.964 /-0.533
CCDC	2116847

4.5. Experimental Methods

General Synthesis of 30/31:

Tetrapyrrane p5 (0.280 g, 0.5 mmol) was taken in a round bottom flask; to it 250 mL of dry DCM was added and stirred for 15 minutes under nitrogen atmosphere to get a clear solution. Azulene-1, 3-bisacrylaldehyde p6 (0.118 g, 0.5 mmol was added to the reaction mixture and stirred for 15 minutes under dark condition. To this, 0.192 mL (2.5 mmol) CF_3COOH was added and reaction mixture was stirred under nitrogen atmosphere in dark for overnight. The reaction mixture was then neutralised with 0.348 mL (2. 5 mmol) triethylamine followed by oxidation with 283 mg (1.25 mmol) of DDQ in open air. After complete removal of solvent from crude mixture by rotary evaporator, the compound was purified using basic alumina grade III where a violet colour band using dichloromethane as eluent and a deep violet colour band using 5% EtOAc- dichloromethane as eluent were obtained. These two fractions were purified further by repeated PTLCs. The desired macrocycles were isolated as extra pure crystalline solids upon further recrystalization.

Compound 30: Yield. ~75mg (20%). R_f = 0.25 (EtOAc/Dichloromethen = 1:99), mp > 300 °C.

^{1}H NMR (500 MHz, $CDCl_3$, 298 K,) δ =: 1.03 (t, 2H, ^3J = 15 Hz, inner *meso* CH), 2.09 (s, 12H, -CH_3), 2.17 (s, 1H, inner azulene CH), 2.58 (s, 6H, -CH_3), 7.26 (s, 4H, mesityl- CH), 7.52-7.54 (m, 1H, azulene-CH), 7.59 (t, ^3J =10 Hz, 2H, azulene-CH), 7.67(d, ^3J =4.9 Hz, 2H, thiophene β-CH), 8.38-8.41(m, 2H, pyrrole β-CH and 2H, azulene CH), 9.43- 9.46 (m, 2H, thiophene β -CH and 2H, pyrrole β -CH), 9.61 (d, 2H, ^3J =12 Hz, outer *meso* CH), 10.1 (d, 2H, ^3J =15 Hz, outer *meso* CH); **^{1}H NMR** (500 MHz, $CDCl_3$, 263 K) δ = 0.61 (t, 2H, ^3J =15 Hz, inner *meso* CH), 2.07 (s, 12H, -CH_3), 2.19 (s, 1H, inner azulene CH), 2.59 (s, 6H, - CH_3), 7.26 (s, 4H, mesityl- CH), 7.53-7.55 (m, 1H, azulene-CH), 7.65 (t, ^3J = 10

Hz, 2H, azulene-CH), 7.76 (d, ^{3}J =4.5 Hz, 2H, thiophene β -CH), 8.48-8.51 (m, 2H, pyrrole β-H and 2H, azulene CH), 9.52 (d, ^{3}J =4.5 Hz, 2H, pyrrole β-H), 9.58 (d, ^{3}J =5.5 Hz 2H, thiophene β-CH), 9.78 (d, 2H, ^{3}J =12 Hz, outer *meso* CH), 10.26 (d, 2H, ^{3}J =15 Hz, outer *meso* CH). HR-MS(ESI-TOF) m/z: $[M]^+$ calcd for $C_{52}H_{42}N_2S_2^+$ 759.2862; found 759.2865 UV-vis (CH_2Cl_2, λ [nm], ([ϵ [M^{-1} $cm^{-1}x10^4$]) 298K) 464.31(30.5), 504.17(27.7), 531.16 (sh), 569.12 (26.6), 678.03 (1.2), 817.87 (5.5), 889.49 (5.4), 1111.03 (br).

Compound 31: Yield. ~118 mg (30%). R_f = 0.3 (EtOAc/Dichloromethen = 3:97), mp > 300 °C.

^{1}H NMR (400 MHz, CD_2Cl_2, 298 K) δ = -2.77 (t, 1H, inner *meso* CH), -2.52 (s, 1H, inner OH), -2.38 (t, 1H, inner *meso* CH), -2.07 (s, 1H, -NH), 2.03 (s, 6H, -CH_3), 2.05 (s, 6H, -CH_3), 2.81 (s, 3H, -CH_3), 2.83 (s, 3H, -CH_3), 6.99 (s, 2H, mesityl-CH), 7 (br, 1H, pyrrole β-H), 7.17 (br, 1H, pyrrole β-H), 7.41 (d, 1H, thiophene β -CH), 7.49 (brs, 1H, pyrrole β-H), 7.55 (m, 1H, pyrrole β-H), 7.57 (s, 2H, mesityl-CH), 7.7 (d, 1H, thiophene β -CH), 8.05 (brs, 1H, thiophene β-CH), 8.47 (m, 1H,Benzene), 9.26 (brs, 1H, thiophene β -CH), 9.43 (d, 1H, 3J = 7.6 Hz, Benzene CH), 9.76 (s, 1H, Benzene CH), 10.23 (brs, 1H, outer *meso* CH), 10.59 (s, 1H, CHO), 11.47 (brs, 2H, outer *meso* CH), 12.03 (brs, 1H, outer *meso* CH); **^{13}CNMR** (100 MHz, CD_2Cl_2, 300 K) δ = 192.67, 167.67, 167.63, 152.22, 152.05, 147.75, 147.68, 147.51, 142.96, 139.46, 139.46, 138.79, 138.70, 137.60, 136.10, 136, 135.54, 135.22, 132.65, 132.54, 131.54, 131.01, 131.01, 128.86, 128.86, 128.61, 128.18, 128.13, 124.84, 124.84, 124.05, 123.59, 121.79, 121.76, 119.09, 119.08, 115.93, 113.88, 113.88, 107.13, 65.59, 64.59, 32.05, 30.19, 29.81, 22.81. HR-MS(ESI-TOF) m/z: $[M]^+$ calcd for $C_{52}H_{42}N_2O_2S_2^+$ 789.2609; found 789.2608. UV-vis-NIR λ [nm], (ϵ [M-1 cm-1x103]), 298K): 419.18 (35.21), 537.41 (85.1), 587.87 (42.49), 687.94 (15.78), 992.64(5.94), 1082.9 (5.12).

General Synthesis of **32**: Tripyrrane **P8** (0.267 g, 0.5 mmol) was taken in a round bottom flask; to it 250 mL of dry DCM was added and stirred for 15 minutes under nitrogen

atmosphere to get a clear solution. Azulene-1, 3-bisacrylaldehyde **P6** (0.118 g, 0.5 mmo) was added to the reaction mixture and stirred for 15 minutes under dark condition. To this, 0.192 mL (2. 5 mmol) CF_3COOH was added and reaction mixture was stirred under nitrogen atmosphere in dark for overnight. The reaction mixture was then neutralised with 0.348 mL (2.5 mmol) triethylamine followed by oxidation with 283 mg (1.25 mmol) of DDQ in open air. After complete removal of solvent from crude mixture by rotary evaporator, the compound was purified using basic alumina grade III where a reddish colour band using dichloromethane as eluent were obtained. After repeated PTLCs chromatography the compound **32** was obtained as green solid using dichloromethane as eluent.

Yield. ~91 mg (30%). R_f = 0.3 (Dichloromethen/Hexane = 4:1), mp > 300 °C.

^{1}H NMR (400 MHz, CD_2Cl_2, 298 K) δ = 1.1 (s, 1H, outer thiophene β -CH), 1.75 (s, 12H, -CH_3), 1.78 (s, 2H, outer *meso*-CH), 1.88 (s, 2H, outer *meso*-CH), 2.05 (s, 6H, -CH_3), 3.8 (br, 2H, pyrrole β-CH), 3.9 (br, 2H, pyrrole β-CH), 6.3 (s, 1H, inner β-H thiophene), 6.4 (br, 4H, *m*- CH), 6.9 (s, 1H), 7.55 (m, 2H), 7.75 (m, 3H), 8.5 (brs, 2H, inner *meso* CH). MALDI-TOF MS *m/z*: $[M]^+$ calcd for $C_{50}H_{40}N_2S_2^+$ 732.2633; found 732.761. ([UV-vis (CH_2Cl_2, λ [nm], ([ϵ [M^{-1} $cm^{-1}x10^3$]), 298K) 517.18 (43.79), 658.2(8.56).

General Synthesis of **33**: Tetrapyrrane **P11** (0.292 g, 0.5 mmol) was taken in a round bottom flask; to it 250 mL of dry DCM was added and stirred for 15 minutes under nitrogen atmosphere to get a clear solution. Azulene-1, 3-bisacrylaldehyde **P6** (0.118 g, 0.5 mmol was added to the reaction mixture and stirred for 15 minutes under dark condition. To this, 0.192 mL (2. 5 mmol) CF_3COOH was added and reaction mixture was stirred under nitrogen atmosphere in dark for overnight. The reaction mixture was then neutralised with 0.348 mL (2.5 mmol) triethylamine followed by oxidation with 283 mg (1.25 mmol) of DDQ in open air. After complete removal of solvent from crude mixture by rotary evaporator, the compound was purified using basic alumina grade III a deep violet colour band using 5% EtOAc- dichloromethane as eluent were obtained. After repeated PTLCs chromatography, the macrocycle **33** was obtained violet solid which was further recrystalized.

MALDI-TOF MS *m/z*: $[M]^+$ calcd for $C_{68}H_{56}N_2S_4^+$1028.3326; found 1028. 451.UV-vis (CH_2Cl_2, λ [nm], (ϵ [M^{-1} $cm^{-1}x10^5$]), 298K): 540 (3.79), 577 (3.81), 800 (1.16), 950 (0.001). 771.2425. UV-vis-NIR λ [nm], (ϵ [M^{-1} $cm^{-1}x10^3$]), 298K): 412.45 (1.25).

Characterization Data

Chapter 4

Mass spectra:

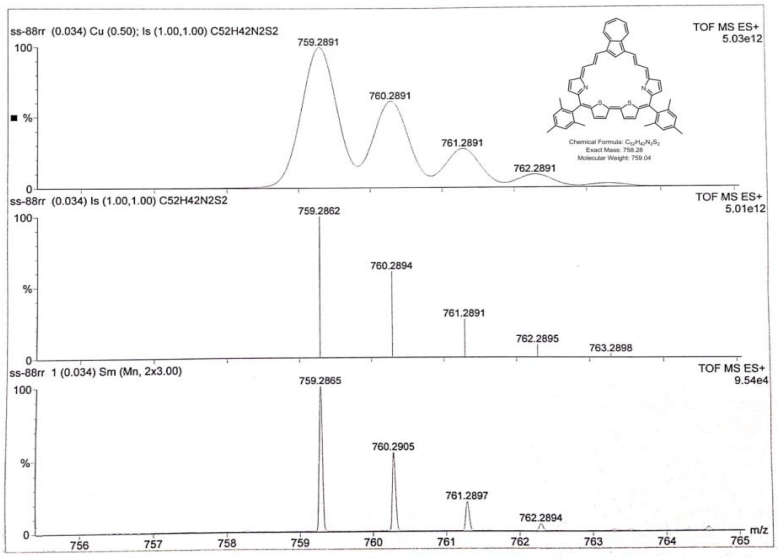

Figure 4.45. HRMS data of 30

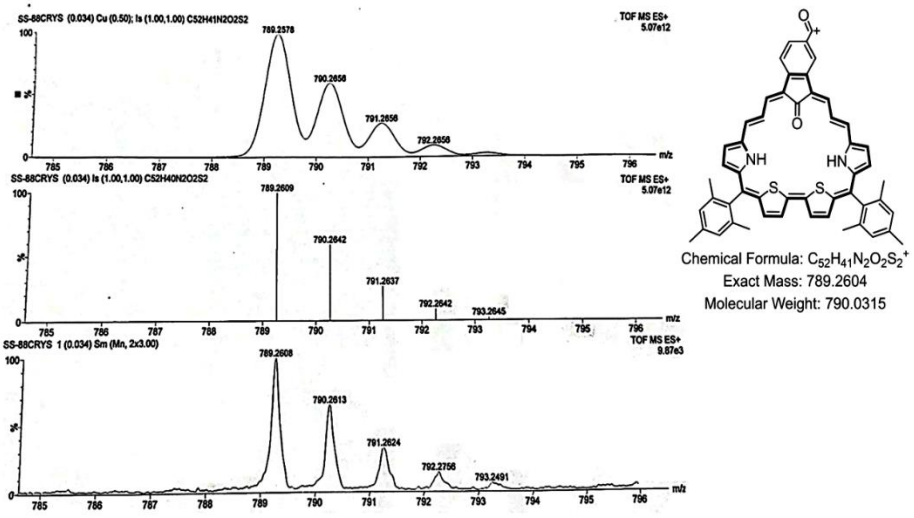

Figure 4.46 HRMS data of **31**

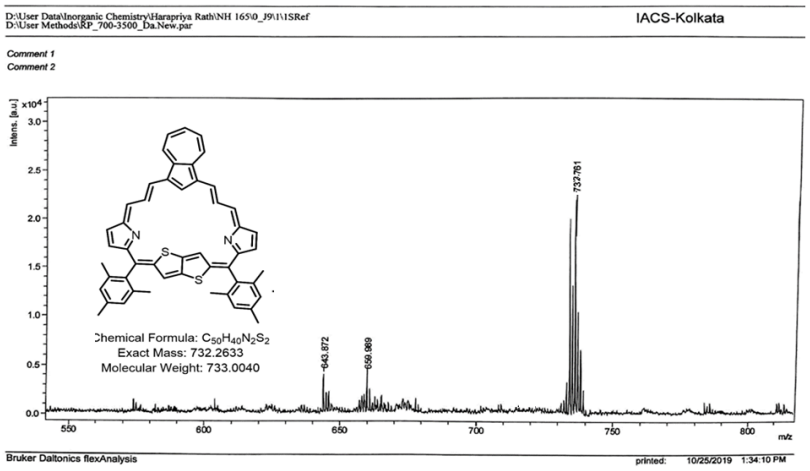

Figure 4.47 MALDI-TOF MS of **32**

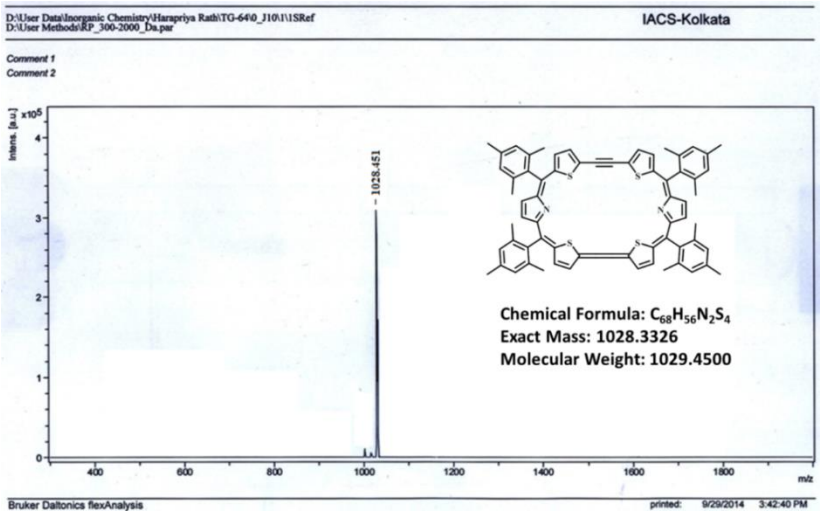

Figure 4.48 MALDI-TOF MS of **33**

4.6. Theoretical Calculation

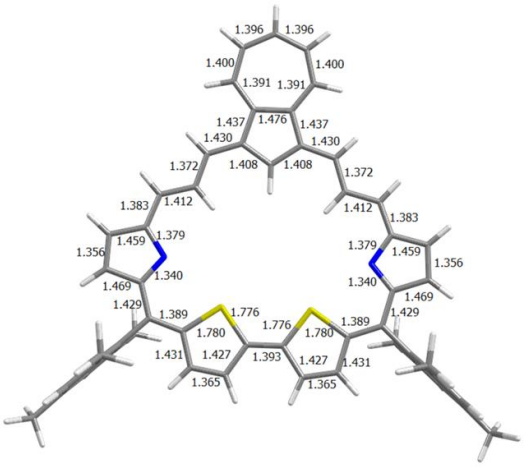

Figure 4.49 Optimized geometry of **30** with selected bond length (Å) computed at the B3LYP/6-31G(d,p) level

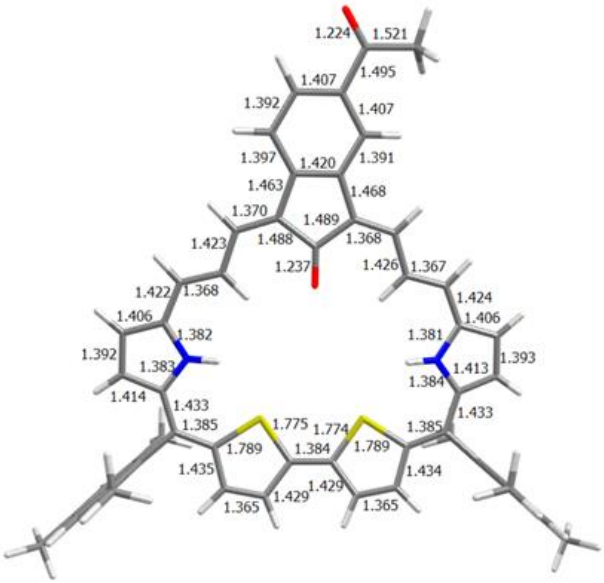

Figure 4.50 Optimized geometry of **31** with selected bond length (Å) computed at the B3LYP/6-31G(d,p) level

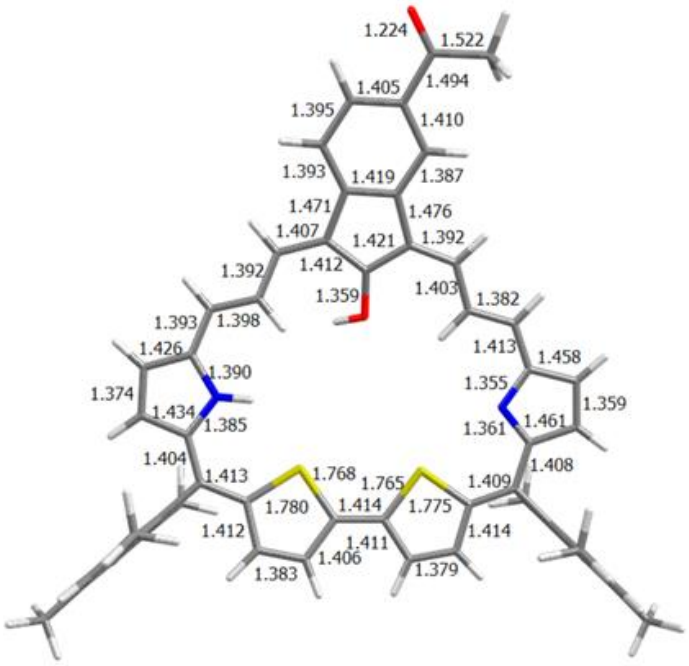

Figure 4.51. Optimized geometry of **31”-1** with selected bond length (Å) computed at the B3LYP/6-31G(d,p) level

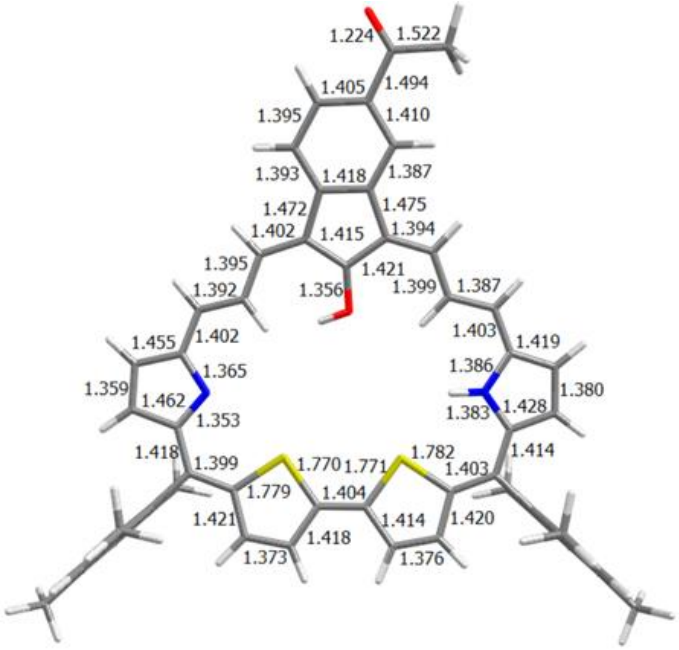

Figure 4.52. Optimized geometry of **31”-2** with selected bond length (Å) computed at the B3LYP/6-31G(d,p) level

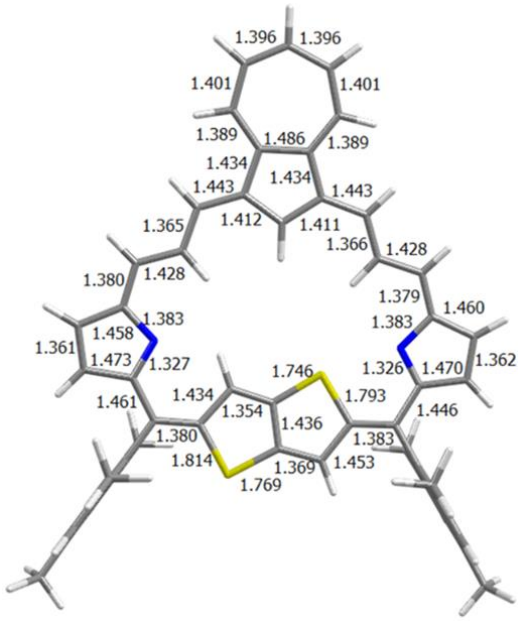

Figure 4.53. Optimized geometry of **32** with selected bond length (Å) computed at the B3LYP/6-31G(d,p) level

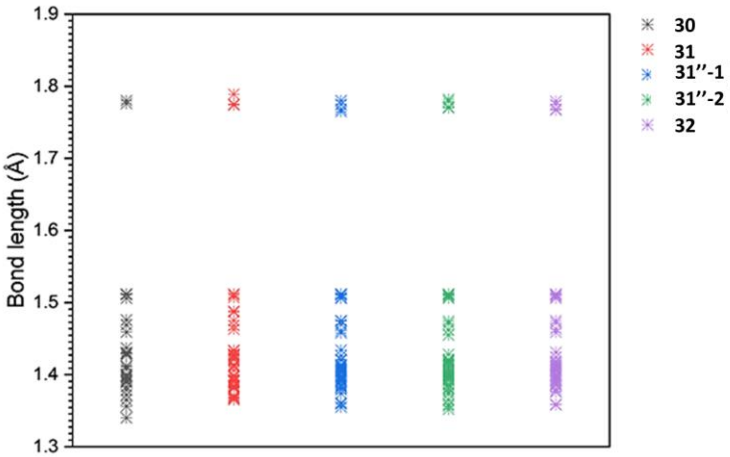

Figure 4.54 Illustration of π-delocalization from calculated C-C, C-S and C-N bond lengths of **30**, **31**, **31**"-1, **31"-2** and **32** at the B3LYP/6-31G (d, p) level

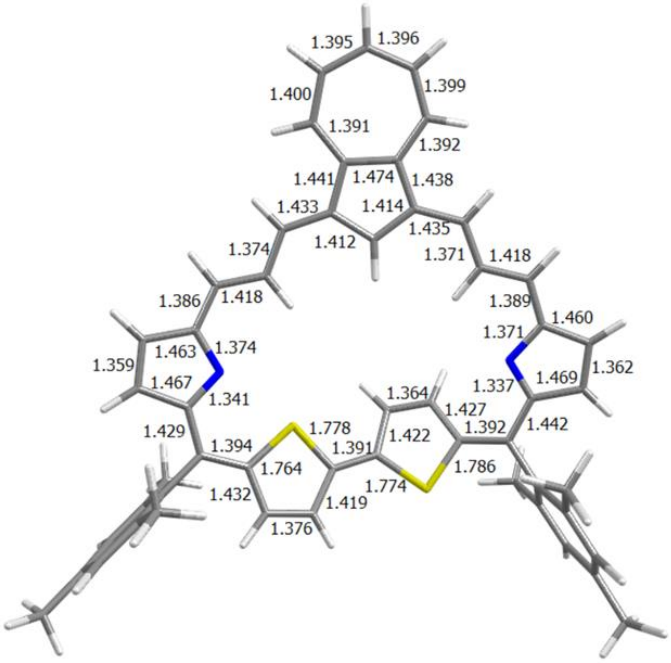

Figure 4.55 Optimized geometry of **30**-Conformer-1 with selected bond length (Å) computed at the B3LYP/6-31G(d,p) level

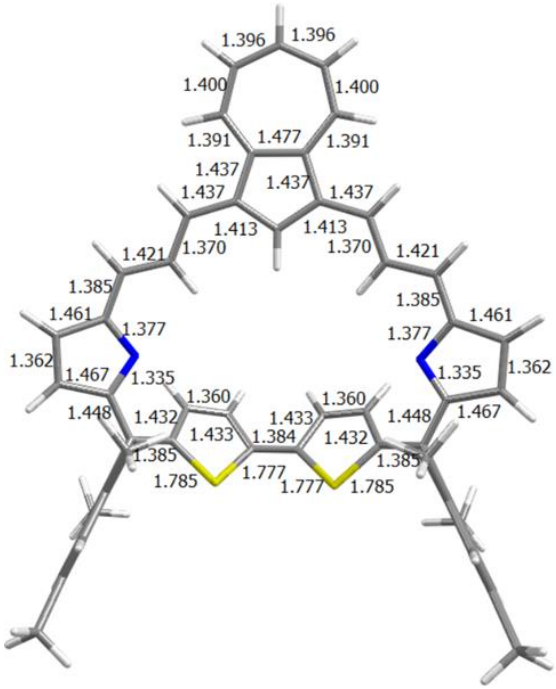

Figure 4.56 Optimized geometry of **30**-Conformer-2 with selected bond length (Å) computed at the B3LYP/6-31G (d,p) level

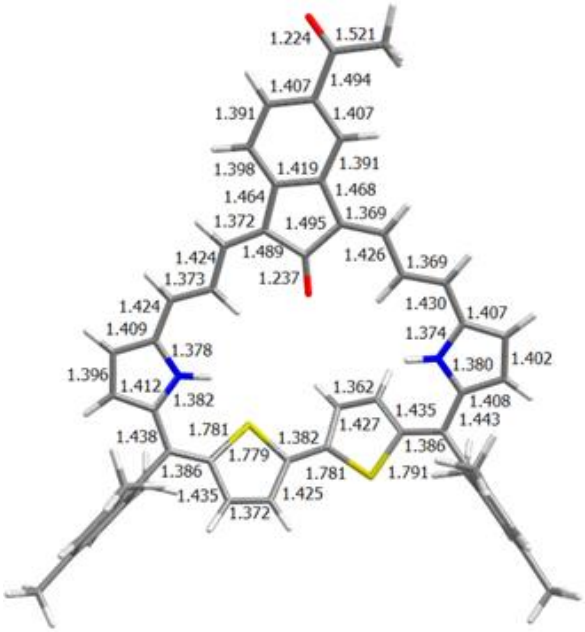

Figure 4.57 Optimized geometry of **31**-Conformer-1 with selected bond length (Å) computed at the B3LYP/6-31G(d,p) level

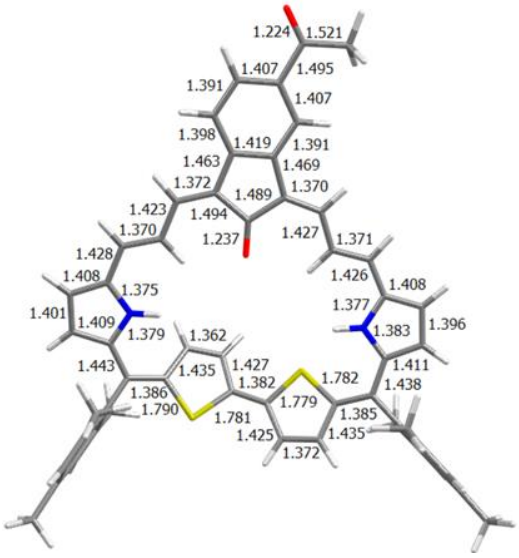

Figure 4.58 Optimized geometry of **31**-Conformer-2 with selected bond length (Å) computed at the B3LYP/6-31G(d,p) level

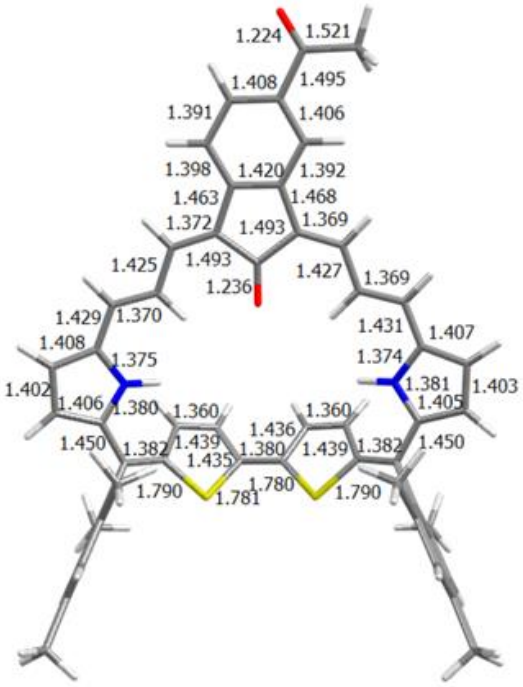

Figure 4.59 Optimized geometry of **31**-Conformer-3 with selected bond length (Å) computed at the B3LYP/6-31G(d,p) level

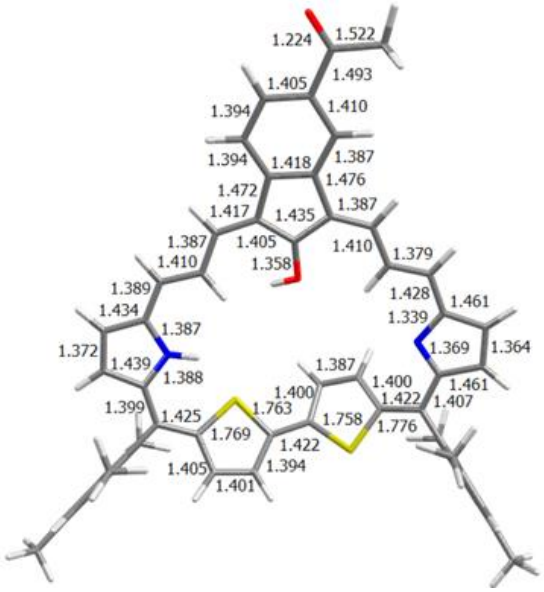

Figure 4.60 Optimized geometry of **31”-1** Conformer-1 with selected bond length (Å) computed at the B3LYP/6-31G (d, p) level

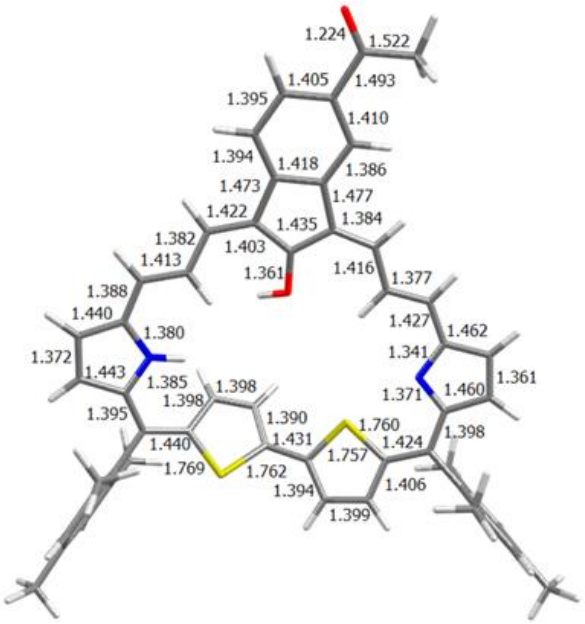

Figure 4.61 Optimized geometry of **31”-1** Conformer-2 with selected bond length (Å) computed at the B3LYP/6-31G(d,p) level

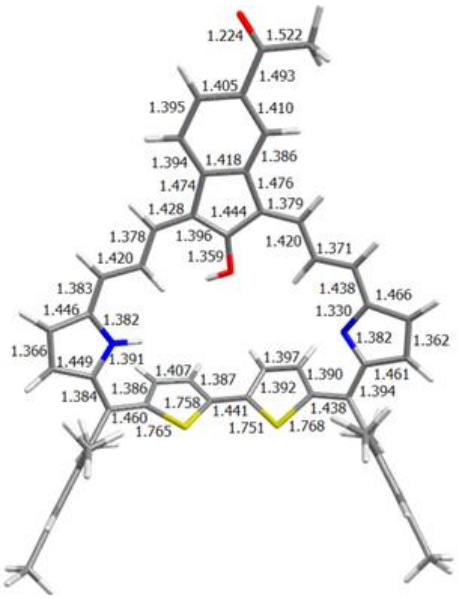

Figure 4.62 Optimized geometry of **31”-1** Conformer-3 with selected bond length (Å) computed at the B3LYP/6-31G (d, p) level

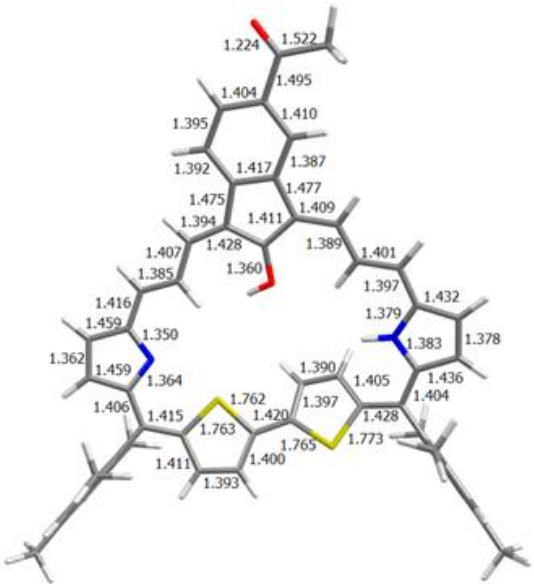

Figure 4.63 Optimized geometry of **31”-2** Conformer-1 with selected bond length (Å) computed at the B3LYP/6-31G (d, p) level

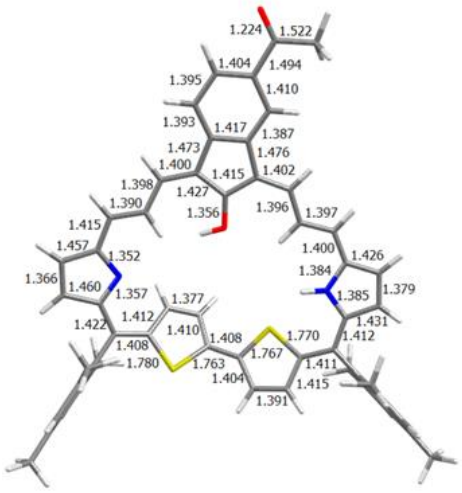

Figure 4.64 Optimized geometry of **31”-2** Conformer-2 with selected bond length (Å) computed at the B3LYP/6-31G (d, p) level

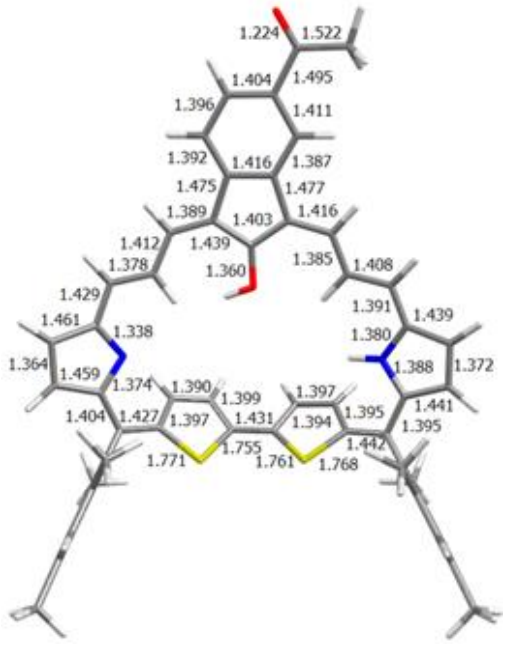

Figure 4.65 Optimized geometry of **31”-2** Conformer-3 with selected bond length (Å) computed at the B3LYP/6-31G (d, p) level

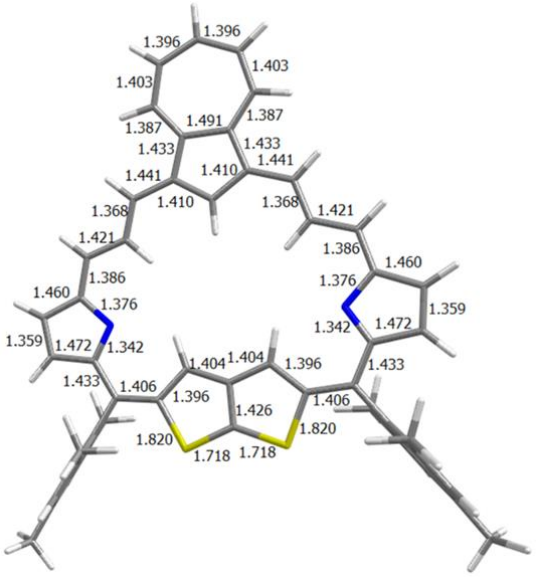

Figure 4.66 Optimized geometry of **32**-Conformer-1 with selected bond length (Å) computed at the B3LYP/6-31G (d, p) level

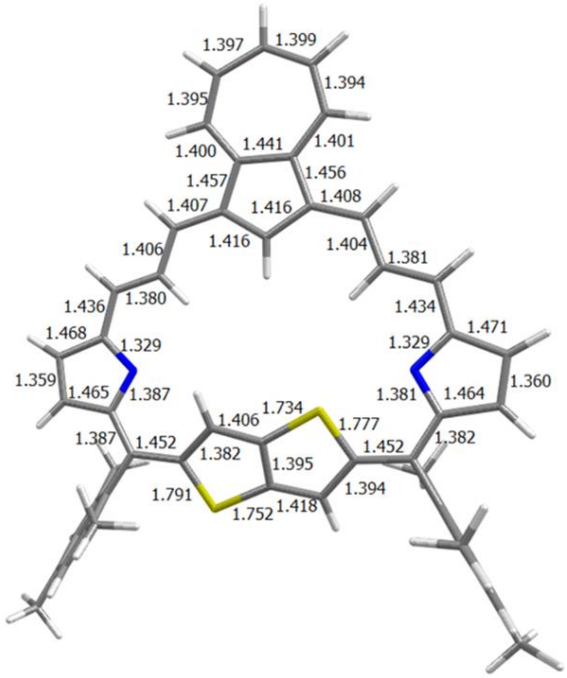

Figure 4.67 Optimized geometry of **32**-Conformer-2 with selected bond length (Å) computed at the B3LYP/6-31G (d, p) level

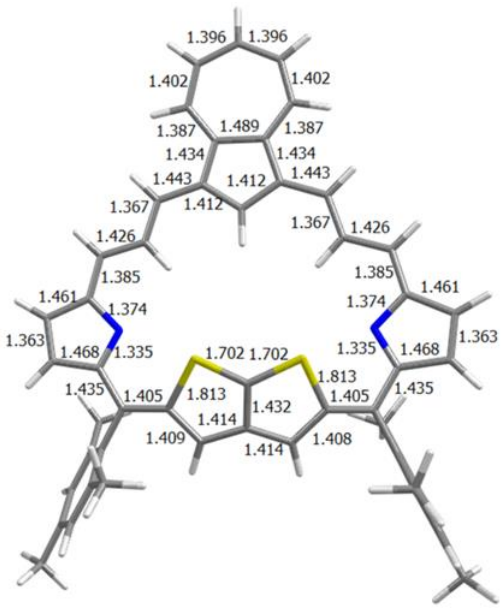

Figure 4.68 Optimized geometry of **32**-Conformer-3 with selected bond length (Å) computed at the B3LYP/6-31G (d, p) level

Table 4 Calculated energies of the optimized structures, zero point energy correction (ZPE), free energy corrections (GFE), relative energies (∆E) and relative Gibbs free energies (∆*G)* for plausible isomers of **30**, **31**, **31”-1**, **31”-2** and **32** at the B3LYP/6-31G(d,p) level.

	ZPE (hartree)	**GFE (hartree)**	**Energy (hartree)**	**∆E (kJ/mol)**	**∆E+ZPE (kJ/mol)**	**∆G (kJ/mol)**
30	0.782713	0.692921	-2912.698637	0.00	0.00	0.00
30-Conformer-1	0.782262	0.693093	-2912.680814	46.80	45.611	47.25
30-Conformer-2	0.782325	0.694043	-2912.653864	117.55	116.53	120.50
31	0.820817	0.726417	-3102.543075	0.00	0.00	0.00
31-Conformer-1	0.821078	0.727618	-3102.529016	36.91	37.60	40.06
31-Conformer-2	0.821092	0.727666	-3102.528934	37.12	37.85	40.41
31-Conformer-3	0.821143	0.728206	-3102.50969	87.65	88.51	92.35
31”-1	0.819331	0.724911	-3102.514288	0.00	0.00	0.00
31”-1-Conformer-1	0.819322	0.72582	-3102.498781	40.71	40.69	42.10
31”-1-Conformer-2	0.819588	0.725851	-3102.501062	34.72	35.40	37.19
31”-1-Conformer-3	0.819362	0.72501	-3102.476037	100.43	100.51	100.68
31”-2	0.819556	0.72517	-3102.518173	0.00	0.00	0.00
31”-2-Conformer-1	0.819454	0.725816	-3102.504887	34.88	34.61	36.58
31”-2-Conformer-2	0.819038	0.725432	-3102.501447	43.91	42.46	44.60
31”-2-Conformer-3	0.819024	0.725138	-3102.478604	103.89	102.49	103.80
32	0.748596	0.660499	-2835.269661	0.00	0.00	0.00
32-Conformer-1	0.746972	0.659657	-2835.242628	70.97	66.71	68.76
32-Conformer-2	0.746867	0.660638	-2835.236551	86.93	82.39	87.29
32-Conformer-3	0.747269	0.661062	-2835.231737	99.57	96.09	101.05

Table 5. Frontier Molecular Orbital compositions (%) in the ground state for **30, 31, 31”-1, 31”-2, 32** at the B3LYP/6-31G (d,p) level.

	Orbital	Energy (eV)	Contribution (%)				
			Thiophene	Pyrrole	π-bridge	Azulene	Mesitylene
30	HOMO-3	-5.922	19.43	56.51	6.40	9.25	8.41
	HOMO-2	-5.918	12.52	37.47	24.73	18.73	6.56
	HOMO-1	-4.848	19.67	27.47	17.13	34.66	1.07
	HOMO	-4.303	34.85	12.54	21.77	4.36	26.48
	LUMO	-2.842	20.20	13.98	21.95	33.91	9.96
	LUMO+1	-2.517	0.07	0.10	0.08	99.74	0.01
	LUMO+2	-2.219	24.60	30.98	31.90	8.53	4.00
	LUMO+3	-1.798	23.62	12.46	7.51	37.12	19.29
31	HOMO-3	-6.240	0.08	0.61	14.96	84.32	0.03
	HOMO-2	-5.465	18.16	8.95	23.04	36.22	13.63
	HOMO-1	-5.172	24.55	34.87	18.8	20.51	1.27
	HOMO	-4.317	33.03	22.66	7.43	20.54	16.34
	LUMO	-2.720	33.85	18.48	12.65	12.75	22.27
	LUMO+1	-2.359	15.18	16.08	33.03	34.36	1.35
	LUMO+2	-1.617	14.64	15.05	22.63	38.03	9.64
	LUMO+3	-0.915	46.12	18.35	8.82	13.23	13.48
31”-1	HOMO-3	-6.147	17.43	57.3	8.05	11.49	5.74
	HOMO-2	-5.671	9.32	11.53	9.39	65	4.76
	HOMO-1	-4.937	26.08	29.06	16.3	23.21	5.35
	HOMO	-4.582	24.02	16.22	21.94	20.01	17.81
	LUMO	-2.791	29.04	18.93	17.55	16.93	17.54
	LUMO+1	-2.668	24.67	24	30.1	11.31	9.92
	LUMO+2	-1.515	16.02	19.56	20.06	33.89	10.46
	LUMO+3	-0.856	27.29	15.89	13.16	35.9	7.76
	HOMO-3	-6.184	17.32	58.34	7.85	11.01	5.48
	HOMO-2	-5.662	9.42	11.32	9.6	63.57	6.09
	HOMO-1	-4.963	24.86	30.62	17.01	24.97	2.53

	Orbital	Energy (eV)	Contribution (%)				
			Thiophene	Pyrrole	π-bridge	Azulene	Mesitylene
31”-2	HOMO	-4.566	26.82	15.23	19.39	18.53	20.04
	LUMO	-2.786	28.81	16.19	17.73	16.31	20.96
	LUMO+1	-2.682	24.77	25.46	32.07	12.79	4.91
	LUMO+2	-1.537	16.62	19.73	20.01	32.53	11.11
	LUMO+3	-0.884	16.01	11.94	9.94	57.05	5.06
32	LUMO	-5.918	83.72	11.48	1.81	1.32	1.67
	LUMO+1	-5.625	28.56	29.36	26.17	12.89	3.02
	LUMO+2	-5.424	13.35	22.65	14.39	32.55	17.07
	LUMO+3	-4.331	24.11	15.36	16.63	21.28	22.62
	LUMO	-2.884	20.92	26.23	35.06	6.45	11.35
	LUMO+1	-2.358	9.79	23.05	19.51	44.22	3.43
	LUMO+2	-2.353	0.11	0.2	0.26	99.39	0.04
	LUMO+3	-1.435	28.99	22.06	14.64	4.98	29.32

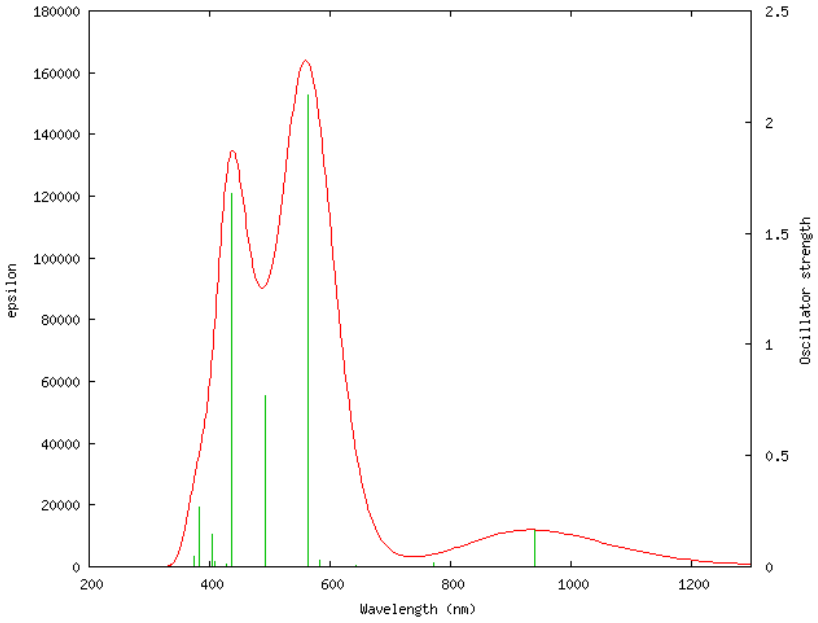

Figure 4.69 Computed absorption spectrum of **30** in solvent phase (CH_2Cl_2) using TD-DFT method at the B3LYP/6-31G(d,p) level

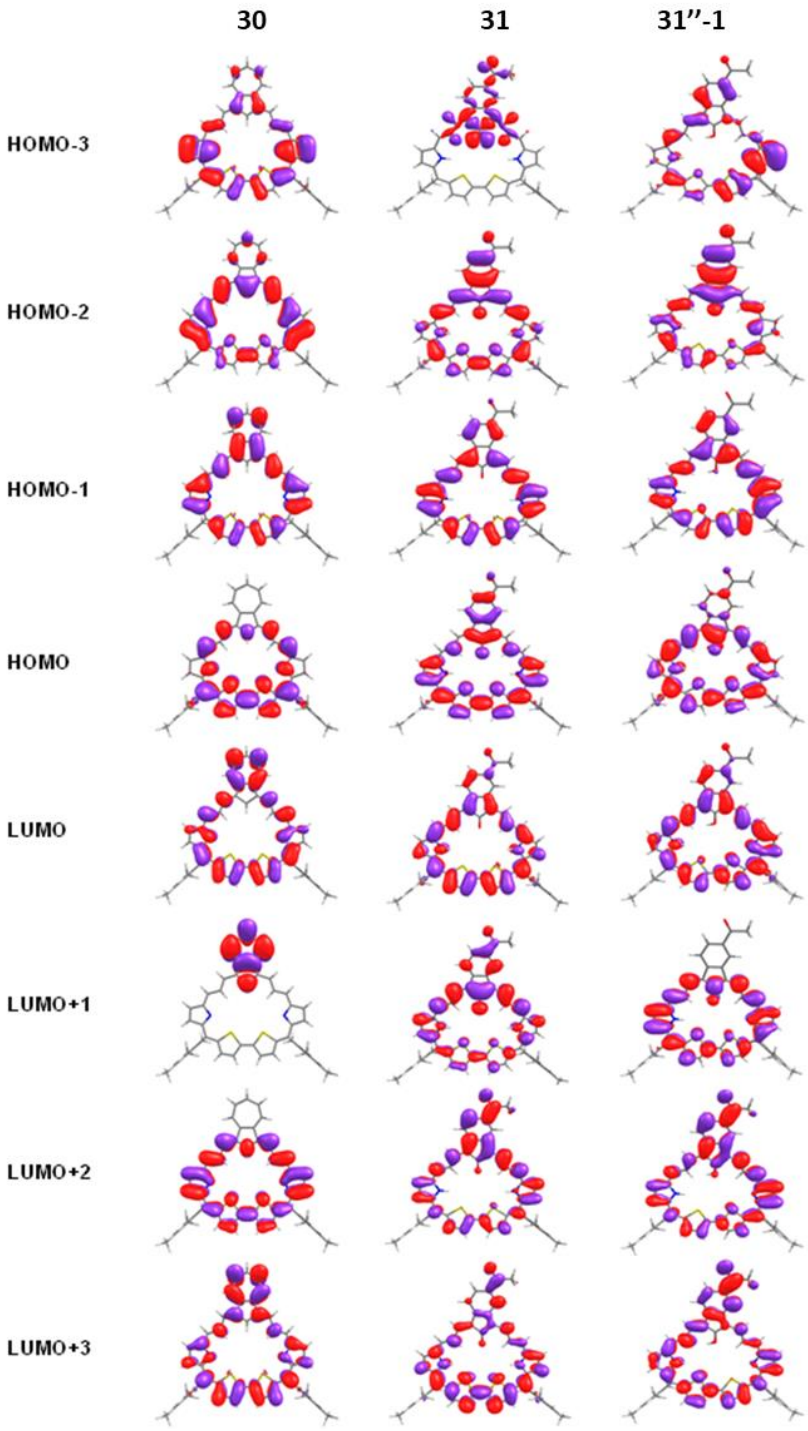

Figure 4.70 Highest occupied molecular orbital and lowest unoccupied molecular orbitals of **30, 31** and **31**"-**1** at the B3LYP/6-31G(d,p) level

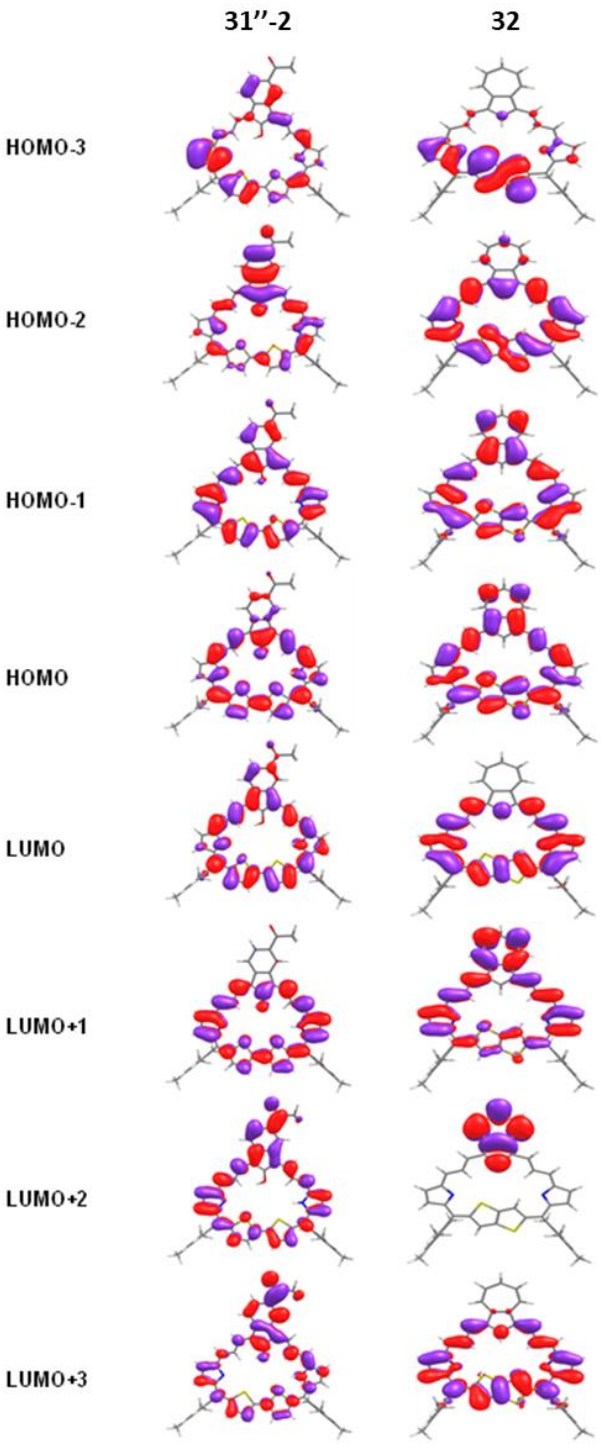

Figure 4.71 Highest occupied molecular orbital and lowest unoccupied molecular orbitals of **31**"-**2** and **32** at the B3LYP/6-31G(d,p) level

Table 6. The calculated NICS (0), NICS (1) and ∑NICS (1) values of each ring centre for **30, 31, 31**”-**1, 31**”-**2** and **32**.

Ring		**30**	**31**	**31**”-**1**	**31**”-**2**	**32**
Imino-type pyrrole -1 [A]	NICS(0)	-1.33	-	0.58	-0.16	-3.29
	NICS(1)	-5.06	-	-3.60	-3.79	-6.56
Imino-type pyrrole -2 [B]	NICS(0)	-1.33	-	-	-	-
	NICS(1)	-5.06	-	-	-	-
Amino-type pyrrole -1 [A]	NICS(0)	-	-11.12	-15.86	-16.55	-3.26
	NICS(1)	-	-9.33	-12.95	-14.00	-5.40
Amino-type pyrrole -2 [B]	NICS(0)	-	-11.04	-	-	-
	NICS(1)	-	-9.31	-	-	-
Thiophene-1 [C]	NICS(0)	-11.77	-8.00	-22.00	-19.35	-6.05
	NICS(1)	-9.97	-6.24	-19.08	-16.58	-4.00
Thiophene-2 [D]	NICS(0)	-11.77	-7.97	-19.80	-21.23	4.53
	NICS(1)	-9.85	-6.22	-16.42	-18.01	4.15
Azulene-5-memebered ring [E]	NICS(0)	-15.58	23.43	13.97	14.75	-16.09
	NICS(1)	-17.11	15.24	7.18	8.43	-17.45
Azulene-6-memebered ring [F]	NICS(0)	-	3.17	-0.57	-0.20	-
	NICS(1)	-	-0.48	-3.65	-3.28	-
Azulene-7-memebered ring [F]	NICS(0)	4.78	-	-	-	-7.82
	NICS(1)	0.70	-	-	-	-9.47
Mesitylene-1 [G]	NICS(0)	-7.72	-8.42	-6.54	-6.70	-9.93
	NICS(1)	-8.94	-9.88	-8.13	-8.28	-11.18
Mesitylene-2 [H]	NICS(0)	-7.72	-8.00	-6.72	-6.54	-9.84
	NICS(1)	-8.94	-6.24	-8.28	-8.08	-11.13
	∑NICS(1)	-64.21	-60.41	-121.87	-119.57	-61.03

Table 7. Harmonic oscillator model of aromaticity (HOMA) values of each ring for **30**, **31**, **31**”-**1**, **31**”-**2** and **32**

	30	**31**	**31**”-**1**	**31**”-**2**	**32**
Imino-type pyrrole-1 [A]	0.3118	-	0.4081	0.4172	0.2908
Imino-type pyrrole-2 [A]	0.3118	-	-	-	0.3065
Amino-type pyrrole-1 [B]	-	0.8610	0.7007	0.7692	-
Amino-type pyrrole-2 [B]	-	0.8638	-	-	-
Thiophene-1 [C]	0.4137	0.3619	0.5933	0.5300	0.1964
Thiophene-2 [D]	0.4137	0.3607	0.6035	0.5300	0.3060
Azulene-5-memebered ring [E]	0.3094	-0.7096	0.1108	0.1065	0.2351
Azulene-6-memebered ring [F]	-	0.9204	0.9227	0.9249	-
Azulene-7-memebered ring [F]	0.7018	-	-	-	0.6322
Mesitylene-1 [G]	0.9364	0.9367	0.9352	0.9371	0.9350
Mesitylene-2 [H]	0.9364	0.9367	0.9375	0.9359	0.9357

Table 8. *H* values for **30, 31, 31**” and **32** at **RCP**

	30	**31**	**31**”-**1**	**31**”-**2**	**32**
Imino-type pyrrole-1 [A]	0.010	-	0.010	0.010	0.011
Imino-type pyrrole-2 [B]	0.010	-	-	-	0.011
Amino-type pyrrole-1 [A]	-	0.012	0.012	0.012	
Amino-type pyrrole-2 [B]	-	0.012	-	-	-
Thiophene-1 [C]	0.009	0.009	0.009	0.009	0.009
Thiophene-2 [D]	0.009	0.009	0.009	0.009	0.009
Azulene-5-memebered ring [E]	0.010	0.010	0.010	0.010	0.010
Azulene-6-memebered ring [F]	-	0.009	-	-	0.004
Azulene-7-memebered ring [F]	0.004	-	0.009	0.009	-
Mesitylene-1 [G]	0.009	0.009	0.009	0.009	0.009
Mesitylene-2 [H]	0.009	0.009	0.009	0.009	0.009
Centre	0.00004	0.00009	0.00010	0.00010	0.00013

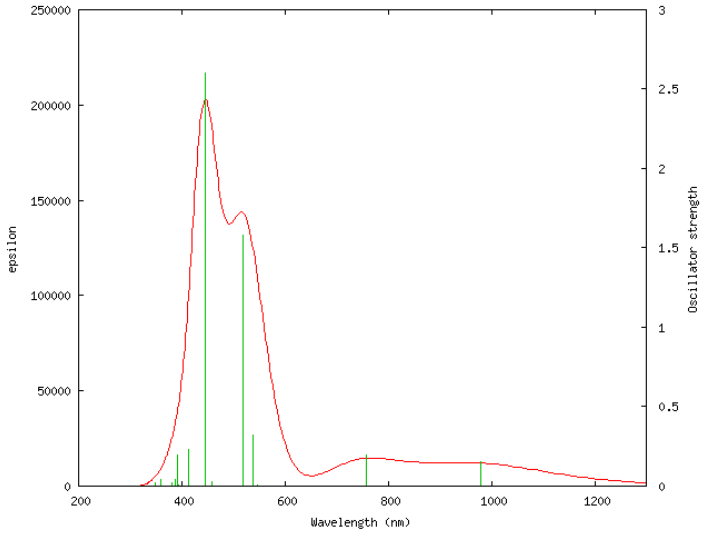

Figure 4.72 Computed absorption spectrum of **31** in solvent phase (CH_2Cl_2) using TD-DFT method at the B3LYP/6-31G(d,p) level

Table 9. Computed absorption maxima (λ_{max} nm), Electronic excitation energies (E, eV), and Oscillator strength (*f*) of **30** in solvent phase (CH_2Cl_2) using TD-DFT method at the B3LYP/6-31G (d, p) level.

No.	Cal. λ_{max} (nm)	Oscillator Strength *f*	E (eV)	Main Contributing Configurations
1	940.3	0.161	1.31	HOMO→LUMO (94%)
2	772.7	0.020	1.60	HOMO-1→LUMO (46%), HOMO→ LUMO +2 (49%)
3	719.1	0.003	1.72	HOMO→ LUMO +1 (96%)
4	643.6	0.005	1.93	HOMO -1→ LUMO +1 (97%)
5	582.3	0.028	2.13	HOMO-1→ LUMO +2 (50%), HOMO→ LUMO +3 (48%)
6	564.3	2.121	2.20	HOMO -1→LUMO (55%), HOMO→LUMO +2 (46%)
7	493.2	0.768	2.51	HOMO -2→LUMO (32%), HOMO -1→LUMO +2 (32%), HOMO→LUMO +3 (33%)
8	447.8	0.001	2.77	HOMO-3→LUMO (35%), HOMO-1→LUMO +3 (62%)
9	437	1.677	2.84	HOMO-2→LUMO (62%), HOMO-1→LUMO+2 (12%), HOMO→LUMO+3 (17%)
10	429	0.010	2.89	HOMO-3→LUMO (57%), HOMO-1→ LUMO+3 (25%)
11	427.8	0.000	2.90	HOMO-4→LUMO (98%)
12	426.4	0.000	2.91	HOMO-5→LUMO (98%)
13	408.8	0.023	3.03	HOMO-6→LUMO (93%)

No.	Cal. λ_{max} (nm)	Oscillator Strength *f*	E (eV)	Main Contributing Configurations
14	408.1	0.000	3.04	HOMO-7→LUMO (98%)
15	404	0.147	3.07	HOMO-8→LUMO (87%)
16	383.7	0.004	3.23	HOMO-3→LUMO+2 (78%)
17	383.6	0.269	3.23	HOMO-9→LUMO (44%), HOMO-2→LUMO+1 (26%), HOMO-2→LUMO+2 (24%)
18	374.4	0.000	3.31	HOMO-3 →LUMO+1 (54%), HOMO→LUMO+4 (33%)
19	373.5	0.036	3.32	HOMO-3→LUMO+1 (29%), HOMO→LUMO +4 (51%)
20	373.3	0.047	3.32	HOMO-2→LUMO+1 (48%), HOMO-2 → LUMO+2 (38%)

Table 10. Computed absorption maxima (λ_{max} nm), Electronic excitation energies (E, eV), and Oscillator strength (*f*) of **31** in solvent phase (CH_2Cl_2) using TD-DFT method at the B3LYP/6-31G(d,p) level.

No.	Cal. λ_{max} (nm)	Oscillator Strength *f*	E (eV)	Main Contributing Configurations
1	980.26	0.156	1.26	HOMO? LUMO (95%)
2	756.83	0.193	1.64	HOMO-1? LUMO (18%), HOMO? LUMO+1 (82%)
3	547.56	0.004	2.26	HOMO-1? LUMO+1 (60%), HOMO? LUMO+2 (27%)
4	538.89	0.322	2.30	HOMO-2? LUMO (34%), HOMO? LUMO+2 (45%)
5	518.91	1.581	2.39	HOMO-1? LUMO (66%), HOMO? LUMO+1 (16%)
6	457.69	0.027	2.71	HOMO-2? LUMO+1 (86%)
7	445.21	2.600	2.78	HOMO-2? LUMO (42%), HOMO-1? LUMO+1 (33%), HOMO? LUMO+2 (18%)
8	423.57	0.000	2.93	HOMO-5? LUMO+1 (83%)
9	413	0.233	3.00	HOMO-1? LUMO+2 (19%), HOMO? LUMO+3 (65%)
10	408	0.000	3.04	HOMO-5? LUMO (84%)
11	394.54	0.004	3.14	HOMO-4? LUMO (90%)
12	394.44	0.001	3.14	HOMO-3? LUMO (90%)
13	391.26	0.195	3.17	HOMO? LUMO+3 (17%), HOMO? LUMO+4 (64%)
14	386.46	0.042	3.21	HOMO-8? LUMO (25%), HOMO-1? LUMO+2 (43%), HOMO? LUMO+5 (19%)
15	380.84	0.000	3.26	HOMO-6? LUMO (98%)
16	380.8	0.000	3.26	HOMO-7? LUMO (97%)
17	379.77	0.021	3.26	HOMO-8? LUMO (15%), HOMO? LUMO+5 (70%)
18	358.42	0.042	3.46	HOMO-2? LUMO+2 (85%)
19	354.65	0.000	3.50	HOMO-9? LUMO (63%), HOMO-9? LUMO+1 (14%), HOMO-9? LUMO+2 (13%)
20	349.4	0.018	3.55	HOMO-10? LUMO (28%), HOMO-8? LUMO+1 (20%), HOMO-3? LUMO+1 (44%)

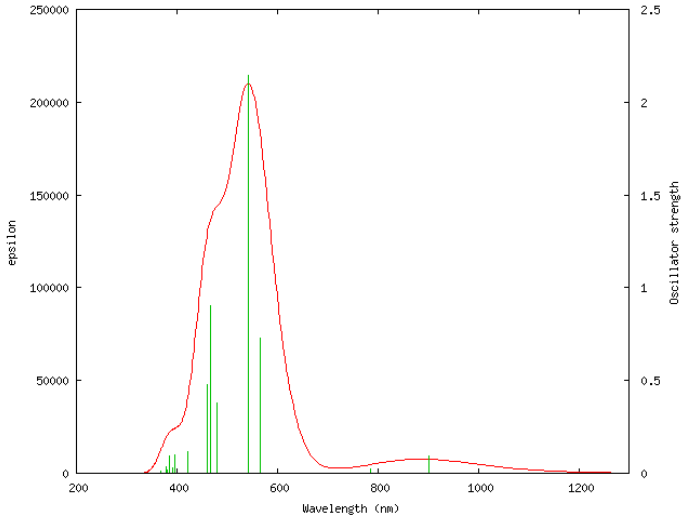

Figure 4.73 Computed absorption spectrum of **31**"-**1** in solvent phase (CH_2Cl_2) using TD-DFT method at the B3LYP/6-31G(d,p) level

Table 11. Computed absorption maxima (λ_{max} nm), Electronic excitation energies (E, eV), and Oscillator strength (*f*) of **31**"-**1** in solvent phase (CH_2Cl_2) using TD-DFT method at the B3LYP/6-31G(d,p) level.

No.	Cal. λ_{max} (nm)	Oscillator Strength *f*	E (eV)	Main Contributing Configurations
1	902.3	0.093	1.37	HOMO-1→LUMO+1 (22%), HOMO→LUMO (73%)
2	784.6	0.025	1.58	HOMO-1→LUMO (37%), HOMO→LUMO+1 (58%)
3	564.9	0.727	2.19	HOMO-2→LUMO (24%), HOMO-1→LUMO+1 (49%), HOMO→LUMO (12%)
4	541.3	2.145	2.29	HOMO-1→LUMO (53%), HOMO-1→LUMO+1 (10%), HOMO→LUMO+1 (35%)
5	480.9	0.380	2.58	HOMO-2→LUMO (53%), HOMO→LUMO+2 (32%)
6	466	0.906	2.66	HOMO-2→LUMO (16%), HOMO-2→LUMO+1 (41%), HOMO-1→LUMO+1 (10%), HOMO→LUMO+2 (20%)
7	459.9	0.479	2.70	HOMO-2→LUMO+1 (41%), HOMO-→LUMO+2 (41%)
8	421	0.115	2.95	HOMO-3→LUMO (44%), HOMO-1→LUMO+2 (45%)
9	417.8	0.001	2.97	HOMO-4→LUMO (97%)
10	407.9	0.002	3.04	HOMO-3→LUMO (30%), HOMO-8→LUMO (16%), HOMO-1→LUMO+2 (33%), HOMO→LUMO+4 (14%)
11	398.3	0.000	3.11	HOMO-6→LUMO (96%)
12	395.6	0.098	3.13	HOMO-3→LUMO+1 (74%)
13	392.5	0.027	3.16	HOMO-5→LUMO (86%)
14	384.6	0.093	3.22	HOMO-8→LUMO (21%), HOMO→LUMO+3 (63%)
15	382.1	0.000	3.24	HOMO-7→LUMO (98%)
16	380.9	0.016	3.26	HOMO-5→LUMO+1 (64%)
17	379.5	0.014	3.27	HOMO-8→LUMO (10%), HOMO-4→LUMO+1 (79%)
18	379	0.038	3.27	HOMO-8→LUMO (30%), HOMO-5→LUMO+1 (29%), HOMO→LUMO+4 (12%), HOMO-4→LUMO+1 (11%)
19	369.5	0.000	3.36	HOMO-7→LUMO+1 (98%)
20	366.9	0.011	3.38	HOMO-8→LUMO+1 (15%), HOMO-6→LUMO+1 (66%)

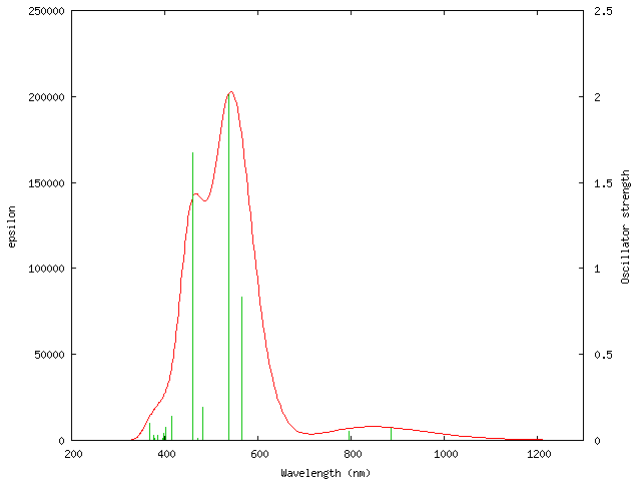

Figure 4.74 Computed absorption spectrum of **31**"-**2** in solvent phase (CH_2Cl_2) using TD-DFT method at the B3LYP/6-31G(d,p) level

Table 12. Computed absorption maxima (λ_{max} nm), Electronic excitation energies (E, eV), and Oscillator strength (*f*) of **31**"-**2** in solvent phase (CH_2Cl_2) using TD-DFT method at the B3LYP/6-31G(d,p) level.

No.	Cal. λ_{max} (nm)	Oscillator Strength *f*	E (eV)	Main Contributing Configurations
1	886.355	0.071	1.40	HOMO-1→LUMO+1 (19%), HOMO→LUMO (62%), HOMO→LUMO+1 (11%)
2	797.167	0.054	1.56	HOMO-1→LUMO (28%), HOMO→LUMO (14%), HOMO→LUMO+1 (53%)
3	565.488	0.835	2.19	HOMO-2→LUMO (22%), HOMO-1→LUMO+1 (47%), HOMO-1→LUMO (13%), HOMO→LUMO (11%)
4	538.988	2.013	2.30	HOMO-1→LUMO (51%), HOMO-1→LUMO+1 (14%), HOMO→LUMO+1 (30%)
5	482.707	0.193	2.57	HOMO-2→LUMO (44%), HOMO→LUMO+2 (49%)
6	470.222	0.012	2.64	HOMO-2→LUMO+1 (88%)
7	459.470	1.674	2.70	HOMO-2→LUMO (29%), HOMO-1-→LUMO+1 (13%), HOMO→LUMO+2 (43%)
8	414.882	0.138	2.99	HOMO-3→LUMO (18%), HOMO-1→LUMO+2 (68%)
9	412.055	0.000	3.01	HOMO-4→LUMO (98%)
10	403.145	0.077	3.08	HOMO-3→LUMO (63%), HOMO→LUMO+4 (15%)
11	398.314	0.044	3.11	HOMO-3→LUMO+1 (75%)
12	395.002	0.010	3.14	HOMO-5→LUMO (82%)
13	393.311	0.001	3.15	HOMO-6→LUMO (87%)
14	385.676	0.026	3.21	HOMO-4→LUMO+1 (19%), HOMO→LUMO+3 (68%)
15	385.484	0.006	3.22	HOMO-4→LUMO+1 (80%), HOMO→LUMO+3 (16%)
16	382.877	0.000	3.24	HOMO-7→LUMO (96%)
17	377.952	0.013	3.28	HOMO-6→LUMO+1 (13%), HOMO-5→LUMO+1 (69%)
18	376.712	0.028	3.29	HOMO-8→LUMO (57%), HOMO-5→LUMO+1 (11%), HOMO→LUMO+4 (23%)
19	371.630	0.003	3.34	HOMO-6→LUMO+1 (83%), HOMO-5→LUMO+1 (15%)
20	368.855	0.098	3.36	HOMO-10→LUMO (25%), HOMO-8→LUMO+1 (55%)

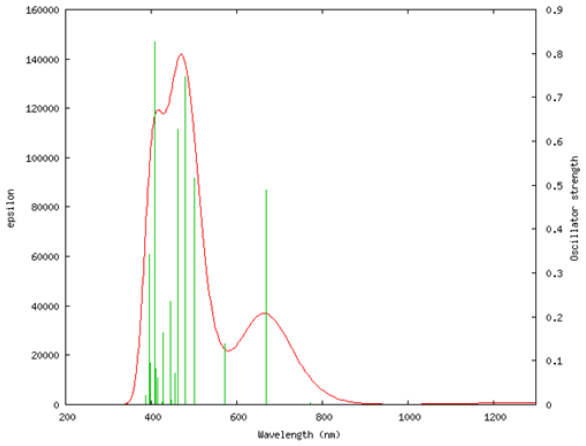

Figure 4.75 Computed absorption spectrum of **32** in solvent phase (CH_2Cl_2) using TD-DFT method at the B3LYP/6-31G(d,p) level

Table13 Computed absorption maxima (λ_{max} nm), Electronic excitation energies (E, eV), and Oscillator strength (*f*) of **32** in solvent phase (CH_2Cl_2) using TD-DFT method at the B3LYP/6-31G (d, p) level.

No.	Cal. λ_{max} (nm)	Oscillator Strength *f*	E (eV)	Main Contributing Configurations
1	1368.0	0.013	0.91	HOMO? LUMO (99%)
2	772.0	0.004	1.61	HOMO? LUMO+2 (96%)
3	669.5	0.488	1.85	HOMO-2? LUMO (10%), HOMO? LUMO+1 (88%)
4	572.4	0.139	2.17	HOMO-1? LUMO (76%), HOMO? LUMO+3 (22%)
5	500.7	0.517	2.48	HOMO-3? LUMO (47%), HOMO-2? LUMO (44%)
6	480.0	0.748	2.58	HOMO-3? LUMO (47%), HOMO-2? LUMO (39%)
7	463.4	0.627	2.68	HOMO-2? LUMO+1 (20%), HOMO-1? LUMO (11%), HOMO? LUMO+3 (54%)
8	455.5	0.071	2.72	HOMO-1? LUMO+2 (85%)
9	447.8	0.011	2.77	HOMO-5? LUMO (20%), HOMO-4? LUMO (73%)
10	444.7	0.038	2.79	HOMO-5? LUMO (72%), HOMO-4? LUMO (18%)
11	444.4	0.235	2.79	HOMO-1? LUMO+1 (79%)
12	428.9	0.164	2.89	HOMO-8? LUMO (75%), HOMO-7? LUMO (12%)
13	425.5	0.000	2.91	HOMO-6? LUMO (90%)
14	425.0	0.006	2.92	HOMO-8? LUMO (14%), HOMO-7? LUMO (78%)
15	416.2	0.062	2.98	HOMO-2? LUMO+2 (45%), HOMO? LUMO+4 (42%)
16	410.4	0.082	3.02	HOMO-10? LUMO (80%)
17	408.7	0.826	3.03	HOMO-2? LUMO+1 (62%), HOMO? LUMO+3 (10%)
18	398.9	0.094	3.11	HOMO-11? LUMO (72%), HOMO-9? LUMO (12%)
19	396.3	0.341	3.13	HOMO-11? LUMO (14%), HOMO-9? LUMO (70%)
20	387.3	0.022	3.20	HOMO-2? LUMO+2 (46%), HOMO? LUMO+4 (36%)

4.7. Reference

1.(a) V. I. Minkin, M. N. Glukhovtsev, and B. Y. Simkin, Aromaticity and Antiaromaticity. Electronic and Structural Aspects; John Wiley and Sons, New York, 1994; (b) A. Stanger, *Chem. Commun*., 2009, 1939-1947;

2. J. K. Park, Z. S. Yoon, M.-C. Yoon, K. S. Kim, S. Mori, J.-Y. Shin, A. Osuka and D. Kim, *J. Am. Chem. Soc.,* 2008, **130**,1824-1825.

3. K. S. Kim, Z. S. Yoon, A. B. Ricks, J.-Y. Shin, S. Mori, J. Sankar, S. Saito, Y. M. Jung, M. R. Wasielewski, A. Osuka and D. Kim,*J. Phys. Chem. A*, 2009, **113**, 4498-4506.

4. S. Saito, J.-Y. Shin, J. M. Lim, K. S. Kim, D. Kim and A. Osuka, *Angew. Chem., Int. Ed.,* 2008, **47**, 9657-9660.

5. (a) P. J. Chmielewski, L. Latos-Grazynski, K. Rachlewicz and T. Glowiak,, *Angew. Chem. Int. Ed. Engl*. 1994, **33**, 777-779; (b) H. Furuta, T. Asano and T. Ogawa, *J. Am. Chem. Soc*. 1994, **116**, 767-777.

6. H. Furuta, H. Maeda and A. Osuka, *J. Am.Chem. Soc*., 2000, **122**, 803-807.

7. Z. Zhang, G. M. Ferrence and T. D. Lash, *Org. Lett*., 2009, **11**, 101-104.

8. T. D. Lash and M. J. Hayes, *Angew.Chem., Int. Ed. Engl.,*1997, ***36***,840-856.

9. T. D. Lash, *Org. Biomol. Chem*., 2015, **13***,* 7846-7878.

10. K. M. Bergman, G. M. Ferrence and T. D. Lash, *J. Org. Chem.,*2004,**69**, 7888-7897.

11.T. D. Lash and S. T. Chaney, *Angew.Chem., Int. Ed. Engl.,* 1997, **36**, 839-840.

12.A. Berlicka, P. Dutka, L. Szterenberg and L. Latos-Grazynski, *Angew.Chem. Int. Ed.,* 2014*,* **53***,* 4885-8889.

13. (a) T. D. Lash, D. A. Colby, S. R. Graham, G. M. Ferrence and L. F. Szczepura, *Inorg.Chem*., 2003, **42**, 7326-7338; (b) L. M. Stateman, G. M. Ferrence and T. D. Lash, *Organometallics,* 2015, **34***,* 3842-3848; (c) T. D. Lash, K. Pokharel, M. Zeller and G. M. Ferrence, *Chem. Commun.,* 2012, **48**, 11793-11795; (d) M. Białek and L. Latos-Grazynski, *Chem. Commun.,* 2014*,* **50**, 9270-9272.

14. (a) S. Venkatraman, V. G. Anand, V. Prabhu Raja, H. Rath, J. Sankar, T. K. Chandrashekar, W. Teng and K. Ruhlandt-Senge*, Chem. Commun.,* 2002, 1660-1661; (b) T. D. Lash, D. A. Colby, S. R. S. Graham and T. Chasey, *J. Org. Chem*., 2004, **69**, 8851-8858
15. V. J. Bauer, D. L. J. Clive, D. Dolphin, J. B. Paine, F. L. Harris, M. M. King, J. Loder, S.-W. C. Wang and R. B. Woodward, *J. Am. Chem. Soc.,* 1983, **105**, 6429-6436.
16. (a) S. B. Brown and T. G. Truscott, *Chem. Br.,* 1993, **29**, 955; (b) R. Bonnett, *Chem. Soc. Rev*., 1995, **24**, 19-33.
17. D. T. Richter and T. D. Lash, *J. Org. Chem.,* 2004, **69**, 8842–8850.
18. S.K. Pushpan, A. Srinivasan, V. G. Anand, S. Venkatraman, T. K. Chandrashekar,B. S. Joshi ,R. Roy and H. Furuta, *J. Am. Chem. Soc.*, 2001, **123**, 5138–5139.
19. G. Karthik, A. Srinivasan and T. K. Chandrashekar, *Org. Lett.*, 2014, **16**, 3472–3475.
20. S. Beckmann, T. Wessel, B. Franck, W. Ho¨nle, H. Borrmann and H.-G. von Schnering,.*Angew.Chem., Int. Ed. Engl.,* 1990, **29***,* 1393-1395.
21. L. Xu, G.M. Ferrence and T.D. Lash, *Org. Lett.* 2006, **8,** 5113-5116.
22. D.R. Reddy and B. G. Maiya, *J. Phys. Chem. A,* 2003, **107**, 6326-6333.
23. W. Tsuzuki , *Chem. Phys. Lip.,* 2010, **163**,741–745.
24. R.Sakashita, Y. Oka, H..Akimaru, P. E. Kesavan, M. Ishida, M.Toganoh, T. Ishizuka, S. Mori, and H.Furuta. *J. Org. Chem.,*2017, **82**, 8686–8696
25. M. Kawamoto, N. Shiga, K. Takaishia and T. Yamashita, *Chem. Commun.* 2010, **46** ,8344-8646
26. R. A. Berger and E. LeGoff, *Tetrahedron Lett.,* 1978,**44**, 4225-4228.
27. M. Gosmann , A. Vogt, and B. Franck, *Liebigs Ann. Chem.* 1990, 163 – 168.
28. M. Gosmann and B. Franck, *Angew Chem.* Int. *Ed. Engl.,*1986, **25**, 1100-1101.
29. (a) E. Vogel *Pure & Appl. Chern.,* **1993**, 65,143-152; (b) R.Bachmann, F. Gemon, C. Pütz and E. Vogel *J. Chem. Soc.*,*Perkin Trans. 2,* **1996,** 541-546.
30. G. Knubel and B. Franck, *Angew. Chem., Int. Ed. Engl.,* 1988, **27**, 1170-1171.

31. (a) T. D. Lash, D. A. Colby, S. R. Graham, G. M. Ferrence, and L. F. Szczepura, *Inorg.Chem*. 2003, **42**, 7326-7338; (b) L. M. Stateman, G. M. Ferrence, and T. D. Lash, *Organometallics,* 2015, **34**, 3842-3848; (c) T. D. Lash, K. Pokharel, M. Zeller, and G. M. Ferrence, *Chem. Commun*. 2012, **48**, 11793-11795; (d) M. Białek, and L. Latos-Grazynski, *Chem. Commun.*2014, **50**, 9270-9272; (e) D. A. Colby, G. M. Ferrence, and T. D. Lash, *Angew.Chem., Int. Ed*. 2004, **43**, 1346-1349.
32. M. Gouterman, *J. Mol. Spectrosc.,* 1963, **11**, 108-127
33. CCDC 2116847 contains the supplementary crystallographic data.
34. B. Franck and A. Nonn, *Angew. Chem., Int. Ed. Engl.,* 1995, **34**, 1795-1811.
35. K. C. Sahoo, K. Gourav, D. Usharani and H. Rath, *J. Org. Chem.,* 2019, **84**, 5203-5212, and references therein;
36. J.-Y. Shin, K. S. Kim, M.-C. Yoon, J. M. Lim, Z. S. Yoon, A. Osuka and D. Kim, *Chem. Soc. Rev.,* 2010, **39**, 2751-2767.
37. J. A. Pople and K. G. Untch, , *J. Am. Chem. Soc*., 1966, **88**, 4811-4845.
38. (a) M. J. Frisch, et al., Gaussian 16, Revision C. 01, Gaussian, Inc., Wallingford, CT, 2019; (b) A. D. Becke, *J. Chem. Phys.,* 1993, **98**, 5648-5652; (c) J. P. Pardew, *Phys. Rev. B*:1986, **33**, 8822-8824; (d) A. D. Becke, *Phys. Rev. A*: 1988, 38, 3098-3100; (e) C. Lee, W. Yang and R. G. Parr, *Phys. Rev. B*, 1988, **37**, 785-789.
39. (a) E. Runge and E. K. U. Gross, , *Phys. Rev. Lett.,* 1984, **52**, 997-1100; (b) R. E. Stratmann, G. E. Scuseria and M. J. Frisch, *J. Chem. Phys.,* 1998, **109**, 8218-8224; (c) R. Bauernschmitt and R. Ahlrichs, *Chem. Phys. Lett.,* 1996, 256, 454-464; (d) T. Yanai, D. P. Tew and N. C. Handy, *Chem. Phys. Lett.,* 2004, **393**, 51-57.
40. D. Geuenich, K. Hess, F. Köhler and R. Herges, *Chem. Rev.,* 2005, **105**, 3758-3772.
41. P. v. R. Schleyer, C. Maerker, A. Dransfeld, H. Jiao and N. J. R. V. E. Hommea, *J. Am. Chem. Soc.,* 1996, **118**, 6317-6318.
42. (a) T. M. Krygowski, *J. Chem. Inf. Comput. Sci.,* 1993, **33**, 77-78; (b) T. M. Krygowski and K. M. Cryański, *Chem. Rev.,* 2001, **101**,1385-1420.

Siamese Vinylogous Carbaporphyrinoids

Chapter 5

5. Abstract

Azulene bridge vinylogous carbaporphyrin has been synthesized following literature known acid-catalyzed condensation protocol. In situ azulene moity rearranged to oxanapthylene unit. The spectroscopic preclusion of aromaticity of these bridge carbaporphyrinoids are confirmed by electronic absorption spectra that exhibited soret band and well defined Q-type bands in the vis-NIR region and NMR spectroscopy.

5.1. Introduction

Bridge porphyrinids have played a central role in understanding the relationship among the structural, electronic characteristics and aromaticity. Such expanded porphyrinoids have found a dual conjugated path, allowing multi-metal coordination site and intramolecular redox reactions.

1,4-Phenylene-Bridged *meso* aryl-substituted expanded Porphyrins was first reported by Osuka and co-workers. The internal 1,4-phenylene bridge was bisected large *meso* aryl-substituted expanded porphyrins **1** and **2**. The presence of diatropic ring current of 1,4-phenylene-bridged [46]decaphyrin **1** was confirmed by its ^{1}H NMR and Uv-Vis-NIR spectra. Upon treatment with DDQ Hückel aromatic 1,4-phenylene-bridged [46]decaphyrin **1** was converted to nonaromatic [44]decaphyrin **2**. A reversible redox interconversion was found between **1** and **2**. The electronic spectrum of **1** exhibited a Soret-like band at 505 nm and strong Q-like split bands at 800 and 856 nm, while that of **2** exhibits broad bands at 454 and 619 nm Interestingly, protonation of **1** with trifluoroacetic acid led to an intense and sharp Soret-like band at 846 nm and a Q-like band at 1221 nm. [1]

Chapter 5

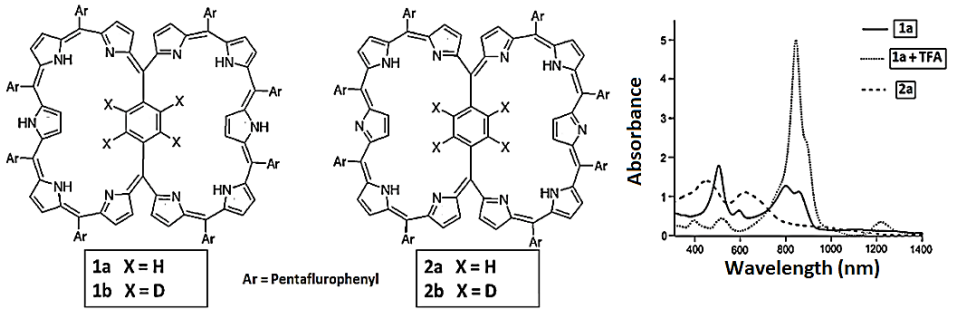

Figure 5.1. 1,4-Phenylene-bridged Decaphyrins

In continuation, the vinylenebridged hexaphyrins **3** and **4** were reported by the same group. The Hückel aromatic vinylene-bridged [26]- **3** is converted to its reduced form **4** Hückel antiaromatic through reduction with $NaBH_4$. These vinylene-bridged hexaphyrins possess rigid structure and exhibited an intramolecular redox conversion between 26π aromatic **3** and 28π antiaromatic **4.**[2]

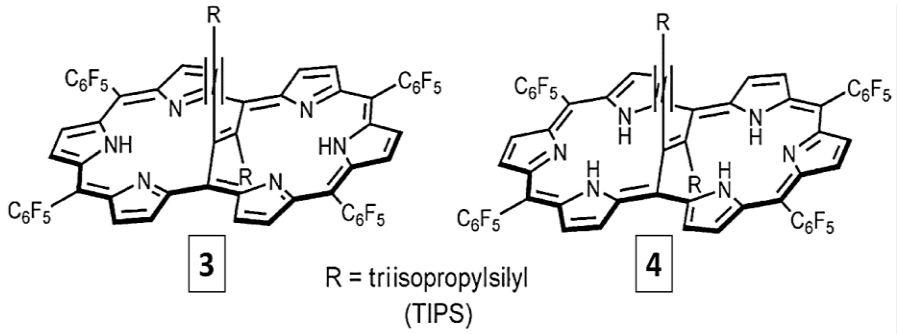

Figure 5.2 Vinylene-bridged [26] hexaphyrin **3** and [28] hexaphyrin **4**.

Internally aromatic strapped [26] porphyrinoids **5**, **6**, and **7** were reported by Osuka and co-workers.[3]

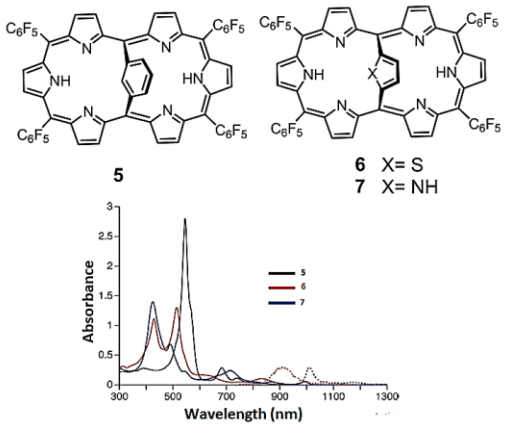

Figure 5.3. Internally m-Phenylene, thiophene and pyrrole Bridged [26]Hexaphyrins

The mentioned porphyrinoids exhibited dual electronic properties. The effective conjugation path of these hexaphyrins can be modulated by internal aromatic straps. Spectroscopic investigations revealed that [26]hexaphyrin network is predominant for **5** because of the negligible involvement of the 1,3-phenylene strap. The active involvement of the 2,5-thienylene and 2,5-pyrrylene straps in the macrocyclic conjugation causes roughly equal contribution of [26]hexaphyrin and [18]thiaporphyrin for **6** and predominant contribution of [18]porphyrin for **7**.

A similar aromatic-bridged system with core modified hexaphyrins **8** and **9** were reported by Chandrashakar and co-workers. Both the macrocycles exhibited dual conjugation of [18] dithiaporphyrin and/or [26] dithiahexaphyrin.[4]

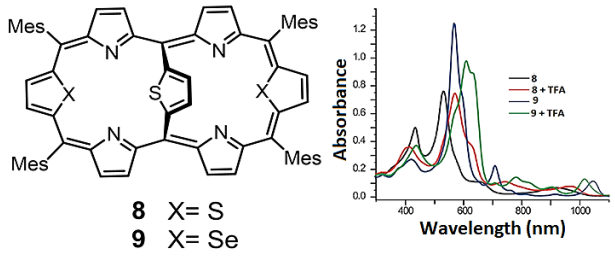

Figure 5.4. Coremodified Internally thoiphene-bridged [26]Hexaphyrins

Chapter 5

In continuation internally 1,3-phenylene- and 2,5-thienylenebridged [46] decaphyrins **10** and **11** were reported by Osuka and co-workers. Internally 1,3-phenylene-bridged [46] decaphyrins **10** exhibits Hückel aromatic whereas 2,5-thienylenebridged [46] decaphyrins **11** display a larger aromatic character on account of the contribution of two twisted Möbius aromatic thia[28]hexaphyrin segments in addition to the global 46π network. Oxidation of **10** gave [44]decaphyrin **12**. The absorption spectrum of **10** showed a relatively broad Soret-like band at 910 nm and distinct Q-like bands at 1189 and 1414 nm whereas, the absorption spectrum of **11** exhibited two Soret-like bands at 603 and 776 nm, that corresponding to the absorption bands of thia[28]hexaphyrin and [46]decaphyrin. [5]

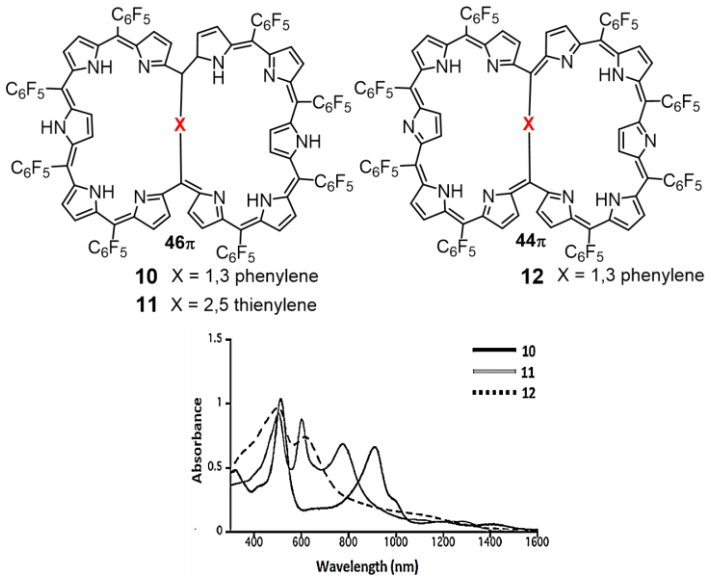

Figure 5.5. Internally 2,5-Thienylene-Bridged [46] Decaphyrin.

In continuation dithienothiophene (DTT)-bridged [34]octaphyrins **13** and **14** were reported by Chandraskekar and co-workers exhibiting Baird-type aromatic in triplet states. The macrocycles **13** and **14** contain competing between 34π and 26π electronic systems in their neutral form. The oxidized form of **13** molecules gave 40π electronically mixed [4n+1] /[4n+1] triplet biradical species in the ground state that possesses global aromaticity in accord with Baird's rule.[6]

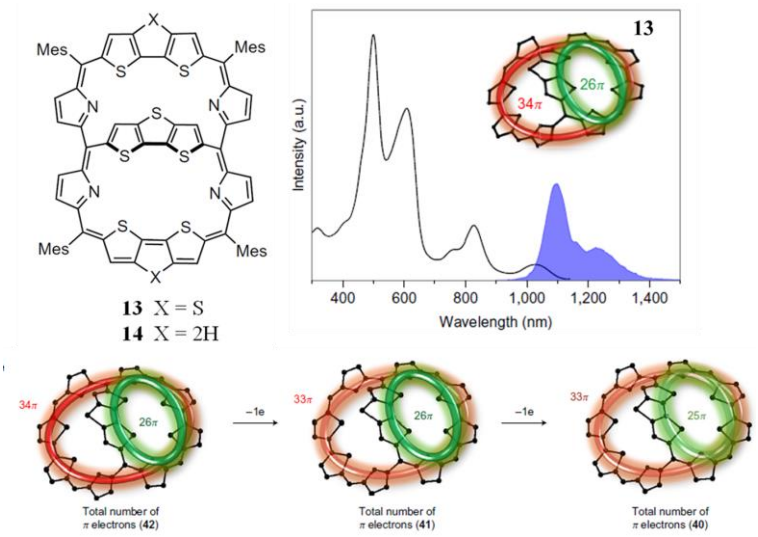

Figure. 5.6. Dithienothiophene (DTT)-bridged porphyrinoids

Azulene bridge hexaphyrin **15** and its palladium complex were reported by L. L. Grażyński and co-workers. The palladium(II) complex of **15** undergoes the hydroxyl-triggered azulene contraction or isomerization to an oxynaphthalene unit and transforming the hexaphyrin framework into *meso*-linked carbaporphyrins **16**. As a result, the conjugation path is changed from 26π electrons to 18π electron pathway.[7]

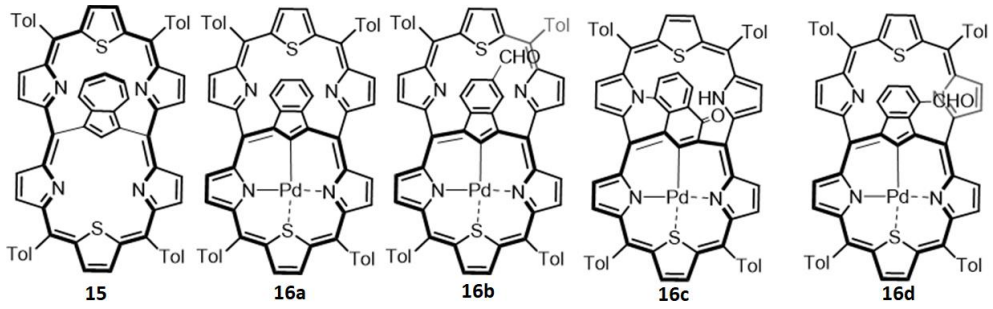

Figure 5.7. Azulene bridge hexaphyrin and its palladium complex

The chemistry of such bridge porphyrinoids are the current focus of modern research because of their unique properties. AS the flexibility of expanded

porpyrinoids can be reduced by the incorporation of a proper internal linker that bounds to two opposite *meso* positions and give the stability to the macrocycle. The conjugation path can go through either the spacer or through the periphery of a macrocycle. For this reason, it is possible to have dual-potential electronic properties and two aromatic pathways that operate independently, which we term as 'dual aromaticity'. Such porphyrinoids have two cavities and their structural diversity and redox properties permit access to a variety of [4n+2] and [4n] π-electronic configuration of Aromatic and antiaromatic compounds.

To date very few examples of such porphyrinods are reported. The chemistry of bridge porphyrins has not explored yet. In my previous chapter I had reported NIR absorptive aromatic core-modified vinylogous azulisapphyrin. The tropilium cation is responsible for the aromaticity of the molecule. In this chapter I have synthesized vinylogous azulene bridge NIR absorptive aromatic core-modified octaphyrin.

5.2. Results and discussion

5.2.1. Synthesis

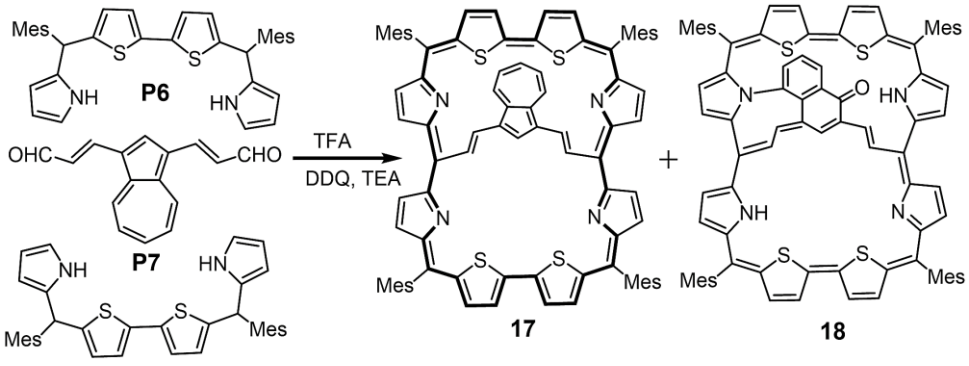

Scheme5.1. Acid-Catalyzed Condensation of core modified bridge carbaporphyrinoid **17**

The new macrocycles were synthesized through acid-catalyzed condensation reaction of tetrapyrrane **P5** with azulene-1,3-bis-acrylaldehyde **P6** in methylene chloride containing ten equivalents of trifluoroacetic acid (TFA) as catalyst followed by oxidation of the macrocycle with DDQ. After purification, the macrocycle **17** and **18** were obtained as blue using 50% dichloromethane and hexane and dark brown using 70% dichloromethane and hexane as eluent respectively

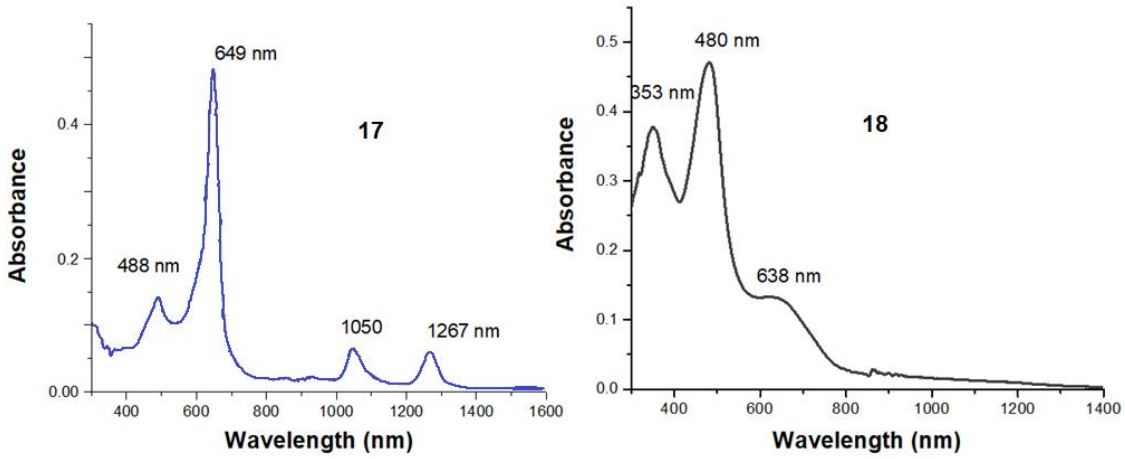

Figure 5.8. UV-vis-NIR Spectrum of **17**(left) and **18**(right)

The structure of this new macrocycles were precluded by various spectroscopic analyses. The heteroannulene **17** and **18** exhibited parent ions peaks at m/z 1310.448 and 1326.4431 in MALDI-TOF and ESI-TOF mass spectrometer respectively accounting for their compositions. The electronic absorption spectra of the macrocycle **17** in the free base exhibited one band at 488nm a sharp Soret band at 649 nm, and two Q-bands at 1050 nm and1267nm indicates the macrocycle is aromatic in nature. While for macrocycle **18** in the free base exhibited two splited Soret bands at 353nm and 480nm, and Q-bands at 638 nm and one stretch band from 800nm to 1300nm indicates the macrocycle is weakly aromatic in nature.

The ^{1}H NMR spectrum of **17** in $CDCl_3$, shows strong diamagnetic ring current present in the macrocycle. In 2D ROESY spectra the macrocycle **17** at 298 K the peaks at 2.35 and 2.15 ppm are individually showing correlation with the signals at 6.99 ppm assigned the peak 6.99 ppm as m-CH protons of the *meso*-mesityl substituents and the peak position at 2.35 and 2.15 ppm corresponding to *ortho* and *para* mesityl-CH_3. In 2D COSY spectra, in most downfield region the two doublets at 11.15 and 10.26 ppm are showing correlation and 2D ROESY doublet at 10.26 ppm is showing correlation with mesityl ortho CH_3 at 2.15 ppm assigned the most two doubles as a bi-thophene β CHS. In 2D COSY spectra, the two doublets at 9.41 and 8.8 ppm are showing the correlation and 2D ROESY the doublet at 8.8 ppm is showing correlation with mesityl ortho CH_3 at 2.15 ppm assigned the two doubles as a pyrrole β CHs In2D COSY spectra, upfield region two doublet at -0.6 and -2.1 ppm. are showing correlation assigned two shielded doublets as internal vinylogous CHs and most shielded singlet at -3.7 ppm is assignd as azulene five-member CH and Δδ value is 14.85 ppm indicates the macrocycle is strongly aromatic in nature Due to ring current effect the azulene sevenmember CHs are resonate in the upfield region. In 2D COSY spectra, the triplet 4.28 ppm is showing correlation with one doublets at 3.98 ppm and another triplet at 5.35 ppm assigned the peaks are azulene seven member CHs.

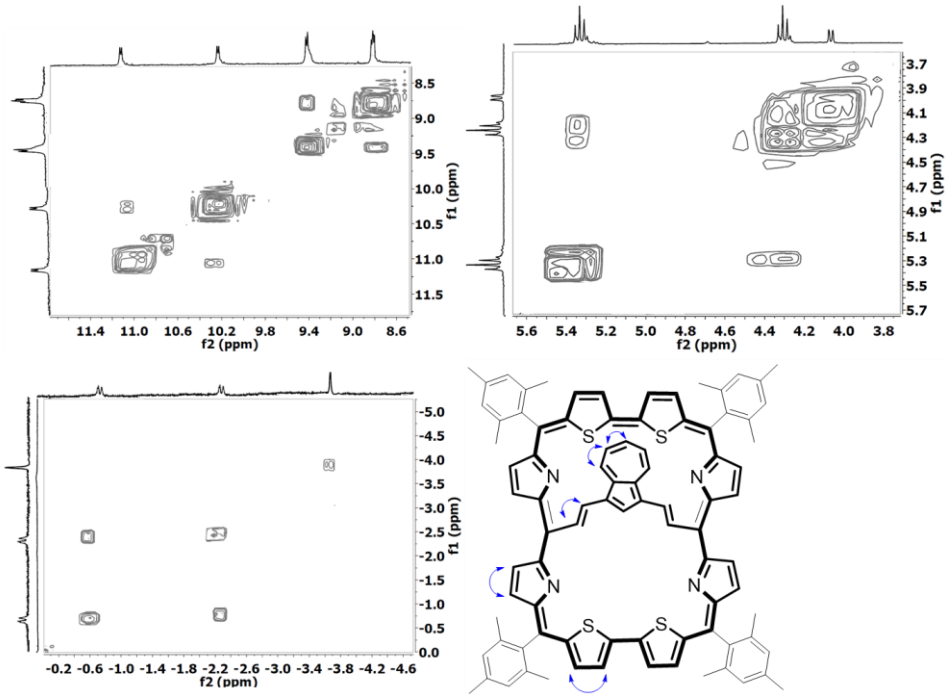

Figure 5.9. 2D COSY Spectra of free base **17** in $CDCl_3$

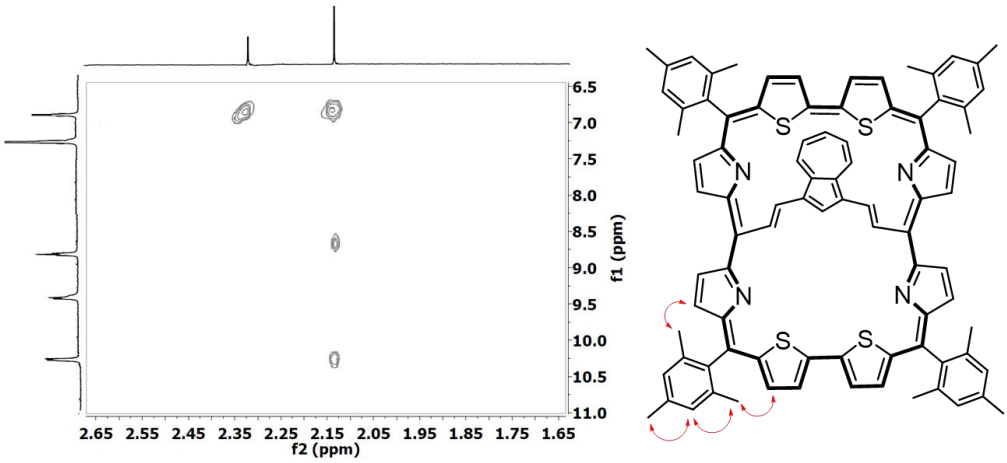

Figure 5.10. 2D ROESY Spectra of free base **17** in $CDCl_3$

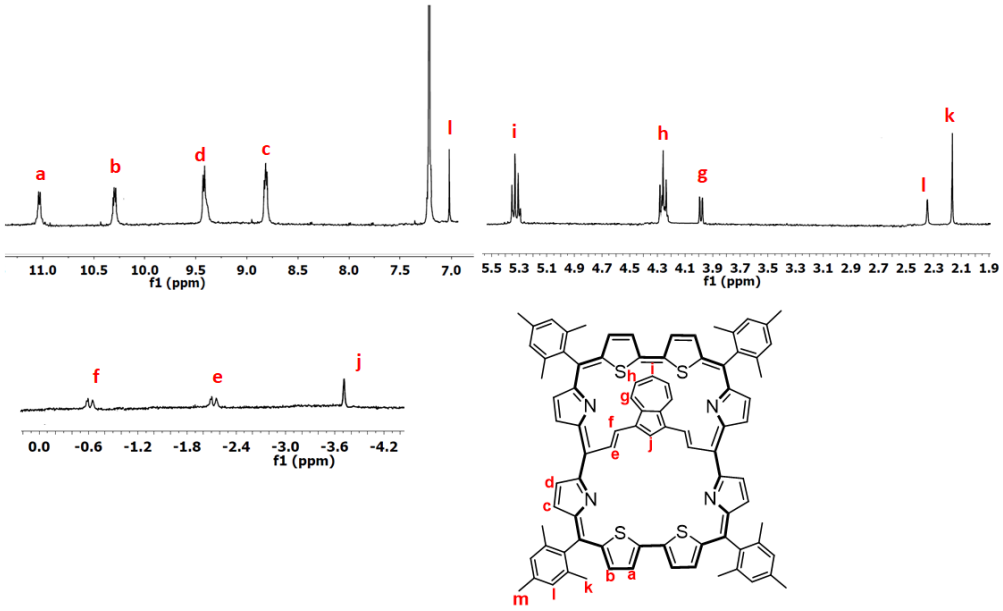

Figure 5.11. Complete assignment of macrocycle **17** in $CDCl_3$

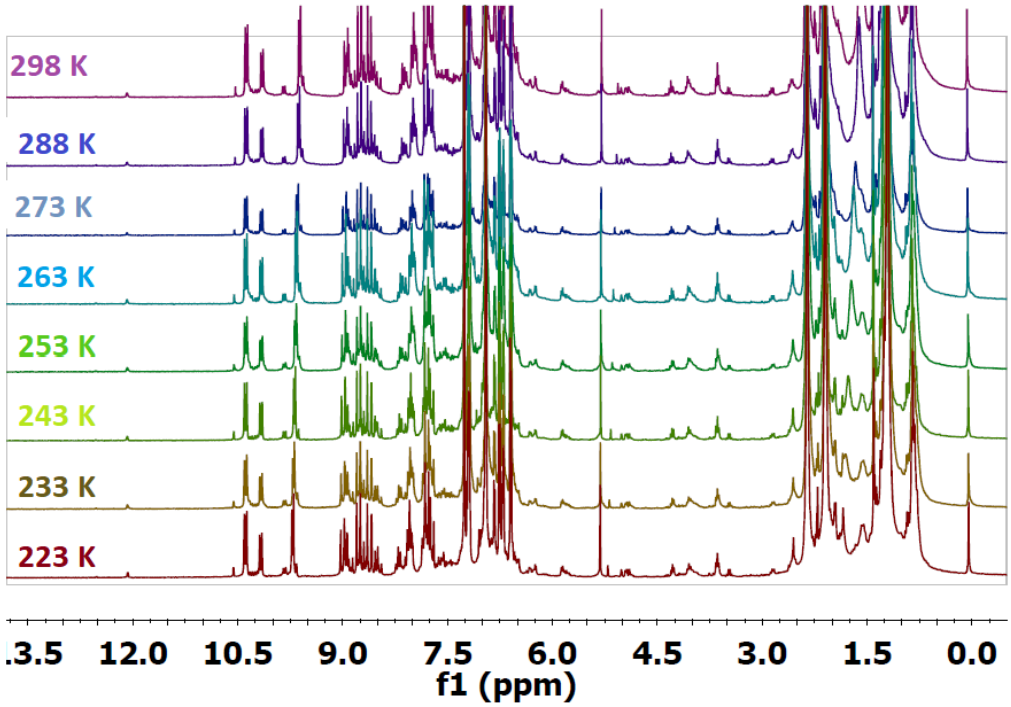

Figure 5.12. Variable temperature ^1H NMR Spectra of free base **18** in $CDCl_3$

The azulene unit becomes rearranges to oxanapthalene unit due to the nucleophilic (water) attack at the seven-member ring. [7] The presence of keto group was confirmed by ^{13}C NMR.the peak at 185.93 which do not show any correlation in 2D HSQC experiment. Upon lowering the temperature, the peaks becomes sharp. In 2D ROESY spectra the macrocycle **18** at 298 K, the peaks at 2.37 and 2.12 were showing the two correlations with 6.75 ppm, indicate the signals at 6.75 m-CH protons of the *meso*-mesityl substituents and the peak position at 2.37 and 2.12 ppm corresponding to *ortho* and *para* mesityl-CH_3.

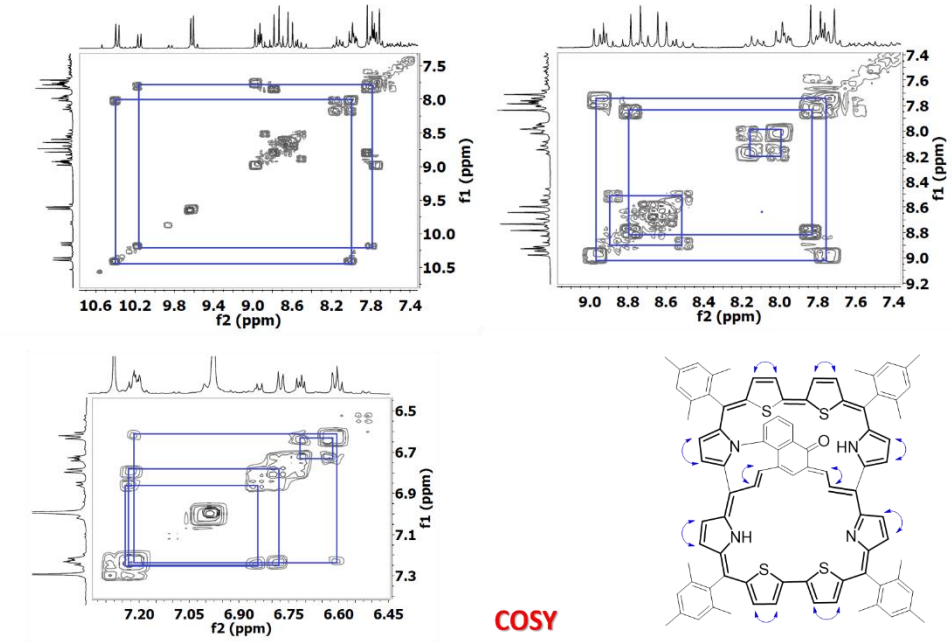

Figure 5.13. 2D COSY Spectra of free base **18** in $CDCl_3$

In 2D ROESY spectra at 298 K, the mesityl *ortho* CH_3 showed two correlations with at 7.21 ppm, 6.76 ppm,6.69ppm and 6.58 ppm In 2D COSY spectra at 298 K, the four sets correlations between the signal at 7.21, 6.58 ppm, 7.21, 6.76, 7.21, 6.82 and 6.58, and 6.69 indicate β–CH protons pyrrole respectively. In deshilded the two broad at 10.52 ppm and. 12.08 ppm assign as two pyrrole NH protons. In 2D COSY spectra at 298 K, the four sets correlations between

the signal peak at 8.92, 7.71 ppm; 8.73, 7.79ppm; 8.14, 7.95ppm and 8.59, 8.92ppm indicates β–CH protons thiophene. In 2D COSY spectra at 298 K, the correlation between the signal peak at 10.37, 7.98 ppm and 10.15 ,7.83 ppm indicates four sets of inner vinylogous CHs. The multiplate at 9.62 ppm is assigned as an outer six-member protons. The singlet signal at 7.83 ppm was inner six-member CH.

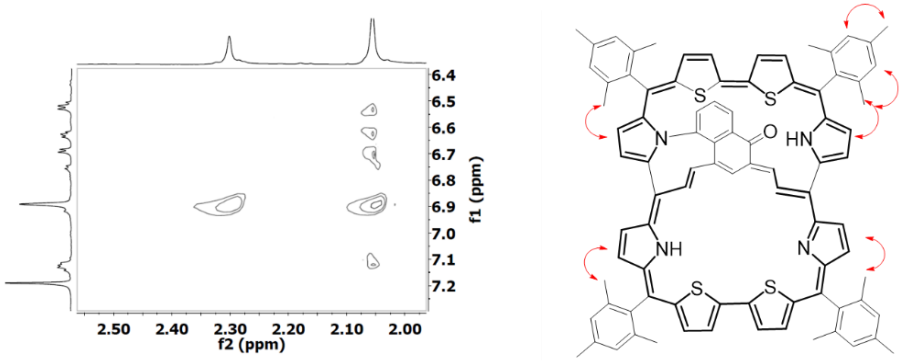

ROESY

Figure 5.14. 2D ROESY Spectrum of free base **18** in $CDCl_3$

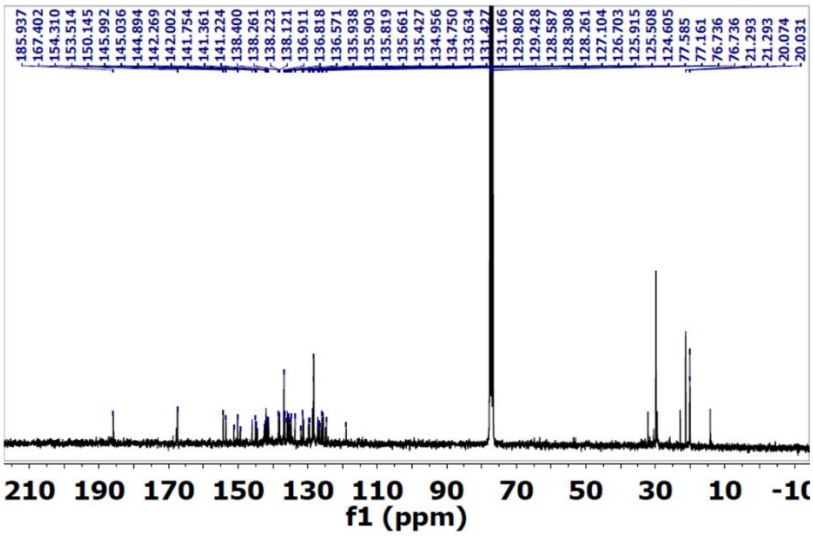

Figure 5.15. ^{13}C NMR Spectrum of free base **18** in $CDCl_3$

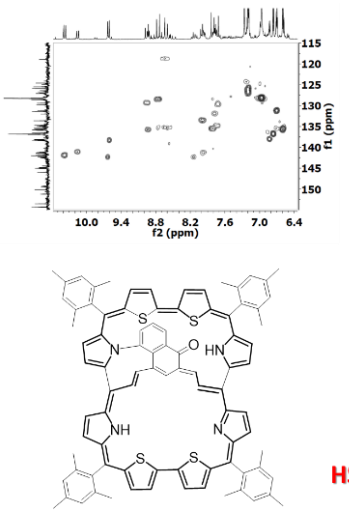

^{1}H NMR ppm	^{13}C NMR ppm	^{1}H NMR ppm	^{13}C NMR ppm
10.37	142.75	8.14	142.43
10.15	141.16	7.98	133.63
9.62	142.27	7.95	141.22
9.59	138.26	7.83	135.42
8.96	129.43	7.79	132.02
8.92	135.82	7.71	129.43
8.77	128.49	7.2	125.92
8.73	128.31	6.82	138.12
8.64	118.95	6.76	136.82
8.59	135.43	6.69	131.42
		6.58	135.66

Figure 5.16. 2D HSQC Spectrum of free base **18** in $CDCl_3$

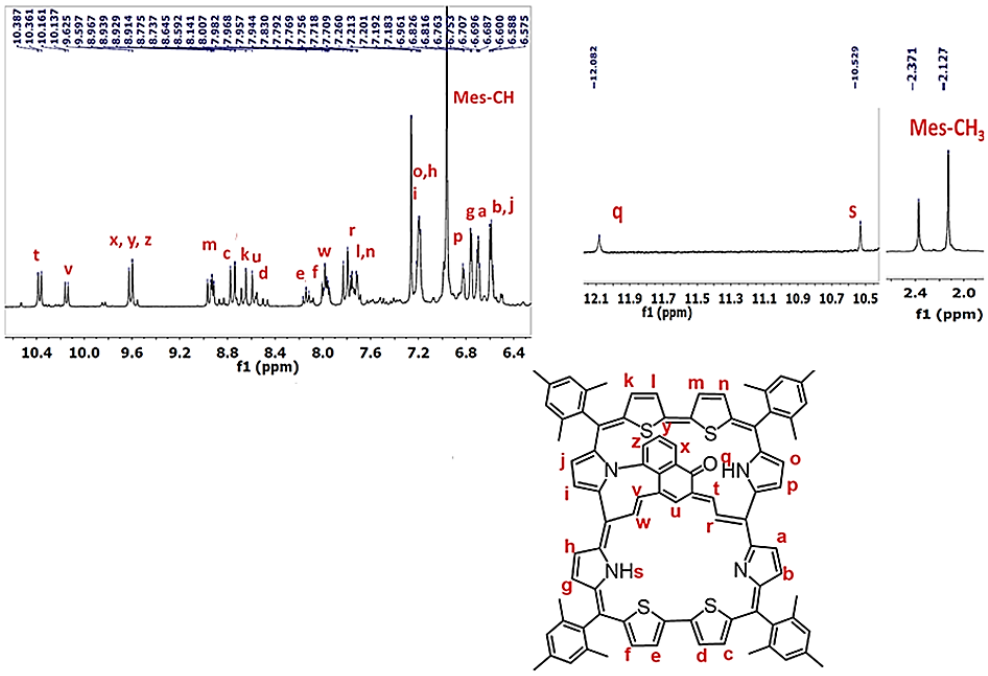

Figure 5.16. Complete assignment of macrocycle **18** in $CDCl_3$

Chapter 5

5.3. Conclusion:

Acid-catalyzed condensation of tetrapyrrane **p5** with azulene-1,3-bis-acrylaldehyde **p6** using TFA as catalyst followed by oxidation with DDQ gave an oxanapthylene bridge expanded carbaporphyrinoid **17** and **18**. In situ under oxidative condition azulene moiety was converted to oxanapthylene moiety. The electronic spectra of **17** and **18** indicates porphyrinic nature with aromaticity and exhibiting NIR absorption. The new macrocycles have two cavities that may be utilized as a receptor. In addition, this macrocycle could be a suitable candidate for use as photosensitizers in photodynamic therapy owing to its long wavelength absorption.

5.4. Experimental Methods

General Synthesis of 17 & 18:

Tetrapyrrane **p5** (280.41 g, 0.5 mmol) was taken in a round bottom flask; to it 250 mL of dry DCM was added and stirred for 15 minutes under nitrogen atmosphere to get a clear solution. Azulene-1, 3-bisacrylaldehyde **p6** (59.02 mg, 0.25 mmol was added to the reaction mixture and stirred for 15 minutes under dark condition. To this, 0.115 mL (1.5 mmol) CF_3COOH was added and reaction mixture was stirred under nitrogen atmosphere in dark for overnight. The reaction mixture was then neutralised with 0.58 mL triethylamine followed by oxidation with 573 mg of DDQ in open air. After complete removal of solvent from crude mixture by rotary evaporator, the compounds were purified using basic alumina grade III and further by repeated PTLCs The compound **17** came as blue band using 50% dichloromethane- Hexane as eluent whereas compound 18 came dark brown color band using 70% dichloromethane- Hexane as eluent.

Compound 17: Yield. ~66mg (10%). R_f = 0.25 (Dichloromethen/ Hexane = 1:1), mp > 300 °C. HR-MS(ESI-TOF) m/z: $[M]^+$ calcd for $C_{88}H_{70}N_4S_4^+$ 1310.4483; found 1310.448 UV-vis (CH_2Cl_2, λ [nm], ([ϵ $[M^{-1}$ $cm^{-1}x10^4]$) 298K) 488.6(25.5), 649.35(89.6), 1050.75 (10.2), 1267.45 (10.2),

^{1}H NMR (400 MHz, $CDCl_3$, 298 K) δ = 11.15 (d, 4H, thiophene β -CHs), 10.26 (d, 4H, thiophene β -CHs), 9.41(d, 4H, pyrrole β-H), 8.8(d, 4H, pyrrole β-H), 6.99(s, 8H, mes-CH), 5.35 (t, 1H, Azulene CH), 4.28 (t, 2H, Azulene CHs), 3.98 (d, 2H, Azulene-CHs), 2.35 (s, 12H, Mes-*p*-CH_3), 2.15 (s, 24H, Mes- *o*-CH_3).,-0.6 (d, 2H, vinylogous CHs), -2.1 (d, 2H, vinylogous CHs), -3.7(s, 1H, Azulene CH),

Compound 18: Yield. ~99mg (15%). R_f = 0.25 (Dichloromethen/ Hexane = 7:3), mp > 300 °C. HR-MS(ESI-TOF) m/z: $[M]^+$ calcd for $C_{88}H_{70}N_4OS_4^+$ 1326.4432; found

1326.4431 UV-vis (CH_2Cl_2, λ [nm], ([ϵ [M^{-1} $cm^{-1}x10^4$]) 298K) 353.25(25.5), 480.35(40.2), 538.12 (10.2), stretch 850-1300nm.

^{1}H NMR (400 MHz, CD_2Cl_2, 298 K) δ = 12.08 (br, 1H, -NH), 10.52 (br, 1H, -NH), 10.37 (d, 1H, vinylogous- CH), 10.15 (d, 1H, vinylogous CH), 9.62 (m, 3H, inner six- member CHs), 8.92 (m, 2H, thiophene β -CHs), 8.73 (m, 1H, thiophene β -CH), 8.64 (s, 1H, inner six- member CH), 8.59 (1H, thiophene β -CH), 8.14 (1H, thiophene β -CH), 7.95 (1H, thiophene β -CH), 7.79 (1H, thiophene β -CH), 7.71 (m, 1H, thiophene β -CH), 7.98 (d, 1H, vinylogous CH), 7.83 (d, 1H, vinylogous CH), 7.21(m, 3H, pyrrole β-H), 6.82(m, 1H, pyrrole β-H), 6.75(s, 8H, mes-CH), 6.76 (m, 1H, pyrrole β-H), 6.69 (m, 1H, pyrrole β-H), 6.58 (m, 2H, pyrrole β-H), 2.37 (s, 12H, -CH_3), 2.12 (s, 24H, -CH_3).
^{13}C NMR (75 MHz, $CDCl_3$) δ 185.94, 167.40, 154.31, 153.51, 151.21, 150.14, 149.49, 149.29, 145.99, 145.04, 144.89, 144.82, 144.46, 142.50, 142.43, 142.27, 142.00, 141.75, 141.36, 141.22, 141.16, 138.40, 138.26, 138.22, 138.12, 136.91, 136.82, 136.57, 135.94, 135.90, 135.82, 135.66, 135.43, 135.14, 134.96, 134.75, 133.63, 132.02, 131.43, 131.17, 129.80, 129.43, 128.59, 128.31, 128.26, 127.10, 127.01, 126.70, 126.44, 125.92, 125.51, 124.91, 124.61, 118.95, 77.59, 77.16, 76.74, 76.74, 21.29, 21.29, 20.07, 20.03.

Characterization Data

Chapter 5

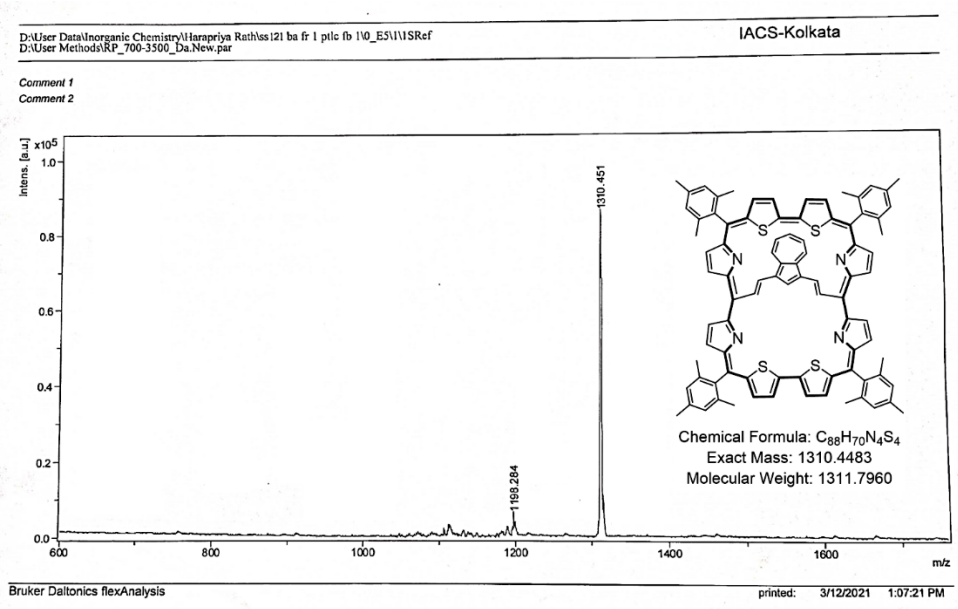

Figure 5.17. MALDI-TOF data of **17**

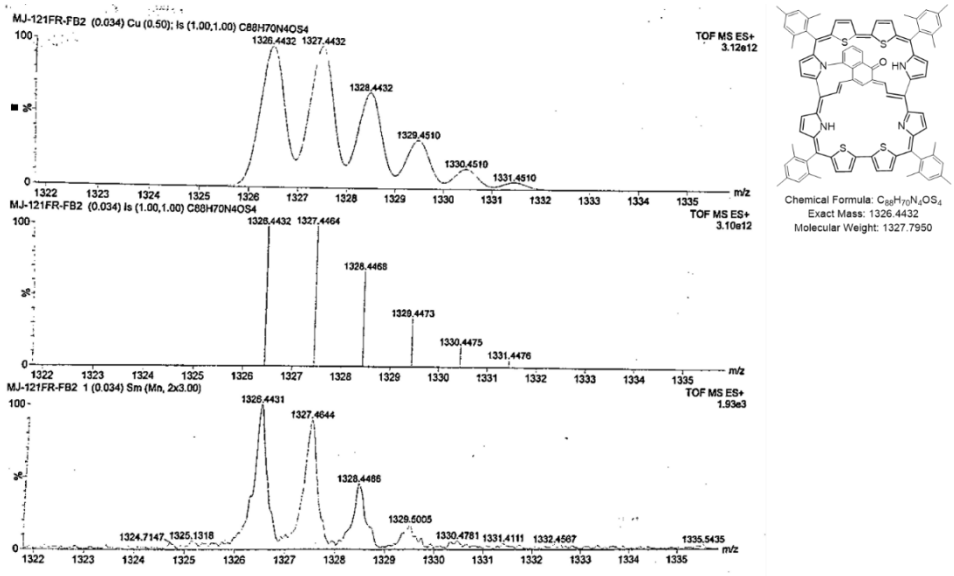

Figure 5.18. HRMS data of **18**

5.5. Reference

1. V. G Anadda, S. Saito and,S. Shimizu and A. Osuka, *Angew. Chem. Int. Ed*. 2005, **44**, 7244 –7248.

2. M.Yoon,S. Cho, M. Suzuki, A. Osuka and D. Kim, *J. Am. Chem. Soc.***,** 2009, **131**, 7360–7367.

3. H. Mori, J. M. Lim, D. Kim and A. Osuka, *Angew. Chem. Int. Ed,* 2013, **52**, 12997 – 13001.
4. G. Karthik, M. Sneha, V. P. Raja,J. M. Lim, D. Kim, A. Srinivasan and T. K. Chandrashekar, *Chem. Eur. J*., 2013, **19**, 1886 – 1890.
5. T. Soya, H. Mori, Y. Hong, Y. H. Koo, D Kim and A, Osuka, *Angew. Chem. Int. Ed*., 2017, **56**, 3232 –3236.
6. W.Y. Cha, T. Kim, A. Ghosh, Z. Zhang, X.S. Ke, R. Ali, V. M. Lynch, J. Jung, W. Kim, S Lee, S. Fukuzumi, J. S. Park, J. L. Sessler, T. K. Chandrashekar and D.Kim, *Nat. Chem*., 2017, **9**, 1243-1248.
7. M. J Białek and L. L. Grażyński, *Chem. Commun.*, 2018, **54**, 1837-1840

List of Publications

1. "NIR absorption of Azulene-bridge Aromatic carabaporphyrinoids Synthesis, Structural and Theoretical characterization". **Sumit Sahoo,** Harapriya Rath *Manuscript under preparation*

2. *"Tailor-Made Aromatic Porphyrinoids with NIR Absorption"* **Sumit Sahoo**, M. Jana and Harapriya Rath*, *Chem. Commun.,* **2022,** 58, 1834-1859.

3. "NIR Absorbing Aromatic (Antiaromatic) Vinylogous Carbasapphyrins (3.3.1.0.1) with built-in Fused Dipolar Aromatic Hydrocarbon: Synthesis and Characterization". **Sumit Sahoo**, V. Gunasekaran, B. Chakraborty, P. Comba* and Harapriya Rath*. *Org. Chem. Front.,* **2021**, *8*, 6909-6915.

4. "Structural isolation of NIR Absorbing Ferrocenyl Bridged N-Confused Fused Expanded Phlorin, N-Confused Porphodimethene and π-extended Corrorin isomer: Synthesis and Characterization". Buddhadeb Chakraborty, **Sumit Sahoo**, R. Narayanasamy, D. Usharani* and Harapriya Rath*, *Dalton Trans.,* **2021**, *50*, 14421 - 14431.

5. "Targeted Synthesis of meso-Aryl Substituted Aromatic *trans*-Doubly N-confused Dithia/Diselena [18] porphyrins (1.1.1.1) with NIR Absorption: Spectroscopic, and Theoretical Characterization" **Sumit Sahoo,** M. Sangeetha, S. Bera, D. Usharanin, Harapriya Rath* *Org.Biomol. Chem.,* **2020,** *18***,** 6058-6062.

6. "Conformational-switch based Strategy Triggered by [18] π Heteroannulenes towards Reduction of Alpha Synuclein (α-Syn) oligomers toxicity" R. Chakraborty, **Sumit Sahoo**, Nyancy Halder, Harapriya Rath.*, Krishnananda Chattopadhyay.* *ACS Chem. Neurosci.* **2019**,10, 573-587.

View Article Online
DOI: 10.1039/D1CC06336G

ARTICLE

Tailor-Made Aromatic Porphyrinoids with NIR Absorption

Sumit Sahoo,[a] Manik Jana [a] and Harapriya Rath *[a]

Received 00th January 20xx,
Accepted 00th January 20xx

DOI: 10.1039/x0xx00000x

The highlight of this article is the recent progress in the state-of the art synthetic design and isolation of artificial porphyrinoids by swapping pyrrole component(s) with diverse functionalized pyrrolic(heterocyclic)/carbacycle building block(s) to compare the impact on the electronic absorption spectra and aromaticity of the incorporated isomeric/expanded porphyrinoids. Attention has been directed towards five distinct criteria of utilizing functionalized pyrrole(heterocycle)/aromatic hydrocarbon as synthons for NIR absorbing aromatic isomeric (N-confusion)/expanded porphyrnoids (with five/six heterocycles): (i) fused or annelated pyrrole (heterocycle), (ii) functionalized bi-pyrrole/bi-thiophene/bi-furan building blocks, (iii) azulene based carbacycle building block, (iv) vinylogous aromatic carbacycle/heterocycle(s) building block and (v) N-confused pyrrole ring(s), and N-confused fused pyrrole ring(s) leading to π-extension. These hybrid porphyrinoids are ideal candidates for basic research into macrocyclic aromaticity and for many potential applications owing to NIR absorption.

[a] *School of Chemical Sciences, Indian Association for the Cultivation of Science, 2A/2B Raja S.C Mullick Road, Jadavpur, Kolkata, West Bengal 700 032, India. ichr@iacs.res.in*

† Footnotes relating to the title and/or authors should appear here.

Electronic Supplementary Information (ESI) available: [details of any supplementary information available should be included here]. See DOI: 10.1039/x0xx00000x

Mr Sumit Sahoo received his BSc from the Department of Chemistry, Egra SSB College in 2014 and MSc from Vidyasagar University, Midnapore, West Bengal, India, in 2016. He is currently pursuing his PhD under the supervision of Dr. Harapriya Rath at the School of Chemical Sciences, Indian Association for the Cultivation of Science, Kolkata, India. His current research efforts focus on the retrosynthetic design and synthesis of NIR absorptive Aromatic core-modified carbaporphyrinoids.

Mr Manik Jana received his BSc from the Department of Chemistry, Garhbeta College in 2015 and MSc from Vidyasagar University, Midnapore, West Bengal, India, in 2017. He is currently pursuing his PhD under the supervision of Dr. Harapriya Rath at the School of Chemical Sciences, Indian Association for the Cultivation of Science, Kolkata, India. His current research efforts focus on the Organometallic Chemistry of Multiply N-Confused Expanded porphyrinoids.

Harapriya Rath received her PhD degree from the Indian Institute of Technology, Kanpur, India on the Nonlinear Optical studies of Core-modified Aromatic Expanded porphyrinoids under the supervision of Prof. T. K. Chandrashekar in 2006. In 2007, she joined the group of Prof. Hiroshi Shinokubo at the Kyoto University, Japan as JSPS Postdoctoral fellow and focused on the subject of Möbius aromaticity (antiaromaticity) and excited state aromaticity of metallated all-aza expanded porphyrinoids. In 2009, she moved to Prof. Richard EP Winpenny's lab at the University of Manchester, United Kingdom as a Royal Society Newton International postdoctoral fellow focusing on hybrid Organic-Inorganic Rotaxanes. In 2012, she started an independent academic carrier at Indian Association for the Cultivation of Science, Kolkata, India as an Assistant professor and Ramanujan Fellow. Since 2017, she is Associate Professor in the School of Chemical Sciences, IACS, Kolkata, India.

Introduction

Current advancements in electronics and bio imaging have sparked renewed interest in the development of next-generation functional dyes. Due to their numerous

View Article Online
DOI: 10.1039/D0OB01243B

COMMUNICATION

Targeted Synthesis of *meso*-Aryl Substituted Aromatic *trans*-Doubly N-confused Dithia/Diselena [18] porphyrins (1.1.1.1) with NIR Absorption: Spectroscopic and Theoretical Characterization

Received 00th January 20xx,
Accepted 00th January 20xx

DOI: 10.1039/x0xx00000x

Sumit Sahoo, [a] Mohandas Sangeetha, [b] Soumita Bera, [a] Dandamudi Usharani *[b,c] and Harapriya Rath*[a]

High yield synthesis and spectroscopic isolation of two hitherto unknown highly stable single conformer of *meso*-aryl substituted dithia/diselena *trans*-doubly N-confused porphyrins with fully π-conjugated [18] annulene structures are reported. In depth solution state spectroscopic measurements and DFT level theoretical calculations strongly conclude the distinct aromaticity with strong NIR absorption of these new macrocycles.

Aromaticity is a multidimensional concept that regulates the intrinsic stability, chemical reactivity and physical properties of π-conjugated molecules.[1] Porphyrins and porphyrin analogues offer multifarious roles in catalysis, sensor development, cancer treatment, nanotechnology, molecular scale information storage owing to their inherent aromaticity.[2] It is worth mentioning that the development of such novel macrocycles with specific functionality has long been an interesting research topic for chemists. In such endeavours, the chemistry of confusion approach to porphyrinoids has grown rapidly since its discovery in 1994 by the Furuta and Latos-Grażyński groups.[3] *N*-Confused porphyrins have witnessed unusual metallation chemistry leading to the formation of metal-carbon bond inside the porphyrin cavity, stabilization of unusual oxidation states of metals and the existence of different tautomeric forms.[4] Core modification of *N*-Confused porphyrin by replacing one or two pyrrole nitrogens by other heteroatom such as O, S, and Se results in the formation of modified *N*-Confused porphyrins with altered electronic structure.[5] The interest in such molecules lies in the fact that they form metal complexes involving weak metal- heteroatom interactions leading to the isolation of some unusual complexes. However, it is pertinent to emphasize that introduction of confusion into tetrapyrrolic macrocycles causes a significant loss of thermodynamic stability.[6f] Consequently, syntheses of multiply *N*-Confused tetrapyrrolic porphyrins have been an intriguingly tough scientific challenge so far. Thus, only a handful of reports (Chart 1) are available in the field of doubly N-confused tetrapyrrolic porphyrins[6] due to limitation of the synthetic means until very recently we adopted a straight forward synthetic methodology for the isolation of the smallest ever antiaromatic [16] *trans*-doubly N-confused porphyrins and redox associated aromaticity reversal.[6e] Thus, easy and efficient synthetic methodologies are most warranted to prepare four membered doubly *N*-Confused porphyrins in high yields for further exploiting their unique chemistry. It was thus this consequence of our scientific interest to study whether and how employment of thiophene/selenophene rings in the development of novel *trans* doubly *N*-Confused porphyrinoids would modify the conformation, electronic properties and the aromaticity of the new macrocycles. The results of such studies are reported herein and provide clues for the further development of new tetrapyrrolic/heterocyclic macrocycles with fine-tuned properties.

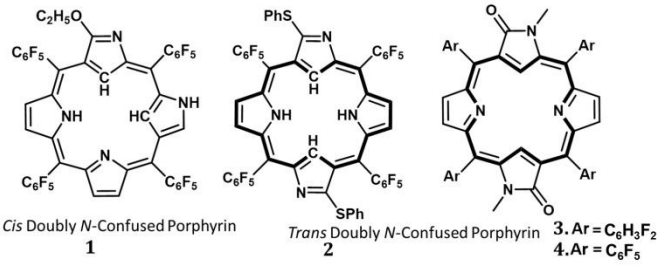

Chart 1. Representative examples of Doubly N-confused porphyrins

Scheme 1 outlines the targeted synthesis of the hitherto unknown *trans*-doubly *N*-Confused dithia/diselena porphyrins

[a] *School of Chemical Sciences, Indian Association for the Cultivation of Science, 2A/2B Raja S.C Mullick Road, Jadavpur, Kolkata, West Bengal 700 032, India. ichr@iacs.res.in*
[b] *Department of Food Safety and Analytical Quality Control Laboratory,CSIR-Central Food Technological Research Institute, Mysuru 700020, Karnataka, India. ushad@cftri.res.in*
[c] *Academy of Scientific and Innovative Research (ACSIR), CSIR-HRDC, Ghaziabad, Uttar Pradesh, India.*

† Footnotes relating to the title and/or authors should appear here.
Electronic Supplementary Information (ESI) available: [Experimental procedure, copy of 1D and 2D NMR spectra, electrochemical data, Theoretical data]. See DOI: 10.1039/x0xx00000x

ORGANIC CHEMISTRY FRONTIERS

RESEARCH ARTICLE

View Article Online
View Journal | View Issue

Cite this: *Org. Chem. Front.*, 2021, **8**, 6909

NIR absorbing aromatic (antiaromatic) vinylogous carbasapphyrins (3.3.1.0.1) with built-in fused dipolar aromatic hydrocarbon: synthesis and characterization†

Sumit Sahoo,[a] Gunasekaran Velmurugan,[b] Buddhadeb Chakraborty,[a] Peter Comba *[b] and Harapriya Rath *[a]

Received 1st September 2021,
Accepted 22nd October 2021

DOI: 10.1039/d1qo01247a

rsc.li/frontiers-organic

Expedient syntheses, spectroscopic, solid state structural proof and theoretical study of three structural variants (with planar geometry) of strongly aromatic (antiaromatic) hybrid [26]/[24] vinylogous carbasapphyrins (3.3.1.0.1) exhibiting strong NIR absorption are reported. The azulene transformations within the macrocycles leading to aromaticity (antiaromaticity) have been supported by DFT based theoretical investigations. Intriguingly, the nature of macrocycles with the (lack of) aromaticity of the related carbaporphyrinoids has been anticipated to be fully triggered by the type of chemically functionalized thiophene based precursor.

Introduction

Azulene, a nonbenzenoid dipolar aromatic hydrocarbon[1] with beautiful blue colour, affords a dissimilar distribution of electron density between the highest occupied (HOMO) and lowest unoccupied molecular orbital (LUMO).[2] The non-mirror-related frontier orbital geometry endows azulene with a small energy gap[2] leading to unique optical and electronic properties. Introduction of an azulene moiety to the porphyrinoid framework[3] has led to borderline macrocyclic aromaticity from dipolar canonical forms that simultaneously give the structure carbaporphyrin and tropylium aromatic characteristics. Current advancements in electronics and bioimaging have sparked renewed interest in the development of next-generation functional dyes. NIR dyes with absorption bands in the biological window (700–900 nm) are in high demand for biological imaging of cells and tissues, as well as for reducing autofluorescence and allowing for deeper light diffusion, all of which contribute to more effective therapy and diagnosis.[4] In such endeavours, controlled modification of the basic framework of expanded porphyrins results in systematic variation of the optical properties, making them efficient NIR dyes in specific instances with strong aromaticity.[5] Among the expanded porphyrinoids known in the literature,[5] sapphyrin is the most widely studied expanded porphyrin,[5i] which has been tremendously investigated over the last two decades for unravelling its potentiality as functional materials, as receptor for neutral molecules toward drug delivery, for anion binding ability and as photosensitizers for photodynamic therapy.[5j–l] We are intrigued by the undisputed scientific fact that a close relationship between the number of π electrons and the topology of the molecular structure (triggered by protonation, solvent polarity, coordination environment) regulates the extent of macrocyclic aromaticity in expanded porphyrinoids.[5b,c,g,h] In this context, it is worthwhile to unravel the impact of amending an azulene moiety on the macrocyclic aromaticity (antiaromaticity) of core modified ring-expanded vinylogous sapphyrins[6] that has hitherto remained unexplored (Chart 1),[3,6] while peculiar transformation of azulene in expanded porphyrinoids has recently been reported[3c] that is in line with the well-known isomerization of azulene to naphthalene.[7] Thus, our scientific interest was to explore the conformation(s), electronic properties and aromaticity (antiaromaticity) of new generation core modified vinylogous carbasapphyrins upon inclusion of the azulene moiety in the macrocyclic conjugation pathway. The results of such scientific studies are reported herein which provide clues for further development of new macrocycles with fine-tuned properties.

[a]*School of Chemical Sciences, Indian Association for the Cultivation of Science, 2A/2B Raja S.C Mullick Road, Jadavpur, Kolkata, West Bengal 700 032, India. E-mail: ichr@iacs.res.in*

[b]*Heidelberg University, Institute of Inorganic Chemistry and Interdisciplinary Center for Scientific Computing, Im Neuenheimer Feld 270, 69120 Heidelberg, Germany. E-mail: peter.comba@aci.uni-heidelberg.de*

†Electronic supplementary information (ESI) available. CCDC 2116847. For ESI and crystallographic data in CIF or other electronic format see DOI: 10.1039/d1qo01247a

Dalton Transactions

ROYAL SOCIETY OF CHEMISTRY

PAPER

View Article Online
View Journal | View Issue

Cite this: *Dalton Trans.*, 2021, **50**, 14421

Structural isolation of NIR absorbing ferrocenyl bridged N-confused fused expanded phlorin, N-confused porphodimethene and the π-extended corrorin isomer: synthesis and characterization†

Buddhadeb Chakraborty,[a] Sumit Sahoo,[a] Raja Narayansamy,[b] Dandamudi Usharani*[b,c] and Harapriya Rath *[a]

Received 19th July 2021,
Accepted 7th September 2021

DOI: 10.1039/d1dt02385c

rsc.li/dalton

Concise syntheses and spectroscopic, solid state X-ray crystal structure and theoretical studies of three electronically appealing new generation hitherto unknown ferrocenyl bridged N-confused heterocyclic macrocycles with (without) fusion are reported. Intriguingly, the expanded N-confused fused phlorin (1.1.1.1.1) with the built-in tripentacyclic [5.5.5] moiety exhibits tailing of the NIR absorption band beyond 1000 nm while the nonconjugated porphodimethene and a new generation π-extended isomeric corrorin analogue exhibit UV-vis absorption.

Introduction

Organic compounds with chromophores that absorb and/or emit in the red or near-infrared (NIR) region are promising materials for a variety of applications including photodynamic therapy dyes,[1] microscopy imaging agents,[2] semiconductors in NIR light emitting diodes,[3] dyes for NIR cut-filters[4] and photosensitizers in NIR-utilizing solar cells.[5] Most organic chromophores with NIR absorption/emission properties fall into one of the four categories: cyanines,[6] phthalocyanines/porphyrins,[7] squaraines[8] and BODIPYs.[9] Because of their unique spectral, structural, chemical, and physical features in comparison with the parent porphyrin system, new porphyrin isomer syntheses continue to attract scientists' interest. Within the context of the generalised extended porphyrin and isomeric porphyrin paradigm, astounding arrays of alterations have been introduced to date by synthetic chemists.[10] In this context, the N-confusion modification[11] approach embedding a peculiar α,β′-linked pyrrole ring (*i.e.*, N-confused pyrrole) into the porphyrin scaffold (Chart 1) has gained attention owing to its aromatic character, relatively long wavelength electronic absorption and facile generation of organometallic derivatives with a large variety of metal ions (transition metals, main group metals and lanthanides) along with the exceptional cases for stabilizing the unusual oxidation states of metals.[12]

The asymmetric flexible skeleton of N-confused porphyrin aids in the reinversion of the N-confused pyrrole ring, resulting in the formation of an intramolecular bond (C–N bond formation between the inverted N-confused pyrrole ring and the neighbouring pyrrole ring) or fusion in the inner core of the porphyrinoid *via* appropriate chemical reactions resulting in the formation of novel N-fused porphyrins (NFPs).[13] NFPs have characteristic absorption[13,14] and emission[13d] in the near-IR range making them viable as near-IR dyes (Chart 2). N-Fused porphyrin possesses a few distinguishing characteristics, making significant contributions to structural organic chemistry, photochemistry, coordination chemistry, and biochemistry.[13b] This has fuelled the rapid development of new structural variants of NIR absorbing/emissive NFPs by varying the extent of π-conjugation and/or the degree of distortion from

[a]*School of Chemical Sciences, Indian Association for the Cultivation of Science, 2A/2B Raja S.C Mullick Road, Jadavpur, Kolkata, West Bengal 700 032, India. E-mail: ichr@iacs.res.in*
[b]*Department of Food Safety and Analytical Quality Control Laboratory, CSIR-Central Food Technological Research Institute, Mysuru 700020, Karnataka, India. E-mail: ushad@cftri.res.in*
[c]*Academy of Scientific and Innovative Research (ACSIR), CSIR-HRDG, Ghaziabad, Uttar Pradesh, India*

†Electronic supplementary information (ESI) available. CCDC 2053405. For ESI and crystallographic data in CIF or other electronic format see DOI: 10.1039/d1dt02385c

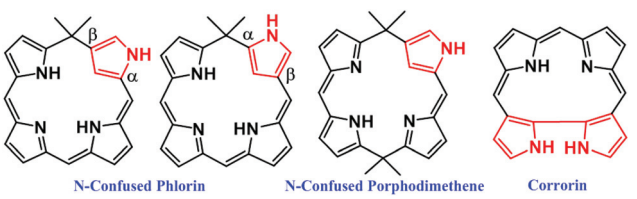

Chart 1 Schematic presentation of N-confused phlorin, N-confused porphodimethene and corrorin.

ACS Chemical Neuroscience
Cite This: ACS Chem. Neurosci. 2019, 10, 573−587
Research Article
pubs.acs.org/chemneuro

Conformational-Switch Based Strategy Triggered by [18] π Heteroannulenes toward Reduction of Alpha Synuclein Oligomer Toxicity

Ritobrita Chakraborty,[†] Sumit Sahoo,[‡] Nyancy Halder,[‡] Harapriya Rath,*[,‡] and Krishnananda Chattopadhyay*[,†]

[†]Structural Biology and Bioinformatics Division, CSIR-Indian Institute of Chemical Biology, 4 Raja S. C. Mullick Road, Kolkata 700032, India

[‡]School of Chemical Sciences, Indian Association for the Cultivation of Science (IACS), 2A/2B Raja S. C. Mullick Road, Kolkata 700032, India

Supporting Information

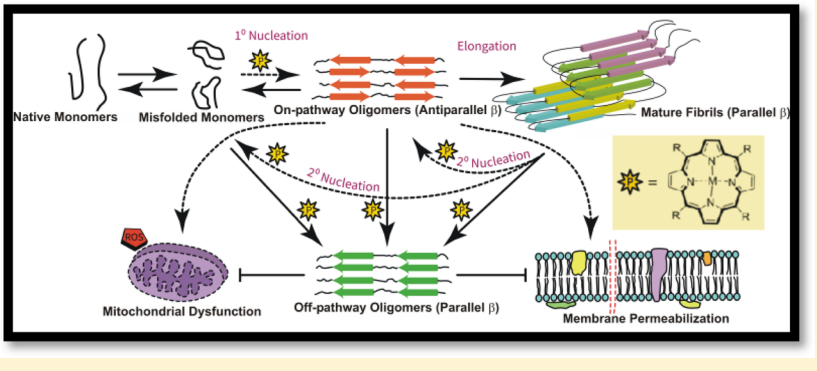

ABSTRACT: A water-soluble *meso*-carboxy aryl substituted [18] heteroannulene (porphyrin) and its Zn-complex have been found to be viable in targeting α-Syn aggregation at all its key microevents, namely, primary nucleation, fibril elongation, and secondary nucleation, by converting the highly heterogeneous and cytotoxic aggresome into a homogeneous population of minimally toxic off-pathway oligomers, that remained unexplored until recently. With the EC_{50} and dissociation constants in the low micromolar range, these heteroannulenes induce a switch in the secondary structure of toxic prefibrillar on-pathway oligomers of α-Syn, converting them into minimally toxic nonseeding off-pathway oligomers. The inhibition of the aggregation and the reduction of toxicity have been studied in vitro as well as inside neuroblastoma cells.

KEYWORDS: *Heteroannulenes, α-Syn, conformational switch, on-pathway oligomer, off-pathway oligomer, neuroblastoma cell*

INTRODUCTION

Alpha synuclein (α-Syn) is a 140 amino acid residue long, natively unfolded protein associated with incurable synucleopathies such as Parkinson's disease (PD), dementia with Lewy bodies, and multiple system atrophy.[1,2] PD is characterized by neuronal loss accompanied by motor and cognitive deficits in patients.[3] The molecular interpretation of PD entails a conformational alteration of the soluble protein α-Syn into misfolded monomers that self-coalesce into intermediate structures ultimately forming well-organized amyloid fibrils. The deposition of these cross-β sheet-rich amyloid fibrils in insoluble cytoplasmic inclusions (Lewy bodies) within the dopaminergic neurons of the substantia nigra pars compacta of the brain is the physiological hallmark of PD.[1]

α-Syn consists of an amphipathic N-terminal domain (residues 1−60), a hydrophobic core domain, also known as the NAC (nonamyloid β component) region (residues 61−95), and an acidic, proline-rich C-terminal domain (residues 96−140).[4] The amino acid sequence of the NAC also occurs individually as a 35 residue long peptide fragment (nonamyloid β) along with the amyloid β peptide in the cytotoxic deposits of related neurodegenerative Alzheimer's disease (AD).[5,6] Interestingly, this NAC sequence is also found as a domain within the α-Syn protein. As a domain within the α-Syn protein, the NAC, due to its hydrophobicity, acts as the initiator of aggregation. Previous studies using paramagnetic relaxation enhancement and NMR dipolar coupling have reported that the native monomeric α-Syn forms an ensemble of fluctuating conformations that are stabilized by a network of long-range intramolecular interactions involving the N and C termini.[7,8] These conformations are ringlike, compact, and relatively stable, and are thought to prevent oligomerization

Received: August 27, 2018
Accepted: October 8, 2018
Published: October 8, 2018

DOI: 10.1021/acschemneuro.8b00436
ACS Chem. Neurosci. 2019, 10, 573−587